Optique Quantique Multimode en Variables Continues

Nicolas Treps

Université Pierre et Marie Curie - Paris VI
Habilitation à diriger des recherches

Nicolas Treps
Laboratoire Kastler Brossel

Optique Quantique Multimode en Variables Continues

Soutenue le 7 décembre 2006

devant le jury composé de :

- Steve Barnett (rapporteur)
- Claude Fabre
- Jean-Marc Frigerio
- Jean-Pierre Gazeau (rapporteur)
- Philippe Grangier (rapporteur)
- Silvania Pereira

Table des matières

Première partie .

Parcours personnel

1. Contexte des activités de recherche et d'enseignement et remerciements

Les travaux que je vais présenter dans les chapitres suivants ont été effectués principalement en deux lieux : le Laboratoire Kastler-Brossel et le département de physique de l'Australian National University, à Canberra, dans le groupe de Hans Bachor. L'origine de cette collaboration date de ma thèse, pendant laquelle nos deux groupes se sont mis en relation pour réaliser une expérience commune, expérience que je suis allé faire à la fin de ma thèse en passant un mois à Canberra. Je vais préciser ici comment s'articulent mes différents travaux entre ces deux endroits, puis je dirai quelques mots de mes activités d'enseignement.

J'ai effectué ma thèse dans le groupe d'optique quantique de Claude Fabre au sein du laboratoire Kastler-Brossel, à l'Université Pierre et Marie Curie. Cette thèse portait sur l'étude des effets quantiques dans les images optiques. J'y ai étudié expérimentalement le comportement des oscillateurs paramétriques concentriques et confocaux au dessus du seuil, à la fois de manière classique en étudiant les motifs optiques émis par de telles cavités, et quantiquement en mettant en évidence le caractère multimode du champ émis par la cavité confocale. Ces études se sont doublées d'une partie théorique sur les propriétés quantiques des solitons et les propriétés quantiques transverses des faisceaux lumineux de manière générale. Un article du groupe ayant montré la possibilité d'améliorer les mesures de position par rapport à la limite quantique standard, nous avons initié la collaboration avec l'Australie -le groupe de Hans Bachor disposant d'une source de vide comprimé de grande qualité- et j'ai pu réaliser l'expérience correspondante à la fin de ma thèse.

C'est donc naturellement que je me suis tourné vers l'Australie pour effectuer mon séjour post-doctoral. Cette fois-ci, je me suis intéressé à la génération d'états non-classiques et aux protocoles d'information quantique, ce qui m'a permis de réaliser, notamment, des expériences d'intrication de polarisation et de téléportation. De plus, j'ai développé en parallèle la théorie de la mesure des images d'intensité pour généraliser à toute mesure les prédictions sur les mesures de position. Ainsi, j'ai également pu pendant ce séjour réaliser une expérience de mesure de position d'un faisceau laser à deux dimensions transverses au delà de la limite quantique standard.

La même année (2002), j'ai été recruté comme Maître de Conférences à l'Université Pierre et Marie Curie, au sein du laboratoire Kastler-Brossel. À mon retour, j'ai participé au renouvellement de l'expérience d'imagerie, qui a pris une autre orientation avec l'amplification sans bruit d'images. Je me suis également intéressé aux expériences sur les oscillateurs paramétriques optiques, qu'elles soient classiques (avec des mesures de brisure de symétrie) ou quantiques (intrication, mesure conditionnelles, bruit basse fréquence, etc...). J'ai ainsi commencé à m'intéresser de manière plus précise aux critères d'intrication et à leur lien avec l'optique quantique multimode.

De plus, je me suis attaché à développer la collaboration avec l'Australie, ce qui nous a permis de recruter un étudiant en thèse en cotutelle entre nos deux institutions. J'ai donc partagé mon temps entre ces différentes activités, en effectuant régulièrement des séjours à Canberra. La grande réussite de cette collaboration vient des bases de son fonctionnement. Tout d'abord, nous avions trouvé un thème commun, novateur, celui de l'optique quantique à petit nombre de modes, où l'on produit à la demande la lumière nécessaire à améliorer une mesure spécifique. Ensuite, il était clair que les expériences se déroulaient en Australie, sous la responsabilité de Hans Bachor, et la théorie était faîte en France, sous ma responsabilité et celle de Claude Fabre. Cette collaboration est toujours en cours et a donné lieu à de nombreuses publications.

Tout cela m'a mené à étudier l'optique quantique multimode, de façon générale, en me penchant à la fois sur les critères d'intrication et les propriétés des champs multimodes. Avec Claude Fabre, nous avons alors défini un nouveau projet de recherche, l'optique quantique avec un peigne de fréquence, pour lequel nous avons obtenu un financement de l'ANR et qui est en cours de montage.

L'ensemble des travaux effectués durant cette période ne sont pas, par soucis de cohérence et de concision, repris dans ce manuscrit. Au delà des extensions et compléments des travaux présentés, certains thèmes ne sont pas abordés. Ainsi, je ne reviendrai pas sur les travaux faits exclusivement pendant ma thèse, ni sur l'étude de la brisure spontanée de symétrie lors de la génération intracavité de second harmonique (article [19] de la liste de publications). Je ne détaillerai pas non plus l'étude des fluctuations quantiques dans les solitons (articles [2,14,17,31] de la liste de publications), études faîtes en partie durant ma thèse et dont les idées physiques sont pour l'essentiel contenues dans les travaux présentés.

Je tiens à insister sur les nombreuses collaborations initiées par le groupe qui ont permis ce travail et l'ont enrichi, que toutes et tous en soit remercié. Je voudrais en particulier citer, tout d'abord, Hans Bachor, puis, dans le désordre, Ping Koy Lam et Magnus Hsu en Australie, Warwick Bowen à Ottago en Nouvelle Zélande, Roman Schnable à Hanovre et Ulrik Andersen à Copenhague. Le groupe de Luigi Lugiato et Alessandra Gatti à Como en Italie, Éric Lantz et son groupe de l'institut Femto ST à Besançon, Mikhail Kolobov du laboratoire Phlam à Lille, Philippe Réfrégier de l'institut Fresnel à Marseille, Yuri et Tania Goliubev de l'université de Saint Petersbourg, German de Valcarcel de l'université de Valence, les brésiliens Paulo Souto-Ribeiro, Antonio Khoury, Paulo Nussenzweig et Carlos Monken.

Je voudrais également mentionner les collaborations internes au laboratoire, tout d'abord l'autre partie du groupe d'optique quantique, notamment Michel Pinard et Alberto Bramati et les thésards successifs de ce groupe. Également Serge Reynaud et Brahim Lamine pour notre début de collaboration sur les mesures de temps. Je n'ai cité ici que les personnes avec lesquelles j'ai collaboré scientifiquement directement, mais bien entendu le laboratoire dans son ensemble, de part son fonctionnement et les personnalités présentes est une clé essentielle de mon travail de recherche. Je remercie aussi en particulier Michèle Leduc, avec laquelle j'ai organisé et participé à de nombreux workshop.

L'équipe elle-même s'est bien malheureusement réduite avec le départ de Thomas Coudreau, merci des moments passés et bonne chance pour la suite ! et celui d'Agnès Maître qui, bien que partie, est toujours présente, disponible et avec qui j'ai maintenant

l'immense plaisir d'enseigner. Enfin, Claude Fabre, lui toujours bien présent, jamais à court d'idées, de conseils ou de projets, et avec qui j'espère vraiment pouvoir continuer à travailler le plus longtemps possible ! Merci à tous les trois.

Enfin, je terminerai par les doctorants avec lesquels j'ai travaillé directement, et sans lesquels, au vu de ma charge d'enseignant chercheur, je n'aurai pu continuer mes activités de recherche, en particulier expérimentales. Ce sont Vincent Delaubert, Laurent Lopez, Gaëlle Keller, Giuseppe Patera, Antonino Chiummo, Sylvain Gigan, Julien Laurat et Laurent Longchambon qui ont fait tout le travail !

Je voudrais aussi profiter de cet espace pour évoquer mes activités d'enseignement et de vulgarisation scientifique. Loin d'être une activité au pire secondaire ou au mieux parallèle à la recherche, l'enseignement fait partie intégrante de notre métier et on se rend compte, au fil des années, que l'un ne peut plus aller sans l'autre. Bien que les conditions d'enseignements ne soient pas toujours idéales, l'organisation compliquée et la charge de travail demandée aux enseignants-chercheurs toujours plus importante, le plaisir des moments passés devant les étudiants compense encore toutes ces difficultés, quel que soit d'ailleurs le niveau et la matière de l'enseignement délivré. J'ai également pris l'habitude de recruter souvent des stagiaires, et je pense que, indépendamment du travail effectué, cela est toujours profitable pour tout le monde, merci à eux et j'espère continuer à avoir les moyens -à la fois en infrastructure mais aussi en temps- de leur proposer des séjours dans notre laboratoire. Je voudrais, pour l'ensemble de mes activités d'enseignement, souligner le soutien dont j'ai pu bénéficier au sein du laboratoire, et en particulier l'aide de Lucile Julien, de Jean-Michel Courty, de Catherine Schwob et d'Agnès Maître.

Je ne vais pas remercier individuellement l'ensemble des personnes avec qui j'ai la chance d'enseigner, mais je voudrais insister sur la confiance qu'elles m'ont en général accordée et sur la liberté dont on dispose du moment que l'on en a la volonté (et le temps !). Cela rend optimiste sur la possibilité de faire évoluer le fonctionnement de notre institution dans le bon sens. Un certain nombre de chantiers sont en cours en particulier sur le rôle de notre enseignement et nos ambitions de formation, et j'espère pouvoir continuer à y participer.

Enfin, j'ai eu la chance de pouvoir, en plus, m'impliquer dans un grand nombre d'activités de vulgarisation, dont la reconstitution de l'expérience de Fizeau constitue la partie visible. Ces activités sont, pour moi, tout à fait similaires à celles de l'enseignement dans leur esprit même si le public y est différent. Merci à ceux qui ont permis ces activités, et en particulier, encore une fois, à Jean-Michel Courty et à Claude Fabre. La diffusion d'une culture de base sur la physique est à mon avis essentielle si l'on veut que cette science ne soit plus considérée, au mieux, comme hermétique par le plus grand nombre. Les efforts de pédagogie faits dans ce cadre sont d'ailleurs tout à fait profitables à la fois à nos activités d'enseignement et à celles de recherche. J'espère voir ces activités se pérenniser, continuer à y impliquer les étudiants du laboratoire et de l'université, afin d'apporter du dynamisme et de la visibilité a notre discipline, mais également afin de continuer à y prendre plaisir !

Deuxième partie .

Présentation générale des travaux

2. Introduction

Les études sur les propriétés spécifiquement quantiques de la lumière ont porté principalement sur deux types distincts d'états quantiques du champ, liés à des techniques de détection très différentes : les états à photons bien isolés d'une part, et les faisceaux intenses ou macroscopiques d'autre part. Le cas des photons uniques donne directement accès à des objets quantiques que l'on peut manipuler pour faire des tests fondamentaux de la mécanique quantique ou mettre en œuvre des protocoles d'information quantique. Cependant, le nombre de particules intriquées très faible limite la gamme des états réalisables, et la technologie des détecteurs (qui permettent difficilement de détecter plus d'un photon à la fois) limite la gamme des états mesurables. Dans le cas des faisceaux macroscopiques, où cette fois-ci le nombre de photons est très grand et où ils ne sont pas distingués individuellement, on a pu réaliser de nombreux états quantiques comme des états comprimés ou des faisceaux intriqués. Cependant, du fait à la fois des non-linéarités atteignables et des techniques de détection, on se trouve dans la limite des petites fluctuations quantiques ce qui interdit de réaliser, par exemple, des états à fonction de Wigner négative. Notre point de départ est pourtant ce deuxième cas, qui englobe la quasi-totalité du travail décrit ici. Dans cette limite des petites fluctuations quantiques, nous allons chercher à augmenter la richesse, et les possibles applications, des états quantiques produits en multipliant le nombre de "modes" -ou degrés de libertés- mis en jeu par le processus de détection. C'est ce que nous appelons l'optique quantique multimode.

La *complexité multimode* introduite permet d'envisager des applications dans le traitement quantique de l'information. On citera l'accroissement des capacités de stockage et de transfert d'information, la réalisation d'intrication plus robuste, le traitement en parallèle de l'information quantique. Mais ces études peuvent également trouver des applications pour améliorer les techniques d'imagerie et de métrologie. Le champ d'étude est donc très vaste et très général, à l'image des multiples applications de l'optique pour les mesures de précisions et les communications. Les enjeux sont à la fois d'étudier avec nos outils des dispositifs bien connus, mais également d'explorer les possibilités nouvelles offertes par une approche quantique appliquée aux degrés de liberté multiples de la lumière.

Dans ce cadre, nous commencerons par un chapitre technique permettant de rappeler quelques notions sur l'écriture de l'opérateur champ électrique multimode, et verrons comment, en pratique, compter le nombre de modes pertinents au sein d'un faisceau lumineux. Puis nous reprendrons la théorie de la mesure optique pour associer le caractère multimode de la lumière à la recherche d'information dans un faisceau. Par cette approche, nous redéfinirons les limites ultimes de la mesure mais nous pourrons également nous pencher sur l'intrication quantique à partir de n'importe quelle grandeur mesurable. La suite de ce mémoire, présentant les travaux effectués et s'appuyant sur une liste d'article, sera alors vue sous l'angle d'illustrations de cette théorie, en partant des expériences monomodes vers les expériences les plus multimodes. Les titres et

les abstracts des articles sont repris dans le texte de manière à l'illustrer. Les articles eux-mêmes sont reproduits en fin de manuscrit.

L'angle multimode sous lequel sont abordés les travaux présentés n'est pas le seul point vue possible ; même s'ils s'intègrent dans ce cadre, ils n'y trouvent pas forcément leur origine. Des domaines comme l'information quantique, l'optique non-linéaire, l'imagerie, etc... ont été souvent moteurs dans ce travail, mais l'approche multimode est celle qui à la fois unifie l'ensemble et permet de présenter, en fin de mémoire, les futurs projets de recherche.

3. Les degrés de liberté de la lumière

3.1. L'opérateur champ électrique

La quantification de la lumière dans le vide permet d'exprimer l'opérateur champ électrique dans la base des ondes planes[1] :

$$\hat{\vec{E}}^{(+)}(\vec{r},t) = i\sqrt{\frac{\hbar}{2\epsilon_0}}\int \frac{d^3k}{(2\pi)^3}\sqrt{\omega}\hat{a}(\vec{k})e^{-i(\omega t-\vec{k}.\vec{r})} \tag{3.1}$$

où nous avons considéré l'opérateur des fréquences positives, qui ne s'écrit qu'en fonction des opérateurs d'annihilation, l'opérateur champ électrique réel étant la somme de cet opérateur et de son hermitien conjugué. Sous cette forme, le continuum de modes est difficile à manipuler, nous allons donc considérer -comme c'est le cas expérimentalement- des conditions aux limites permettant de s'en affranchir. Nous choisissons une direction de propagation privilégiée, z, et supposons que, transversallement, le champ s'annule à l'infini. De plus, nous nous plaçons dans l'approximation paraxiale. Enfin, nous allons supposer que la détection du champ se fait pendant un temps d'intégration[2] T. Ces conditions aux limites, à la fois spatiales et temporelles, permettent de remplacer le continuum par un nombre dénombrable de modes et ainsi écrire le champ :

$$\hat{\vec{E}}^{(+)}(\vec{\rho},u) = \sum_i \mathcal{E}_i\hat{a}_i\vec{u}_i(\vec{\rho},u). \tag{3.2}$$

Dans cette équation, $\mathcal{E}_i$ est une constante qui dépend du mode considéré, $\hat{a}_i$ est l'opérateur d'annihilation d'un photon dans le mode i. Un mode est une fonction qui dépend des différents paramètres de la propagation : transverse ($\vec{\rho} = x\vec{i} + y\vec{j}$), temporel ($u = z - ct$) et polarisation, qui est normalisée et qui vérifie l'équation de propagation du champ dans le vide. L'ensemble des modes considérés dans la décomposition précédente forme une base dans laquelle tous champ lumineux peut être décomposé, en associant au champ son amplitude sur chacun de ces modes. Connaissant cette décomposition, on connaît le champ en n'importe quel point de l'espace des paramètres. Les modes sont normalisés et orthogonaux entre eux de telle sorte que :

$$[\hat{a}_i, \hat{a}_j^\dagger] = \delta_{ij} \tag{3.3}$$

et chacun est un oscillateur harmonique, un degré de liberté quantique.

[1] On pourra se reporter à M. I. Kolobov, Rev. Mod. Phys. **71**, 1539 (1999) où sont également posées les bases de l'optique quantique multimode spatiale

[2] On pourrait à la place d'introduire le temps de détection supposer que le champ s'annule aux temps -ou mieux, aux u- plus et moins l'infini, mais l'introduire dès maintenant permet d'obtenir plus rapidement les expressions qui nous intéressent.

Cette dernière équation permet de traiter tous les problèmes que nous allons aborder ici, cependant, dans l'essentiel des cas nous pourrons faire une hypothèse supplémentaire : que le champ est de fréquence centrale ω_0 et de largeur en fréquence $\Delta\omega$ petite devant ω_0. Dans ce cas, les constantes de normalisation sont toutes égales et l'opérateur champ s'écrit :

$$\hat{\vec{E}}^{(+)}(\vec{\rho}, u) = \mathcal{E} \sum_i \hat{a}_i \vec{u}_i(\vec{\rho}, u). \tag{3.4}$$

où $\mathcal{E} = i\sqrt{\frac{\hbar\omega_0}{2\epsilon_0 cT}}$.

Enfin, pour alléger les calculs, nous travaillerons souvent directement avec l'opérateur $\hat{A}$ tel que :

$$\hat{\vec{A}}^{(+)}(\vec{\rho}, u) = \sum_i \hat{a}_i \vec{u}_i(\vec{\rho}, u) \tag{3.5}$$

où l'intégrale sur tout l'espace des paramètres de $\hat{\vec{A}}^{(+)\dagger}\hat{\vec{A}}^{(+)}$ est homogène à un nombre de photons.

C'est dans la somme sur i présente dans l'expression de l'opérateur champ électrique que sont présents les degrés de liberté de la lumière. En effet, comme nous l'avons déjà dit, chaque mode représente un oscillateur harmonique indépendant et donc un degré de liberté. Les paramètres mis en jeu sont ρ, u et la polarisation, nous serons donc à même de décrire des systèmes multimodes en polarisation, transversalement, temporellement ou frequentiellement. L'espace considéré est donc très riche et nous verrons, dans les chapitres suivants, comment tirer parti indépendamment de chacun de ces paramètres. Pour ce faire, l'expression 3.4 est bien adaptée car, la constante étant la même pour tous les modes, les changement de bases sont particulièrement aisés. En effet, pour passer d'une base $\{u_i, \hat{a}_i\}$ à une base $\{v_i, \hat{b}_i\}$, connaissant la matrice de passage entre les modes : $v_i = \sum_j c_{ij} u_j$, les opérateurs de créations se déduisent des mêmes relations : $\hat{b}_i^\dagger = \sum_j c_{ij} \hat{a}_j^\dagger$. De plus dans le cas, fréquent, où cette matrice est réelle, cette relation est également valable pour les opérateurs d'annihilation.

3.2. Lumière monomode, multimode

Il convient maintenant de décrire l'état quantique de la lumière. Cependant, et afin de fixer le vocabulaire, rappelons ici que nous appellerons *mode* les modes u_i comme nous venons de les définir, *état quantique de la lumière dans le mode i* ou *état du mode i* l'état quantique de l'oscillateur harmonique caractérisé par l'opérateur $\hat{a}_i$ et enfin *l'état quantique de la lumière* le ket[3] $|\Psi>$ représentant l'état complet de la lumière dans tous les modes et s'écrivant, sous sa forme la plus générale et, pour chaque mode, dans sa base des états de Fock :

$$|\Psi> = \sum_{n_1,\ldots,n_i,\ldots} C_{n_1,\ldots,n_i,\ldots} |n_1, \ldots, n_i, \ldots> \tag{3.6}$$

où $|n_1, \ldots, n_i, \ldots>$ représente l'état quantique produit tensoriel des états de Fock n_1 photons dans le mode 1, n_2 photons dans le mode 2, etc ...

[3] les même considérations peuvent se faire en matrice densité, mais les notions deviennent alors un peu plus difficiles à manier et ne sont pas nécessaires pour le travail présenté ici

mode	lumière monomode	lumière multimode
v_0, $\hat{b}_0$	état quelconque de valeur moyenne $\vec{E}^{(+)}(\vec{\rho}, u)$	état quelconque de valeur moyenne $\vec{E}^{(+)}(\vec{\rho}, u)$
v_1, $\hat{b}_1$	vide	état non-classique tel que $< \Psi \vert \hat{b}_1 \vert \Psi >= 0$
$\vdots$	$\vdots$	$\vdots$
v_n, $\hat{b}_n$	vide	état non-classique tel que $< \Psi \vert \hat{b}_n \vert \Psi >= 0$
v_{n+1}, $\hat{b}_{n+1}$	vide	vide
$\vdots$	$\vdots$	$\vdots$

Tab. 3.1.: Comparaison entre un champ monomode et un champ multimode dans la base du champ moyen

L'ensemble des calculs menant à une définition propre du caractère monomode ou multimode de la lumière est présenté dans l'article **1** (reproduit en page 54). Nous allons voir ici que quelques considérations simples permettent d'en comprendre la substance. Donnons nous une base de modes $\{\vec{u}_i, \hat{a}_i\}$ et un ket $|\Psi>$ décrivant l'état de la lumière. La valeur moyenne du champ électrique, qui correspond au champ classique, s'écrit :

$$\vec{E}^{(+)}(\vec{\rho}, u) =< \Psi | \hat{\vec{E}}^{(+)}(\vec{\rho}, u) | \Psi > . \tag{3.7}$$

On peut alors définir une nouvelle base $\{\vec{v}_i, \hat{b}_i\}$, que nous appellerons base du champ moyen, telle que

$$\vec{v}_0(\vec{\rho}, u) = \frac{\vec{E}^{(+)}(\vec{\rho}, u)}{||\vec{E}^{(+)}(\vec{\rho}, u)||} \tag{3.8}$$

et on choisit les autres modes v_i afin de former une base othonormale et complète. Comme nous l'avons dit, les opérateurs d'annihilation $\hat{b}_i$ se déduisent des $\hat{a}_i$ avec les même relations que celles permettant de passer des u_i aux v_i. Dans cette base, le champ électrique moyen est porté uniquement, par définition, par le premier mode. Autrement dit $< \Psi | \hat{b}_i | \Psi >= 0$ pour tout $i \neq 0$. On peut à partir de cette base donner une définition des champs monomode et multimode, illustrée dans le tableau 3.2. La lumière monomode est telle que seul le mode de champ moyen est dans un état différent du vide, alors que, pour le cas multimode, des modes autres que le mode de champ moyen sont non-classiques (mais la valeur moyenne du champ électrique y est nulle, nous qualifierons par abus de langage ces modes de *vide*, mais toujours en italique pour les différentier du vide électromagnétique proprement dit). Nous avons choisi ici $(n-1)$ modes non-classiques, décrivant alors un champ d'ordre n (en supposant que l'on se soit placé dans la base où n est le plus petit possible). On notera également que des corrélations peuvent exister entre les modes dans le cas multimode, mais elles n'apparaissent pas dans le tableau.

En résumé, une superposition d'états cohérents, dans des modes différents, reste un champ monomode selon notre critère, car il suffit de se placer dans la base de champ moyen. Un état non-classique l'est également puisqu'il se décrit à l'aide d'un seul mode non-classique, les autres modes étant vides. Le caractère multimode est donc donné par les fluctuations quantiques non-classiques, i.e. différentes de celles du vide, des modes

autres que celui de champ moyen. On peut interpréter cela en disant que les fluctuations du vide -donc celles des états cohérents- sont parfaitement aléatoires et donc les analyser suivant n'importe quelle base n'en change pas la nature. Alors que les fluctuations non-classique sont organisées, et que le paramètre d'ordre s'applique pour un mode du rayonnement bien défini, regarder les fluctuations selon une autre base en change donc la nature -car on les mélange avec des fluctuations du vide-.

Nous avons considéré ici des cas purs, donc en particulier sans fluctuations classiques. Nous avons fait une première extension de ce critère au cas des matrices densités, en étendant la notion d'état monomode à celle d'un état dont la matrice densité s'écrit comme le produit tensoriel d'une matrice densité quelconque sur un mode et la matrice densité du vide sur les autres modes. Ces calculs étant préliminaires, ils ne sont pas détaillés ici, mais permettent d'envisager une extension de nos critères au cas général. En particulier, dans les lasers communément appelés multimodes par exemples, ce sont des modes au dessus du seuil qui sont en compétition, et qui ont des fluctuations classiques différentes : multimodes. Ce cas pourrait être inclus dans l'approche matrice densité, de même que le cas où on part d'états purs et on considère des pertes (ce qui rajoute des fluctuations du vides). Néanmoins, ces différents exemples concernent des réalités physiques assez différentes, non utilisées dans le présent manuscrit, et leur étude générale fait l'objet de nos projets de recherches.

4. La mesure optique

4.1. Définition

Le champ étant bien décrit, nous allons maintenant le mesurer. Un détecteur optique intègre, sur un domaine de l'espace des paramètres, soit l'intensité soit l'amplitude du champ. Nous allons donc considérer ces deux types de détections, en appelant $\mathbf{x}$ le paramètre général qui prend en compte, outre les dimensions transverses et fréquentielles, celles de polarisation. De cette façon, nous allons oublier le caractère vectoriel de l'opérateur champ donné en équation 3.5, mais en comprenant que l'expression $\int d\mathbf{x}$ est une intégrale sur les paramètres continus et une somme sur ceux discrets (ici uniquement la polarisation). Le détecteur d'intensité est alors modélisé par :

$$\hat{S}_I = \int g_I(\mathbf{x}) \hat{A}^{(+)\dagger}(\mathbf{x}) \hat{A}^{(+)}(\mathbf{x}) d\mathbf{x} \tag{4.1}$$

où g_I est la fonction de gain, réelle et sans dimension, qui prend en compte la géométrie et les propriétés du détecteur. $\hat{S}_I$ est homogène à un nombre de photons. Nous ne considérons ici que des détecteurs linéaires. On voit dans les figures ci-dessous deux exemples simples de mesures où la fonction de gain ne prend que deux valeurs différentes, $+1$ et -1, dans un cas en fonction de la polarisation, dans l'autre en fonction de la position :

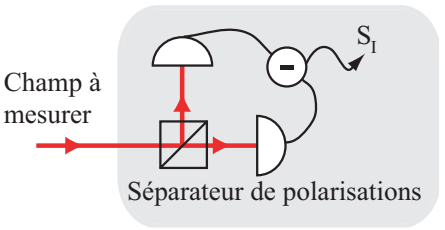

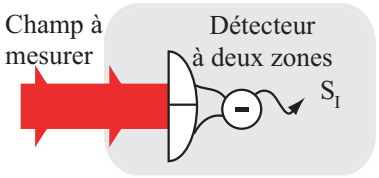

De la même façon le détecteur d'amplitude s'écrit :

$$\hat{S}_E = \int g_E(\mathbf{x}) \hat{A}^{\theta(\mathbf{x})}(\mathbf{x}) d\mathbf{x} \tag{4.2}$$

où g_E est de nouveau la fonction de gain, et $\hat{\vec{A}}^{\theta(\mathbf{x})}(\mathbf{x})$ l'opérateur de quadrature du champ défini par

$$\hat{A}^{\theta(\mathbf{x})}(\mathbf{x}) = \hat{A}^{(+)}(\mathbf{x}) e^{-i\theta(\mathbf{x})} + \hat{A}^{(+)\dagger}(\mathbf{x}) e^{i\theta(\mathbf{x})}. \tag{4.3}$$

Ce détecteur est défini ici d'une manière totalement abstraite où l'on suppose qu'il existe des dispositifs capables de détecter les quadratures du champ en appliquant un gain qui dépend de la position dans l'espace des paramètres. On remarque qu'il est nécessaire de faire le choix de la quadrature à mesurer via le choix de la fonction $\theta(\mathbf{x})$.

Pour réaliser un tel détecteur il est nécessaire d'utiliser un dispositif interférométrique de type homodyne. Un exemple en est donné ci-contre, où une nouvelle fois la fonction de gain peut prendre deux valeurs en fonction de la position, et sur chaque position on détecte une quadrature du champ. Nous verrons par la suite que changer la forme de l'oscillateur local permet également d'agir sur la fonction de gain.

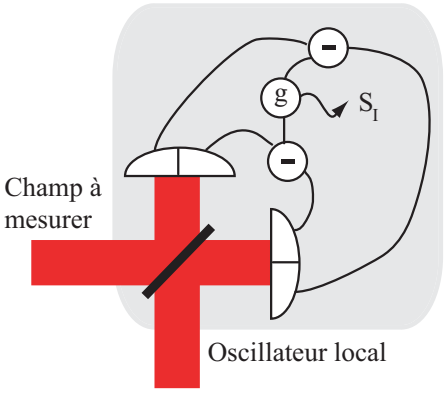

4.2. Mode propre

Les mesures telles que nous les avons définies réalisent une combinaison linéaire des valeurs locales du champ pour en extraire une seule information. Le but de cette section est donc de déterminer quelle est cette information, et comment elle peut être décrite simplement. Nous allons voir que, en choisissant la bonne base dans la description du champ donnée en équation 3.5, l'opérateur de mesure défini ci-dessus, qu'il soit d'intensité où d'amplitude, se ramène à la mesure de l'état du champ dans un seul mode, que l'on appelle alors mode de détection. Il est de plus possible d'expliciter ce mode en fonction de la définition de la mesure et de la forme du champ mesuré.

Prenons l'exemple de la mesure de la différence des polarisations verticales et horizontales de la figure de la section précédente. Dans le cas où le champ incident est polarisé verticalement (respectivement horizontalement), S_I mesure le mode de polarisation verticale (respectivement, au signe près, horizontale). Mais, quand le champ incident est polarisé à $+45^o$, S_I, de valeur moyenne nulle dans ce cas, est sensible aux fluctuations de polarisation orthogonales à la polarisation incidente, le mode de détection est donc dans ce cas le mode à -45^o.

Pour généraliser cette approche, supposons que l'opérateur champ électrique de l'équation 3.5 est écrit dans la base du champ moyen (c'est à dire que le premier mode de la décomposition est proportionnel au champ, et que tous les autres sont *vides*). À partir de cette décomposition, il est possible de construire le mode de détection de la mesure, celui dont l'état est mesuré par notre appareil. Nous appelons ce mode w_1, et il est défini par :

$$w_1(\mathbf{x}) = \frac{1}{f} g_I(\mathbf{x}) u_0(\mathbf{x}) \tag{4.4}$$

où f assure la normalisation du mode. En effet, en utilisant les opérateurs différentiels ($\delta\hat{a} = \hat{a} - < \hat{a} >$) et en se plaçant dans la limite des petites fluctuations (les termes en carré d'opérateurs de fluctuations sont négligés), les fluctuations de l'opérateur $\hat{S}_I$ peuvent s'exprimer uniquement en fonction de celles du mode w_1 :

$$\begin{aligned} \delta\hat{S}_I &= f\alpha_0(\delta\hat{b}_1^\dagger + \delta\hat{b}_1) \\ &= f\alpha_0\delta\hat{X}_{w_1}^+ \end{aligned} \tag{4.5}$$

où α_0 est la valeur moyenne de $\hat{a}_0$ -opérateur d'annihilation associé au mode de champ moyen u_0- , supposée réelle (sans perte de généralité), $\delta\hat{b}_1$ est l'opérateur de fluctuations associé au mode w_1 et $\delta\hat{X}^+_{w_1}$ l'opérateur de quadrature amplitude correspondant[1]. Les fluctuations mesurées par notre appareil sont donc celles de la quadrature amplitude du mode de détection w_1. On voit dans son expression que ce mode correspond au mode de champ moyen u_0 pondéré par la fonction de gain g_I. En reprenant l'exemple de la mesure de polarisation où la fonction de gain est égale à $+1$ pour la polarisation verticale et -1 pour l'horizontale, quand le champ incident est polarisé à $+45^o$, le mode de détection est bien celui à -45^o.

Les même idées sont valables pour les mesures d'amplitudes, nous en donnerons des exemples dans le chapitre suivant, ici nous allons nous limiter au calcul du mode. Comme nous le verrons au chapitre suivant, cette détection peut être réalisée à l'aide d'une détection homodyne où la forme de l'oscillateur local est donnée par $g_E(\mathbf{x})e^{i\theta(\mathbf{x})}$. Ainsi, définissons le mode de détection par :

$$w_1(\mathbf{x}) = \frac{1}{f} g_E(\mathbf{x}) e^{i\theta(\mathbf{x})} \tag{4.6}$$

où f est encore une fois un facteur de normalisation que nous n'explicitons pas. Il est alors possible de construire une base de mode $\{w_i\}$ dont le mode w_1 est donné par l'équation précédente, et d'exprimer l'opérateur champ dans cette base. Dans ce cas, dans l'intégrale 4.2 seule l'intégrale de recouvrement avec w_1 est non nulle et il vient, sans avoir besoin de se placer dans la limite des petites fluctuations :

$$\begin{aligned} \hat{S}_E &= f(\hat{b}_1^\dagger + \hat{b}_1) \\ &= f\hat{X}^+_{w_1}. \end{aligned} \tag{4.7}$$

Comme pour les mesures d'intensité, l'opérateur de mesure d'amplitude est proportionnel à la quadrature amplitude d'un seul mode, que nous appelons mode de détection, et qui se détermine à partir des caractéristiques de la détection et du mode de champ moyen. Il est important de souligner que ce mode dépend donc de la valeur moyenne locale du champ lui-même.

Nous venons de montrer que toute mesure se ramène à la considération d'un seul mode, que nous savons décrire à partir du mode de champ moyen et des propriétés du détecteur. En particulier, le bruit sur la détection provient exclusivement des propriétés de bruit de ce mode. En agissant sur ses fluctuations on peut donc modifier -et en particulier améliorer !- la sensibilité de la mesure. Lorsque plusieurs détections sont effectuées simultanément, l'action doit porter sur chacun des modes de détection correspondants. Nous avons ainsi les outils théoriques pour réaliser et détecter de la lumière multimode. L'article regroupant l'essentiel de ces idées est le suivant :

Article 1, reproduit en page 54

Quantum noise in multipixel image processing

N. Treps, V. Delaubert, A. Maître, J.M. Courty and C. Fabre

[1] On appelle quadrature amplitude celle pour laquelle $\theta = 0$: $\hat{X}^+_{w_1} = \hat{b}_1^\dagger + \hat{b}_1$, et quadrature de phase celle pour laquelle $\theta = \pi/2$: $\hat{X}^-_{w_1} = i(\hat{b}_1^\dagger - \hat{b}_1)$

Phys. Rev. A **71**, 013820 (2005)

Abstract : We consider the general problem of the quantum noise in a multipixel measurement of an optical image. We first give a precise criterium in order to characterize intrinsic single mode and multimode light. Then, using a transverse mode decomposition, for each type of possible linear combination of the pixels' outputs we give the exact expression of the detection mode, i.e. the mode carrying the noise. We give also the only way to reduce the noise in one or several simultaneous measurements.

4.3. Mesure d'un paramètre p

4.3.1. Limite de Cramer-Rao

Nous avons décrit en détail le comportement d'un appareil de mesure, l'étape suivante consiste à adapter et optimiser cet appareil relativement à la quantité à mesurer. Considérons que la lumière transporte de l'information que l'on désire retrouver. Cette information peut par exemple provenir de l'interaction entre le faisceau et un échantillon physique dont on souhaite retrouver certaines propriétés. Elle peut également avoir été directement inscrite dans faisceau pour, par exemple, des communications quantiques. En tous les cas, nous pouvons modéliser cette modification du faisceau par un paramètre p qui affecte uniquement le mode de champ moyen $u_0(\mathbf{x}, p)$, l'action du paramètre étant supposée classique (elle n'agit pas sur les fluctuations).

Nous cherchons à caractériser le meilleur estimateur possible de p (que p soit petit ou non). Pour cela, nous considérons un estimateur non biaisé (i.e. dont la valeur moyenne sur un grand nombre de mesures est p) et cherchons sa variance. Ce problème est classique et est résolu par la théorie de l'information[2], en introduisant une quantité appelée information de Fisher I_F. Cette quantité, dont nous ne donnons pas le détail du calcul ici, permet d'évaluer la quantité d'information disponible sur p en fonction de la statistique de la lumière (son bruit) et, cela, indépendamment de l'appareil de mesure utilisé, seul le type de mesure (intensité ou amplitude) devant être défini. On peut en déduire la variance de l'estimateur : $\sigma^2 = 1/I_F$, et ainsi la plus petite valeur de p pouvant être mesurée (définie par un rapport signal sur bruit égal à 1). Cette limite absolue s'appelle la limite de Cramer-Rao. Dans notre cas, et en considérant de la lumière cohérente (statistique poissonienne), on obtient ce que nous appelons la limite quantique standard, qui s'écrit respectivement pour les mesures d'amplitude et d'intensité :

$$p^{\min}_{\text{amplitude}} = \frac{A}{2\sqrt{N}} \quad \text{où} \quad \left.\frac{\partial u_0(\mathbf{x},p)}{\partial p}\right|_{p=0} = \frac{1}{A} v_A(\mathbf{x}) \tag{4.8}$$

$$p^{\min}_{\text{intensité}} = \frac{a}{2\sqrt{N}} \quad \text{où} \quad \left.\frac{\partial |u_0(\mathbf{x},p)|}{\partial p}\right|_{p=0} \cdot \frac{u_0(\mathbf{x})}{|u_0(\mathbf{x})|} = \frac{1}{a} v_I(\mathbf{x}) \tag{4.9}$$

où v_A et v_I sont des modes normalisés et A et a les constantes de normalisation, réelles positives, correspondantes. N est le nombre total de photons. On observe que pour la mesure d'amplitude, la normalisation est donnée par la dérivée du mode champ moyen ;

[2]Voir par exemple *Théorie du bruit et applications en physique*, P. Réfrégier, Lavoisier (2002)

ceci est à mettre en parallèle avec la variation du mode champ moyen pour une petite variation du paramètre p :

$$\begin{aligned} u_0(\mathbf{x}, p) &\approx u_0(\mathbf{x}) + p \left.\frac{\partial u_0(\mathbf{x}, p)}{\partial p}\right|_{p=0} \\ &= u_0(\mathbf{x}) + \frac{p}{A} v_A(\mathbf{x}). \end{aligned} \tag{4.10}$$

Le mode v_A est celui qui porte l'information, et nous verrons que pour réaliser cette limite il faut un système de détection dont le mode de détection est justement v_A. Les mêmes considérations sont valables pour la mesure en intensité, exceptée la prise en compte d'une norme dans l'équation 4.9 nécessaire si le paramètre p ne modifie pas uniquement l'amplitude du champ, mais également sa phase (signal auquel n'est pas sensible la détection en intensité).

4.3.2. Les appareils de mesure optimaux

La connaissance à la fois du mode portant le signal, indépendamment de l'appareil de mesure, et du mode de détection pour un détecteur donné permet d'optimiser le détecteur relativement au paramètre mesuré. Le cas de la mesure d'amplitude étant le plus simple, nous allons ici détailler les calculs, qui permettent d'appréhender le problème de façon synthétique. En effet, en utilisant la décomposition de Taylor de l'équation 4.10 pour calculer la valeur moyenne de l'opérateur $\hat{S}_E$ de l'équation 4.2, on trouve, en omettant le terme ne dépendant pas de p (ce qui revient à calibrer la détection en ajoutant une constante, mesurable en l'absence de signal) :

$$< \hat{S}_E(p) >= \frac{p}{A} \alpha_0 f \int \left[w_1^*(\mathbf{x}) v_A(\mathbf{x}) + w_1(\mathbf{x}) v_A^*(\mathbf{x}) \right] d\mathbf{x}. \tag{4.11}$$

où, on le rappelle, w_1 est le mode de détection associé à l'appareil de mesure et v_A est le mode qui porte l'information à mesurer. Le rapport signal sur bruit, dans le cas des états cohérents, est alors égal à :

$$\frac{< \hat{S}_E(p) >^2}{< \delta \hat{S}_E(p)^2 >} = p^2 \frac{N}{A^2} \left[\int \left[w_1^*(\mathbf{x}) v_A(\mathbf{x}) + w_1(\mathbf{x}) v_A^*(\mathbf{x}) \right] d\mathbf{x} \right]^2 \tag{4.12}$$

L'intégrale est une intégrale de recouvrement entre deux modes normalisés, elle n'est donc maximale que lorsque ces modes sont identiques, le meilleur choix pour w_1, et donc du gain et de la phase de la détection comme explicité en éq. 4.6, est v_A.

On obtient dans ce cas, et pour des états cohérents, que la plus petite valeur du paramètre mesurable, définie par un rapport signal sur bruit égal à 1, est donnée :

$$p_{min} = \frac{A}{2\sqrt{N}} \tag{4.13}$$

limite identique à celle de Cramer-Rao. Nous avons déjà dit que cette mesure d'amplitude correspondait à une détection homodyne dont l'oscillateur local a la forme de w_1 (voir figure ci-contre), nous avons donc un schéma expérimental permettant d'atteindre la limite de Cramer-Rao (qui sera mis en œuvre au chapitre suivant).

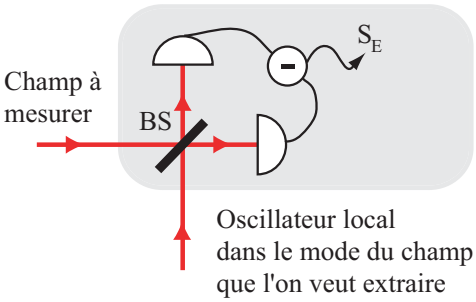

Pour la mesure d'intensité, les mêmes considérations peuvent se faire avec une petite complication technique du fait du module apparaissant dans la dérivée. Cependant, on trouve cette fois-ci que le gain permettant d'optimiser le rapport signal sur bruit est donné par :

$$g_I(\mathbf{x}) \propto \frac{1}{|u_0(\mathbf{x})|} \left.\frac{\partial |u_0(\mathbf{x},p)|}{\partial p}\right|_{p=0} \tag{4.14}$$

qui mène, comme pour la mesure d'amplitude, à la limite de Cramer-Rao.

Ce système est matérialisé par un détecteur multipixel : un pixel par valeur de $\mathbf{x}$ (voir figure ci-contre) et peut donc être implémenté, au moins de manière approchée, expérimentalement.

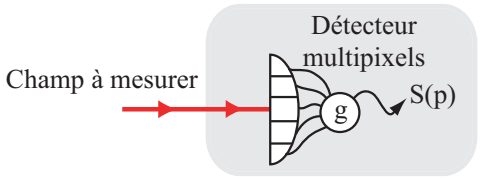

Article 2, reproduit en page 62

Quantum limits in image processing

V. Delaubert, N. Treps, C. Fabre, H.A. Bachor and P. Refrégier

Soumis à Phys. Rev. Lett.

Abstract : We determine the bound to the maximum achievable sensitivity in the estimation of a scalar parameter from the information contained in an optical image in the presence of quantum noise. This limit, based on the Cramer-Rao bound, is valid for any image processing protocol. It is calculated both in the case of a shot noise limited image and of a non-classical illumination. We also give practical experimental implementations allowing us to reach this absolute limit.

4.3.3. Facteur de bruit et amplification

Les limites données précédemment concernent des détecteurs parfaits (sans bruit électronique) et au gain ajustable indéfiniment. Or, lorsque les signaux sont faibles, ou

lorsque la distance de propagation est grande et donc les pertes importantes, il est souvent nécessaire d'amplifier la lumière. Nous allons voir ici rapidement l'effet de cette amplification sur notre mesure.

Notre amplificateur agit sur le champ en entrée $\{\hat{a}_i\}$ pour produire le champ en sortie $\{\hat{b}_i\}$. On le modélise par un processus du type Bogoliubov[3] généralisé, qui agit sur les opérateurs d'annihilation et de création. On suppose de plus qu'il existe une base multimode propre, c'est à dire inchangée par cette transformation (qui ne couple donc pas ces modes entre eux). Ce cas correspond à la plupart des amplificateurs (et aussi les lames séparatrices) linéaires pour lesquels on peut trouver une base découplant les modes. Nous considérons de plus que des sources de bruit externes peuvent intervenir. Les modes de sortie s'écrivent :

$$\hat{b}_i = U_i \hat{a}_i + V_i \hat{a}_i^\dagger + \sum_k (\alpha_{ki} \hat{v}_{ki} + \beta_{ki} \hat{v}_{ki}^\dagger). \tag{4.15}$$

où tous les coefficients sont réels. Chacune de ces transformation devant être unitaire, il vient

$$U_i^2 - V_i^2 + \sum_k (\alpha_{ki}^2 - \beta_{ki}^2) = 1. \tag{4.16}$$

C'est cette dernière relation la plus importante. Elle montre qu'un amplificateur simpliste -seul $U \neq 0$ par exemple- n'est pas autorisé par la mécanique quantique, et donc que tout processus d'amplification est susceptible de rajouter du bruit.

Deux cas sont à dégager dans les processus d'amplification. Tout d'abord, le cas où $V_i = 0$. Dans ce cas, les modes de bruit étant des modes vides ne contribuant pas au signal, le gain du processus est simplement $G_i = U_i^2$, c'est ce qu'on appelle l'amplification insensible à la phase. On définit le facteur de bruit du processus F_{PIA}^i (donné en puissance de bruit dans cette section) comme le quotient entre le rapport signal sur bruit avant amplification et le rapport signal sur bruit après amplification. Il se calcule simplement en utilisant les équations précédentes et on obtient, en tenant compte de l'unitarité :

$$F_{PIA}^i = 2 - \frac{1}{G_i} + 2\frac{\sum_k \beta_{ki}^2}{G_i}. \tag{4.17}$$

Il apparaît le résultat bien connu que, même en annulant le dernier terme de cette équation, le processus rajoute $3dB$ de bruit pour un gain infini.

Le deuxième cas est celui où ni U ni V ne sont nuls, communément appelé sensible à la phase. Le calcul du gain est un peu plus délicat, mais si l'on suppose qu'en entrée nous avons des états cohérents $\alpha_i = |\alpha_i| e^{i\phi_i}$, alors le gain s'écrit $G_i = U_i^2 + V_i^2 + 2U_i V_i \cos(2\phi_i)$, il est bien sensible à la phase du champ. En considérant alors la quadrature d'amplitude, pour laquelle le gain est maximal, il vient pour le facteur de bruit :

$$F_{PSA}^i = 1 + \sum_i \frac{(\alpha_{ki} + \beta_{ki})^2}{G}. \tag{4.18}$$

Dans ce cas, et uniquement sur la bonne quadrature, il est possible d'obtenir de l'amplification sans bruit ajouté en s'affranchissement des entrées de vide supplémentaires, ce

[3] Voir N.N. Bogoliubov, J. Phys. (USSR) **11**, 23 (1947) et également C.M. Caves, *Quantum limits on noise in linear amplifiers*, Phys. Rev. D. **26**, 1817-1839 (1982) pour une étude approfondie des processus d'amplification.

qui impose $U_i^2 - V_i^2 = 1$. Ce type d'amplificateur permet d'améliorer les mesures dans le cas de détecteurs d'efficacité quantique faible par exemple. On montre en effet dans ce cas que, en prenant en compte l'efficacité de détection dans le calcul du facteur de bruit, on peut obtenir un facteur de bruit effectif inférieur à un, c'est à dire améliorer la mesure de notre paramètre grâce à de l'amplification sans bruit[4].

Nous verrons en fin de ce mémoire comment réaliser cette amplification à l'aide d'un amplificateur paramétrique optique. On notera ici la grande généralité des équations présentées qui permettent de modéliser les processus passifs tels les lames séparatrices, mais aussi de prédire les propriétés non-classiques des champs émis par les amplificateurs paramétriques optiques par exemple.

4.4. États non-classiques, intrication et information quantique

Comme nous l'avons vu au début de ce mémoire, les champs multimodes quantiques sont liés à la présence d'états non-classiques de la lumière. Nous venons de voir également qu'une mesure optique était caractérisée par son mode de détection, et donc en particulier ses propriétés de bruit. Ceci nous a permis de donner et d'atteindre la limite quantique standard, liée à l'utilisation de lumière cohérente. Il est possible, en changeant les propriétés de bruit du mode de détection -et en particulier en utilisant dans ce mode de la lumière comprimée- d'aller au delà de la limite de Cramer-Rao standard, puisque le bruit de la mesure lui est directement proportionnel. Ainsi, dès lors que ce mode est différent du mode de champ moyen, de la lumière multimode quantique est nécessaire pour améliorer la mesure.

L'expression 4.7 donnant la mesure d'amplitude en fonction de son mode de détection recèle d'autres possibilités. En effet, la définition du mode w_1 est très libre (contrairement à la mesure d'intensité où g_I est réel) et notamment, en changeant la phase dans sa définition de $\pi/2$, on accède à la quadrature de phase $\delta\hat{X}^-_{w_1}$ de ce mode. Expérimentalement, cela est réalisé simplement en déphasant l'oscillateur local. Ainsi, pour chaque mesure, on a accès très simplement à l'observable conjuguée $\hat{S}^-_E = f\delta\hat{X}^-_{w_1}$ telle que

$$[\hat{S}_E, \hat{S}^-_E] = 2if^2. \tag{4.19}$$

Il est possible de réaliser de l'intrication multimode en adressant individuellement les propriétés quantiques des modes de détection de deux faisceaux. Ainsi, avec ces mesures d'amplitude, l'extension multimode des protocoles d'information quantique monomode est évidente, et on peut penser paralléliser le traitement de l'information quantique pour, par exemple, augmenter les débits, mais également en augmenter la sécurité.

On peut finalement se demander quel est le cadre adéquat pour décrire l'intrication quantique. En effet, si nous considérons deux champ monomodes intriqués (comme cela sera décrit au chapitre suivant), il est possible de les caractériser, comme nous allons le faire, via les critères d'intrication usuels. Pour les champs multimodes intriqués nous ferons alors de même en isolant, dans ces champs, les paires de modes intriqués et en les caractérisant via les même critères. Cependant, et pour revenir à l'exemple de deux faisceaux monomodes, il est possible de décrire ce système comme un seul système quantique multimode, en fusionnant les deux bases de modes. En se placant alors dans

[4]Voir par exemple A. Mosset, F. Devaux et E. Lantz, Phys. Rev. Lett. **94**, 223603 (2005)

la base du champ moyen le mode de champ moyen devient comprimé en phase et le premier mode vide comprimé en intensité (comme cela est le cas lorsqu'on mélange nos deux champs intriqués, en phase, sur une lame 50/50 : l'une des sortie est intense et comprimée en phase, l'autre est *vide* et comprimée en intensité). Cependant, les notions de non-séparabilités et de non-localité, par exemple, n'ont plus beaucoup de sens lorsque les deux bases sont mélangées et nous avons donc choisi de nous en tenir aux critères d'intrication habituels et de restreindre nos champs multimodes à des champs dont tous les modes sont copropageants. On notera pourtant que l'autre approche rappelle celle qui consiste à regrouper les états quantiques via des classes d'équivalences définies par des opérations locales, et est un sujet de recherche que nous poursuivons car il peut être très riche pour la caractérisation des états multimodes.

5. Du monomode au tout multimode

5.1. La mesure monomode : intrication et téléportation

Une mesure est dite monomode lorsqu'un seul détecteur mesure l'ensemble du champ, ou, pour une détection homodyne, lorsque l'oscillateur local a la forme du champ moyen. Dans ce cas, le mode de détection n'est autre que le mode de champ moyen et, même si la lumière est multimode, la détection ne sera pas sensible aux propriétés non-classiques des modes *vides*. C'est le régime habituel de l'optique quantique en variables continues et dans ce cadre il est possible de réaliser des expériences de génération d'états non-classiques, d'intrication, et de les utiliser pour des protocoles d'information quantique. Ces types d'expériences étant maintenant bien connus, nous ne donnerons que peu de détails, en insistant cependant sur la difficulté de caractériser ces états et en particulier les corrélations, caractérisation autrement appelée la *science des critères*. Nous allons décrire ici des expériences qui mettent en évidence successivement différents niveaux de corrélations.

5.1.1. Photons jumeaux et mesures conditionnelles

Le premier niveau de corrélation entre deux champs, n'impliquant qu'une seule quadrature de chaque champ, est appelé gémellité, par extension des photons jumeaux qui reflètent des corrélations d'intensité. Les corrélations entre deux champ sont dites quantiques quand elles ne peuvent être expliquées par une théorie semi-classique (où le champ est traité classiquement). Ce critère, très simple dans le cas symétrique mais un peu technique dans le cas général, signifie qu'en faisant une somme (ou différence) pondérée entre les deux quadratures des deux champ on obtient une quantité dont les fluctuations quantiques sont inférieures à celles d'un état cohérent de même puissance. Il est décrit en détail, dans l'article suivant, qui contient aussi l'ensemble des critères que nous allons évoquer dans ce chapitre :

Article 3, reproduit en page 68

Criteria of quantum correlation in the measurement of continuous variables in optics

N. Treps, and C. Fabre
Laser Physics **15**, 187 (2005)

Abstract : The purpose of this short tutorial paper is to review various criteria that have been used to characterize the quantum character of correlations in optical systems, such as "gemellity", QND correlation, intrication, EPR correlation and Bell correlation, to discuss and compare them.

This discussion, restricted to the case of measurements of continuous optical variables, includes also an extension of known criteria for "twin beams" to the case of imbalanced correlations.

Nous réalisons au laboratoire des photons jumeaux à l'aide d'un oscillateur paramétrique optique. Cette cavité, à l'intérieur de laquelle se trouve un cristal non-linéaire de type 2 (du KTP), génère, lorsqu'elle est pompée avec de la lumière à 532nm, naturellement des faisceaux signal et complémentaire corrélés en intensité, du fait de la conservation de l'énergie lors du processus de génération paramétrique. La très grande stabilité de notre cavité semi-monolithique permet d'obtenir un seuil bas (d'une dizaine de milliwatts) et un bruit sur la différence de 7,5 dB inférieur au bruit quantique standard, en utilisant le critère de gémellité.

Ces fortes corrélations nous ont permis de mettre en place un protocole original de génération conditionnelle d'état sub-poissonien. L'idée consiste à mesurer les fluctuations d'intensité du complémentaire ce qui, du fait de la forte corrélation existante, nous renseigne sur celles du faisceau signal. Ainsi, on peut sélectionner dans le faisceau signal les moments où les fluctuations du faisceau complémentaire sont comprises dans une certaine bande de valeurs -proche de zéro par exemple-. Le nouveau faisceau signal produit (une version hachée de l'original, générée conditionnellement à la mesure du complémentaire) possède alors des fluctuations proches de zéro, modulo la taille de la bande de sélection et la valeur des corrélations. L'expérience a été faite en mesurant et stockant informatiquement les fluctuations d'intensité du signal et du complémentaire, puis en faisant une post-sélection sur le signal à partir des valeurs du complémentaire. Nous avons pu de cette façon produire un faisceau dont les fluctuations en intensité sont réduites de 4,4 dB sous le bruit quantique standard, partant de 7,5 dB de photons jumeaux. Cette méthode originale est très intéressante car elle s'apparente aux techniques utilisées en photon uniques et permet d'envisager la création, de manière conditionnelle, de nombreux états quantiques. Les détails en sont donnés dans :

Article 4, reproduit en page 77

Conditionnal Preparation of a Quantum State in the Continuous Variable Regime : Generation of a sub-Poissonian State from Twin Beams

J. Laurat, T. Coudreau, N. Treps, A. Maître and C. Fabre

Phys. Rev. Lett. **21** 213601 (2003)

Abstract : We report the first experimental demonstration of conditional preparation of a nonclassical state of light in the continuous variable regime. Starting from a nondegenerate optical parametric oscillator which generates above threshold quantum intensity correlated signal and idler "twin beams," we keep the recorded values of the signal intensity only when the idler intensity falls inside a band narrower than its standard deviation. By this very simple technique, we generate a sub-Poissonian state 4.4 dB (64%) below shot noise from twin beams exhibiting 7.5 dB (82%) of noise reduction in the intensity difference.

5.1.2. Intrication

Avec la même cavité, nous avons généré de l'intrication. Les faisceaux signal et complémentaire émis dans un OPO sont naturellement corrélés en intensité, mais également en phase. Cependant, la diffusion de phase vient modifier la fréquence du signal et complémentaire et donc, même si la somme de leurs phases reste bien fixée, la différence elle peut varier et empêche de détecter simplement les corrélations. Pour fixer ces fréquences nous avons donc introduit à l'intérieur de la cavité un couplage (une lame quart d'onde) qui mélange très légèrement les polarisations signal et complémentaire. Deux oscillateurs légèrement couplés, s'ils ont des fréquences suffisamment proches se verrouillent l'un à l'autre pour osciller à une fréquence commune. C'est le phénomène qui se produit dans l'OPO lorsque la température du cristal est suffisamment proche de la température de dégénérescence[1].

Néanmoins, pour des raisons qui restent encore à explorer -mais que nous supposons venir du bruit de phase du laser de pompe- nous n'avons pas pu observer de corrélations de phase, au niveau quantique, au dessus du seuil. Le système, une fois réglé, est donc utilisé au dessous du seuil d'oscillation, et ce sont les fluctuations des champs *vides* émis que nous analysons. Pour caractériser ces doubles corrélations, nous avons utilisé le critère de Duan décrit en équation (20) de l'article **3**, et qui reflète le caractère intriqué, ou non-séparable, de l'état quantique produit. Non-séparable signifiant que sa fonction d'onde ne peut pas s'écrire comme le produit tensoriel de deux fonctions d'onde (une pour chacun des faisceaux), où comme la superposition statistique de tels produits. La non-séparabilité mesurée reste, a l'heure d'aujourd'hui, la meilleure jamais mesurée (0,33, à comparer à 1 pour des états cohérents). L'article correspondant est :

Article 5, reproduit en page 81

Compact source of Einstein-Podolsky-Rosen entanglement and squeezing at very low noise frequencies

J. Laurat, T. Coudreau, G. Keller, N. Treps and C. Fabre
Phys. Rev. A **70** 042315 (2004).

Abstract : We report on the experimental demonstration of strong quadrature Einstein-Podolsky-Rosen entanglement and squeezing at very low noise sideband frequencies produced by a single type-II, self-phase-locked, frequency degenerate optical parametric oscillator below threshold. The generated two-mode squeezed vacuum state is preserved for noise frequencies as low as 50 kHz. Designing simple setups able to generate nonclassical states of light in the kHz regime is a key challenge for high sensitivity detection of ultraweak physical effects such as gravitational wave or small beam displacement.

Dans cet article, nous avons également démontré le caractère *basse fréquence* des fluctuations non-classiques, ce qui signifie que pour des fréquences d'analyse d'environ 50kHz nous observons encore des effets quantiques. Cette propriété très intéressante n'avait pas été observée jusqu'alors et vient de ce que, en théorie, le bruit de la pompe ne se couple pas aux champs émis lorsque l'on travaille sous le seuil. Nous n'avons pas exploré cette

[1] Voir l'expérience originale de E. J. Mason et N. C. Wong, Opt. Lett. **23** 1733 (1998)

voie plus avant, mais cela prouve que ce genre de système peut être utilisé avec profit dans des dispositifs où il est nécessaire d'avoir des propriétés quantiques sur une grande bande de fréquence (lecture optique de l'information, détection d'ondes gravitationnelles, etc...).

Le niveau suivant de corrélation est celui de l'intrication dite EPR[2]. Dans ce cas, où comme pour l'inséparabilité il y a des corrélations entre les deux quadratures des deux champs, on caractérise l'intrication via la variance conditionnelle. Celle-ci représente la variance d'une quadrature d'un champ connaissant les fluctuations de la même quadrature de l'autre champ (c'est ce qu'on obtiendrait en rétroagissant sur un champ de manière optimale grâce aux mesures faites sur l'autre champ). Dans le cas des corrélations EPR, les produits des variances conditionnelles des deux quadratures du même champ connaissant celles de l'autre champ viole l'inégalité de Heisenberg, on parle alors de *violation apparente* de cette inégalité[3]. Ce critère est identique à celui de Duan pour des cas purs, mais est beaucoup plus sensible aux pertes : au delà de 50% de pertes les corrélations EPR ne peuvent subsister. Or, 50% de perte signifient que, potentiellement, une tierce partie a pu prélever plus de la moitié du faisceau et donc posséder une copie de l'original plus fidèle que celle des opérateurs. En ce sens, le critère EPR est relié au théorème de *non-clonage* qui explique qu'il n'est pas possible de réaliser deux copies identiques d'un état quantiques, et est pertinent pour, comme nous allons le voir, les expériences de téléportation[4].

5.1.3. Téléportation quantique

L'intrication quantique est utilisée dans nombre de protocoles d'information quantique, le plus célèbre étant la téléportation. Ce protocole est très intéressant car il permet de mettre en évidence le caractère non-classique des faisceaux autrement que via un critère direct. La téléportation a d'abord été introduite pour des états à photons uniques, puis a été étendue aux variables continues à la fois théoriquement et expérimentalement [5]. Rappelons-en ici le principe, la figure ci-dessous donnant un exemple de téléportaiton classique :

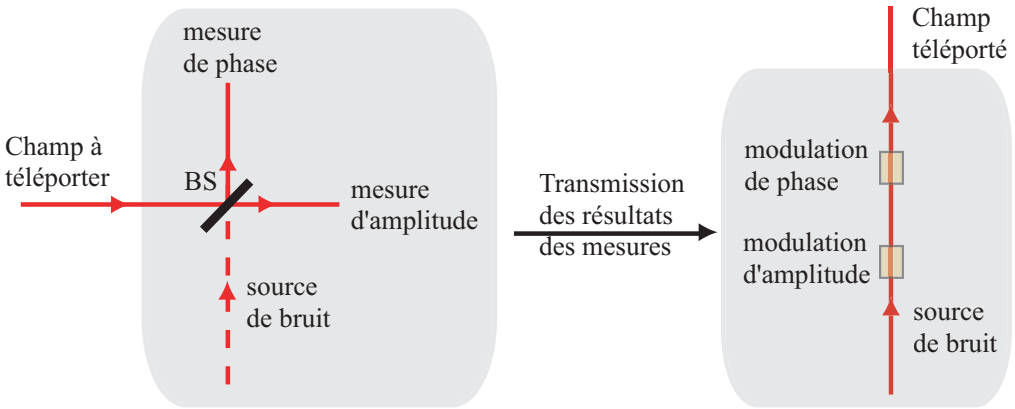

[2] A. Einstein, B. Podolsky and N. Rosen, Phys. Rev. **47**, 777 (1935)
[3] Voir par exemple M. Reid and P. Drummond, Phys. Rev. Lett. **60**, 2731 (1989)
[4] Voir à ce sujet F. Grosshans et P. Grangier, Phys. Rev. A **64**, 010301 (2001)
[5] Voir en particulier C.H. Bennett *et al.*, Phys. Rev. Lett. **70**, 1895 (1993) et A. Furusawa *et al.*, Science **282**, 706 (1998)

Lors d'une mesure effectuée sur un faisceau lumineux, si l'on désire mesurer à la fois son intensité et sa phase du bruit est introduit dans cette mesure du fait de la non-commutabilité des observables. Le dispositif modèle pour mettre en œuvre ces mesures consiste à séparer en deux le faisceau sur une lame séparatrice et utiliser une des sorties pour mesurer l'intensité et l'autre pour mesurer la phase. Dans ce cadre, le bruit de la mesure vient de l'entrée non-utilisée de la lame séparatrice, par laquelle arrivent des fluctuations du vide.

De la même façon, si on désire utiliser les informations de la mesure pour reconstruire le faisceau un peu plus loin, une autre source de bruit apparaît inévitablement : le support sur lequel est faîte cette reconstruction, le faisceau que l'on cherche à moduler par exemple. Ainsi, dans une expérience complète de téléportation deux quantas de bruit sont introduits, un à la mesure, un à la reconstruction. L'idée, pour aller au delà de cette limite, consiste à corréler ces deux sources de bruit de telle sorte qu'elles se compensent à la fin de l'expérience. En utilisant deux faisceaux EPR, l'un à l'entrée vide de la lame séparatrice et l'autre à la reconstruction, on réalise exactement ce système et, idéalement, une téléportation parfaite est alors possible. Nous avons, en Australie, réalisé une telle expérience :

Article 6, reproduit en page 85

Experimental investigation of continuous-variable quantum teleportation

W. P. Bowen, N. Treps, B. C. Buchler, R. Schnabel, T. C. Ralph, H.-A. Bachor, T. Symul, and P. K. Lam

Phys. Rev. A. 67, 032302 (2003)

Abstract : We report the experimental demonstration of quantum teleportation of the quadrature amplitudes of a light field. Our experiment was stably locked for long periods, and was analyzed in terms of fidelity F and with signal transfer $T_q = T^+ + T^-$ and noise correlation $V_q = V^+_{in|out} V^-_{in|out}$. We observed an optimum fidelity of 0.64 ± 0.02, $T_q = 1.06 \pm 0.02$, and $V_q = 0.96 \pm 0.10$. We discuss the significance of both $T_q > 1$ and $V_q < 1$ and their relation to the teleportation no-cloning limit.

La technique pour générer les faisceaux EPR est, dans cette expérience, différente de celle présentée en section précédente, elle repose sur le mélange de deux faisceaux comprimés produit chacun dans des Amplificateurs Paramétriques Optiques (OPA). Le mélange de deux états comprimés en amplitude, déphasés de $\pi/2$, sur une lame 50/50 génère directement des états intriqués. La technique utilisée ici pour produire ces états comprimés est le processus de de-amplification dans un amplificateur paramétrique optique. En effet, ce dispositif réalise, dans le cas idéal, une transformation des champs du type proposé en équation 4.15 où on peut s'affranchir des sources de bruits externes et donc, pour le cas monomode, $U^2 - V^2 = 1$. On montre dans ce cadre facilement que pour un processus de de-amplification où $U = \cosh x$ et $V = -\sinh x$ on obtient $< (\hat{\delta} X_b^+)^2 >= e^{-2x}$, le champ sortant est comprimé. Expérimentalement, on place un cristal non-linéaire d'ordre 2 dans une cavité, on choisira généralement du type I pour assurer simplement la dégénérescence entre signal et complémentaire. Cette cavité est pompé, dans nos expériences, à $532nm$ et injectée à $1064nm$; sa longueur est asservie sur

une résonance infrarouge et, souvent, nous la choisirons non résonnante pour la pompe. Étant en configuration sensible à la phase, l'ajustement de la phase relative entre la pompe et le signal permet de se placer en régime de dé-amplification, et d'obtenir un champ sortant dans l'infrarouge comprimé en intensité. La puissance de ce champ sortant peut être très faible -la dizaine de microwatts- mais, n'étant pas nulle, on a une référence de phase permettant de réaliser des asservissements dans les expériences en aval[6].

Nous avons ici mis, en particulier, l'accent sur la caractérisation de l'expérience. En effet, de nombreux critères sont utilisés : la Fidélité -intégrale de recouvrement entre l'état original et l'état produit-, le transfert de signal -la quantité d'information utile transmise, critère originellement introduit dans le cadre des mesures quantiques non déstructives -, et les variances conditionnelles -comment le caractère non-classique des faisceaux se transmet- ; et nous avons de plus étudié l'influence de l'incertitude de mesure de différents paramètres (comme le gain, l'efficacité quantique de détection, etc...) sur les résultats trouvés. Les valeurs mesurées pour ces critères étaient à l'époque les meilleures jamais atteintes, néanmoins la limite du "non-clonage", reflétant que le faisceau téléporté est forcément la meilleure copie existante de l'original, bien qu'ayant été approchée de près n'a pas été battue, seule sa version restreinte au transfert de signal l'ayant été[7].

La téléportation quantique étant une pierre essentielle des protocoles d'information quantiques, et notamment pour les réseaux de communications, nous avons étudié, de manière théorique, comment ses principes pouvaient s'étendre aux ensembles atomiques. Nous proposons ici un protocole de téléportation basé sur le transfert des propriétés quantiques des atomes vers la lumière, une mesure de la lumière et une reconstruction effectuée directement sur le nuage atomique :

Article 7, reproduit en page 89

Teleportation of an atomic ensemble quantum state

A. Dantan, N. Treps, A. Bramati and M. Pinard

Phys. Rev. Lett. 94, 050502 (2005)

Abstract : We propose a protocol to achieve high fidelity quantum state teleportation of a macroscopic atomic ensemble using a pair of quantum-correlated atomic ensembles. We show how to prepare this pair of ensembles using quasiperfect quantum state transfer processes between light and atoms. Our protocol relies on optical joint measurements of the atomic ensemble states and magnetic feedback reconstruction.

5.2. La mesure de polarisation

L'espace de la polarisation d'un faisceau lumineux est un espace à deux dimensions, à deux modes comme nous les avons définis au début de ce mémoire, par exemple les

[6] Voir par exemple le livre de Hans Bachor et Tim Ralph, *A guide to experiments in quantum optics*, Wiley-VCH, Weinheim, (2005) pour plus de précisions sur ces techniques maintenant standard.

[7] Depuis cette limite à été dépassée par N. Takei, H. Yonezawa and A. Furusawa, Phys. Rev. Lett. **94**, 220502 (2005)

modes de polarisation horizontale et verticale. Par rapport à la section précédente un degré de liberté en plus est disponible et l'espace des états est donc plus riche, mais plus complexe à évaluer. Commençons par définir la réduction de bruit en polarisation. En accord avec notre premier chapitre, il faut, pour évaluer un faisceau donné, se placer dans la base du champ moyen : le mode de champ moyen est alors celui de la polarisation de la valeur moyenne du champ et le deuxième mode est sa composante orthogonale. Dans ce cadre, les propriétés quantiques du mode de champ moyen ne nous intéressent pas, car c'est ce qui est détecté par une détection monomode. Nous dirons donc que nous avons de la réduction de bruit en polarisation lorsque le mode de polarisation orthogonal au champ moyen est non-classique, en accord avec ce qui a été proposé par N.V. Korolkova *et al.*[8].

Nous avons réalisé en Australie une expérience de réduction de bruit de polarisation, dont les résultats ont été obtenu préalablement à l'achèvement de la théorie présentée ici. Ainsi, la définition de la réduction de bruit de polarisation y est différente. Nous nous étions placé dans l'espace des paramètres de Stockes, dont l'extension quantique par rapport à la définition classique est immédiate (voir l'article). Cet espace est intéressant car les quatre paramètres de Stokes peuvent être mesurés grâce à des mesures d'intensité (et ne nécessitent donc pas de référence de phase). C'est d'ailleurs pourquoi les variables de polarisation suscitent beaucoup d'intérêt pour les protocoles de communication. La réduction du bruit d'un des paramètres de Stokes en dessous de sa valeur dans le cas cohérent nous permettait d'affirmer que le faisceau était comprimé en polarisation. Néanmoins, et afin de ne pas reproduire des expériences monomodes, nous avions réduit simultanément les fluctuations de 3 sur 4 des paramètres, ce qui implique que le faisceau est comprimé en accord avec la définition donnée au paragraphe précédent. Les résultats sont exposés dans :

Article 8, reproduit en page 94

Stokes-operator-squeezed continuous-variable polarization states

R. Schnabel, W. P. Bowen, N. Treps, T.C. Ralph, H.-A. Bachor et P.K. Lam

Phys. Rev. A 67, 012316

Abstract : We investigate nonclassical Stokes-operator variances in continuous-wave polarization-squeezed laser light generated from one and two optical parametric amplifiers. A general expression of how Stokes-operator variances decompose into two-mode quadrature operator variances is given. Stokes parameter variance spectra for four different polarization-squeezed states have been measured and compared with a coherent state. Our measurement results are visualized by three-dimensional Stokes-operator noise volumes mapped on the quantum Poincaré sphere. We quantitatively compare the channel capacity of the different continuous-variable polarization states for communication protocols. It is shown that squeezed polarization states provide 33% higher channel capacities than the optimum coherent beam protocol.

Pour produire cette réduction de bruit nous avons utilisés deux faisceaux comprimés -les mêmes que ceux de la téléportation- que nous avons mélangé grâce à un cube sépara-

[8] Natalia Korolkova and Rodney Loudon, Phys. Rev. A **71**, 032343 (2005).

teur de polarisation. L'analyse complète du faisceau produit à été faite ce qui nous permis de tracer notre état produit -et le faire varier- à l'intérieur de la sphère de Poincaré.

La suite logique de cette expérience consiste à réaliser de l'intrication de polarisation. Nous avons donc cherché, dans une approche similaire à celle de l'article précédent, à intriquer les paramètres de Stokes de deux faisceaux différents. Nous avions choisi également de réaliser une intrication non-triviale -qui serait uniquement celle des champs moyens- et avons donc réalisé une intrication équivalente à l'intrication des modes *vides* des deux faisceaux, intrication qui rentre donc dans le cadre que nous avons défini et que nous pouvons donc appeler intrication multimode en polarisation.

Il est à noter que nous avons développé des critères basés sur les paramètres de Stokes -du fait de leur utilité en information quantique-, mais que les critères généraux d'intrication multimode manquent encore. On remarquera également la similitude formelle entre cette expérience et l'intrication spatiale proposée en section suivante (voir figure ci-contre).

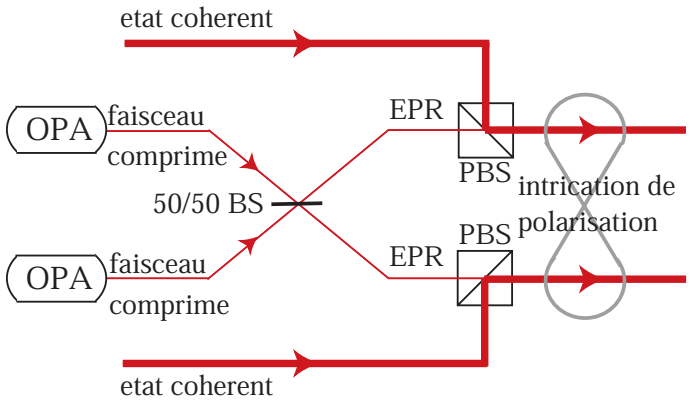

Article 9, reproduit en page 105

Experimental demonstration of continuous variable polarization entanglement

W.P. Bowen, N. Treps, R. Schnabel et P.K. Lam
Phys. Rev. Lett. 89, 253601 (2002)

Abstract : We report the experimental transformation of quadrature entanglement between two optical beams into continuous variable polarization entanglement.We extend the inseparability criterion proposed by Duan et al. [Phys. Rev. Lett. 84, 2722 (2000)] to polarization states and use it to quantify the entanglement.We propose an elaboration utilizing two quadrature entangled pairs for which all three Stokes operators between a pair of beams are entangled.

5.3. Le nano-positionnement

Originellement, ce sont les degrés de libertés transverses de la lumière ($\vec{\rho} = x\vec{i} + y\vec{j}$) qui nous ont conduit vers l'étude du multimode. Ces paramètres décrivent la distribution du champ électrique dans un plan transverse à sa propagation, ce que nous appelons ici une image. Les mesures et caractérisations des images se heurtent, ultimement, au bruit quantique de la lumière. La volonté d'aller au delà de cette limite suscita les études menées, qui mêlent à la fois des techniques d'imagerie, de théorie du signal et d'optique quantique. Plusieurs approches ont été utilisées, l'une consistant à considérer chaque position transverse $\vec{\rho}$ comme un degré de liberté -nous l'évoquerons dans le dernier chapitre de ce mémoire- et l'autre à décomposer la lumière en modes transverses -comme les modes gaussiens- et à en dégager ceux importants pour l'application considérée. Cette

dernière approche ne met en jeu simultanément que quelques modes, et c'est celle que nous allons évoquer ici.

5.3.1. Les détecteurs à quadrants

Les études expérimentales sont ici la conséquence directe de la théorie présentée en début de ce mémoire. Nous nous sommes penchés sur des appareils de mesure et avons tenté d'atteindre, puis de dépasser, la limite quantique standard associée. Premier appareil considéré, le détecteur à deux zones qui permet, en faisant la différence des photocourants délivrés par ces deux zones, de déterminer la position du faisceau relativement au détecteur. Ce détecteur de position, très sensible, est utilisé dans de nombreux appareils tel, par exemple, le microscope à force atomique.

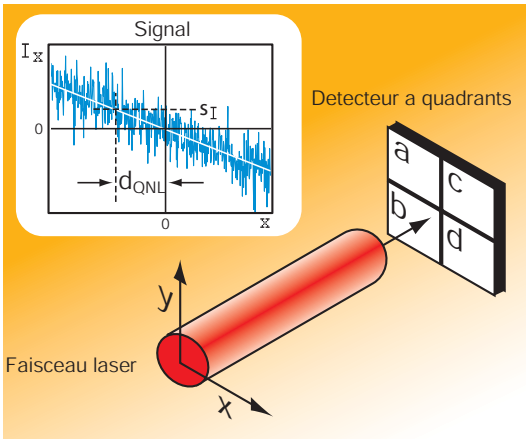

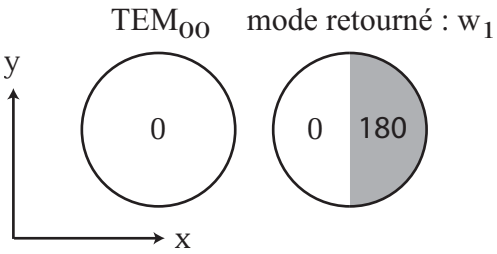

FIG. 5.1.: Figure de phase des deux modes intervenant dans une mesure de position : un champ gaussien et un champ gaussien retourné.

Nous nous plaçons donc dans le cadre d'une mesure d'intensité, comme définie par l'équation 4.1, où le gain est égal à -1 pour $x < 0$ et $+1$ pour $x > 0$. Le mode de détection w_1 associé -dont on rappelle qu'il est égal au mode de champ moyen pondéré par le gain du détecteur- est donc un mode identique à celui du champ moyen pour $x > 0$ et égal à moins celui du champ moyen pour $x < 0$, mode que l'on appelle mode retourné. Il se trouve de plus que, lorsque le faisceau est pratiquement centré -ce qui est le cas dans toutes les expériences- le mode retourné est orthogonal au mode de champ moyen, et ces deux modes forment donc le début d'une base. Cette précision est importante car elle signifie qu'il est possible d'adresser directement, au moins en théorie, le mode retourné sans perturber celui de champ moyen. Tous calculs faits, on trouve que le plus petit déplacement mesurable est donné dans cette expérience, avec un faisceau gaussien TEM_{00} de taille w_0, par :

$$d_{min}^{split} = \frac{w_0}{2\sqrt{N}}\sqrt{\frac{\pi}{2}} \cdot \sqrt{< \delta \hat{X}_{w_1}^{+2} >}. \tag{5.1}$$

On voit apparaître deux paramètres important : le nombre de photons détecté pendant le temps de mesure-plus il est grand, plus la mesure est précise- et le bruit du mode retourné -plus il est petit, plus la mesure est sensible-. Dans l'expérience suivante nous

avons réalisé un tel montage, et nous avons produit un mode retourné *vide* et comprimé en intensité en plaçant une lame de phase sur le faisceau comprimé dont nous disposions. Ce faisceau était mélangé sur une lame avec le champ moyen, puis déplacé -à une fréquence d'oscillation de quelques MHz- et enfin mesuré. Nous avons pu mesurer des déplacements de l'ordre de l'Angström et aller au delà de la limite quantique standard :

Article 10, reproduit en page 111

Surpassing the standard quantum limit for high sensitivity measurements in optical images using non classical light

N. Treps, U. Andersen, B. Buchler, P. K. Lam, A. Maître, H.-A. Bachor, C. Fabre

Phys. Rev. Lett. 88, 203601 (2002)

Abstract : Using continuous wave superposition of spatial modes, we demonstrate experimentally displacement measurement of a light beam below the standard quantum limit. Multimode squeezed light is obtained by mixing a vacuum squeezed beam and a coherent beam that are spatially orthogonal. Although the resultant beam is not squeezed, it is shown to have strong internal spatial correlations. We show that the position of such a light beam can be measured using a split detector with an increased precision compared to a classical beam. This method can be used to improve the sensitivity of small displacement measurements.

Le faisceau produit dans cette expérience est, d'après notre partie théorique, un faisceau multimode quantique à deux modes. Ce fut la première mise en évidence expérimentale d'un tel faisceau dans le domaine spatial.

L'étape suivante consista à étudier le détecteur à quadrants -4 cases de taille identique- qui permet de mesurer simultanément les positions verticale et horizontale du faisceau. Les modes de détections associés à ces mesures sont les versions horizontale et verticale du mode retourné décrit plus haut. Ces deux modes étant, de nouveau, orthogonaux entre eux et orthogonaux au mode de champ moyen, nous avons les trois premiers modes d'une base orthonormale. Les plus petits déplacements mesurables dans chaque direction sont identiques et donnés par l'équation 5.1. La difficulté de l'expérience réside dans le mélange sans perte des modes ; en effet, seul le mode de champ moyen pouvant subir des pertes sans voir son état modifié, il y a au moins un mélange sans pertes à effectuer. Nous avons donc développé des dispositifs permettant le mélange de modes transverses orthogonaux. Celui utilisé dans l'expérience suivante est une cavité en anneau, résonnante pour un des modes qu'elle transmet donc parfaitement, et non résonnante pour l'autre qu'elle peut donc réfléchir sur son miroir de sortie afin de le mélanger parfaitement au faisceau transmis[9]. L'efficacité d'un tel système nous a permis de réaliser un faisceau multimode quantique à trois modes et de l'utiliser pour faire des mesures au delà de la limite quantique standard dans les deux directions transverses simultanément :

[9]Les différentes méthodes développées pour mélanger des modes transverses, ainsi que nombre de techniques expérimentales, sont détaillées dans l'article N. Treps, N. Grosse, W. Bowen, M.T.L. Hsu, A. Maître, C. Fabre, H.-A. Bachor et P.K. Lam, *Nano-displacement measurements using spatially multimode squeezed light*, J. Opt. B : Quantum Semiclass. Opt **6** S664-S674 (2004), non reproduit ici par soucis de concision.

Article 11, reproduit en page 115

A Quantum Laser Pointer

N. Treps, N. Grosse, W. P. Bowen, C. Fabre, H.-A. Bachor, and P. K. Lam

Science Aug 15 2003 : 940-943

Abstract : The measurement sensitivity of the pointing direction of a laser beam is ultimately limited by the quantum nature of light. To reduce this limit, we have experimentally produced a quantum laser pointer, a beam of light whose direction is measured with a precision greater than that possible for a usual laser beam. The laser pointer is generated by combining three different beams in three orthogonal transverse modes, two of them in a squeezed-vacuum state and one in an intense coherent field. The result provides a demonstration of multichannel spatial squeezing, along with its application to the improvement of beam positioning sensitivity and, more generally, to imaging.

5.3.2. Mesure optimale de déplacement et d'inclinaison

D'après l'équation 4.8 le mode de détection associé à une mesure de déplacement est la dérivée par rapport à la dimension transverse -le déplacement- du mode de champ moyen, un TEM_{00} dans notre cas. Or, la dérivée du mode TEM_{00} n'est autre que le mode TEM_{01}. Il nous faut donc mesurer la composante TEM_{01} du faisceau pour en déduire sa position. Pour ce faire, reconsidérons le principe d'une détection homodyne : le champ à mesurer arrive sur une lame 50/50, où il interfère avec un champ intense incident sur l'autre entrée de la lame et que l'on appelle oscillateur local. Deux détecteurs mesurent les deux sorties de la lame et le signal de différence est enregistré. Il est bien connu que si l'oscillateur local est suffisamment intense ce signal est proportionnel aux fluctuations du champ à caractériser. Ceci est du aux interférences entre les deux champs sur la lame. En terme multimode, cela signifie que le mode du champ qui est effectivement mesuré est celui qui interfère parfaitement avec l'oscillateur local. Une détection homodyne dont l'oscillateur local est un TEM_{01} nous permettra donc de mesurer cette composante du champ incident. Le plus petit déplacement mesurable est dans ce cas, en calculant la constante de normalisation de l'équation 4.8 :

$$d_{min}^{homodyne} = \frac{w_0}{2\sqrt{N}} \sqrt{< \delta \hat{X}_{w_1}^{+2} >} \tag{5.2}$$

où w_1 est le mode de détection, donc la composante TEM_{01} du faisceau incident. On observe un facteur d'amélioration $\sqrt{\frac{\pi}{2}}$ par rapport à la détection avec un détecteur à quadrant, qui n'était donc pas optimale (alors qu'ici, comme nous l'avons montré, nous atteignons la limite de Cramer-Rao). On a de plus, du fait de la détection homodyne, accès à la quantité conjuguée mesurée en déphasant l'oscillateur local de $\pi/2$. On montre que cette nouvelle observable correspond, comme attendu, à l'inclinaison du faisceau, quantité conjuguée du déplacement, de manière analogue à la dualité entre position et impulsion d'une particule -en effet, l'inclinaison du faisceau est équivalente à une impulsion transverse-.

Nous avons réalisé cette expérience de mesure optimale en mettant en place une détection homodyne 'spatiale' dont l'oscillateur local est un mode TEM_{01} -produit en faisant

passer un faisceau gaussien légèrement désaligné dans une cavité vide asservie sur le mode à produire-. Le faisceau à mesurer, un mode TEM_{00} est mélangé avec un mode TEM_{01} comprimé pour réaliser le faisceau comprimé en position. Le mode comprimé est réalisé directement en asservissant la cavité de l'OPA sur ce mode et en adaptant température de cristal et forme de l'injection.

Il est mélangé avec le champ moyen grâce, cette fois-ci, à un interféromètre de Mach-Zehnder avec un miroir supplémentaire pour le rendre sensible à la parité du mode comme illustré dans la figure ci-contre.

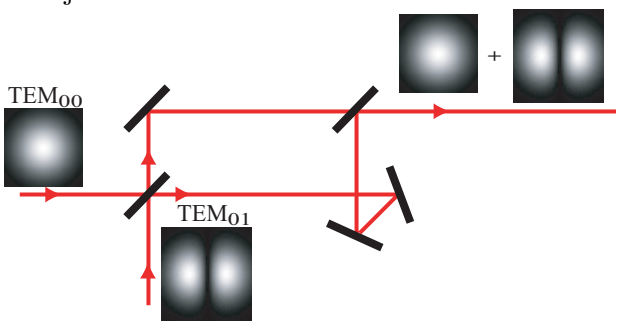

Nous avons pu mettre en évidence les mesures optimales de la position et de l'inclinaison d'un faisceau gaussien, et ensuite aller au delà de la limite quantique standard :

Article 12, reproduit en page 119

Quantum measurements of spatial conjugate variables : Displacement and tilt of a Gaussian beam

V. Delaubert, N. Treps, C.C. Harb, P.K. Lam and H.-A. Bachor
Optics Letters 31 1537-1539 (2006)

Abstract : We consider the problem of measurement of optical transverse profile parameters and their conjugate variable. Using multimode analysis, we introduce the concept of detection noise modes. For Gaussian beams, displacement and tilt are a pair of transverse-profile conjugate variables. We experimentally demonstrate the optimal encoding and detection of these variables with a spatial homodyning scheme. Using higher-order spatial mode squeezing, we show the sub-shot-noise measurements for the displacement and tilt of a Gaussian beam.

Ces mesures ayant montré la faisabilité expérimentale des détections homodyne multimode ainsi que l'accès aux quantités conjuguées, nous avons cherché à développer une *boîte à outils* permettant de faire de l'information quantique multimode spatiale. Nous avons montré comment produire, adresser individuellement, comprimer et mesurer différents modes transverses :

Article 13, reproduit en page 122

Tools for multi-mode quantum information : modulation, detection and squeezing of spatial laser modes

M.Lassen, V.Delaubert, C.C.Harb, P.K.Lam, N.Treps, P.Buchhave, C.Fabre, and H-A.Bachor
Soumis à Phys. Rev. Lett.

Abstract : We present here all the required tools for continuous variable parallel quantum information protocols based on multi-mode quantum correlations and entanglement. We describe our ability to encode and detect quantum information with high efficiency. We experimentally demonstrate the generation of spatial correlations or optical squeezing in higher order transverse Hermite-Gauss modes. The higher order mode squeezing is achieved by the mode selective tuning of the phase matching condition and the cavity resonance condition of the nonlinear $\chi^{(2)}$ optical parametric amplification.

5.3.3. Intrication spatiale

La possibilité de mesurer, à la limite quantique, deux observables conjuguées d'un même faisceau permet d'envisager la réalisation d'intrication. Il est remarquable, comme nous l'avons évoqué dans la section précédente, que les deux observables mises en jeu correspondent précisément à la position et l'impulsion du faisceau. On notera cependant que ceci n'est vrai que pour un faisceau TEM_{00}. En effet, autant il est toujours vrai que la transformée de Fourier du déplacement est l'impulsion (et ceci est réalisé couramment en faisant simplement une transformation champ proche - champ lointain avec une lentille), autant le produit des variances des observables correspondantes n'est minimum que lorsque que l'on part d'une forme gaussienne, comme c'est le cas pour la position et l'impulsion d'une particule. Néanmoins, partant de deux faisceaux gaussiens, il est donc possible de les intriquer en position et impulsion comme nous l'avons proposé.

La méthode proposée ici consiste à réaliser deux faisceaux individuellement comprimés en position, identiques à celui réalisé en section précédente. Ces deux faisceaux sont ensuite mélangés sur une lame 50/50 et les faisceaux de sortie sont, comme cela se passe pour les champs monomodes, intriqués en position et impulsion.

On remarquera l'analogie formelle avec l'intrication de polarisation puisque, ici aussi, on travaille avec une base à deux modes et on intrique les modes *vides* de chacun des faisceaux. La réalisation expérimentale de cette proposition est prévue très prochainement dans le cadre de notre collaboration avec l'Australie.

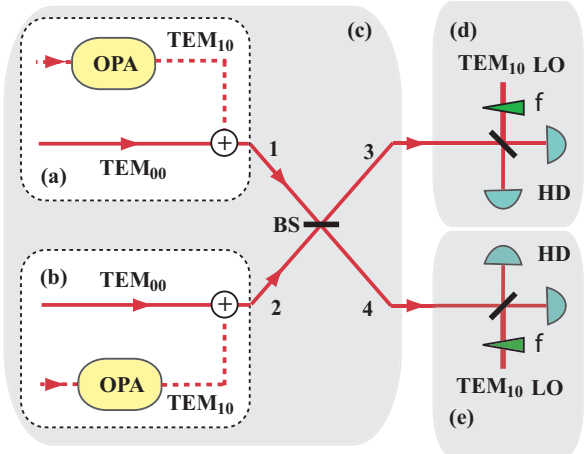

Article 14, reproduit en page 127

Continuous-Variable Spatial Entanglement for Bright Optical Beams

M.T.L. Hsu, W.P. Bowen, N. Treps and P.K. Lam

Phys. Rev. A 72, 013802 (2005)

Abstract : A light beam is said to be position squeezed if its position can be determined to an

accuracy beyond the standard quantum limit. We identify the position and momentum observables for bright optical beams and show that position and momentum entanglement can be generated by interfering two position, or momentum, squeezed beams on a beam splitter. The position and momentum measurements of these beams can be performed using a homodyne detector with local oscillator of an appropriate transverse beam profile. We compare this form of spatial entanglement with split detection-based spatial entanglement.

5.3.4. Lecture optique de l'information

La possibilité de caractériser et d'améliorer toute mesure effectuée avec un détecteur à pixels permet d'envisager des applications pour la lecture optique de l'information. Nous nous sommes penchés sur un système modèle, le disque optique (CD), et avons cherché à en augmenter la capacité en introduisant des méthodes de lecture permettant de dépasser la limite de diffraction.

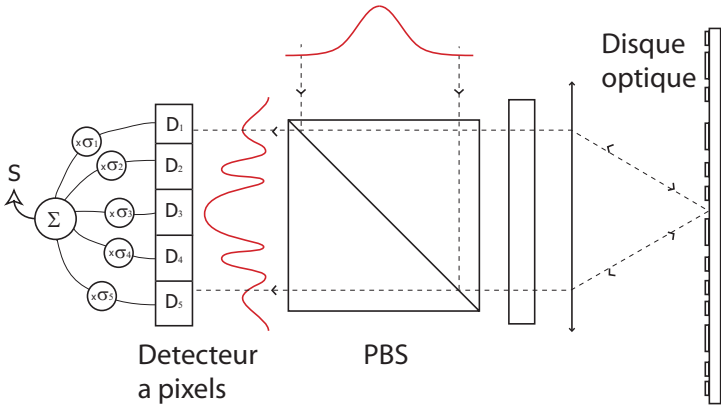

FIG. 5.2.: Principe général de la lecture optique de l'information à l'aide d'un détecteur à pixels.

La reconstruction du champ lu avec un détecteur à pixel n'est a priori pas limitée par la diffraction, puisque nous avons accès à la valeur de l'intensité et des techniques de superrésolution permettent de reconstruire l'image avec précision. Cependant, pour des images complexes, ces techniques se trouvent très vite limitées par le bruit (qu'il soit d'origine électronique ou quantique) et les améliorations obtenues par rapport à la limite de diffraction sont faible. La situation est toute autre quand on désire n'extraire que quelques paramètres -comme défini au premier chapitre de ce mémoire- car dans ce cas la grande quantité d'information a priori rend caduque la limite de diffraction. En effet, dans le cas de la mesure d'un paramètre où on connaît tout sauf la valeur de p elle-même, les limites de précision sont imposées par la mécanique quantique et non plus par la théorie de la diffraction. Ceci car l'information a priori permet d'adapter le détecteur à la quantité que nous voulons mesurer. Ainsi, si plusieurs informations sont disposées sur le support optique dans une tache de diffraction -une information consistant en un trou d'une profondeur un quart de longueur d'onde- la distribution d'intensité du faisceau réfléchi en champ lointain, lue par un détecteur à pixels, doit permettre de faire la différence entre les quelques combinaisons de bit possibles. C'est la proposition que nous avons faîte, où pour chaque combinaison de bit possible on adapte la configuration des gains du détecteur pour que le mode de détection soit le plus proche possible du mode portant l'information. Nous avons montré qu'il était ainsi possible de faire la différence

entre les 8 combinaisons possibles induites par 3 bits dans la tache de diffraction à l'aide d'un détecteur à 5 zones. De plus, en cas de faible flux de photons (pour un temps de lecture court par exemple) il est possible d'augmenter le rapport signal sur bruit en comprimant les mode de détections pertinents. De la lumière multimode quantique à quelques modes permet dans ce cas d'augmenter significativement la capacité de stockage des supports optiques.

L'article suivant reprend ce principe en détail, et revient sur un certain nombre de difficultés que nous n'avons pas abordées ici, comme le calcul de la propagation du champ avec de grandes ouvertures numériques et des détails sub longueur d'onde, l'interaction entre le champ et le support, la géométrie de l'ensemble, etc... :

Article 15, reproduit en page 134

Optical storage of high density information beyond the diffraction limit : a quantum study

V. Delaubert, N. Treps, G. Bo and C. Fabre
Phys. Rev. A 73, 013820 (2006)

Abstract : We propose an optical readout scheme allowing a proof of principle of information extraction below the diffraction limit. This technique, which could lead to improvement in data readout density onto optical disks, is independent from the wavelength and numerical aperture of the reading apparatus, and involves a multipixel array detector. Furthermore, we show how to use nonclassical light in order to perform a bit discrimination beyond the quantum noise limit.

5.4. Le tout multimode : les cavités dégénérées

Dans les sections précédentes nous avons étudié des exemples où les modes mis en jeu étaient bien identifiés, et les modes importants en nombre réduit. Cette approche de synthèse de mode est bien adaptée lorsque l'on dispose d'information a priori sur la quantité à mesurer, mais est limitée, du fait des techniques expérimentales, à un nombre de mode restreints et donc à des problèmes simples. Lorsque l'on désire de manière générale caractériser une image et en extraire le plus de détails possibles, sans savoir à l'avance où il se trouvent, on utilise un détecteur possédant un grand nombre de pixels et des techniques de superrésolution. Ces techniques se ramènent *in fine* à des combinaisons linéaires de pixel et sont sensibles, comme toutes mesures, au bruit de modes de détection. Cependant, l'absence d'information a priori ne permet pas de connaître à l'avance la forme de ces modes et donc d'en réduire le bruit préalablement à la mesure. Pour aller plus loin, il faut abandonner l'approche de la synthèse de mode et tenter de réduire simultanément le bruit de tous les modes, ce que l'on appelle la réduction de bruit locale. C'est le principe des configurations dégénérées où tous les modes sont équivalents[10]. Nous étudions ici ce cas pour les dimensions transverses, nous verrons en section suivante le même type d'approche pour les dimensions temporelles.

[10]Une étude précise du bruit quantique dans la supperésolution et des modes transverses à comprimer est faite dans V. Beskrovnyy and M. Kolobov, Phys. Rev. A **71**, 043802 (2005)

Notre outil de base est encore une fois la génération paramétrique. En effet, aux propriétés quantiques de photons jumeaux et d'intrication s'ajoutent, lors de ce processus, des propriétés spatiales remarquables car les champ émis sont également corrélés en impulsion du fait de l'accord de phase dans le cristal. De plus, en configuration d'amplification, si le cristal est suffisamment mince, chaque point transverse du cristal se comporte comme un amplificateur indépendant et une amplification point à point -donc multimode- d'un champ incident peut être réalisée.

5.4.1. Images et cavités

Dans le régime des variables continues il est nécessaire, lorsque les puissances disponibles ne sont pas élevées, de placer le cristal à l'intérieur d'une cavité. Or les cavités habituelles possèdent des modes propres détruisant le caractère multimode du processus paramétrique. Nous avons donc étudié les propriétés des cavités dégénérées transversallement : des cavités résonnantes, pour une longueur donnée, pour un grand nombre de modes transverses simultanément.

Un point de vue intéressant consiste à écrire la matrice ABCD correspondant à la propagation de la lumière sur un tour de cavité. Une condition nécessaire et suffisante pour que la cavité soit dégénérée est qu'il existe un entier N tel que cette matrice élevée à la puissance N soit égale à l'identité. Cela signifie simplement qu'au bout de N tours dans la cavité un rayon revient sur lui même. Cependant, cette matrice ne prend pas en compte la phase accumulée par ce rayon, et l'ordre de dégénérescence est défini de manière plus précise dans :

Article 16, reproduit en page 144

Image transmission through a stable paraxial cavity

S. Gigan, L. Lopez, N. Treps, A. Maître, and C. Fabre

Phys. Rev. A **72** 023804 (2005)

Abstract : We study the transmission of a monochromatic "image" through a paraxial cavity. Using the formalism of self-transform functions, we show that a transverse degenerate cavity transmits the self-transform part of the image, with respect to the field transformation over one round-trip of the cavity. This formalism gives insight into the understanding of the behavior of a transverse degenerate cavity, complementary to the transverse mode picture. An experiment of image transmission through a hemiconfocal cavity shows the interest of this approach.

Il existe plusieurs types de cavités dégénérées. Les cavités parfaitement dégénérées, pour lesquelles la matrice $ABCD$ est l'identité, sont aussi appelées auto-imageantes, elles reproduisent le champ à l'identique en un tour de cavité et cela signifie que toute image incidente sur la cavité est transmise sans déformation. Nous avons étudié une telle cavité et montré qu'elle permettait de transférer une image du champ fondamental au champ second harmonique en configuration de doublage de fréquence.

Cependant, cette cavité est complexe à manipuler et nous avons donc étudié des cavités partiellement dégénérées, pour lesquelles $N \neq 1$. Dans ce cas, le champ transmis par la cavité est la somme du champ incident, plus le champ ayant subi un tour de cavité,

jusqu'à celui ayant subi $N-1$ tours de cavité. Les images transmises sans déformation par la cavité sont donc celles invariantes par une telle transformation. Ce sont des fonctions *auto-transformes* comme défini dans l'article précédant. Notons simplement que, en revenant dans la base des modes gaussiens, cela signifie que seul 1 mode sur N est résonnant dans la cavité.

5.4.2. Propriétés quantiques d'un OPO confocal

La cavité confocale est une cavité composée de deux miroirs sphériques, de même rayon de courbure R et espacés d'une distance R. La matrice $ABCD$ d'une telle cavité est égale à moins l'identité, un rayon se reboucle sur lui-même en deux tours de cavité. Ainsi, suivant le réglage fin de sa longueur, cette cavité transmet soit tous les modes pairs, soit tous les modes impairs ; c'est la configuration modes pairs que nous avons utilisée exclusivement.

Avec un cristal non-linéaire d'ordre deux placé à l'intérieur, cela forme un OPO confocal. Nous considérons ici le cas d'un cristal de type II, du KTP, tel que les faisceaux signal et complémentaire sont polarisés orthogonalement, il est donc possible de les séparer pour mesurer des propriétés de photons jumeaux. La cavité n'étant résonnante que pour les modes pairs, elle mélange les photons d'impulsion transverse (i.e. la composante du vecteur d'onde orthogonale à l'axe de la cavité) $\vec{k}_T$ avec ceux d'impulsion $-\vec{k}_T$, une géométrie intéressante pour regarder les effets quantiques consiste donc à considérer les cônes d'émission d'angle d'ouverture l'angle du vecteur $\vec{k}$ avec l'axe de la cavité. Nous avons réglé à dégénérescence une telle cavité et regardé les corrélations d'intensité entre les champs signal et complémentaire (photons jumeaux). Puis, pour observer des effets multimodes, nous avons placé un diaphragme pour couper le faisceau émis en fonction de l'angle d'émission. Nous avons pu montrer que les propriétés quantiques des faisceaux ainsi coupés spatiallement n'étaient pas linéaires avec la puissance transmise, ce qui serait le cas pour un champ monomode. Nous avons donc montré le comportement multimode quantique de l'OPO confocal :

Article 17, reproduit en page 154

Experimental study of the spatial distribution of quantum correlations in a confocal optical parametric oscillator

M. Martinelli, N.Treps, S. Ducci, S. Gigan, A. Maître et C. Fabre
Phys. Rev. A 67, 023808 (2003)

Abstract : We study experimentally the spatial distribution of quantum noise in the twin beams produced by a type-II optical parametric oscillator operating in a confocal cavity above threshold. The measured intensity correlations are at the same time below the standard quantum limit and not uniformly distributed inside the beams. We show that this feature is an unambiguous evidence for the multimode and nonclassical character of the quantum state generated by the device.

L'étude théorique précise, au delà des considérations de symétries simples utilisés dans l'expérience précédente, d'une telle cavité nécessite la prise en compte des propriétés transverses de la cavité en même temps que la propagation du champ dans le cristal où,

quand on parle d'image, les effets de diffraction sont essentiels. Nous avons donc écrit les relations d'entrée-sortie complètes de la cavité en utilisant des opérateurs locaux, et nous avons résolu numériquement ces équations. Ces études ont confirmé en grande partie les prédictions précédentes, moyennant la prise en compte d'une longueur de cohérence

$$l_{coh} = \sqrt{\frac{\lambda l_c}{\pi n_s}} \tag{5.3}$$

où l_c est la longueur du cristal et n_s l'indice optique. Si on s'intéresse aux effets quantiques en champ proche (i.e. dans le plan du cristal), pour des détecteurs de taille caractéristique supérieure à l_c on retrouve les prédictions de photons jumeaux intuitives, alors que pour des détecteurs de taille inférieure ces effets disparaissent. En d'autres termes, l'aire de cohérence, induite par la diffraction dans le cristal, correspond à la taille caractéristique des modes pouvant osciller indépendamment, et donc en divisant l'aire du faisceau par l'aire de cohérence on peut obtenir une estimation du nombre de modes mis en jeu dans l'expérience :

Article 18, reproduit en page 163

Multimode squeezing properties of a confocal optical parametric oscillator : Beyond the thin-crystal approximation

L. Lopez, S. Gigan, N. Treps, A. Maître, C. Fabre, and A. Gatti
Phys. Rev. A 72, 013806 (2005)

Abstract : Up to now, transverse quantum effects usually labeled as "quantum imaging" effects which are generated by nonlinear devices inserted in resonant optical cavities have been calculated using the "thin-crystal approximation," i.e., taking into account the effect of diffraction only inside the empty part of the cavity, and neglecting its effect in the nonlinear propagation inside the nonlinear crystal. We introduce in the present paper a theoretical method which is not restricted by this approximation. It allows us in particular to treat configurations closer to the actual experimental ones, where the crystal length is comparable to the Rayleigh length of the cavity mode. We use this method in the case of the confocal optical parametric oscillator, where the thin-crystal approximation predicts perfect squeezing on any area of the transverse plane, whatever its size and shape. We find that there exists in this case a "coherence length" which gives the minimum size of a detector on which perfect squeezing can be observed, and which gives therefore a limit to the improvement of optical resolution that can be obtained using such devices.

5.4.3. Amplification d'image

La dernière étape de ces expériences en cavité partiellement dégénérée consiste en l'amplification sans bruit d'images. Comme nous l'avons vu au début de ce mémoire, ce processus permet de régénérer des images et également de s'affranchir de la mauvaise efficacité quantique de détecteur. De plus, naturellement, l'amplification via un milieu paramétrique crée des états non-classiques très intéressants.

Pour réaliser de l'amplification multimode, nous avons choisi, pour des raisons pratiques, comme cavité dégénérée une cavité semi-confocale, composée d'un miroir plan et d'un miroir sphérique de rayon de courbure R distants de $R/2$. Il faut élever la matrice $ABCD$ de ce dispositif à la puissance 4 pour obtenir l'identité, un seul mode transverse sur 4 y est donc résonnant. On se reportera à l'article **16** pour les propriétés de cette cavité.

L'oscillateur paramétrique optique, sous le seuil et injecté par un signal, réalise exactement le processus d'amplification que nous avons évoqué au début de ce mémoire. En type II, où signal et complémentaire sont polarisés orthogonalement, l'injection selon une des polarisations réalise un amplificateur insensible à la phase alors que l'injection à 45^o des polarisations propres réalise un amplificateur sensible à la phase. Nous n'avons pu, du fait du mélange -même faible- des polarisations induit par notre cavité, ne réaliser que le deuxième, qui est celui le plus pertinent car sans bruit.

La cavité elle même est en configuration de double cavité, comme expliqué dans :

Article 19, reproduit en page 173

Noiseless Optical Amplification of Images using transverse degenerate OPOs

L. Lopez, N. Treps, C. Fabre and A. Maître

En préparation

Abstract :

Nous avons pu mettre en évidence de l'amplification d'image en type II, puis montrer que cette amplification rajoutait moins de bruit qu'une amplification classique et était donc dans le régime sans bruit. Ces résultats remarquables ont été pris à chaque fois en mesurant une modulation d'intensité sur l'ensemble de l'image, et nous avons montré que le facteur de bruit de notre amplificateur ne dépend pas de l'image injectée, démontrant ainsi son caractère multimode quantique. De plus, nous avons pu passer d'une configuration d'amplification à une configuration de de-amplification, et dans ce cas observer de la réduction du bruit d'intensité quelle que soit l'image transmise. La prochaine étape de cette expérience est de remplacer la cavité semi-confocale par la cavité auto-imageante pour ne plus déformer les images. De plus, dans cette configuration, sous le seuil, nos calculs théoriques ont montré que les propriétés locales des champs sont quantiquement remarquables, et nous pourront alors faire des mesures locales pour mettre en évidence le caractère multimode, plutôt que des mesures globales en changeant le mode injecté comme nous l'avons fait jusqu'à présent.

5.5. Multimode en temps et fréquence : futures directions

5.5.1. L'OPO en mode synchrone

Les degrés de liberté non encore explorés des faisceaux continus sont ceux de temps et fréquence, ce qui paraît naturel car, traditionnellement, un faisceau continu est monochromatique et stationnaire. Cependant, la description théorique donnée en premier chapitre autorise ce degré de liberté, d'ailleurs mis en œvre sous des formes diverses par

plusieurs groupes à travers le monde. Ici, et afin de garder l'aspect cohérent inhérent à notre approche, nous avons choisi de considérer les peignes de fréquence, qui sont une superposition cohérente de différentes fréquences optiques. Ces peignes sont émis en général par les lasers à impulsions à verrouillage de modes et se traduisent, dans le domaine temporel, par un train d'impulsions cohérentes entre elles. Vu sous l'angle des fréquences, l'analogie est parfaite avec notre approche de l'imagerie, où une image est une superposition cohérente de différents modes transverses. Ce domaine est l'objet de notre nouveau projet de recherche et l'expérience correspondante est en cours d'installation. Nous ne présentons ici que les études théoriques que nous avons menées jusqu'à présent.

Le système modèle que nous avons considéré est celui d'un oscillateur paramétrique optique pompé en mode synchrone. Cet OPO est tel que le temps que met la lumière à faire un tour de cavité est égal au temps entre deux impulsions successives de la pompe, ainsi les différentes impulsions pompe se superposent dans la cavité et les champs émis par l'OPO sont de nouveaux des peignes de fréquences. Le bilan de puissance dans ce dispositif est alors très intéressant, car du fait de sa cohérence ce système se comporte comme un OPO continu, mais sa puissance crête, de l'ordre de 5 ordres de grandeurs supérieure, augmente de manière considérable les non-linéarités et réduit les seuils. De plus, cette cavité est dégénérée puisque toutes les fréquences du peigne de fréquence y sont résonnantes simultanément. Ainsi, dans ce dispositif, et ce contrairement au cas spatial, la dégénérescence est assurée dès que l'on obtient l'oscillation.

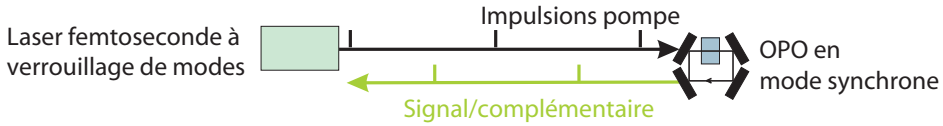

Nous avons étudié théoriquement les propriétés quantiques d'un tel système, dans le cas où signal et complémentaire sont dégénérés. Comme la cavité ne sélectionne pas naturellement de modes, cette sélection est effectuée à la fois par la forme de la pompe et par les propriétés d'accord de phase du cristal. On voit ainsi apparaître naturellement une nouvelle base de modes, que l'on appelle super-modes, où chaque mode est une combinaison linéaire de modes monochromomatiques, ce sont donc des peignes de fréquence. La forme, dans le domaine des fréquences, de ces modes est similaire, sous certaines hypothèses, à celle des modes de Hermite-Gauss. On trouve alors que lorsque l'on s'approche du seuil d'oscillation, le super-mode le plus proche du seuil devient comprimé. Mais ce qui est remarquable est qu'il existe des domaines de valeur des paramètres où un grand nombre de super-modes ont des seuils comparables, et dans ce cas tous ces modes ont des propriétés quantiques comparables mais indépendantes, on atteint un régime multimode :

Article 20, reproduit en page 178

Squeezing frequency combs

G.J. de Valcarcel, G. Patera, N. Treps and C. Fabre

Soumis à Phys. Rev. A

Abstract : We have developed the full multimode theory of a synchronously pumped type I

optical parametric oscillator (SPOPO). We derive expressions for the oscillation threshold and the characteristics of the generated mode-locked signal beam. We calculate the output quantum fluctuations of the device, and find that, in the degenerate case (coincident signal and idler set of frequencies), significant squeezing is obtained when one approaches threshold from below for a set of well defined "super-modes", or frequency combs, consisting of a coherent linear superposition of signal modes of different frequencies which are resonant in the cavity.

Ces études ont plusieurs objectifs. Tout d'abord, du fait des non-linéarités disponibles nous espérons non-seulement améliorer les expériences existantes mais de plus explorer de nouveaux états quantiques. D'un autre côté, la dimension multimode en temps/fréquence permet d'envisager des applications par exemple en métrologie des fréquences -qui utilise maintenant des peignes de fréquences- et en transfert de temps. C'est cette dernière configuration que nous avons commencé à étudier.

5.5.2. Le transfert de temps

Le transfert de temps consiste en le partage, entre deux opérateurs distants, de la variable u définie au début de ce mémoire, variable qui est invariante lors de la propagation de la lumière dans le vide. Une petite variation du temps de trajet de la lumière entre les deux opérateurs induit donc une variation de u à l'arrivée. Une mesure de haute sensibilité de cette variable permet une optimisation du transfert de temps, nous sommes donc exactement dans le cadre de notre théorie de la mesure multimode. En effet, ce que nous cherchons à mesurer est une petite variation du u sous l'action d'un paramètre qui agit directement sur u lui-même, de manière analogue aux mesures de position où l'on mesure la position du faisceau sous l'action d'un déplacement. Le mode de détection associé à la mesure est donc la dérivée du champ par rapport à u.

Ainsi, considérons que le faisceau lumineux partagé est une impulsion gaussienne, que nous supposerons simplement de durée grande devant le cycle de la lumière (soit la femtoseconde pour une impulsion dans le proche infrarouge), ce qui permet de la supposer quasi-monochromatique et d'utiliser la décomposition 3.5. En omettant les variables autres que u, le mode de champ moyen est de la forme $u_0(u) = \frac{1}{\pi^{1/4}\tau^{1/2}} e^{-\frac{u^2}{2t^2}} e^{-i\omega_0 u}$. Il vient, pour une petite variation ϵ de u :

$$\begin{aligned} u_0(u-\epsilon) &\approx u_0(u) + \frac{\epsilon}{a} u_1(u) \\ &= u_0(u) + \epsilon \left[i\omega_0 u_0(u) + \frac{1}{\tau\sqrt{2}} v_1(u) \right] \end{aligned} \tag{5.4}$$

où u_1 est la dérivée normalisée de u_0, v_1 est un mode TEM_{01} dans l'espace temporel, équivalent au mode de signal des petits déplacements, qui s'écrit $v_1(u) = \frac{\sqrt{2}}{\pi^{1/4}\tau^{3/2}} u e^{-\frac{u^2}{2t^2}} e^{-i\omega_0 u}$, et $\omega_0\tau$ est égal au nombre d'oscillations du champ à l'intérieur d'une impulsion. Nous avons ici explicité les modes afin de souligner les analogies, mais surtout les différences, avec les mesures de déplacement. Contrairement à ce dernier cas, où le mode de signal est simplement le TEM_{01}, il apparaît ici un terme nouveau proportionnel, mais en quadrature, à u_0. Ce terme apparaît car la variable mesurée est également la variable de la propagation. Le mode de signal, qui est l'ensemble de l'expression entre crochets, est donc plus subtil que dans le cas spatial et nous avons choisi de le séparer en ses composantes u_0 et v_1 car elles recouvrent deux approches différentes.

Le terme proportionnel à u_0 est un terme de déphasage, qui exprime simplement que si le temps de trajet d'un faisceau augmente légèrement, il s'en trouvera déphasé à l'arrivée. Mesurer ce déphasage correspond donc à faire du suivi de phase du faisceau, et peut se faire avec un champ partagé continu (qui rentre dans le cadre de notre approche en faisant tendre τ vers l'infini). Le terme en u_1 est celui auquel nous sommes maintenant habitué et est induit par un décalage global de l'enveloppe du champ. En définissant la mesure de temps comme le temps de trajet du maximum de l'enveloppe, c'est ce terme qui lui correspond. Ces deux termes, liés dans le vide, peuvent différer dans un milieu dispersif où la vitesse de phase est différente de la vitesse de groupe.

Une mesure de temps effectuée en mesurant le temps de trajet de l'enveloppe d'impulsions lumineuses pourra donc être réalisée de manière optimale via une détection homodyne dont l'oscillateur local est dans le mode u_1. De plus, en utilisant par exemple un OPO en mode synchrone, il est possible de réduire le bruit de ce mode et donc d'améliorer la mesure de temps. L'article correspondant, réalisé en collaboration avec B. Lamine, S. Reynaud et C. Fabre et que nous avons intitulé "Quantum enhancement of time transfer", est en préparation.

6. Conclusion et perspectives

L'effort à la fois théorique et expérimental présenté dans ce mémoire n'est pas isolé et suit une tendance internationale vers l'exploration de la complexité, en particulier en optique quantique. L'imagerie quantique est par exemple le fruit du réseau européen QUANTIM, qui découle lui-même de travaux pionniers effectués en Europe et en Russie. Depuis, le département de la défense américain a financé un projet "Quantum Imaging, New Methods and Applications" pour lequel nous sommes collaborateurs. Nous sommes de plus engagés, avec un nouveau groupe de laboratoires européens issus en partie du réseau QUANTIM, dans la rédaction d'un nouveau projet visant spécifiquement à explorer la complexité de l'intrication en optique quantique.

En parallèle, sous l'impulsion en particulier de l'information quantique, la nécessité de générer des états plus complexes et permettant des protocoles plus riches et plus efficaces a mené la communauté au mélange de techniques de variables continues et de photons uniques. On citera en particulier la génération d'états à fonction de Wigner négative, à la fois dans le domaine impulsionnel[1] et dans le domaine continu[2], qui reposent dans les deux cas sur la soustraction d'un seul photon au champ -à l'aide d'une lame faiblement réfléchissante et d'un détecteur de photons uniques- à laquelle on conditionne la caractérisation du champ restant. De la même façon, des idées permettant de caractériser le champ via les corrélations entre ce photon soustrait et les fluctuations du champ transmis ont été proposées et commencé à être mises en œuvre[3].

Finalement, les travaux en optique quantique à petit nombre de modes trouvent un écho dans la recherche d'application de la lumière comprimée à la mesure optique. Nos partenaires australiens ont également un protocole pour améliorer les performances du CD[4], projet aussi à l'étude, via des techniques dites classiques, par des laboratoires en Hollande, au Royaume-Uni et en Allemagne. Avec ces différents groupes nous sommes en train de monter un consortium européen pour fédérer les approches classiques et quantiques à l'amélioration de la densité d'information accessible par des moyens optiques. Il est intéressant de rapprocher ces études des efforts faits par la communauté pour réaliser de la réduction de bruit quantique à basse fréquence[5]. Motivées par l'amélioration de la

[1] *Generating Optical Schrödinger Kittens for Quantum Information Processing* A. Ourjoumtsev, R. Tualle-Brouri, J. Laurat et P. Grangier, Science **312**, 83-86 (2006).

[2] *Generation of a Superposition of Odd Photon Number States for Quantum Information Networks* J. S. Neergaard-Nielsen, B. Melholt Nielsen, C. Hettich, K. Mølmer, and E. S. Polzik, Phys. Rev. Lett. **97**, 083604 (2006)

[3] *Giant Violations of Classical Inequalities through Conditional Homodyne Detection of the Quadrature Amplitudes of Light* H. J. Carmichael, H. M. Castro-Beltran, G. T. Foster, and L. A. Orozco, Phys. Rev. Lett. **85**, 1855-1858 (2000)

[4] *A quantum study of multi-bit phase coding for optical storage*, Magnus T.L. Hsu, Vincent Delaubert, Warwick P. Bowen, Claude Fabre, Hans-A. Bachor, Ping Koy Lam, quant-ph/0602132

[5] *Coherent Control of Vacuum Squeezing in the Gravitational-Wave Detection Band* Henning Vahlbruch, Simon Chelkowski, Boris Hage, Alexander Franzen, Karsten Danzmann, and Roman Schnabel Phys. Rev. Lett. **97**, 011101 (2006). *Squeezing in the Audio Gravitational-Wave Detection Band* Kirk

sensibilité des détecteurs à ondes gravitationelles, ces études trouvent un écho dans la recherche d'application à la lecture optique où de la réduction de bruit large bande est nécessaire.

On le voit, les différents thèmes de recherche présenté dans ce mémoire sont poursuivis de manière active au niveau international et, en particulier, européen. La suite de ces recherches s'inscrit dans ces différents cadres en s'appuyant en particulier sur l'expérience d'optique quantique avec des peignes de fréquences que nous sommes en train d'installer, mais également en poursuivant l'expérience d'imagerie et celle de génération d'intrication. Le nouveau réseau IRCOQ, financé par l'ANR et dont je suis coordinateur, dont l'acronyme signifie "Intrication et Réseau de Communication Quantique" fédère ces différentes approches sous l'angle de l'information quantique en regroupant les acteurs principaux de l'optique quantique en variables continues en France.

Tout d'abord, à court terme, l'étude quantique de l'oscillateur paramétrique optique en cavité auto-imageante s'impose. Le but en est non-seulement de réaliser de l'amplification d'image parfaitement multimode mais également, en configuration sous le seuil et sans injection, de générer pour la première fois du vide comprimé localement. Les calculs que nous avons fait prédisent ces compressions, et prédisent de plus que l'analyse en champ lointain des fluctuations quantiques émises par ce dispositif permet d'observer des corrélations EPR locales. La mise en évidence de telles corrélations serait une étape majeure dans l'étude de la complexité en optique quantique mais également dans la perspective d'applications en imagerie. Ainsi, suivant les résultats obtenus dans cette expérience nous pourrons envisager de mettre en œuvre des applications à la mesure optique où à l'information quantique multimode. Le réseau IRCOQ se prête parfaitement à ces études où nous pourrons évaluer la possibilité d'un réseau de communications quantiques multimode.

Du côté de la génération d'états intriqués, nous voulons poursuivre l'étude théorique et expérimentale de la caractérisation de l'intrication et des critères associés. En particulier, la qualité des faisceaux EPR produits par l'expérience permet d'envisager l'étude de corrélations dites "photons-champ" entre la statistique de photon et celle des fluctuations de quadrature. Au delà des avantages en terme de sensibilité vis-à-vis des pertes et de caractérisation nouvelle de la réduction de bruit, ces études nous permettront de mettre en œuvre, à la fois théoriquement et expérimentalement, des critères d'intrication d'un type nouveau. Nous en attendons une meilleure compréhension des propriétés des états quantiques à plusieurs modes mais également d'étudier la possibilité de générer des états à fonction de Wigner négative en configuration multimode. Enfin, ces études permettent bien évidemment d'étudier quelles sont les meilleures configurations pour générer des états non-classiques pour les communications quantiques.

L'essentiel de nos efforts va néanmoins se porter sur l'études des nouvelles variables que sont le temps et la fréquence, et les applications envisagées grâce à l'utilisation de peignes de fréquences. Nous sommes en train d'installer une expérience consistant en un oscillateur paramétrique optique pompé en mode synchrone, comme décrit dans le dernier chapitre de ce manuscrit. Ce système à très bas seuil -du fait de l'intensité crête très importante- et à très grande longueur de cohérence permet dans un premier temps de revisiter un certain nombre d'expériences d'optique quantique en variables continues

McKenzie, Nicolai Grosse, Warwick P. Bowen, Stanley E. Whitcomb, Malcolm B. Gray, David E. McClelland, and Ping Koy Lam Phys. Rev. Lett. **93**, 161105 (2004)

avec des non-linéarités supérieures de plusieurs ordres de grandeurs à celle utilisées habituellement. Dans un second temps, nous prévoyons de mettre en œuvre la théorie présentée au chapitre précédent visant à générer des "super-modes" au propriétés quantiques remarquables. Nous étudierons alors les domaines de comportement monomode et multimode de notre oscillateur et envisagerons de réaliser une expérience de mesure de temps par détection homodyne.

À plus long terme, cette expérience doit nous permettre d'étudier l'intrication à un grand nombre de modes, quelle que soit leur origine : fréquence - en intriquant les différentes dents des peignes produits- temps -en intriquant les super-modes- et bien sur spatiales. Ces études seront portées par un effort théorique visant à étudier quelles sont les meilleures configurations pour les réseaux de communications quantiques mais également quelles sont les applications en terme de métrologie du temps et des fréquences. Ce système est intrinsèquement très riche et ses possibles applications sont multiples, ces recherches ont donc un caractère exploratoire très important. Nous pourrons étudier, par exemple, l'application de la lumière produite par notre cavité aux protocoles mêlant photons uniques et détection homodyne. En effet, les très fortes non-linéarités, qui induisent une non-linéarité par photon très importante, permettent de se diriger vers des états à nombre de photons mésoscopique, intermédiaires entre les photons uniques et les variables continues.

Troisième partie .

Sélection d'articles

Sont reproduits ici les articles cités dans la partie précédente et sélectionnés pour recouvrir l'ensemble des travaux de recherche. La structure générale du corps du texte est reprise, et chaque partie est précédée des abstracts des articles sélectionnés.

La mesure optique

Article 1, reproduit en page 54

Quantum noise in multipixel image processing

N. Treps, V. Delaubert, A. Maître, J.M. Courty and C. Fabre

Phys. Rev. A **71**, 013820 (2005)

Abstract : We consider the general problem of the quantum noise in a multipixel measurement of an optical image. We first give a precise criterium in order to characterize intrinsic single mode and multimode light. Then, using a transverse mode decomposition, for each type of possible linear combination of the pixels' outputs we give the exact expression of the detection mode, i.e. the mode carrying the noise. We give also the only way to reduce the noise in one or several simultaneous measurements.

Article 2, reproduit en page 62

Quantum limits in image processing

V. Delaubert, N. Treps, C. Fabre, H.A. Bachor and P. Refrégier

Soumis à Phys. Rev. Lett.

Abstract : We determine the bound to the maximum achievable sensitivity in the estimation of a scalar parameter from the information contained in an optical image in the presence of quantum noise. This limit, based on the Cramer-Rao bound, is valid for any image processing protocol. It is calculated both in the case of a shot noise limited image and of a non-classical illumination. We also give practical experimental implementations allowing us to reach this absolute limit.

PHYSICAL REVIEW A **71**, 013820 (2005)

Quantum noise in multipixel image processing

N. Treps, V. Delaubert, A. Maître, J. M. Courty, and C. Fabre
Laboratoire Kastler Brossel, UPMC, Case 74, 4 Place Jussieu, 75252 Paris cedex 05, France
(Received 29 July 2004; published 31 January 2005)

We consider the general problem of the quantum noise in a multipixel measurement of an optical image. We first give a precise criterion in order to characterize intrinsic single-mode and multimode light. Then, using a transverse mode decomposition, for each type of possible linear combination of the pixels' outputs we give the exact expression of the detection mode, i.e., the mode carrying the noise. We give also the only way to reduce the noise in one or several simultaneous measurements.

DOI: 10.1103/PhysRevA.71.013820 PACS number(s): 42.50.Dv, 42.30.−d, 42.50.Lc

INTRODUCTION

Multipixel photodetectors such as diode arrays or charge-coupled device (CCD) sensors are now frequently used to record images. These sensors provide signals in which the useful information is mixed with random noise. A contribution to this noise originates from the quantum nature of light: the arrival of individual photons is a random process. Contrarily to technical noise, due to imperfections in the source, the optical system, or the detector, this quantum noise cannot be reduced by eliminating the defects in the measurement process. The purpose of this paper is to determine the precise origin of this noise and to analyze whether and how it can be reduced. With the analysis of the spatial distribution of this noise, we will single out the precise transverse modes whose fluctuations are at the origin of this quantum noise, and determine the parameters that have to be changed in order to reduce this noise.

As images are complex objects which carry a great deal of information, there are actually many ways to extract information from them, depending on the image user needs [1–3]. We will focus our attention on the extraction from the image of one or several continuous parameters, the variation of which modifies the light distribution in the image plane and not its total intensity. In such a case, the quantity of *a priori* information on the image is very important, as one assumes that the variation of the image under observation is due only to the variation of a searched parameter M. A second use to which our calculations can apply is the determination of predefined patterns in the image, such as given shapes, surfaces, borders, textures, and so on. It is a very difficult problem *per se*, and the incidence of quantum noise on it, to the best of our knowledge, has not been precisely studied so far. In contrast, we do not consider the search for the smallest possible details, where resolution is at stake. In this problem, there is very little to none *a priori* information and the problem of quantum limits to resolution has been already considered in other publications [4,5].

In most cases, the light used to carry the image comes from "classical sources," such as lamps or the usual lasers, in which the photons are randomly distributed in the image plane. This gives rise to a spatial shot noise which will yield a "standard quantum limit" in the measurement of a very small variation of M. It is now well known that "nonclassical light," such as squeezed light or sub-Poissonian light, is likely to reduce quantum fluctuations on a given measurement [6]. The aim of the last part of the present paper is to identify the best nonclassical light enabling us to reduce the quantum noise in the measurement of the quantity M performed in the image. It has been already shown [7] that nonclassical light in a single transverse mode, though very effective in reducing the noise for a measurement performed on the total beam, is of little use for a measurement performed on an image. One therefore needs multi-transverse-mode nonclassical light for our purpose. This is the reason why we devote the first section of this paper to a precise analysis of such a concept, before considering in the second section the problem of information extraction: we identify the exact noise source in the measurement of M, and show how to choose the best configuration which allows us to measure a variation of M with a sensitivity beyond the standard quantum limit.

I. "INTRINSIC" MULTIMODE LIGHT

We consider the propagation of light in the vacuum along the z direction, and call the transverse coordinate $\vec{r}$. We assume that the light frequency is ω_0 with a linewidth $\delta\omega$ much smaller than ω_0, and that it has a well defined polarization. One knows that it is possible to find several bases of transverse modes $\{u_i(\vec{r},z)\}$, such that each mode verifies the propagation equation of the field in vacuum projected onto the polarization axis,

$$\Delta(u_i e^{ikz}) + \frac{\omega_0^2}{c^2} u_i = 0; \tag{1}$$

it is an orthonormal basis,

$$\int u_i^*(z,\vec{r}) u_j(z,\vec{r}) d^2r = \delta_{ij}; \tag{2}$$

and it satisfies a completeness relation,

$$\sum_i u_i^*(z,\vec{r}) u_i(z,\vec{r}') = \delta(\vec{r}-\vec{r}'). \tag{3}$$

For instance, the usual Laguerre-Gauss TEM_{pq} basis satisfies these conditions. Considering a light beam, the electric field is written as the sum of the positive and negative frequencies components:

$$E(\vec{r},z,t) = E^{(+)}(\vec{r},z)e^{-i(\omega_0 t - kz)} + \text{c.c.} \tag{4}$$

It is possible to expand the electric field positive frequency envelope in the transverse modes basis as

$$E^{(+)}(\vec{r},z) = \sum_i \mathcal{E}_i u_i(\vec{r},z). \tag{5}$$

A. Single-mode or multimode light: Classical approach

For a TEM_{pq} basis field expansion, when more than one $\mathcal{E}_i$ is nonzero, it seems at first sight natural to say that this field is multimode. However, if the $\mathcal{E}_i$ coefficients are fixed (i.e., we consider a *coherent superposition of modes* and not a statistical one), one can always define a new transverse mode

$$v_0 = \frac{1}{\sqrt{\sum_i |\mathcal{E}_i|^2}} \sum_i \mathcal{E}_i u_i \tag{6}$$

and construct a basis $\{v_i\}$ in which v_0 is the first element. In this basis, the field is proportional to v_0 which means it is single mode. We can conclude that for a coherent superposition of modes, there is no intrinsic definition of a multimode beam (i.e., a definition independent of the choice of the basis). We will restrict our analysis to spatial variables, but it can be applied to any physical dimension. For instance, in the time domain, a mode locked laser is single mode, as it is a coherent superposition of many temporal modes. If the temporal modes are incoherent with each other then the system is unambiguously multimode. More precisely, if the field is a stochastic superposition of modes, the v_0 mode cannot be defined and the multimode character has a clear meaning. We will exclude this case in the following.

B. Single-mode light: Quantum approach

In order to give the quantum description of the transverse plane of a light beam, it is very common to quantize the field starting from a transverse mode basis such as the one we just defined in the previous section. In order to obtain standard formulas, we consider that all measurements are performed in an exposure time T and associate to each vector of the mode basis a set of creation and annihilation operators $\hat{a}_i^\dagger$ and $\hat{a}_i$ such that the field $\mathcal{E}_i$ of the previous section is replaced by the operator $i\sqrt{\hbar\omega_0/2\epsilon_0 cT}\hat{a}_i$. With these notations we obtain the standard commutation relations $[\hat{a}_i,\hat{a}_j^\dagger]=\delta_{ij}$, and the positive field envelope operator can be written as [8]

$$\hat{E}^+(\vec{r},z) = \sqrt{\frac{\hbar\omega_0}{2\epsilon_0 cT}}\hat{A}^+(\vec{r},z) \tag{7}$$

with

$$\hat{A}^{(+)}(\vec{r},z) = \sum_i \hat{a}_i(z)u_i(\vec{r},z), \tag{8}$$

so that $\hat{A}^{(+)\dagger}\hat{A}^{(+)}$ is a photon number per unit surface.

In order to give a proper definition of the single-mode case, let us write the most general state of the field in the Fock state basis $|n_1,\ldots,n_i,\ldots\rangle$, where n_i stands for the number of photons in the mode i:

$$|\psi\rangle = \sum_{n_1,\ldots,n_i,\ldots} C_{n_1,\ldots,n_i,\ldots}|n_1,\ldots,n_i,\ldots\rangle \tag{9}$$

and the mean value of the electric field is given by

$$\langle\psi|\hat{A}|\psi\rangle = \sum_i \left(\sum_{n_1,\ldots,n_i>1,\ldots} C^*_{n_1,\ldots,n_i-1,\ldots}C_{n_1,\ldots,n_i,\ldots}\right)\sqrt{n_i}u_i(\vec{r}). \tag{10}$$

Following the definition for the classical beams, we can give a definition of a single-mode beam.

Definition 1. A state is single mode if a mode basis $\{v_0,v_1,\ldots\}$ exists in which it can be written

$$|\psi\rangle = |\phi\rangle \otimes |0,\ldots,0,\ldots\rangle$$

where $|\phi\rangle$ is the state of the field in the first transverse mode.

The question is now whether, in contrast with the classical states, quantum states exist that cannot be written as (1). To answer this question, we will demonstrate the following proposition.

Proposition 1. A quantum state of the field is single mode if and only if the actions on it of all the annihilation operators of a given basis give collinear vectors.

One can note that if this property stands for a given basis, it then stands for the action of any annihilation operator.

Let us assume first that our field $|\psi\rangle$ is single mode with respect to the basis $\{u_i,\hat{a}_i\}$; then

$$\hat{a}_0|\psi\rangle = |\psi_0\rangle \quad \text{and} \quad \hat{a}_i|\psi\rangle = 0 \quad \forall\ i\neq 0. \tag{11}$$

Consider now any linear combination of the operators

$$\hat{b} = \sum_i c_i\hat{a}_i \tag{12}$$

where $\Sigma_i|c_i|^2=1$ which ensures that $[\hat{b},\hat{b}^\dagger]=1$. The action of this operator on the field is given by

$$\hat{b}|\psi\rangle = \sum_i c_i\hat{a}_i|\psi\rangle = c_0|\psi_0\rangle. \tag{13}$$

This demonstrates the first implication of our proposition: all the actions of annihilation operators on the field are proportional.

To prove the other implication, consider now a field $|\psi\rangle$ on which the action of any annihilation operator $\hat{a}_i$ is proportional to $|\psi_0\rangle$. This is in particular true for the basis $\{u_i,\hat{a}_i\}$:

$$\hat{a}_i|\psi\rangle = \alpha_i|\psi_0\rangle. \tag{14}$$

If we assume that $\Sigma_i|\alpha_i|^2=1$ (which is always possible by changing the normalization of $|\psi_0\rangle$), we can define a new basis $\{v_i(\vec{r},z),\hat{b}_i\}$ such that

$$\hat{b}_0 = \sum_i \alpha_i^*\hat{a}_i, \quad v_0 = \sum_i \alpha_i^* u_i, \tag{15}$$

and complete the basis by defining a unitary matrix $[c_{ij}]$ such that

$$\hat{b}_i = \sum_j c_{ij}\hat{a}_j \quad \text{with } c_{0j} = \alpha_j^* \quad \text{and} \quad \sum_j c_{ij}c_{kj}^* = \delta_{ik}. \tag{16}$$

It is then straightforward to show that

$$\hat{b}_i|\psi\rangle = \delta_{0i}|\psi_0\rangle, \tag{17}$$

which concludes the demonstration.

In addition to the proposition, Eq. (15) gives the expression of the mode in which "lies" the mean field, knowing the action of a particular basis. We can also note that to show that a field is single mode, it is sufficient to show that all its projections on the annihilation operators of one particular basis are proportional.

To illustrate the proposition, if one considers the superposition of coherent states

$$|\psi\rangle = |\alpha_1\rangle \otimes \cdots \otimes |\alpha_i\rangle \otimes \cdots \tag{18}$$

it is straightforward to show that the actions of all the annihilation operators on this state are proportional to the state itself; we have a single-mode beam. The basis in which it is single mode is the same as the one for the classical case, setting v_0 as in Eq. (6).

Using this proposition, we can also look for the different states that satisfy our definition of a single-mode quantum beam. As a state that cannot be written as follows in any mode basis:

$$|\psi\rangle = |\phi_1\rangle \otimes \cdots \otimes |\phi_i\rangle \otimes \cdots \tag{19}$$

is obviously not a single-mode beam, we will consider now such a factorized state of the field, on which the action of the annihilation operators gives

$$\hat{a}_i|\psi\rangle = |\phi_1\rangle \otimes \cdots \otimes (\hat{a}_i|\phi_i\rangle) \otimes \cdots. \tag{20}$$

Consequently, there are only two possibilities to have all these states proportional: either only one of the actions is different from zero, which means we are already in the basis in which the state is single mode; or all the states are coherent states.

We have described here all the possible single-mode states, and they agree with the intuitive description one might have. For instance, if one considers the superposition of several transverse modes, if at least one of them is a noncoherent state, one gets a quantum multimode state.

C. Multimode light: Quantum approach

A beam of light is said to be multimode, from a quantum point of view, when it is not single mode according to Definition 1. We can characterize such a beam by its degree n (this degree equals 1 for a single-mode beam).

Definition 2. For a beam $|\psi\rangle$, the minimum number of modes necessary to describe it (or the minimum number of nonvacuum modes in its modal decomposition), reached by choosing the appropriate basis, is called the degree n of a multimode beam. Any corresponding basis is called a minimum basis for the field $|\psi\rangle$.

The degree of a multimode beam can also be related to the generalization of Proposition 1 to an n-mode beam. Using the same technique, one can show that a quantum field is an n-mode beam if and only if the action on it of all the annihilation operators belongs to the same n-dimensioned subspace.

Whereas the previous paragraph gives a good definition of the degree of a multimode beam, it is not very convenient as one has no information on the basis in which the beam is exactly described by n modes. We can, however, define a particular basis, useful for calculations.

Proposition 2. For a beam $|\psi\rangle$ of degree n, it is always possible to find a basis $\{u_i,\hat{a}_i\}$ such that the mean value of the electric field is nonzero only in the first mode; and, it is a minimum basis for the field $|\psi\rangle$. We will call that basis an eigenbasis.

In order to demonstrate this proposition, let us consider a minimum basis $\{u_i,\hat{a}_i\}$ for the field $|\psi\rangle$. This basis is supposed to be ordered such that the n first modes are the relevant ones. We can then define a new basis $\{v_i,\hat{b}_i\}$ such that

$$v_0 = \frac{1}{\sqrt{\sum_{i=0}^{n-1}\langle\hat{a}_i\rangle^2}}\sum_{i=0}^{n-1}\langle\hat{a}_i\rangle u_i,$$

$$v_{i,0<i<n} = \sum_{j=0}^{n-1} c_{ij}u_j,$$

$$v_{i,i\geqslant n} = u_i, \tag{21}$$

where the coefficients $\{c_{ij}\}$ are chosen in order to get an orthonormal basis. Definitions similar to the one of Eq. (21) apply for the annihilation operators. The first vector of this basis is the same as the one defined for a classical beam in Eq. (6). In that basis, the mean field is single mode in a classical sense. However, the energy lying in all the other modes is not necessarily zero; only the electric field mean value is zero for these modes, and as the modes for $i\geqslant n$ were not changed, this new basis is still a minimum one for the field $|\psi\rangle$. This demonstrates the proposition. The demonstration illustrates the construction of a basis as defined in Proposition 2 from a minimum basis, even though thanks to the $\{c_{ij}\}$ coefficients an infinite number of bases are possible.

The existence of this basis is also a confirmation of the intuitive idea of the difference between single-mode and multimode quantum light. Indeed, for a single-mode beam, the spatial variation of the noise is the same as the one of the mean field. For a multimode beam, the previous description shows that some of the modes orthogonal to the mean field are sources of noise but do not contribute to the mean field. This implies that the variation of the noise is independent of the one of the mean field. This property can be used to experimentally characterize the multimode character of light. For instance, one can show the quantum multimode character of the light using a variable spatial filter. This idea has been implemented to study the semiconductor lasers output by cutting the field with a razor blade [9], and, more recently, we have shown that spatial quantum behavior of a spatially

multimode optical parametric oscillator can be demonstrated using an iris whose aperture size is continuously varied [10].

We have defined the theoretical basis required to develop a study on optical image measurements. The following section on information extraction will indeed strongly rely on the propositions and definitions of the first part.

II. DIFFERENCE MEASUREMENTS

A. Description

A widely used technique in optics, and more generally in physics, to improve the signal to noise ratio in a measurement is to perform a *difference measurement*. It consists in producing two identical signals from the light source used in the experiment. When one monitors the difference between these two signals, one gets of course a zero mean signal, but one also cancels all the common mode noises, for example, the one arising from the classical intensity fluctuations of the source. The remaining noise arises from the noise sources affecting the two channels differently.

One simple way to produce two identical beams is to use a 50% beam splitter. In this case, the vacuum noise coming from the unused side of the splitter is such a not-common-mode noise and remains in the difference measurement: whatever the actual excess noise of the beam impinging on the beam splitter, the remaining noise corresponds to the shot noise of this beam.

This simple technique of noise cancellation is used, for example, to measure very small absorptions [11] by inserting the absorbing medium in one of the arms of the difference setup, or very small frequency shifts, by inserting a Fabry-Pérot cavity in one of the arms. It is also extensively used in multipixel measurements, with either split detectors or quadrant detectors, to measure submicrometer displacements, for example of nanoscale fluorophores in biological samples [12] and in atomic force microscopy [13], and ultrasmall absorptions by the mirage effect [14].

The problem of the determination of the origin of quantum noise on a split detector and of its reduction has been already investigated theoretically [7] and experimentally [15–17]. We will here extend these considerations to more general configurations.

More formally, we consider the measurement by a detector consisting of a set of pixels, each one occupying a transverse area D_i. The pixels cover the whole transverse plane, with no overlap between them. Each photodetector delivers a power given by

$$\hat{I}(D_i) = \int_{D_i} 2\epsilon_0 c \hat{E}^\dagger(\vec{r})\hat{E}(\vec{r})d^2r. \tag{22}$$

This can also be written as the photon number measured during the exposure time T of the detector:

$$\hat{N}(D_i) = \int_{D_i} \hat{A}^\dagger(\vec{r})\hat{A}(\vec{r})d^2r. \tag{23}$$

In this section, the measurement M is defined by

$$\hat{M}(\{\sigma_i\}) = \sum_i \sigma_i \hat{I}(D_i) \quad \text{such that } \sigma_i = \pm 1 \tag{24}$$

or again in terms of number of photons per second:

$$\hat{N}(\{\sigma_i\}) = \sum_i \sigma_i \hat{N}(D_i), \tag{25}$$

where $\sigma_i = \pm 1$ corresponds to the electronic gain of detector i.

Considering a light beam in state $|\psi\rangle$, the measurement is a difference measurement for that beam if its mean value is zero, i.e., if

$$\langle \hat{N}(\{\sigma_i\})\rangle = 0. \tag{26}$$

B. One difference measurement

If one considers one difference measurement performed with a coherent state, which has spatially uncorrelated quantum fluctuations, the noise arising from the measurement will not depend on the choice of $\{\sigma_i\}$ if $\sigma_i = \pm 1$, and will be equal to the square root of the total number of photons. This is what is called the standard quantum noise. In the general case, in order to compute the noise, an analysis equivalent to the one performed in the case of a small displacement measurement, as done in Ref. [7], is necessary. We recall it here and extend it to the general case of transverse modes of any shape, in order to show the following proposition.

Proposition 3. The noise on a difference measurement performed on a beam $|\psi\rangle$ originates from a single mode, orthogonal to the mean field: the "flipped mode." In order to reduce the noise in that measurement, it is necessary and sufficient to inject a squeezed state in this flipped mode.

In order to perform the general noise calculation, let us define the two "detectors":

$$D_+ = \bigcup_{i,\sigma_i=+1} D_i,$$

$$D_- = \bigcup_{i,\sigma_i=-1} D_i, \tag{27}$$

which gives

$$\hat{N}_- = \hat{N}(D_+) - \hat{N}(D_-) = \sum_{i,j} \hat{a}_i^\dagger \hat{a}_j \left[\int_{D_+} u_i^*(\vec{r})u_j(\vec{r})d^2r - \int_{D_-} u_i^*(\vec{r})u_j(\vec{r})d^2r \right]. \tag{28}$$

Considering small quantum fluctuations for which $\delta\hat{a}_i = \hat{a}_i - \langle \hat{a}_i \rangle$, the fluctuations of $\hat{N}_-$ are

$$\delta\hat{N}_- = \hat{N}_- - \langle \hat{N}_- \rangle = \sum_i [\delta\hat{a}_i^\dagger C_-^i + \delta\hat{a}_i C_-^{i*}], \tag{29}$$

with C_-^i defined as

$$C_-^i = \sum_j \langle \hat{a}_j \rangle \left[\int_{D_+} u_i^*(\vec{r}) u_j(\vec{r}) d^2r - \int_{D_-} u_i^*(\vec{r}) u_j(\vec{r}) d^2r \right]$$
$$= \int_{D_+} u_i^*(\vec{r}) A_\psi(\vec{r}) d^2r - \int_{D_-} u_i^*(\vec{r}) A_\psi(\vec{r}) d^2r$$

and where $A_\psi(\vec{r})$ is the mean value of the electric field $\langle \psi | \hat{A}(\vec{r}) | \psi \rangle$. The C_-^i coefficients are the partial overlap integrals between the modes u_i and the mean field.

We can now compute the noise related to this measurement:

$$\langle \delta \hat{N}_-^2 \rangle = \sum_i |C_-^i|^2 + \left[\sum_{i,j} \langle \delta \hat{a}_i^\dagger \delta \hat{a}_j^\dagger \rangle C_-^i C_-^j + \langle \delta \hat{a}_i^\dagger \delta \hat{a}_j \rangle C_-^i C_-^{j*} + \text{c.c.} \right]. \quad (30)$$

Using the completeness relation, the first term of the last equation can be shown to be equal to the total number of incident photons per second, N_0. This shows that the noise related to this measurement arises *a priori* from all the modes.

We will now demonstrate that the noise comes in fact from a single mode when we write $\langle \delta \hat{N}_-^2 \rangle$ in the appropriate basis. We indicate by v_0 the mode of the mean field as defined in the previous part:

$$v_0(\vec{r}) = \frac{1}{\sqrt{N_0}} A_\psi(\vec{r}). \quad (31)$$

If v_0 is the first mode of a basis, the mean value of the electric field in all the other modes will be zero, as shown in the previous section. We define now the mode v_1, which we will refer to as the flipped mode of v_0, such that

$$v_1(\vec{r}) = \begin{cases} v_0(\vec{r}) & \text{if } r \in D_+, \\ -v_0(\vec{r}) & \text{if } r \in D_-. \end{cases} \quad (32)$$

As we have assumed that the mean value of the measurement is zero, v_1 is orthogonal to v_0, which means that we can find a basis $\{v_i, \hat{b}_i\}$ where v_0 and v_1 are the two first modes. In that basis, the overlap integrals become

$$C_-^i = \sqrt{N_0} \left[\int_{D_+} v_i^*(\vec{r}) v_0(\vec{r}) d^2r - \int_{D_-} v_i^*(\vec{r}) v_0(\vec{r}) d^2r \right]$$
$$= \sqrt{N_0} \int_D v_i^*(\vec{r}) v_1(\vec{r}) d^2r = \sqrt{N_0} \delta_{i,1}. \quad (33)$$

These integrals are different from zero only for the flipped mode. The noise of Eq. (30) becomes

$$\langle \delta \hat{N}_-^2 \rangle = N_0 \langle (\delta \hat{b}_1^\dagger + \delta \hat{b}_1)^2 \rangle, \quad (34)$$

which shows that the noise arises only from the quadrature of the flipped mode of v_0 in phase with the mean field mode. For this reason, we call this mode the eigenmode of the measurement. Another standard notation is

$$\langle \delta \hat{N}_-^2 \rangle = N_0 \langle \delta X_1^{+2} \rangle, \quad (35)$$

where $X_1^+ = \hat{b}_1 + \hat{b}_1^\dagger$ is the quadrature of the flipped mode, and N_0 represents the shot noise. Consequently, having a squeezed state in that mode is necessary and sufficient to reduce the noise related to the measurement.

This calculation shows that, for a difference measurement, the noise in the measurement is exactly the one of the flipped mode. Changing the noise properties of the flipped mode is then the only way to change the noise in the measurement. We have a necessary and sufficient condition to improve the measurement compared to the standard quantum limit.

This demonstration imposes the noise properties of only one quadrature of the flipped mode, but there is no condition on the other quadrature, and all the other modes can be in any state. Then, there is not only one practical solution.

C. Multiple difference measurement

We have demonstrated which mode one needs to squeeze in order to perform one difference measurement on a beam. We can now expand this analysis in the case of several difference measurements. Let us consider n difference measurements of the type of Eq. (26). We will assume that these measurements are independent, which means that none of them is a linear combination of the others. One can show that the corresponding flipped modes are then also linearly independent. We have shown that in order to improve simultaneously the sensitivity of all these measurements it is necessary, and sufficient, to squeeze all these flipped modes. Practically these modes are in general not orthogonal, but one can find an orthogonal basis of the subspace generated by these modes. Injecting squeezed vacuum states in each of these modes will result in squeezed states in each of the flipped modes.

Regarding the degree of the beam necessary to improve simultaneously all the measurements, it is clear that in order to perfectly squeeze all the flipped modes, a beam of degree $n+1$ is necessary (and sufficient). We can summarize all the considerations of Sec. II into a proposition.

Proposition 4. In order to reduce the noise simultaneously in n independent difference measurements it is necessary and sufficient to use a beam of degree at least $n+1$ that can be described in a transverse mode basis $\{\hat{a}_i, u_i\}$ such that u_0 is proportional to the electric field profile of the beam; $\{u_i\}_{0<i\leqslant n}$ is the basis of the space vector generated by the flipped modes of the measurements; and all these modes are perfectly squeezed.

III. LINEAR MEASUREMENT

Difference measurements are obviously not the only ones performed in image processing [1–3]. The extraction of the pertinent information arises generally from the numerical computation of a function $F(I(D_1), I(D_2), \ldots, I(D_n))$ from the intensities $I(D_i)$ $(i=1, \ldots, n)$ measured on each pixel. To simplify the following discussion, we will restrict ourselves to the case when this function is *linear* with respect to the intensities $I(D_i)$, as is a case often encountered in real situa-

tions, for example, when one wants to determine the spatial Fourier components of the image, or when the variations of the parameter to measure are small enough so that the function F can be linearized.

In the formalism of Eqs. (24) and (25), using a linear function corresponds to letting the gain σ_i of the detectors take any real value and not only ± 1:

$$\hat{M}(\{\sigma_j\}) = \sum_j \sigma_j \hat{I}(D_j),$$

$$\hat{N}_\sigma = \sum_j \sigma_j \hat{N}(D_j). \tag{36}$$

We emphasize that, contrary to the previous section, the mean value of the measurement is not necessarily zero. In that case, we will show the following proposition.

Proposition 5. Consider a field state $|\psi\rangle$ described in an eigenbasis $\{\hat{b}_i, v_i\}$, and consider a linear measurement performed with an array of detectors D_i, each detector having a gain σ_i. The noise on the measurement, $\hat{N}_\sigma = \Sigma_j \sigma_j \hat{N}(D_j)$, arises only from the generalized flipped mode w defined by

$$\forall\ \vec{r},\vec{r} \in D_i \Rightarrow w_1(\vec{r}) = \frac{1}{f}\sigma_i v_0(\vec{r}) \tag{37}$$

where f is a normalization factor.

Here, there is not much sense in defining the positive and negative gain domains. We can anyway extend the notion of overlap integral between a basis vector and the mean field:

$$C_\sigma^i = \sum_j \sigma_j \int_{D_j} u_i^*(\vec{r}) A_\psi(\vec{r}) d^2r, \tag{38}$$

which leads to a formula equivalent to Eq. (30)

$$\langle \delta\hat{N}_\sigma^2 \rangle = \sum_i |C_\sigma^i|^2 + \left[\sum_{i,j} \langle \delta\hat{a}_i^\dagger \delta\hat{a}_j^\dagger \rangle C_\sigma^i C_\sigma^j + \langle \delta\hat{a}_i^\dagger \delta\hat{a}_j \rangle C_\sigma^i C_\sigma^{j*} + \text{c.c.} \right]. \tag{39}$$

Recalling that $A_\psi(\vec{r}) = \sqrt{N_0} v_0(\vec{r})$, we can also extend the notion of the flipped mode, and define a *detection mode* by

$$\forall\ \vec{r},\vec{r} \in D_i \Rightarrow w_1(\vec{r}) = \frac{1}{f}\sigma_i v_0(\vec{r}), \tag{40}$$

where f ensures the normalization of w_1:

$$f^2 = \sum_j \sigma_j^2 \int_{D_j} v_0^*(\vec{r}) v_0(\vec{r}) d^2r. \tag{41}$$

However, as the mean value of the measurement can be different from zero, the detection mode w_1 is not in general orthogonal to the mean field mode v_0. In order to calculate the noise in the measurement, it is necessary to construct a basis that contains the detection mode w_1. As the mean value of the electric field in this mode is different from zero, it is not possible to obtain an eigenbasis with w_1, but we can still choose w_0 such that the mean field mode v_0 is a linear combination of w_0 and w_1. Choosing all the other modes w_i (with $i \geqslant 2$) in order to obtain an orthonormal basis, we obtain a basis such that the mean field is distributed in the two first modes, the detection mode is w_1, and the mean value of the electric field in all the other modes is zero. We can then perform a calculation similar to the one of the previous section, which gives

$$C_\sigma^i = \sqrt{N_0} f \int_D w_i(\vec{r}) * w_1(\vec{r}) d^2r = \sqrt{N_0} f \delta_{i,1}. \tag{42}$$

Once again the detection mode is the only one that is relevant for the calculation of the noise related to the measurement. Taking into account that the normalization giving rise to the shot noise has changed,

$$\sum_i |C_\sigma^i|^2 = |C_\sigma^1|^2 = N_0 f^2, \tag{43}$$

the noise formula becomes

$$\langle \delta\hat{N}_\sigma^2 \rangle = f^2 N_0 \langle (\delta\hat{c}_1^\dagger + \delta\hat{c}_1)^2 \rangle, \tag{44}$$

where the $\{\hat{c}_i\}$ are the annihilation operators associated with the transverse mode basis $\{w_i\}$.

The f^2 factor is a global effect of the gain, and modifies both the measured signal and shot noise level. In any case, if the flipped mode is perfectly squeezed, we can still perform a perfect measurement. However, the experimental configuration is much more complicated as, in general, the mean value of the electric field in mode w_1 is different from 0, which means that, as is shown in the Appendix, generating the good mode is difficult. An appropriate approach would be to describe the field back into an eigenbasis, and check how to set the noise of the different modes in that basis. We will see in the Appendix how this can be done in a simple case. The important result of this part is that whatever the measurement we perform the noise arises only from one mode. Changing the noise of this mode allows us to improve the sensitivity of the measurement. As in the previous section, it is also possible in that general case to perform several simultaneous measurements, and to identify the subspace of modes responsible for the noise.

It is interesting to note that, in the particular case of a measurement where the gains are adapted to have $\langle \hat{M}(\{\sigma_j\}) \rangle = 0$, the mode v_0 coincides with w_0. Indeed, v_0 is here orthogonal to w_1:

$$\int_D w_1^*(\vec{r}) v_0(\vec{r}) d^2r = \sum_j \frac{\sigma_j}{f} \int_{D_j} v_0^*(\vec{r}) v_0(\vec{r}) d^2r \propto \left\langle \sum_j \sigma_j \hat{N}(D_j) \right\rangle = 0; \tag{45}$$

hence the basis is an eigenbasis of the field. Again, that case is relevant experimentally as it means that one can act on the noise without perturbing the mean field mode.

CONCLUSION

We have shown in this article how to properly define the degree of multimode character of a light beam. We have used the basis decomposition associated with that definition in

order to single out, in a linear transverse measurement, the transverse mode carrying the noise. We have shown that it is possible to go beyond the standard quantum noise limit by injecting in that mode squeezed light, and that this can be done simultaneously for several independent measurements.

It order to implement the theory developed here to complex experimental configurations we have shown that it was preferable that the various detection modes be orthogonal to the mean field (i.e., they do not contribute to the mean electric field), and it is necessary to mix them without introducing losses. For instance, one can use the proposal we have detailed in [17] and used to mix two nonclassical beams in orthogonal transverse modes, and a mean coherent field, in order to improve the sensitivity of the transverse position measurement of a laser beam.

In this paper, we have analyzed in great detail the origin of quantum noise in a multipixel measurement. What remains to be considered now is the signal, and not only the noise in the measurement. This will be the natural continuation of our work, and we will describe in a future publication what is the influence of the gain configuration on the signal to noise ratio and how to optimize a given measurement in an optical image.

ACKNOWLEDGMENTS

Laboratoire Kastler Brossel, of the Ecole Normale Supérieure and University Pierre et Marie Curie, is associated with the CNRS. This work has been supported by the European Union within the framework of the QUANTIM network (Contract No. IST 2000-26019).

APPENDIX: TWO-ZONE MEASUREMENT

In this article, we have exhibited the mode structure of the light in a multipixel measurement, using a basis that contains the detection mode. However, when the mean value of the measurement is different from zero, we have shown that this detection mode has a mean electric field value different from zero. In that configuration, it is very difficult experimentally to address the detection mode without modifying the mean field distribution. We have shown that the only basis pertinent for such a task is an eigenmode basis. We will show here what is the structure of that basis for a two-zone measurement of nonzero mean value.

Using the notations of the previous sections, we consider two detectors D_+ and D_- whose gains are, respectively, +1 and −1. We recall here the mode structure defined in the main text of this article. v_0 is the transverse mode carrying the mean field of the beam and w_1 is the detection mode as defined in Eq. (40) [which, in this case, is equivalent to the flipped mode of Eq. (32)]. w_0 is the mode orthogonal to w_1 in the subspace generated by v_0 and w_1. Let us call the partial integrals of v_0 on each zone i_+ and i_-,

$$i_+ = \int_{D_+} v_0^*(\vec{r}) v_0(\vec{r}) d^2r \quad \text{and} \quad i_- = \int_{D_-} v_0^*(\vec{r}) v_0(\vec{r}) d^2r.$$

A simple calculation gives

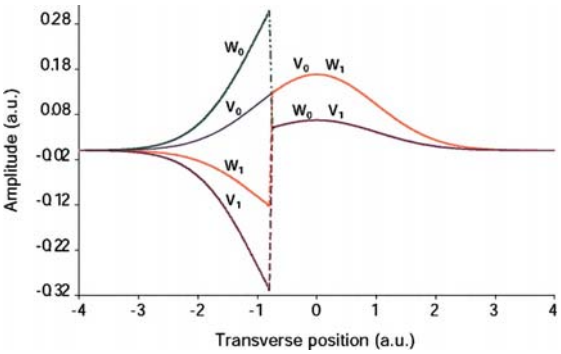

FIG. 1. Electric field profile of the constituent modes used to form the nonclassical multimode beam.

$$w_0(\vec{r}) = \begin{cases} \sqrt{\dfrac{i_-}{i_+}} v_0(\vec{r}) & \text{if } r \in D_+, \\ \sqrt{\dfrac{i_+}{i_-}} v_0(\vec{r}) & \text{if } r \in D_-. \end{cases} \tag{A1}$$

The first mode of an eigenbasis for the field is v_0. The second one, v_1, is defined as the mode orthogonal to v_0 in the subspace generated by w_0 and w_1. Its expression is found to be v_1 such that

$$v_1(\vec{r}) = \begin{cases} w_0(\vec{r}) & \text{if } r \in D_+, \\ -w_0(\vec{r}) & \text{if } r \in D_-. \end{cases} \tag{A2}$$

As w_0 is orthogonal to w_1, which is the flipped mode of v_0, one can show that v_0 is orthogonal to v_1, which is the flipped mode of w_0 (see Fig. 1). In order to calculate the noise in the measurement using that basis, the flipped mode is expressed as a linear combination of the two first modes of the eigenbasis:

$$w_1 = \alpha v_0 + \beta v_1, \tag{A3}$$

where $\alpha = i_+ - i_-$ and $\beta = 2\sqrt{i_+ i_-}$, which leads to

$$\langle (\delta\hat{c}_1^\dagger + \delta\hat{c}_1)^2 \rangle = \alpha^2 \langle (\delta\hat{b}_0^\dagger + \delta\hat{b}_0)^2 \rangle + \beta^2 \langle (\delta\hat{b}_1^\dagger + \delta\hat{b}_1)^2 \rangle + 2\alpha\beta \langle (\delta\hat{b}_0^\dagger + \delta\hat{b}_0)(\delta\hat{b}_1^\dagger + \delta\hat{b}_1) \rangle. \tag{A4}$$

Expressed in an eigenbasis that does not contain the detection mode, we see that the noise arises from the individual noise of the two first modes and from their correlation function. In that basis, in order to reduce the noise we have several solutions: either the two first modes are perfectly squeezed, or they are perfectly correlated, or any solution in between. Anyway, we can assume that if we want to make a lot of different measurements, it is very difficult to produce correlation between the mean field and the different vacuum modes; hence the easiest solution is to have the mean field squeezed, and the corresponding vacuum squeezed. The same argument as before applies, and we show that we still need an extra mode for each piece of extra information.

[1] M. Bertero and P. Boccacci, *Introduction to Inverse Problems in Imaging* (IOP Publishing, Bristol, 1998).
[2] A. K. Jain, *Fundamentals of Digital Image Processing*, Information and System Sciences Series (Prentice-Hall, Englewood Cliffs, NJ, 1989).
[3] A. K. Katsaggelos, *Digital Image Restoration*, Springer Series in Information Sciences Vol. 23 (Springer-Verlag, Berlin, 1991).
[4] M. Bertero and E. R. Pike, Opt. Acta **29**, 727 (1982).
[5] M. I. Kolobov and C. Fabre, Phys. Rev. Lett. **85**, 3789 (2000).
[6] H-A. Bachor, *A Guide to Experiments in Quantum Optics* (Wiley-VCH, Weinheim, 1998).
[7] C. Fabre, J. B. Fouet, and A. Maître, Opt. Lett. **25**, 76 (1999).
[8] C. Fabre, in *Quantum Fluctuations*, edited by S. Reynaud, E. Giacobino, and J. Zinn-Justin, 1995 Proceedings of the Les Houches Summer School of Theorectical Physics, LXIII (Elsevier Science, Amsterdam, 1997).
[9] J. P. Poizat, T. Chang, O. Ripoll, and P. Grangier, J. Opt. Soc. Am. B **15**, 1757 (1998); J.-P. Hermier, A. Bramati, A. Z. Khoury, E. Giacobino, J.-Ph. Poizat, T. J. Chang, and Ph. Grangier, *ibid.* **16**, 2140 (1999).
[10] M. Martinelli, N. Treps, S. Ducci, S. Gigan, A. Maitre, and C. Fabre, Phys. Rev. A **67**, 023808 (2003).
[11] C. Schwob, P. H. Souto Ribeiro, A. Maître, and C. Fabre, Opt. Lett. **22**, 1893 (1997), and references therein.
[12] C. Tischer, S. Altmann, S. Fisinger, J. K. H. Hrber, E. H. K. Stelzer, and E.-L. Florin, Appl. Phys. Lett. **79**, 3878 (2001).
[13] Tim J. Senden, Curr. Opin. Colloid Interface Sci. **6**, 95 (2001).
[14] C. Boccara, D. Fournier, and J. Badoz, Appl. Phys. Lett. **36**, 130 (1980).
[15] N. Treps, U. Andersen, B. Buchler, P. K. Lam, A. Maître, H-A. Bachor, and C. Fabre, Phys. Rev. Lett. **88**, 203601 (2002).
[16] N. Treps, N. Grosse, W. P. Bowen, C. Fabre, H-A. Bachor, and P. K. Lam, Science **301**, 940 (2003).
[17] N. Treps, N. Grosse, W. Bowen, M. T. L. Hsu, A. Maître, C. Fabre, H. A. Bachor, and P. K. Lam, J. Opt. B: Quantum Semiclassical Opt. **6**, S664 (2004).

Quantum limits in image processing

V. Delaubert[1,2], N. Treps[1], C. Fabre[1], H.A. Bachor[2], and P. Réfrégier[3]
[1]*Laboratoire Kastler Brossel, Université Pierre et Marie Curie-Paris6, CC74, 4 Place Jussieu, 75252 Paris cedex 05, France*
[2]*ARC Centre of Excellence for Quantum-Atom Optics, Australian National University, Canberra, ACT 0200, Australia and*
[3]*Physics and Image processing group, Fresnel Institute,UMR 6133, Domaine Universitaire de Saint-Jérôme, 13397 Marseille cedex 20, France*
(Dated: September 22, 2006)

We determine the bound to the maximum achievable sensitivity in the estimation of a scalar parameter from the information contained in an optical image in the presence of quantum noise. This limit, based on the Cramer-Rao bound, is valid for any image processing protocol. It is calculated both in the case of a shot noise limited image and of a non-classical illumination. We also give practical experimental implementations allowing us to reach this absolute limit.

PACS numbers: 42.50.Dv; 42.30.-d; 42.50.Lc

Introduction. - Many of the most sensitive techniques for the measurement of a physical parameter - which we will call p in the following and assume to be a scalar - are optical. In some cases, the total intensity or amplitude of the light beam varies with p and conveys the information. It is then well known [1–4] that there exists a standard quantum limit in the sensitivity of the measurement of p when the light beam is in a coherent state, and that it is possible to go beyond this limit using sub-Poissonian or squeezed light. In other cases, the parameter p of interest only modifies the distribution of light in the transverse plane and not its total intensity. The present paper deals with this latter situation. For example, the parameter p modifies the position or direction of a light beam. This configuration has been studied at the quantum level, both theoretically and experimentally using split detectors [5–7] or homodyne detection [8, 9]. But in many instances the parameter p affects in a complicated way the field distribution in the detection plane (that we will call here the image). For example a fluorescent nano-object imbedded in a biological environment modifies the image recorded through a microscope in a complex way because of diffraction. Nevertheless its position can be determined from the information contained in the image with a sensitivity which can be much better than the wavelength [10]. In order to extract the parameter value in such experiments, one needs to use detector arrays or CCD cameras and to combine in an appropriate way the information recorded on the different pixels.

When all the sources of technical noise have been removed in the apparatus, quantum fluctuations still affect the optical measurement and limit its sensitivity, in a way that can be readily calculated for each specific measurement protocol. The purpose of this paper is much broader. It is to answer the following question: what is the lowest limit imposed by quantum noise to the accuracy of the determination of p, independently of the information processing protocol used for the extraction of information? As we will see, this optimum limit depends only on the statistics of the fluctuations of the incoming light. We use an approach based on the Cramer-Rao Bound. This tool, widely used in the signal processing community [11], has already been applied to different domains, such as gravitational wave detection [12] or diamagnetism [13].

Notations and assumptions. - The parameter p is measured relative to an *a priori* value chosen for simplicity to be 0. Because of the quantum fluctuations in the optical measurements, there will be an uncertainty on its estimation. An evaluation of this uncertainty thus provides the precision on the determination of the parameter p around a zero value.

The mean value of the local complex electric field operator in the image plane, normalized to a number of photons, will be written for a given value of the parameter as

$$\bar{E}(\vec{r},p) = 2\sqrt{N}u_0(\vec{r},p), \tag{1}$$

where N refers to the total number of photons detected in the mean field during the integration time of the detector. N is assumed to be independent of p, as stated previously. $u_0(\vec{r},p)$ is the p-dependent transverse distribution of the mean field, complex in the general case, and normalized to 1 (its square modulus integrated over the transverse plane equals 1). The local mean photon number detected during the same time interval is

$$\bar{n}(\vec{r},p) = \frac{\bar{E}^*(\vec{r},p)\bar{E}(\vec{r},p)}{4} = N|u_0(\vec{r},p)|^2. \tag{2}$$

Intensity measurements. - We first assume that p is determined by processing the information contained in the measurement of the local intensity, i.e. local number of photons. The best possible local intensity detection device would consist in a set of indexed pixels paving the entire transverse plane, in the limit when their spatial extension approaches 0. Let $\mathbf{n} = [n_1, ..., n_k, ...]$ be one measurement of the photon distribution with such a hypothetical detector, where n_k corresponds to the number of photons detected on pixel k. Because of the noise

present in the light, the sample $\mathbf{n}$ differs from its statistical mean value $\bar{\mathbf{n}}(p) = [\bar{n}_1(p), ..., \bar{n}_k(p), ...]$. Let $L(\mathbf{n}|p)$ be the likelihood of its observation. Note that $\mathbf{n}$ corresponds to a single measurement and hence does not explicitly depend on p, contrarily to the average on all the possible realizations.

The achievable precision on the estimation of p is limited by the Cramer-Rao Bound (CRB). More precisely, the variance of any unbiased estimator of p is necessarily greater than $\sigma^2_{min} = 1/I_F$, where the Fisher information I_F is given, when the actual value of p is 0, by [11]:

$$I_F = -\int \frac{\partial^2}{\partial p^2} l(\mathbf{n}|p)\Big|_{p=0} L(\mathbf{n}|0) d\mathbf{n}, \tag{3}$$

where we have introduced the log-likelihood $l(\mathbf{n}|p) = \ln L(\mathbf{n}|p)$. The integration spans continuously over all possible photon distributions that can be detected when the parameter value is $p = 0$. This information is thus highly dependent on the noise statistics.

Let us first assume that the illumination is coherent, and therefore that the local intensity noise is Poissonian. The probability of measuring n_k photons on pixel k, when the parameter equals p is given by

$$P_{k,p}(n_k) = \frac{\bar{n}_k(p)^{n_k}}{n_k!} e^{-\bar{n}_k(p)}. \tag{4}$$

Restricting our analysis to spatially uncorrelated beams, the likelihood $L(\mathbf{n}|p)$ simply corresponds to the product of all local probabilities given in Eq. 4. Then, taking the limit of infinitely small pixels and using Eq. 3, one can show that the Fisher information equals

$$I_F^{Poisson} = \int \left[\frac{\bar{n}'(\vec{r},0)^2}{\bar{n}(\vec{r},0)} - \bar{n}''(\vec{r},0) \right] d^2r, \tag{5}$$

where the $'$ denotes a derivative relative to p. Using Eq. 1, one finally finds that

$$I_F^{Poisson} = \frac{4N}{a^2}, \tag{6}$$

where a is a global positive parameter characterizing the variation of the image intensity with p, defined by

$$\frac{1}{a^2} = \int \left[\frac{\partial}{\partial p} |u_0(\vec{r},p)| \right]^2_{p=0} d^2r. \tag{7}$$

The smallest value of p that can be distinguished from the shot noise - i.e. corresponding to a signal to noise ratio (SNR) equal to 1 -, whatever the algorithm used to determine it from the local intensity measurements, provided that it gives an unbiased estimation of p, is finally greater than $a/2\sqrt{N}$. This value sets the standard quantum noise limit for intensity measurements of p, imposed by the random time arrival of photons on the detector. It is inversely proportional to the square root of the number of photons, as expected, and is related, through the dependence with a, to the modification of the mean intensity profile with p.

We now consider a non-classical illumination, still with identical mean intensity, but with local sub-Poissonian quantum fluctuations described by a noise variance $\sigma_P^2 < 1$ (assumed to be the same over the entire transverse plane). One can show that the CRB leads to

$$p_{min}^{sub-Poisson} \geq \frac{a\sigma_P}{2\sqrt{N}}. \tag{8}$$

As we have already noticed, the limit given by Eq. 8 is valid for any measurement strategy. Nevertheless, a practical way enabling us to reach such an absolute limit remains to be found. This is what is presented in the next paragraph.

Let us assume that an image processor calculates a given linear combination of the local intensity values recorded by the pixels of an array detector, as represented in Fig. 1. Assuming that the pixels are small compared

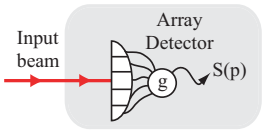

FIG. 1: Array detector as an optimal intensity detection. g refers to the pixel gain distribution. $S(p)$ is the p-dependent processed signal.

to the characteristic variation length of the image, the mean value $\bar{S}(p)$ of the computed signal can be written as an integral over the transverse plane as follows

$$\bar{S}(p) = \int g(\vec{r}) \bar{n}(\vec{r},p) d^2r, \tag{9}$$

where $g(\vec{r})$ is the local gain on the pixel localized at position $\vec{r}$, which can be positive or negative. Assuming that p is small, $|u_0(\vec{r},p)|$ can be expanded at first order into

$$|u_0(\vec{r},p)| = |u_0(\vec{r},0)| + \frac{p}{a} u_I(\vec{r}), \tag{10}$$

where a has been defined in Eq. 7, and u_I is a transverse function normalized to 1, already introduced in a particular case in reference [8]. The gains are chosen such as $\bar{S}(p=0) = 0$ (difference measurement), so that $\bar{S}(p)$ is given, at first order, by

$$\bar{S}(p) = \frac{2Np}{a} \int g(\vec{r}) |u_0(\vec{r},0)| u_I(\vec{r}) d^2r, \tag{11}$$

For a coherent illumination, because the local quantum fluctuations are uncorrelated, the noise variance ΔS^2 on on $\bar{S}(p)$ is equal to the shot noise on each pixel weighted by $g^2(\vec{r})$ [14]. Moreover, as p is small, the noise is independent of p at the first order, and we get

$$\Delta S^2 = N \int g^2(\vec{r}) |u_0(\vec{r},0)|^2 d^2r. \tag{12}$$

It is then possible to optimize the gain factor $g(\vec{r})$ in order to get the highest possible SNR defined by SNR= $\bar{S}(p)^2/\Delta S^2$. Using Cauchy-Schwartz inequality, one can show that the highest SNR value for the present measurement strategy is given by SNR= $4Np^2/a^2$, and is obtained for an optimal value of the gain distribution given by

$$g_{opt}(\vec{r}) = \beta \frac{u_I(\vec{r})}{|u_0(\vec{r},0)|}, \tag{13}$$

where β is an arbitrary constant. The minimum measurable value of p - corresponding to comparable signal and noise, i.e. SNR= 1 - is given by $p_{min} = a/2\sqrt{N}$, which is precisely equal to the CRB for classical illumination. The present measurement strategy is therefore optimal as it allows to reach the CRB for small values of the parameter p, with the certainty that no other measurement strategy can do better. Note that we have not proven that it is the unique way to reach the CRB.

We can even extend this result to the use of non classical light. Indeed, using a bimodal field composed of a bright mode u_0 in a coherent state carrying the mean field, and a squeezed vacuum mode in the mode u_I, the detected noise power is modified into

$$\Delta S^2 = N\sigma_P^2, \tag{14}$$

when the noise variance on the amplitude quadrature of the mode u_I is given by σ_P^2 [14]. Note that the use of a locally squeezed beam would not provide any improvement as u_I is the only mode contributing to the measurement noise, referred to as the *noise-mode of detection* [8, 14]. The minimum measurable p value is in this case

$$p_{min} = \frac{a\sigma_P}{2\sqrt{N}}. \tag{15}$$

We have thus found a way to reach the bound, i.e. the minimum accessible p-value given in Eq.8. Moreover, our scheme requires minimum quantum resources, namely a bimodal field with squeezing in only one mode.

Field measurements. - We now assume that the information about p is extracted from the knowledge of the local complex field, i.e. local amplitude and phase, that can be obtained by interferometric techniques. Similarly to the previous section, the best possible detection would here access the local complex field on k-indexed areas paving the entire transverse plane, in the limit when their spatial extension approaches 0. Let $\mathbf{E} = [E_1, ..., E_k, ...]$ be a single measurement of the field distribution, hence independent of p, where E_k corresponds to the complex field detected on area k. Again, because of the noise present in the light, the sample $\mathbf{E}$ differs from its statistical mean value $\bar{\mathbf{E}}(p) = \left[\bar{E}_1(p), ..., \bar{E}_k(p), ...\right]$. Let $L(\mathbf{E}|p)$ be the likelihood of its observation.

A bound to the maximal precision on p can again be calculated from the CRB, which, for a field measurement, is the inverse of the following Fisher information

$$I_F = -\int \left[\frac{\partial^2}{\partial p^2} l(\mathbf{E}|p)\right]_{p=0} L(\mathbf{E}|0) d\mathbf{E}, \tag{16}$$

We assume that the local field fluctuations in the transverse plane can be described by a Gaussian probability density function independent of the mean field. Moreover, we consider a classical or non classical illumination whose amplitude and phase quadrature fluctuations are described by the noise variances σ_P^2 and σ_Q^2, respectively. These factors neither depend on $\vec{r}$ nor on p, as we assume the fluctuations to be homogeneous and independent of the parameter p.

The probability to measure a field given by $E_k = P_k + iQ_k$ on area k, where P_k and Q_k correspond to the local field quadratures, is, for a parameter value p

$$\mathcal{P}_{k,p}(E_k) = \frac{1}{2\pi\sigma_P\sigma_Q} e^{-\left[\frac{(P_k - \bar{P}_k(p))^2}{2\sigma_P^2} + \frac{(Q_k - \bar{Q}_k(p))^2}{2\sigma_Q^2}\right]}, \tag{17}$$

where $\bar{P}_k(p)$ and $\bar{Q}_k(p)$ are the local quadratures statistical averages, satisfying: $\bar{E}_k(p) = \bar{P}_k(p) + i\bar{Q}_k(p)$. Without loss of generality, we define the orientation of the Fresnel diagram relative to the phase of the mean field, i.e. $\bar{P}(\vec{r},p) = 2\sqrt{N}u_0(\vec{r},p)$ and $\bar{Q}(\vec{r},p) = 0$, taking the limit of infinitely small detection areas. Assuming no spatial correlations in the field fluctuations, one can show that the Fisher information is given by

$$I_F^{Gauss} = \int \frac{1}{\sigma_P^2} \left[\frac{\partial \bar{P}(\vec{r},p)}{\partial p}\right]_{p=0}^2 d^2r. \tag{18}$$

We now introduce b, a second global positive parameter, characterizing the variation of the image field with p

$$\frac{1}{b^2} = \int \left[\frac{\partial}{\partial p} u_0(\vec{r},p)\right]_{p=0}^2 d^2r. \tag{19}$$

Using Eq.1 and 19, the Fisher information simplifies into

$$I_F^{Gauss} = \frac{4N}{b^2\sigma_P^2}. \tag{20}$$

The smallest value of p that can be distinguished from the quantum noise using a field detection of the optical beam is finally greater than the CRB:

$$p_{min}^{Gauss} \geq \frac{b\sigma_P}{2\sqrt{N}}. \tag{21}$$

Again, we can propose an experimental scheme enabling to reach this limit in the case of a small parameter p, and for which the mean value of the complex electric field can be written at first order

$$\bar{E}(\vec{r},p) = 2\sqrt{N}\left[u_0(\vec{r},0) + \frac{p}{b}u_E(\vec{r})\right], \tag{22}$$

where b has been introduced in Eq.19, and where $u_E(\vec{r})$ is a transverse function normalized to 1.

Let us consider a balanced homodyne detection, as represented in Fig. 2, with a local oscillator (LO) chosen to be defined by the following complex field operator

$$\bar{E}_{LO}(\vec{r}) = 2\sqrt{N_{LO}}u_E(\vec{r})e^{i\theta_{LO}}, \tag{23}$$

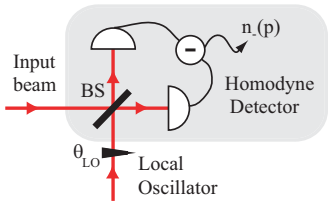

FIG. 2: Balanced homodyne detection as an optimal field detection. $n_-(p)$ is the p-dependent signal. ϕ_{LO} is the local oscillator phase. BS : 50/50 beamsplitter.

where N_{LO} corresponds to the number of photons detected in the entire LO beam during the integration time. The LO is much more intense than the image, i.e. $N_{LO} \gg N$. θ_{LO} is the LO phase. The mean intensity difference n_- between the photocurrents of the two detectors is given in terms of number of photons by

$$\bar{n}_-(p) = \frac{1}{4}\int \left[\bar{E}^*_{LO}(\vec{r})\bar{E}(\vec{r},p) + \bar{E}^*(\vec{r},p)\bar{E}_{LO}(\vec{r})\right] d^2r \quad (24)$$

Note the similarity with Eq.9, as incident field amplitude and LO field play here identical roles of incident intensity and electronic gain, respectively. Though detectors do not resolve the spatial distribution of the beams and no processing of the spatial information is made, the balanced homodyne technique directly provides an "analog" computation of the quantity of interest.

When the LO phase is tuned to the maximum of the p-dependent term, the homodyne signal becomes

$$\bar{n}_- = 2\sqrt{NN_{LO}}\frac{p}{b}. \quad (25)$$

For coherent illumination, the noise power on the homodyne signal corresponds to N_{LO}, i.e. to the shot noise of the LO. The SNR of the homodyne measurement is thus given by SNR$= 4Np^2/b^2$. The minimum measurable value of p - corresponding to a SNR of 1 - with homodyne detection is given by

$$p_{min} = \frac{b}{2\sqrt{N}}. \quad (26)$$

Moreover, when the component of the image selected by the LO is in a non classical state , i.e. allowing a squeezed vacuum u_E mode with a noise variance σ_P^2 on the amplitude quadrature within the incoming beam, we get

$$p_{min} = \frac{b\sigma_P}{2\sqrt{N}}. \quad (27)$$

This result corresponds exactly to the CRB calculated for amplitude measurements of p. The homodyne detection scheme with the appropriate LO shape and phase is therefore an optimal field detection of p. Again, it uses minimal resources as only one source of squeezed light is needed to reach the non classical CRB.

Comparison and conclusion. - We have presented two efficient - i.e. reaching the associated CRB - signal processing techniques for the extraction of information contained in an image. We can show that the CRB for field measurements, in which all quadratures can be accessed, is smaller than the one for intensity measurements, i.e. $a \geq b$. Yet, both schemes are useful: the intensity scheme is interesting since it is not restricted to monochromatic light, whereas the amplitude scheme is useful since it does not require pixellized detectors.

Let us finally note that this work provides limits which are valid for a shot noise limited light of any shape. However it is not valid so far for any kind of non-classical light, as we have restricted our analysis to homogeneous squeezed states. In a forthcoming publication, we will study the situation of quantum fields with quantum spatial correlations in the transverse plane and will investigate for the corresponding modifications of the CRB.

Acknowledgements. We would like to acknowledge the support of the Australian Research Council scheme for Centre of Excellence. Laboratoire Kastler Brossel, of the Ecole Normale Supérieure and Université Pierre et Marie Curie, is associated with the CNRS.

[1] M. Xiao et al., Phys. Rev. Lett. **59**, 278 (1987).
[2] P. H. Souto Ribeiro et al., Opt. Lett. **22**, 1893 (1997).
[3] J. Gao et al., Opt. Lett. **23**, 870 (1998).
[4] H.A. Bachor et al., *A guide to experiments in quantum optics*, Wiley-VCH (2003).
[5] C. Fabre et al., Opt. Lett.**25**, 76 (2000).
[6] N. Treps et al., Phys. Rev. Lett. **88** 203601 (2002)
[7] N. Treps et al., Science, **301**, 940 (2003).
[8] V. Delaubert et al., Opt. Let. **31**, 1537 (2006)
[9] V. Delaubert et al., preprint quant-ph/**0607142**.
[10] A. Rohrbach et al., Rev. Sci. Instrum. **75**, 2197 (2004)
[11] P. Réfrégier, *Noise Theory and Application to Physics*, Springer, New-York, (2004).
[12] D. Nicholson et al., Phys. Rev. D **57**, 4588 (1998).
[13] S. Curilef et al., Phys. Rev. B, **71**, 024420 (2005).
[14] N. Treps et al., Phys. Rev. A **71**, 013820 (2005).

La mesure monomode : intrication et téléportation

Article 3, reproduit en page 68

Criteria of quantum correlation in the measurement of continuous variables in optics

N. Treps, and C. Fabre
Laser Physics **15**, 187 (2005)

Abstract : The purpose of this short tutorial paper is to review various criteria that have been used to characterize the quantum character of correlations in optical systems, such as "gemellity", QND correlation, intrication, EPR correlation and Bell correlation, to discuss and compare them. This discussion, restricted to the case of measurements of continuous optical variables, includes also an extension of known criteria for "twin beams" to the case of imbalanced correlations.

Article 4, reproduit en page 77

Conditionnal Preparation of a Quantum State in the Continuous Variable Regime : Generation of a sub-Poissonian State from Twin Beams

J. Laurat, T. Coudreau, N. Treps, A. Maître and C. Fabre
Phys. Rev. Lett. **21** 213601 (2003)

Abstract : We report the first experimental demonstration of conditional preparation of a nonclassical state of light in the continuous variable regime. Starting from a nondegenerate optical parametric oscillator which generates above threshold quantum intensity correlated signal and idler "twin beams," we keep the recorded values of the signal intensity only when the idler intensity falls inside a band narrower than its standard deviation. By this very simple technique, we generate a sub-Poissonian state 4.4 dB (64%) below shot noise from twin beams exhibiting 7.5 dB (82%) of noise reduction in the intensity difference.

Article 5, reproduit en page 81

Compact source of Einstein-Podolsky-Rosen entanglement and squeezing at very low noise frequencies

J. Laurat, T. Coudreau, G. Keller, N. Treps and C. Fabre
Phys. Rev. A **70** 042315 (2004).

Abstract : We report on the experimental demonstration of strong quadrature Einstein-Podolsky-Rosen entanglement and squeezing at very low noise sideband frequencies produced by a single type-II, self-phase-locked, frequency degenerate optical parametric oscillator below threshold. The generated two-mode squeezed vacuum state is preserved for noise frequencies as low as 50 kHz. Designing simple setups able to generate nonclassical states of light in the kHz regime is

a key challenge for high sensitivity detection of ultraweak physical effects such as gravitational wave or small beam displacement.

Article 6, reproduit en page 85

Experimental investigation of continuous-variable quantum teleportation

W. P. Bowen, N. Treps, B. C. Buchler, R. Schnabel, T. C. Ralph, H.-A. Bachor, T. Symul, and P. K. Lam

Phys. Rev. A. 67, 032302 (2003)

Abstract : We report the experimental demonstration of quantum teleportation of the quadrature amplitudes of a light field. Our experiment was stably locked for long periods, and was analyzed in terms of fidelity F and with signal transfer $T_q = T^+ + T^-$ and noise correlation $V_q = V^+_{in|out} V^-_{in|out}$. We observed an optimum fidelity of 0.64 ± 0.02, $T_q = 1.06 \pm 0.02$, and $V_q = 0.96 \pm 0.10$. We discuss the significance of both $T_q > 1$ and $V_q < 1$ and their relation to the teleportation no-cloning limit.

Article 7, reproduit en page 89

Teleportation of an atomic ensemble quantum state

A. Dantan, N. Treps, A. Bramati and M. Pinard

Phys. Rev. Lett. 94, 050502 (2005)

Abstract : We propose a protocol to achieve high fidelity quantum state teleportation of a macroscopic atomic ensemble using a pair of quantum-correlated atomic ensembles. We show how to prepare this pair of ensembles using quasiperfect quantum state transfer processes between light and atoms. Our protocol relies on optical joint measurements of the atomic ensemble states and magnetic feedback reconstruction.

Criteria of quantum correlation in the measurement of continuous variables in optics

N. Treps, C. Fabre
Laboratoire Kastler Brossel, UPMC, Case 74, 4 Place Jussieu, 75252 Paris cedex 05, France
(Dated: May 30, 2006)

The purpose of this short tutorial paper is to review various criteria that have been used to characterize the quantum character of correlations in optical systems, such as "gemellity", QND correlation, intrication, EPR correlation and Bell correlation, to discuss and compare them. This discussion, restricted to the case of measurements of continuous optical variables, includes also an extension of known criteria for "twin beams" to the case of imbalanced correlations.

PACS numbers: 42.50.Dv; 42.30.-d; 42.50.Lc

I. INTRODUCTION

One of the most striking features of quantum mechanics is the existence of the so-called entangled states, i.e. of quantum states $|\Psi>$ describing a system made of two separable parts which cannot be written as a tensor product of quantum states $|\Psi_1>$ and $|\Psi_2>$ describing separately each of the subsystems :

$$|\Psi> \neq |\psi_1> \otimes |\psi_2> \tag{1}$$

In such states, there exist strong correlations between measurements performed on the sub-systems. These correlations have been widely studied, almost from the onset of quantum physics, but they still keep a part of their mystery, and therefore of their attraction. The discovery that quantum correlations play an irreplaceable role in information processing gave recently a new impetus to their study.

The existence of correlations between different measurements is obviously not a specific property of quantum physics : it is simply the consequence of a former interaction, whatever its character, between the two parts submitted to the measurement. Consequently, the observation or prediction of a correlation, even perfect, between the measurements of two variables is not at all a proof of the quantum character of the phenomenon under study, in contrast to what can be found sometimes in articles. One can find in the literature a great deal of criteria setting a border between the classical and the quantum effects, differing by the definitions of the quantum character of a given physical situation. The purpose of the present paper is mainly tutorial : it is to give a short overview of the different criteria which are already well-known and extensively used in the literature, to compare them and discuss their domain of relevance. We will also introduce slight original additions to some already known criteria, especially for the criterion of "gemellity" in the case where the two correlated systems do not play symmetrical roles.

Of course, it is impossible to treat the problem of quantum correlations in all its generality in such a short review. We will restrict ourselves here to the domain of the so-called *continuous variables in optics*. More precisely we will consider correlations between measurements performed on light beams in the case where the photons cannot be distinguished individually, and leave aside the correlations between photo-counts and between measurements performed on other observables than the ones arising from photodetection. One of the important application of this work is to be able to precisely assess the quantum aspects of the correlations appearing between two points of the transverse plane of an optical image.

After a short paragraph devoted to the introduction of the problem and of the notations, we will successively focus on the different criteria of quantum correlations, involving either a single correlation measurement, and assessing first the impossibility of a classical description of the phenomenon, then the QND character of the correlation, or involving the measurement of two correlations on non-commuting observables, and assessing first the intrication of the state describing the system, then its EPR character, and finally its impossibility of description in terms of local hidden variables.

II. POSITION OF THE PROBLEM, NOTATIONS

Let us consider two modes of the electromagnetic field, labelled 1 and 2, that can be separated without introducing losses in the system, and that are measured by detectors situated at different locations : the modes can differ either by the frequency, the direction of propagation, the polarization, the transverse shape, or by several of these characteristics. $\hat{a}_1$ and $\hat{a}_2$ are the corresponding annihilation operators, and

$$\hat{X}_i^+ = \hat{a}_i + \hat{a}_i^\dagger \quad \hat{X}_i^- = \frac{\hat{a}_i - \hat{a}_i^\dagger}{i} \quad (i = 1, 2) \tag{2}$$

the quadrature operators. The measurement performed on these modes can be either a direct photodetection, which measures the fluctuations of the amplitude quadrature component, parallel to the mean field $\bar{E}_i$ in the Fresnel representation plane, or a balanced homodyne detection, which measures any quadrature component. We will call in a generic way $\hat{X}_i$ the quadrature component which is measured, and $\delta\hat{X}_i$ its fluctuations.

¿From the fluctuations measured on a single detector, one can deduce the quantity :

$$F_i = \langle \delta\hat{X}_i^2 \rangle \tag{3}$$

equal to 1 when the field is in a coherent state. F_i is the Fano factor [1, 2] of the beam in the case of a direct photodetection, and the quadrature noise normalized to shot noise in a homodyne measurement.

The simultaneous recording of the fluctuations measured by the two detectors allows us to determine the normalized correlation coefficient :

$$C_{12} = \frac{\langle \delta X_1 \delta X_2 \rangle}{(F_1 F_2)^{1/2}} \tag{4}$$

which varies between -1 (perfect anti-correlation) and 1 (perfect correlation).

For the sake of simplicity, we will assume in the following, when it turns out to be necessary, that the system under study has correlations, and not anti-correlations, and therefore that C_{12} is positive. All our following discussion can be readily extended to the case of anti-correlations by exchanging the role of sum and differences between the quantities measured on the two modes. One can also note that the study performed here can be applied to the fluctuations of non-optical physical systems, as soon as a protocol exists to transfer these fluctuations to an optical field, as is done in the case of cold atoms and entanglement between light and cold atoms [3, 4].

Let us consider now the case of an optical experiment which gives an experimental value of C_{12} close to 1. In which respect can one claim the quantum nature of the observed correlations ? That is the question that we will address in the following sections.

III. NON CLASSICAL CHARACTER OF THE CORRELATED BEAMS : "TWIN BEAMS"

One knows that most of the optical phenomena can be explained by using the so-called *semi-classical approach of the light-matter interaction*, in which a quantized matter interacts with the electro-magnetic field treated as a classical quantity, possibly endowed with classical fluctuations. Even the photo-electric effect, for which the photon was introduced by Einstein [5] lies in this category, which also includes all interference effects that are directly measured on the intensity of the field. In this model, the fluctuations which exist in the photo-detection signal are due to the random character of the "quantum jump" occurring in the atom because of its irradiation by the classical field. The minimum noise measured on the photo-detector is the shot noise, or standard quantum noise limit. As explained in many textbooks on Quantum Optics [1, 6, 7], it was realized in the seventies that there existed light states which gave rise to measurements that could not be accounted for within the semi-classical approach. These states are named "non-classical states", and are unveiled by measurements involving either intensity correlations between two photocurrents, or intensity fluctuations of a given photocurrent around the mean. The observation of photon antibunching using single photon states has been historically the first unambiguous experimental situation[8] where a classical description of the field was not able to account for the observed results. Let us note that Herbert Walther has played a major role in the study of these effects, using the light emitted by a single trapped ion [9, 10]. One can therefore define a first level of quantum correlation by the following statement :

Quantum correlation, level 1 : *The correlation measured in the system cannot be described by a semi-classical model involving classical electromagnetic fields having classical fluctuations.*

In the domain of continuous variables and intense beams to which we restrict the present discussion, one shows that the situations where one records quadrature fluctuations above the standard quantum noise limit can be described using the semi-classical approach with classical stochastic electro-magnetic fields [1, 11], and that quantum fluctuations below the this limit are only produced by non-classical states. Squeezed states are one example of non-classical states. The border between the classical and quantum world corresponds to the situation where all the beams used in the experiment are in coherent and vacuum states (Fano factor of 1). Furthermore, it is easy to show that *the classical character of the field is preserved by linear "passive" optical devices*, which involve only linear, energy-preserving, optical elements like beamsplitters and free propagation.

To ascertain whether the correlation between two given beams can be described in a classical frame or not, the simplest way is therefore to process the two beams by all possible linear passive optical devices : if one is able to

produce in such a way a beam having fluctuations below the quantum noise limit, the correlation will be termed as "non-classical". This procedure is easy to implement if the two beams have the same frequency. If the two beams have different frequencies ω_1 and ω_2, it is more difficult but still possible, at least in principle : the noise reduction will then be measured by a homodyne detection scheme using a local oscillator at frequency $(\omega_1 + \omega_2)/2$, and will appear at a noise frequency $\Omega = |\omega_1 - \omega_2|/2$.

A. Classical correlation

Let us first consider the simplest way to produce correlated beams by classical means : one inserts a 50% beamsplitter in a given classical beam, which is thus divided into two output beams having a degree of correlation that can be simply calculated. Taking into account the vacuum mode entering through the unused port of the beamsplitter, one obtains the following value for the correlation obtained by splitting an input classical field on a 50% beamsplitter :

$$[C_{12}]_{class} = \frac{F_{in} - 1}{F_{in} + 1} \tag{5}$$

where F_{in} is the Fano factor of the input beam on the beamsplitter, or equivalently by :

$$[C_{12}]_{class} = 1 - \frac{1}{F} \tag{6}$$

where F is the common value of the Fano factor of the two beams at the output of the beamsplitter ($F = (F_{in}+1)/2$).

Let us note that C_{12} tends to 1 when F_{in} goes to infinity, i.e. when the vacuum noise of the second input can be neglected with respect to the proper noise of the input beam. A very strong correlation is therefore not always the sign of a quantum origin : it can be just the reverse, and due to the fact that the quantum fluctuations can be neglected in the problem ! The normalized correlation factor C_{12} is thus not the most unambiguous way to appreciate the quantum character of a correlation.

B. "Gemellity"

Let us now exploit the operational definition of the quantum character of the correlation given at the beginning of this section, which is to use a linear passive operation which transforms the correlation into a sub-shot noise beam. In the case of two beams, this operation simply consists of recombining the beams on a beamsplitter of variable transmission and reflection after variable optical paths. The phases are adjusted so that one mixes the relevant quadrature components X_1 and X_2. One eventually obtains a beam having quadrature fluctuations $\delta\hat{X}_{out}$ given by :

$$\delta\hat{X}_{out} = r\delta\hat{X}_1 - t\delta\hat{X}_2 \tag{7}$$

r and t being adjustable amplitude reflection and transmission coefficients. If the minimum noise on this beam is below the standard quantum limit, we are sure that the initial correlation can only be described in a full quantum frame. We will name by the neologism "gemellity" ("twinship") the minimum variance of this quantity, labelled G, which can be found to be :

$$G = \frac{F_1 + F_2}{2} - \sqrt{C_{12}^2 F_1 F_2 + \left(\frac{F_1 - F_2}{2}\right)^2} \tag{8}$$

and state :

$$G < 1$$
$$\Downarrow$$
Impossibility of a classical description of correlated beams

C. Balanced case

Let us first consider the case of two beams of equal means and noises, so that $F_1 = F_2 = F$. In this case, the gemellity has a very simple expression :

$$G = F(1 - |C_{12}|) \tag{9}$$

The reflection and transmission amplitude coefficients r and t are both equal in this case to $1/\sqrt{2}$, so that G can also be written as :

$$G = \frac{\langle \left(\delta \hat{X}_1 - \delta \hat{X}_2\right)^2 \rangle}{2} \tag{10}$$

It is nothing else than the normalized noise on the difference between the fluctuations of the two measurements, and can be easily monitored by simple electronic means. In the classical case described in the previous paragraph, it is easy to show that G takes the value 1, whatever the initial Fano factor F_{in} of the beam. If the gemellity G has a value smaller than 1, the two beams have identical mean values and almost identical fluctuations (within the quantum noise). Such beams are usually named "twin beams", in a way reminiscent of the "twin photons" studied in the photon counting regime. One can distinguish between "intensity twin beams", where the measured quadrature is the amplitude quadrature (in that case, the measured gemellity is equivalent to the normalized difference of the intensity fluctuations of the two beams), and which are produced by above threshold OPOs [12, 13] or by the mixing on a 50% beamsplitter of a coherent state and a squeezed vacuum [14], and "quadrature twin beams", which are produced by non degenerate OPOs below threshold [15, 16]. The smallest measured value of the gemellity G is to the best of our knowledge $G = 0.11$ [17].

The non-classical region ($G < 1$) corresponds to correlations C_{12} larger than $1 - 1/F$. The correlation likely to produce non-classical twin beams has a lower limit which is more and more close to 1 when the two fields have more and more excess noise. If each field is at shot noise, any non-zero correlation is a proof of gemellity, and therefore of non-classical character.

D. Unbalanced case

Unbalanced beams may have also strong, or even perfect, classical correlations. To produce classically correlated fields of unequal intensities and fluctuations, one can use a non equal beam-splitter with different amplitude transmission and reflection coefficients. In this case, the correlation C_{12} is found to be

$$[C_{12}]_{class} = \sqrt{(1 - \frac{1}{F_1})(1 - \frac{1}{F_2})} \tag{11}$$

which is the generalization of relation (6). This amount of correlation, as expected, gives a value larger than or equal to 1 to the gemellity G, defined by Eq(8).

If F_1 or F_2 is equal to 1, Expression(8) implies that any non-zero correlation C_{12} gives a value of G smaller than 1 : any correlation between a field at shot noise and another field has thus a quantum origin.

In order to experimentally determine the gemellity, one uses the operational definition : it is the minimum noise -normalized to shot noise - obtained when one mixes the two considered beams on a beamsplitter of variable transmission and reflection. The gemellity criterion for a non-classical correlation between unbalanced beams is interesting from an experimental point of view, because in a given experimental situation the two measured beams do not have necessarily the same mean power and noise [18, 19, 20].

IV. NON-CLASSICAL CHARACTER OF THE MEASUREMENT PROVIDED BY THE CORRELATION : "QND-CORRELATED BEAMS"

When two observables M_1 and M_2 are perfectly correlated, the measurement of M_2 gives without uncertainty the value of M_1. The first measurement is thus a *Quantum Non Demolition measurement* (QND) of the observable M_1 performed on the second sub-system.

We can now define a second level in the quantum character of correlations :

Quantum correlation, level 2 : *The information extracted from the measurement on one field provides a Quantum Non Demolition measurement of the other.*

In the last decade, many studies have been devoted to the precise definition of QND criteria[21], that we can use now in our discussion. In the present case, the "Non Demolition" part of the measurement is automatically ensured, as the measurement, performed on beam 2, does not physically affect the measured system, which is beam 1. Its quantum character is effective when the measurement is able to provide enough information on the instantaneous quantum fluctuations of the other beam so that it is possible, using the information acquired on mode 2, to correct mode 1 from its quantum fluctuations and transform it into a non-classical state in the meaning of the previous section by a feed-back or feed-forward electronic device. This criterion is well known in QND studies[22], where it is shown that it is equivalent to state that the *conditional variance* $V_{1|2}$ of beam 1 knowing beam 2 takes a value smaller than 1. The conditional variance has the following expression in terms of the Fano factor of beam 1 and the normalized correlation C_{12} between the two :

$$V_{1|2} = F_1(1 - C_{12}^2) \tag{12}$$

A. Balanced case

Let us first consider the case where the two beams have identical mean values and fluctuations ($F_1 = F_2 = F$). In this case there is only one conditional variance $V_{1|2} = V_{2|1} = V$, and the criterion for "QND-correlated beams" is :

$$V_{1|2} = V_{2|1} = V < 1 \tag{13}$$

The conditional variance and the gemellity are related by :

$$V = G(1 + C_{12}) = 2G - \frac{G^2}{F} \tag{14}$$

so that :

$$G \leq V \leq 2G \tag{15}$$

One notices that the conditional variance is always bigger than the gemellity, so that all the QND-correlated beams are twin beams, whereas the reverse is not true. We see also that a small enough gemellity, namely smaller than 0.5, implies that the beams are QND-correlated.

It is possible to show [22] that the conditional variance can be directly measured by using an adjustable amplification on one of the two photocurrents, i.e. by measuring the quantity :

$$\hat{X}_g = \hat{X}_1 - g\hat{X}_2 \tag{16}$$

The conditional variance is equal to the minimum value of $< \delta\hat{X}_g^2 >$ when g is varied.

B. Unbalanced case

In this case the two conditional variances are different, and there are two possible criteria $V_{1|2} < 1$ and $V_{2|1} < 1$. They are not always simultaneously satisfied : there exist situations where $V_{1|2} < 1$ and $V_{2|1} > 1$ for example. This shows that the QND criterion evaluates the correlation from the point of view of one beam, and the information that one can have on this beam from measurements on another one, and does not intrinsically quantize the quantum correlation between the two fields.

It is easy to show that it is enough to have one of the two conditional variances smaller than 1 to have twin beams. In contrast, there are regions of the parameter space where G is smaller than 0.5 and where one of the two conditional variances is bigger than 1.

We will therefore give an "asymmetrical" criterion to characterize this second level of quantum correlation :

$$V_{1|2} < 1 \quad \textbf{or} \quad C_{12} > \sqrt{1 - \tfrac{1}{F_1}}$$

$$\Downarrow$$

Possibility of a QND measurement of beam 1 using the correlation between beams 1 and 2

V. IMPOSSIBILITY OF DESCRIPTION BY A STATISTICAL MIXTURE OF FACTORIZABLE STATES : "INSEPARABLE BEAMS"

We now define a new level in the quantum character of correlations, related to the entangled character of the state, as already stated in the introduction :

Quantum correlation, level 3 : *The correlation arises from a system which can be described only by an entangled or non-separable quantum state.*

Let us first consider the case of a pure state, which is described by a state vector $|\Psi>$. If this vector can be written as a tensor product of states belonging to each Hilbert sub-space (i.e it is not entangled nor non-separable), the mean value of a product of observables $\hat{O}_1$ and $\hat{O}_2$ acting separately in the two sub-spaces (1) and (2) will be the product of the mean value of each observable : there will be therefore no correlations in such a system, whatever the two observables. So, if one finds a non-zero correlation on a single couple of observables, even when this correlation is weak, it is a proof that the system is in an entangled state : correlation implies entanglement for pure cases.

Reciprocally, if the system is described by an entangled state $|\Psi>$ of the form (1), what are the conditions to get a non-zero correlation between two observables $\hat{O}_1$ and $\hat{O}_2$? One knows that $|\Psi>$ can be written in the following form (Schmidt decomposition [23]) :

$$|\Psi>=\sum_j |\psi_{1,j}>\otimes|\psi_{2,j}> \tag{17}$$

where the states $|\Psi_{i,j}>$ belong to the Hilbert space of the sub-system labelled (i) ($i = 1, 2$). Non-zero correlations will happen when, firstly, the measurement on sub-system (1) is performed on an observable $\hat{O}_1$ which has not all the states $|\Psi_{1,j}>$ in the same eigenspace, so that the state reduction due to the measurement changes the total state $|\Psi>$. Secondly, in order to affect the measurement performed on an observable $\hat{O}_2$ on system (2) the states $|\Psi_{2,j}>$ must not be in the same eigenspace of $\hat{O}_2$.

These arguments prove that the presence of entanglement in a pure state does not imply that any couple of observable will be correlated, and, if a correlation between two observables is obtained, it does not imply that the correlation has reached even the level 1 of quantum correlation. The requirement of the quantum description of the correlation (twin beams) is therefore stronger than the requirement of having an entangled state.

The situation is completely different if one allows the system to be in a *statistical mixture of quantum states*, so that it is described by a density matrix instead of a state vector: in this case, the existence of a correlation between two measured quantities does not imply that the system is in an entangled state. A single correlation, even perfect, between a given observable of sub-system (1) and a given observable of sub-system (2) can be obtained with "separable states" in the meaning of [24], i.e. with states that are classical statistical mixtures of factorizable states. They can be written as :

$$\rho = \sum_j p_j |\psi_{1,j}>\otimes|\psi_{2,j}><\psi_{1,j}|\otimes<\psi_{2,j}| \tag{18}$$

with p_j positive real numbers such that $\sum_j p_j = 1$. States which cannot be written as (18) will be called non-separable. They are also named "entangled states" in an extended meaning.

Let us consider as an example the system described by the separable density matrix :

$$\rho = \sum_n p_n |n:1, n:2><n:1, n:2| \tag{19}$$

where $|n:1, n:2>$ is a Fock state with the same number n of photons in the two modes (1) and (2). This state yields a perfect intensity correlation between the two modes, and satisfies the two previous criteria : the correlation C_{12} is 1, and therefore the gemellity G is zero, as well as the conditional variances $V_{1|2}$ and $V_{2|1}$.

Note that the state described by (19) is indeed very "quantum", in spite of not being entangled or non-separable, as it is built from Fock states having exactly the same number of photons in the two modes, which cannot be produced classically, but only through cascade processes, such as parametric down-conversion. We see here that quantum correlations and entanglement are different notions, which are of course related, but not in a straightforward and simple way.

Duan et al. [24] have shown that in order to ascertain the separable character of the physical state of a system, one needs to make *two joint correlation measurements on non-commuting observables* on the system, and not only

one, as was the case in the two previous sections. They have shown that in the case of Gaussian states, there exists a necessary and sufficient criterion of separability in terms of the quantity S_{12}, that we will call "separability", and is given by :

$$S_{12} = \frac{1}{2}\left(\langle\delta(\hat{X}_{+1} - \hat{X}_{+2})^2\rangle + \langle\delta(\hat{X}_{-1} + \hat{X}_{-2})^2\rangle\right) \tag{20}$$

The separability S_{12} appears as the sum of the gemellity G_+ measuring the correlations between real quadrature components of the two beams, and the (anti)gemellity G_- measuring the anticorrelation between the imaginary quadrature component of the same beams (defined with a + instead of a − in equation (**??**)).

The third level of quantum correlation is evaluated by the well-known Duan criterion, which writes :

$$S_{12} < 2$$
$$\Downarrow$$
Quantum correlation arising from an entangled or non-separable state

This criterion allows us to establish some relations between the different levels of quantum correlations that we have already considered.

For example, classical beams will give values larger than 1 for the gemellities measured on any variables, and in particular on $\hat{X}_+$ and $\hat{X}_-$. In this case, the quantity S_{12} is larger than 2, and the two beams are therefore separable. A contrario, non separable beams imply that at least one of the two gemellities is smaller than 1, and therefore that the beams are at least "twins", in intensity or in phase. For quadrature measurements on statistical mixtures of Gaussian states, the non-separability criterion implies that the criterion 1 is fulfilled and is therefore stronger than this latter one. Note that the beams are not necessarily QND-correlated in one of these variables., so that level 2 is not necessarily reached.

Non separable beams are usually prepared by mixing two non-classical states, such as squeezed states, on a beam-splitter [25], but it has been shown [26] that one can generate an entangled state from a single squeezed beam mixed with a coherent state plus some well adapted linear processing of the two output beams.

VI. POSSIBILITY OF QND MEASUREMENT OF TWO CONJUGATE VARIABLES : "EPR BEAMS"

In their famous paper, Einstein, Podolsky and Rosen [27] have exhibited the following wavefunction for the continuous variables position $\hat{x}_i$ and momentum $\hat{p}_i$ $(i = 1, 2)$ of two particles :

$$\psi(x_1, x_2) = \int_{-\infty}^{+\infty} e^{ip(x_1 - x_2 + x_0)/\hbar} dp \tag{21}$$

where x_0 is a constant, and shown that it provides perfectly correlated position measurements and perfectly anti-correlated momentum measurements of the two particles. This state, which is obviously entangled, can be readily transferred in the domain of quadrature operators of two light modes [28]. In quantum optics terms, it allows us to perform perfect QND measurements of the two quadrature components of mode 1, by measurements performed only on beam 2. This perfect information that one eventually gets on the two quadratures of the field apparently contradicts the fact that these measurements are associated to two non-commuting operators, and therefore obey a Heisenberg inequality.

We now reach a fourth level in the quantum character of the correlations :

Quantum correlation, level 4 : *The information extracted from the measurement of the two quadratures of one field provides values for the quadratures of the other which violate the Heisenberg inequality*

This situation has been extensively considered and discussed by M. Reid and co-workers [28, 29], which have shown that this violation is only apparent, and does not violate the basic postulate of Quantum Mechanics. They have introduced the following criterion to characterize this fourth level of quantum correlation of the so-called "EPR beams" :

$$V_{X_{+1}|X_{+2}} V_{X_{-1}|X_{-2}} < 1$$
$$\Downarrow$$
Possibility of an apparent violation of the Heisenberg inequality for the quadratures components of beam 1 through measurements performed on beam 2

where $V_{X_{+1}|X_{+2}}$ is the conditional variance of X_{+1} knowing X_{+2}, and $V_{X_{-1}|X_{-2}}$ is the conditional variance of X_{-1} knowing X_{-2}.

This condition is related somehow to the QND-correlated beams of section 4. It can be written in terms of the normalized correlation $C_{X_{+1}X_{+2}}$ and anticorrelation $C_{X_{-1}X_{-2}}$:

$$\left(1 - C^2_{X_{+1}X_{+2}}\right)\left(1 - C^2_{X_{-1}X_{-2}}\right) > \frac{1}{F_+F_-} \tag{22}$$

where F_+ and F_- are the noise variance on quadratures + and − normalized to shot noise (fulfilling $F_+F_- > 1$).

The EPR correlation turns out to be stronger than the non-separability correlation, in the same way as the QND criterion of section 4 is stronger than the non-classical criterion of section 3 : it has been shown [30] that all EPR beams are non-separable, whereas the reverse is not true. In the same article, *Bowen et al.* show that for pure states the two criteria correspond to the same physical states. However, *Duan* criteria is robust with respect to the mixed character of the fields states, whereas the EPR criteria can not be fulfilled in the presence of more than 50% of losses. Let us stress that this behaviour is linked to the *no-cloning* theorem : it has been proved that linear amplification and a 50/50 beam-splitter produces the best possibles two copies (clones) of any input state [31]. Hence, when two beams are EPR correlated, i.e. that less than 50% losses are present, on a quantum information point of view we are sure than no spy has a better copy of the state. This is in the same way relevant for the success of teleportation [32].

VII. IMPOSSIBILITY OF DESCRIPTION OF THE MULTIPLE CORRELATION BY LOCAL CLASSICAL STOCHASTIC VARIABLES : "BELL BEAMS"

Quantum fluctuations can be mimicked in many instances by classically-looking stochastic supplementary variables. This is the case in particular when one uses the approach of "vacuum fluctuations", behaving as classical fluctuations, but with a variance given by quantum mechanics and carrying no energy. This is to be distinguished from the classical stochastic fields, originating from the uncontrolled variations of the classical parameters of the light source. Bell [33] has shown that such a stochastic modelling was not likely to reproduce all the correlations that can be encountered in quantum mechanical systems when these supplementary stochastic variables (usually named "hidden variables") were local, i.e. attached to the sub-system under measurement. He introduced inequalities fulfilled by any local hidden variable models, and violated in some very specific situations of quantum mechanical correlated systems.

We must therefore introduce a new level of quantum correlations :

Quantum correlation, level 5 : *The multiple correlations of the system cannot be described by local hidden variable approaches*

The corresponding criterion for this level of quantum correlation is the celebrated Bell inequality [33]. We will not go into the details of it here for the following reason : one shows in Quantum Optics that all phenomena can be described through the use of quasi-probability distributions [1, 7], such as the Wigner representation or others. For the special case of light beams having a Gaussian statistics, which the case of all the physical situations encountered so far in the regime of continuous variables in optics, the Wigner representation is everywhere positive : the quasi-probability distribution becomes a true probability distribution, the evolution of which can be mapped into stochastic equations for fluctuating fields : these stochastic fields constitute in this case the local "hidden" variables which account for all the observed quantity, including the variances and the correlations between measurements. This means that there is never a violation of the Bell inequality in the continuous variable regime with Gaussian states, and the level 5 of quantum correlations is never reached in this case.

To reach it, one needs to deal with non Gaussian states, with partly negative Wigner functions, such as the Fock states, Schrödinger cat states [34], or states produced through conditional non-Gaussian measurements like photon-counting. The discussion of such situations is beyond the scope of this simple introductory paper on quantum correlations.

VIII. CONCLUSION

The exploration of the quantum world, in which professor Walther has undoubtedly played a major role, has unveiled physical situations which are looking more and more strange for an observer only acquainted to the certainties of classical physics. We have tried in this short review to assess and classify the "degree of oddness" of quantum optical phenomena. In the last decades, theoreticians and experimentalists have gone higher and higher in such a ladder of

pure quantum effects. There is no doubt that they are far from reaching the top of the quest, and that new heights of even stranger quantum properties will be attained in the future.

IX. ACKNOWLEDGMENTS

We would like to thank Philippe Grangier and Thomas Coudreau for fruitful discussions. Laboratoire Kastler Brossel, of the Ecole Normale Supérieure and University Pierre et Marie Curie, is associated to CNRS. This work has been supported by the European Union in the frame of the QUANTIM network (contract IST 2000-26019).

[1] Bachor H.A., Ralph T.C., 2004, *A guide to experiments in quantum optics* (Wiley-VCH)
[2] Fano U., 1947, Phys. Rev. **72**, 26
[3] Julsgaard B., Kozekhin A.,Polzik E.S., 2000, Nature (London) **413** 400
[4] Dantan A., Pinard M., 2004, Phys. Rev. A **69**, 043810
[5] Einstein A., 1905, Annalen der Physik **17** 132
[6] Mandel L., Wolf E., 1995, *Optical coherence and quantum optics* (Cambridge University Press)
[7] Walls D.F., Milburn G.J., 1994, *Quantum Optics*(Springer-Verlag)
[8] Kimble H.J., Dagenais M., Mandel L., 1977, Phys. Rev. Letters **39**, 691
[9] Cresser J.D., Haeger J., Leuchs G., Rateike M., Walther H., 1983, *Dissipative systems in quantum optics*, p.21, R. Bonifacio ed., (Springer Verlag)
[10] Diedrich F., Walter H., 1987, Phys. Rev. Lett. **58**, 203
[11] Loudon R., 1973, *Quantum theory of light* (Oxford University Press)
[12] Heidmann A., Horowicz R.J., Reynaud S., Giacobino E., Fabre C., Camy G., 1987, Phys. Rev. Letters *59*, 2555
[13] Aytur O, Kumar P., 1990, Phys. Rev. Letters **65**, 1551
[14] Slusher R., Hollberg L., Yurke B., Mertz J., Valley J., 1985, Phys. Rev. Letters **55**, 2409
[15] Ou Z.Y., Pereira S.F., Kimble H.J., Peng K.C., 1992, Phys. Rev. Letters **68**, 3663
[16] Laurat J., Longchambon L., Coudreau T., Keller G., Treps N., Fabre C., 2004, "Experimental Generation of Quadrature Entanglement with a Self-Phase-Locked ND-OPO Below Threshold", preprint
[17] Laurat J., Coudreau T., Keller G., Treps N., Fabre C., 2004, "Compact source of EPR entanglement and squeezing at very low noise frequencies", quant-ph/0403224
[18] Martinelli M., Treps N., Ducci S., Gigan S., A. Maître, Fabre C., 2003, Phys. Rev. A **67**, 023808
[19] Romanelli M., Giacobino E., Bramati A., 2004, Opt. Lett. **29**, 1629
[20] Karr J. Ph., Baas A., Giacobino E., 2004, Phys. Rev. A **69**, 063807
[21] Grangier P., Courty J.M., Reynaud S., 19912, Optics Commun. **89**, 99
[22] Poizat J.P., Roch J.F., Grangier P., 1994, Ann. Phys. Fr. **19**, 265
[23] Knight P.L., 1997, *Quantum fluctuations in optical systems*, Les Houches Session 63, p. 1, S. Reynaud, E. Giacobino, J. Zinn-Justin eds. (North-Holland)
[24] Duan L.M., Giedke G., Cirac I., Zoller P., 2000, Phys. Rev. Lett. **84**, 2722
[25] Furusawa A., Sorensen J.L., Braunstein S., Fuchs C.A., Kimble H.J., Polzik E.S., 1998, Science **282**, 706
[26] Bowen W.P., Lam P.K., Ralph T.C., 2003, Journ. of Mod. Opt. **50**, 801
[27] Einstein A., Podolsky B., Rosen N., 1935, Phys. Rev. **47**,777
[28] Reid M., Drummond P., 1989, Phys. Rev. Lett. **60**, 2731
[29] Reid M., Drummond P., 1991, Phys. Rev **A41**, 3930
[30] Bowen W.P., Schnablel R., Lam P.K., Ralph T.C., 2004, Phys. Rev. A, **69**, 012304
[31] Cerf N.J., Ipe A., Rottenberg X., 2000, Phys. Rev. Lett. **85**, 1754
[32] Grosshans F., Grangier P., 2001, Phys. Rev. A **64**, 010301
[33] Bell J., 1965, Physics, **1**, 195
[34] Yurke B., Stoler D., 1986, Phys. Rev. Lett. **57**, 13

VOLUME 91, NUMBER 21 PHYSICAL REVIEW LETTERS week ending 21 NOVEMBER 2003

Conditional Preparation of a Quantum State in the Continuous Variable Regime: Generation of a sub-Poissonian State from Twin Beams

J. Laurat, T. Coudreau,*,† N. Treps, A. Maître,* and C. Fabre

Laboratoire Kastler Brossel, UPMC, Case 74, 4 Place Jussieu, 75252 Paris Cedex 05, France

(Received 16 April 2003; published 18 November 2003)

We report the first experimental demonstration of conditional preparation of a nonclassical state of light in the continuous variable regime. Starting from a nondegenerate optical parametric oscillator which generates above threshold quantum intensity correlated signal and idler "twin beams," we keep the recorded values of the signal intensity only when the idler intensity falls inside a band narrower than its standard deviation. By this very simple technique, we generate a sub-Poissonian state 4.4 dB (64%) below shot noise from twin beams exhibiting 7.5 dB (82%) of noise reduction in the intensity difference.

DOI: 10.1103/PhysRevLett.91.213601 PACS numbers: 42.50.Dv, 42.65.Yj

A well-known technique to generate a single photon state from quantum correlated photons ("twin photons") is to use the method of conditional measurement: if one labels (1) and (2) the two modes in which the twin photons are emitted, it consists of retaining in the information collected on mode (1) only the counts occurring when a photon is detected in mode (2) (within a given time window ΔT). This method has been widely and very successfully used over the past decades, first with twin photons generated by an atomic cascade [1], then by using the more efficient technique of parametric down-conversion [2]. Various protocols have been proposed to use conditional preparation in order to generate other kinds of nonclassical states, for example, Schrödinger cat states using a squeezed vacuum state transmitted through a beam splitter and a measurement conditioned by the counts detected on the reflected port [3]. In a similar way, teleportation of a quantum state of light can be achieved by using conditional measurements [4] and the degree of entanglement can be improved by photon subtractions [5]. In cavity QED, conditional measurements on the atomic state have also led to the experimental generation of nonclassical photon states [6].

State reduction is obviously not restricted to the case of photon counting, so that it may be interesting to extend this technique to the continuous variable regime, where a continuously varying photocurrent is measured instead of a series of photocounts. Continuous detection conditioned by a photon counting event has been implemented in various schemes [7]. Closer to our proposal where continuous measurements are used both for triggering and characterizing the generated state, many theoretical protocols have been suggested relying on a two-mode squeezed vacuum produced by a nondegenerate optical parametric amplifier [8,9]. For instance, homodyne measurements on the idler can be used to condition the detection of the signal and would reduce it to a squeezed state [8].

In a conditional state preparation, the generation of the nonclassical state can be seen as the collapse of the entangled wave function induced by the measurement on one of its components. However, very frequently, the measurement is made by postselection of the relevant events in the record of all the values measured on the two channels, which can be made after the end of the physical measurement, so that no wave-function collapse actually occurs during the experiment. Note that, in contrast to the methods of direct generation of a nonclassical state, the exact time window when the state is produced is not controlled in a conditional measurement, and what we call the "preparation probability," i.e., the probability of generating the nonclassical state in a given time interval, is an important parameter to characterize its efficiency.

To the best of our knowledge, no scheme has been suggested so far to generate nonclassical intense beams by the technique of conditional measurement performed on continuous variables. This is the purpose of the present Letter, which proposes a very simple way of conditionally preparing a bright sub-Poissonian beam from twin beams, and reports on its experimental implementation. The theory of the presented technique will be detailed in a forthcoming publication [10].

It is well-known that a nondegenerate optical parametric oscillator (ND-OPO) produces above threshold an intense signal and idler twin beams [11]: in the ideal case of a system without losses, the Fourier components of the signal and idler intensity quantum fluctuations which lie inside the cavity bandwidth are perfectly correlated. The correlations are characterized by the "gemellity," which is the remaining noise on the intensity difference between the signal and idler intensities normalized to the corresponding quantum noise level [12]. The instantaneous values of the signal and idler photocurrents play therefore the role of the occurrence of counts in the photon counting regime. The conditional technique that we propose consists of selecting the signal

photocurrent I_s only during the time intervals when the idler intensity I_i has a given value I_0 (within a band ΔI smaller than the photocurrent standard deviation). The measurements outside these time intervals are discarded. If the correlation is perfect and the interval ΔI close to zero, the recorded signal intensity is perfectly constant, and an intense number state is generated.

In a real experiment, the correlation between the signal and idler photocurrents is not perfect, and the selection band ΔI is finite, so that the method will not prepare a perfect number state, but a sub-Poissonian state instead. The density matrix describing the state of light which is produced by such a state reduction technique can be determined within the approximation that the signal and idler photon distributions are Gaussian [10]. In the limit where ΔI is very small, one finds that, whatever the initial intensity noise of the beams are, the conditional measurement produces a sub-Poissonian signal beam, characterized by a Fano factor equal to the conditional variance of the intensity fluctuations of the signal beam knowing the intensity fluctuations of the idler beam, which plays an important role in the characterization of quantum nondemolition measurements [13]. In other words, in the limit of large correlations, the intensity noise reduction on the conditionally prepared state is equal to the twin beam noise reduction minus 3 dB.

Obviously, if ΔI is very small, the probability that the idler intensity lies within the chosen band is also very small, and the preparation probability of the nonclassical state production by such a conditional measurement is also very low. Computer simulations, as well as analytical calculations [10], show that the Fano factor of the generated state remains almost constant in a wide range of ΔI values, whereas the preparation probability of the method increases quickly. It is only when ΔI reaches values comparable to the shot noise standard deviation that the postselection process becomes less efficient, and the Fano factor tends to its uncorrected value.

The present conditional measurement technique has strong analogies with the method of active feed-forward correction of the signal beam intensity, by optoelectronics techniques, using the information obtained from the measurement of the idler intensity [14,15], which produces a sub-Poissonian state with a Fano factor also equal to the conditional variance. The present technique is much simpler to implement, whereas the active correction technique is nonconditional and has the advantage of producing the nonclassical state at all times.

The experimental setup is shown in Fig. 1. A continuous frequency-doubled Nd:YAG laser pumps a triply resonant ND-OPO above threshold, made of a semimonolithic linear cavity: in order to increase the mechanical stability and reduce the reflection losses, the input flat mirror is directly coated on one face of the 10-mm-long KTP crystal. The reflectivities for the input coupler are 95.5% for the pump (532 nm) and almost 100% for the

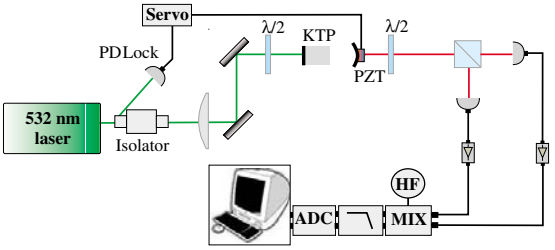

FIG. 1 (color online). Experimental layout. The 1064 nm orthogonally polarized bright twin beams generated by the ND-OPO are separated by a polarizing beam splitter and detected. The high frequency components of the photocurrents are amplified and demodulated at a given Fourier frequency. The two channels are digitized and simultaneously recorded on a computer.

signal and idler beams (1064 nm). The output coupler ($R = 38$ mm) is highly reflecting for the pump and its transmission is 5% for the infrared. At exact triple resonance, the oscillation threshold is less than 15 mW. The OPO is actively locked on the pump resonance by the Pound-Drever-Hall technique: we detect by reflection a remaining 12 MHz modulation present in the laser and the error signal is sent to a homemade proportional-integral controller. In order to stabilize the OPO infrared output intensity, the crystal temperature has to be drastically controlled (within a mK). The OPO can operate stably during more than one hour without mode hopping. The signal and idler orthogonally polarized beams (1–5 mW range) generated by the OPO are then separated by a polarizing beam splitter and detected on a pair of balanced high quantum efficiency InGaAs photodiodes (Epitaxx ETX300, quantum efficiency: 95%). A half-wave plate is inserted before the polarizing beam splitter. When the polarization of the twin beams is turned by 45° with respect to its axes, it behaves as a 50% usual beam splitter, which allows us to measure the shot noise level [11].

In almost all the bright twin beam experiments to date [11], the photocurrents are subtracted and the difference is sent onto a spectrum analyzer which gives the variance of the photocurrent distribution. We have implemented a different protocol to have access to the full photon-number quantum statistics of the signal and idler beams at a given Fourier frequency Ω (see also [16]): each photocurrent is amplified and multiplied by a sinusoidal current at frequency Ω produced by a signal generator, and filtered by a 22 kHz low-pass filter in order to obtain the instantaneous value of the photocurrent Fourier component at frequency Ω, which is then digitized at a sampling rate of 200 kHz by a 12-bit, 4-channel acquisition card, which also simultaneously records the instantaneous values of the dc photocurrents. Two successive acquisitions (200 000 points for each channel) are required, one for calibrating the shot noise by rotating the

VOLUME 91, NUMBER 21 PHYSICAL REVIEW LETTERS week ending 21 NOVEMBER 2003

half-wave plate and the other to record the quantum correlated signals.

Figure 2 sums up the measurements obtained with a demodulation frequency $\Omega/2\pi = 3.5$ MHz. Figure 2(a) shows the actual recording of the fluctuations of the idler beam during a time interval of 100 ms. As the OPO is pumped close to threshold, the signal and idler beams have intensity fluctuations which are much larger than the standard quantum limit, as can be seen on curve 2(b), giving the probability distribution of the intensity fluctuations normalized to the shot noise. The corresponding Fano factor exceeds 100 (20 dB above the shot noise level). One can calculate the noise variance on the difference between the signal and idler intensities. It reaches a value of 7.5 dB below the standard quantum limit (8.5 dB after correction of dark noise), in good agreement with the value of the noise variance measured on the spectrum analyzer. The dark noise, which is more than 6 dB below all measurements, is not subtracted in the following experimental results.

The conditional measurement is performed in the following way: the signal intensity values are kept only if the idler intensity values recorded at the same time fall inside a narrow band around its mean value. The remaining ensemble of values of the signal intensity is given in Fig. 2(c), in which the shot noise is given at the same time: one indeed observes a significant narrowing of the probability distribution below the shot noise level. Let us

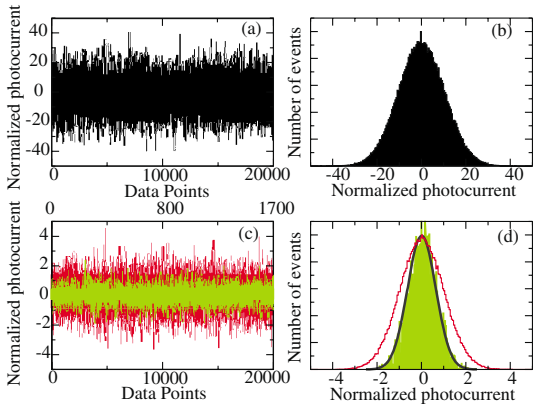

FIG. 2 (color online). Experimental results: (a) idler intensity fluctuations: 200 000 acquired points at 3.5 MHz demodulation frequency (only 20 000 shown). (b) Corresponding probability distribution. The unit is the width σ_0 of the Poisson distribution of the same mean intensity (shot noise). (c) Values of the signal intensity conditionally selected by the value of the idler intensity recorded at the same time (selection bandwidth ΔI equal to $0.2\sigma_0$ around the mean), superimposed to the corresponding experimentally measured shot noise. (d) Corresponding probability distribution, compared to the Poisson distribution (grey line), displaying the sub-Poissonian character of the conditionally generated state. The black line is a Gaussian fit of the intensity distribution.

stress that the shot noise is unchanged by this selection process: the beam exists only in the selection intervals so that the unselected intervals do not contribute to the average value. Figure 2(d) gives the probability distribution of the intensity fluctuations of the conditionally prepared state normalized to the shot noise, together with the Poissonian distribution of photons for the same mean intensity. With a selection bandwidth ΔI equal to 0.2 times the standard deviation σ_0 of a coherent state having the same power (shot noise level), the conditionally prepared light state exhibits 4.4 dB of noise reduction below the Poisson distribution. This value is very close to the theoretical expectation in the case of a vanishingly narrow intensity band. The preparation probability of the conditional preparation is around 0.85% (1700 points out of 200 000 are accepted). This value would be higher for an initial state with less excess noise.

The preparation probability can be improved by increasing the selection bandwidth, at the expense of a decreased nonclassical character of the selected state. Figure 3 shows the measured residual noise in the conditionally produced state, and the preparation probability of the state generation, as a function of the selection bandwidth normalized to σ_0. The noise reduction turns out to be almost constant until the normalized selection bandwidth becomes of the order of 0.1, whereas the preparation probability steadily increases, in very good agreement with numerical simulations. However, one can see a slight increase in the noise when the selection bandwidth becomes very narrow. This artifact is due to the sampling process on a finite range of bits, which restricts the resolution of the acquisition.

In Fig. 4, we give the measured residual noise for different amounts of intensity correlations between the beams, which can be varied by inserting losses on the OPO beams. One checks on the figure the validity of the prediction that the noise reduction is equal to the

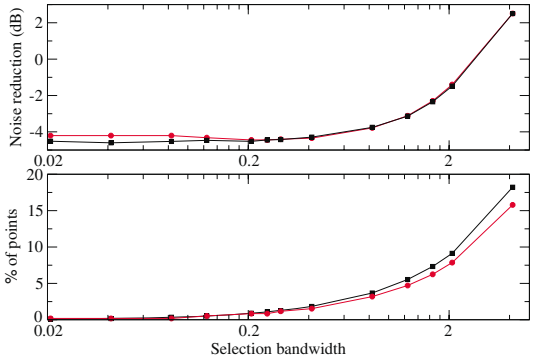

FIG. 3 (color online). Measured intensity noise on the post-selected signal (a) and preparation probability (proportion of selected points) (b) as a function of the selection bandwidth on the idler normalized to σ_0. Circles: experimental data. Squares: theoretical predictions.

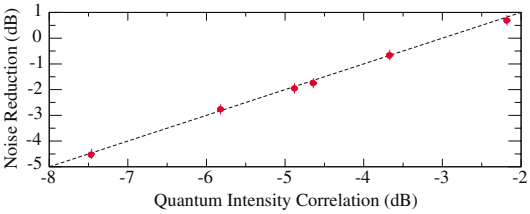

FIG. 4 (color online). Measured intensity noise reduction for different values of the signal-idler correlation. The selection bandwidth is taken equal to 0.2 times the shot noise. Circles: experimental data. Dotted line: theoretical prediction at the limit of a very small selection bandwidth (gemellity minus 3 dB).

gemellity minus 3 dB. One also observes that, when the intensity difference noise is reduced by less than 3 dB below the standard quantum level, the conditional state has reduced intensity noise fluctuations in comparison with the very noisy initial beam, but that it is not a nonclassical sub-Poissonian state.

The continuous variable regime offers a unique possibility to improve dramatically the efficiency of conditional strategy, by choosing multiple selection bands with different mean values on the idler intensity. Independent selection bands will correspond to independent sets of time windows. By using hundreds of independent intervals, one keeps most of the values of the signal, each of these intervals reducing the signal to a given sub-Poissonian state. Figure 5 shows that the noise reduction does not depend of the band center and that the preparation probability follows the initial Gaussian noise distribution.

To conclude, we have shown the first experimental demonstration of conditional preparation of a quantum state in the continuous variable regime. We have studied the influence of the selection bandwidth on the obtained nonclassical state and on the preparation probability of its preparation and shown that many sub-Poissonian states can be produced in parallel. This method to generate nonclassical states of light in the continuous variable regime is equivalent to sending the signal beam through an intensity modulator which either totally transmits the beam when the idler beam has the right value, or blocks it when it is not the case. It therefore drastically changes the light state and seems to be very different from the usual technique which consists of correcting the beam fluctuations by a feed-forward or feedback optoelectronic loop which only slightly modifies the quantum fluctuations. This strongly nonlinear character of the action on the light may lead to the generation of non-Gaussian states. One could also envision other criteria of conditioning the quantum state than simply imposing to the idler beam intensity to lie within a given band. This could also lead to the generation of new families of nonclassical bright states of light.

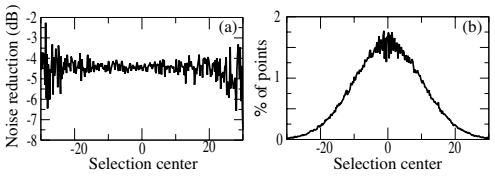

FIG. 5. Measured intensity noise on the reduced state (a) and preparation probability (b) as a function of the band center normalized to σ_0. The selection bandwidth is taken equal to 0.4 times the shot noise.

Laboratoire Kastler-Brossel, of the Ecole Normale Supérieure and the Université Pierre et Marie Curie, is associated with the Centre National de la Recherche Scientifique (UMR 8552). We acknowledge support from the European Commission project QUICOV (IST-1999-13071) and from ACI Photonique (Ministère de la Recherche).

*Also at the Pôle Matériaux et Phénomènes Quantiques FR CNRS 2437, Université Denis Diderot, Paris, France.
†Electronic address: coudreau@spectro.jussieu.fr

[1] P. Grangier, G. Roger, and A. Aspect, Europhys. Lett. **1**, 173 (1986).
[2] C. K. Hong and L. Mandel, Phys. Rev. Lett. **56**, 58 (1986).
[3] M. Dakna *et al.*, Phys. Rev. A **55**, 3184 (1997).
[4] C. H. Bennett *et al.*, Phys. Rev. Lett. **70**, 1895 (1993); D. Bouwmeester *et al.*, Nature (London) **390**, 575 (1997).
[5] T. Opatrny, G. Kurizki, and D. G. Welsch, Phys. Rev. A **61**, 032302 (2000); P. T. Cochrane, T. C. Ralph, and G. J. Milburn, Phys. Rev. A **65**, 062306 (2002).
[6] J.-M. Raimond, M. Brune, and S. Haroche, Rev. Mod. Phys. **73**, 565 (2001).
[7] G. T. Foster *et al.*, Phys. Rev. Lett. **85**, 3149 (2000); A. I. Lvovsky *et al.*, Phys. Rev. Lett. **87**, 050402 (2001).
[8] K. Watanabe and Y. Yamamoto, Phys. Rev. A **38**, 3556 (1988); J. Fiurásek, Phys. Rev. A **64**, 053817 (2001).
[9] G. M. D'Ariano *et al.*, Phys. Rev. Lett. **83**, 2490 (1999).
[10] J. Laurat, T. Coudreau, N. Treps, A. Maître, and C. Fabre (to be published)
[11] A. Heidmann *et al.*, Phys. Rev. Lett. **59**, 2555 (1987); J. Mertz *et al.*, Opt. Lett. **16**, 1234 (1991); J. Gao *et al.*, Opt. Lett. **23**, 870 (1998).
[12] S. Reynaud, C. Fabre, and E. Giacobino, J. Opt. Soc. Am. B **4**, 1520 (1987)
[13] P. Grangier, J.-M Courty, and S. Reynaud, Opt. Commun. **83**, 251 (1991); J.-Ph Poizat, J. F. Roch, and P. Grangier, Ann. Phys. (Paris) **19**, 265 (1994).
[14] J. Mertz *et al.*, Phys. Rev. Lett. **64**, 2897 (1990)
[15] J. Mertz, A. Heidmann, and C. Fabre, Phys. Rev. A **44**, 3229 (1991)
[16] Y. Zhang, K. Kasai, and M. Watanabe, Opt. Lett. **27**, 1244 (2002); M. Martinelli *et al.*, Phys. Rev. A **67**, 023808 (2003).

PHYSICAL REVIEW A **70**, 042315 (2004)

Compact source of Einstein-Podolsky-Rosen entanglement and squeezing at very low noise frequencies

J. Laurat,[1] T. Coudreau,[1,2,*] G. Keller,[1] N. Treps,[1] and C. Fabre[1]
[1]*Laboratoire Kastler Brossel, UPMC, Case 74, 4 place Jussieu, 75252 Paris Cedex 05, France*
[2]*Laboratoire Matériaux et Phénomènes Quantiques, Université Denis Diderot, 2 place Jussieu, 75251 Paris Cedex 05, France*
(Received 30 March 2004; published 25 October 2004)

We report on the experimental demonstration of strong quadrature Einstein-Podolsky-Rosen entanglement and squeezing at very low noise sideband frequencies produced by a single type-II, self-phase-locked, frequency degenerate optical parametric oscillator below threshold. The generated two-mode squeezed vacuum state is preserved for noise frequencies as low as 50 kHz. Designing simple setups able to generate nonclassical states of light in the kHz regime is a key challenge for high sensitivity detection of ultraweak physical effects such as gravitational wave or small beam displacement.

DOI: 10.1103/PhysRevA.70.042315 PACS number(s): 03.67.Mn, 04.80.Nn, 42.50.Dv, 42.50.Lc

Since the pioneering work of Caves [1], which showed that it is possible to improve the sensitivity of interferometric measurements by the use of squeezed light, and its experimental demonstrations [2], various protocols involving squeezed light have been discussed in order to beat the standard quantum limit in gravitational wave detectors [3]. As next generations of gravitational wave detectors will be designed to be shot noise limited in the acoustic band from 10 Hz to 10 kHz, such techniques appear as quite promising ways to improve their sensitivity. Recently, a squeezing-enhanced power-recycled Michelson interferometer has been experimentally demonstrated and signal-to-noise ratio improvement obtained [4]. However, the injected squeezing bandwidth lies around 5 MHz and not in the frequency band of gravitational waves. A source of low-frequency squeezing is thus a key point for the implementation of future squeezed-input interferometers.

More generally, many high sensitivity measurements performed at low modulation frequency can benefit from such a device. In [5], a "quantum laser pointer" has been experimentally demonstrated and an improvement of modulated small displacement measurements in two orthogonal directions in the transverse plane has been reported. Improved beam positioning sensitivity below the shot-noise limit is obtained at the frequency where squeezing is available, a few MHz in the case of this experiment. Two sources of low-frequency squeezing are needed to apply this promising displacement measurement technique to actual instruments where frequency modulation is generally low. This could be applied, for instance, to AFM microscopy in the tapping mode where the cantilever oscillates at its resonant frequency which is typically a few hundreds of kHz. Such a squeezing source should also improve the thermo-optical spectroscopy technique called the "mirage effect" [6], which enables the measurement of very weak absorption: a thermo-optical modulation on a sample induces a periodic refractive index gradient and results in a low-frequency modulated probe beam deflection.

Broadband and low-frequency squeezing is also very useful even if the information is not carried by a single frequency modulation. When a beam is detected during a finite time, the signal-to-noise ratio depends on the noise in an extended range of sideband frequencies. Broadband squeezing with a cutoff frequency as low as possible is thus required. A great number of measurements can be improved in that way, for instance the detection of weak pulsed signals or the reduction of the bit error rate in the readout of digitized optical information.

In [7], quantum noise reduction on the intensity difference of twin beams has been observed down to 90 kHz. However, only two experiments to date have demonstrated continuous-wave squeezing at low frequencies. Both experiments are based on an optical noise cancellation scheme where sources of squeezing are inserted within a Mach-Zehnder interferometer: squeezing has been obtained around 220 kHz with a pair of independent optical parametric amplifiers (OPA) [8] and very recently around 100 kHz with a single OPA [9]. This frequency range is rather unusual in the experimental quantum optics field where nonclassical properties are generally observed in the MHz range due to the presence of large classical noise at lower frequencies. In this paper, we report on what is to our knowledge the first experimental demonstration of very-low-frequency continuous-wave squeezing without the need of an optical noise cancellation scheme. Broadband vacuum squeezing is observed for frequencies down to 50 kHz. Furthermore, our setup generates not only single-mode squeezing but also Einstein-Podolsky-Rosen (EPR) entanglement, which is a basic requisite in quantum information protocols such as teleportation, dense-coding, or optical-atomic interfacing [10].

Our setup relies on a frequency degenerate type-II phase-matched optical parametric oscillator (OPO) below threshold, in which a quarter-wave plate inserted in the cavity adds a linear coupling between the signal and idler fields. In this paper, we focus on the case where the plate is rotated by a very small angle (smaller than 0.02°) relative to the principal axis of the nonlinear crystal. In such a configuration, the signal and idler modes are entangled: they show quantum correlations and anticorrelations on orthogonal quadratures

*Electronic address: coudreau@spectro.jussieu.fr

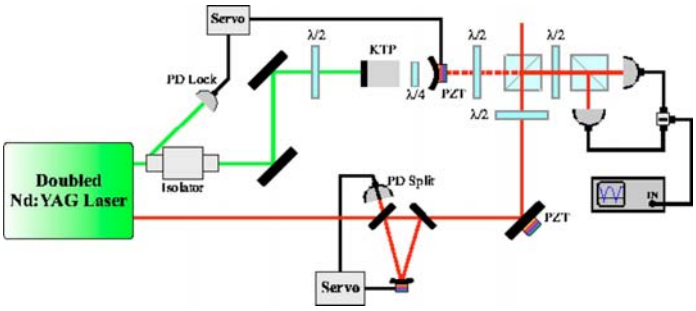

FIG. 1. Experimental layout. A continuous frequency-doubled Nd:YAG laser pumps below threshold a frequency degenerate type-II phase-matched OPO with a quarter-wave plate inserted inside the cavity. The generated two-mode state is characterized by homodyne detection and the difference of the photocurrents is sent onto a spectrum analyzer. PD Lock: FND-100 photodiode for locking of the OPO. PD Split: split two-element InGaAs photodiode for tilt-locking of the filtering cavity.

for noise frequencies inside the bandwidth of the cavity. This nonclassical behavior exists also without the plate. However, the linear coupling—even for a plate rotated by a very small angle—facilitates the finding of experimental parameters for which entanglement is observed. When our setup is operated above threshold, frequency degenerate operation is obtained in a small locking zone and not only for a precise value of experimental parameters [11], which corresponds also to the required parameters below threshold. When this zone is found, the OPO can be operated below threshold and the entanglement is maximized by fine tuning of the crystal temperature. Furthermore, the degenerate operation with bright beams opens the possibility to match the homodyne detection without infrared injection of the OPO. In prior experiments with KTP crystals and green pump, the pairing of crystals in order to compensate walk-off [2] or using α-cut KTP for noncritical phase matching and frequency-doubled Nd:YAP laser [12] was necessary to generate entangled states of light.

Instead of directly measuring the quantum correlations and anticorrelations of the signal and idler fields, A_1 and A_2, we characterize the noise of the superposition modes oriented ±45° from the axes of the crystal,

$$A_+ = \frac{A_1 + A_2}{\sqrt{2}}, \quad A_- = \frac{A_1 - A_2}{\sqrt{2}}.$$

These two modes have squeezed fluctuations due to the correlations and anticorrelations between signal and idler fields. The amount of entanglement between signal and idler can be inferred from the amount of squeezing available on these superposition modes. We have developed in [13] a theoretical study of this original device named "self-phase-locked OPO" in the above-threshold regime. Below threshold, theoretical and experimental behavior for various birefringent plate angles will be reported on in a forthcoming paper [14].

The experimental setup is shown in Fig. 1. A continuous-wave frequency-doubled Nd:YAG laser ("Diabolo" without option "noise eater," Innolight GmbH) pumps a triply resonant type-II phase-matched OPO, made of a semimonolithic linear cavity: in order to increase the mechanical stability and reduce the reflection losses, the input flat mirror is directly coated on one face of the 10-mm-long KTP crystal (θ=90°, φ=23.5°, Raicol Crystals Ltd.). The reflectivities for the input coupler are 95.5% for the pump at 532 nm and close to 100% for the signal and idler beams at 1064 nm. The output coupler with a radius of curvature of 38 mm is highly reflecting for the pump and its transmission is 5% for the infrared. A birefringent plate—$\lambda/4$ for the infrared and almost λ for the pump—is inserted inside the cavity. Rotation as small as 0.01° can be obtained thanks to a rotating mount controlled by a piezoelectric actuator. At exact triple resonance and for a very small angle of the plate relative to the axes of the crystal, the oscillation threshold is less than 20 mW, close to the threshold without the plate [15]. The OPO is actively locked on the pump resonance by the Pound-Drever-Hall technique: we detect by reflection a 12 MHz modulation and the error signal is sent to a home-made proportional-integral controller. The OPO can operate stably during more than one hour without mode-hopping using a drastic control of the crystal temperature within the mK range and an optical table isolated from floor vibrations by pneumatic feet (Newport I-2000).

The 1064 nm laser output is used as a local oscillator for homodyne detection of the generated state. This beam is spatially filtered and intensity-noise cleaned by a triangular-ring 45-cm-long cavity with a high finesse of 3000, which is locked on the maximum of transmission by the tilt-locking technique [16]. The homodyne detection is based on a pair of balanced high quantum efficiency InGaAs photodiodes (Epitaxx ETX300, quantum efficiency: 95%) and the fringe visibility reaches 0.97. The shot noise level of all measurements is easily obtained by blocking the output of the OPO. A half-wave plate inserted at the output of the OPO, just before the first polarizing beam splitter of the homodyne detection, enables us to choose the field to characterize signal or idler modes which are entangled, or the ±45° rotated modes which are squeezed. The homodyne detection can be locked on the squeezed quadrature during more than an hour using a standard dither and lock technique. The error signal is extracted from the demodulated noise at a given frequency after envelope detection.

Figure 2 shows the experimental broadband noise reduction observed in the ±45° vacuum modes for frequencies between 300 kHz and 10 MHz. One observes that these two modes are squeezed well below the standard quantum limit, except around 1 MHz, where the narrow peak of excess noise is due to the relaxation oscillation of the laser. One can note that this excess is less important on the mode A_+, which is sensitive to phase noise of the laser. A noise eater implemented on the Nd:YAG laser should permit us to largely

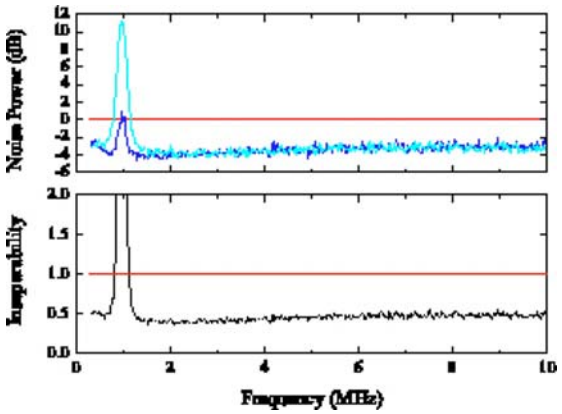

FIG. 2. Normalized noise variances from 300 kHz to 10 MHz of the ±45° vacuum modes and inseparability criterion for signal and idler modes defined as the half-sum of the previous squeezed variances. The resolution bandwidth is set to 100 kHz and the video bandwidth to 300 Hz.

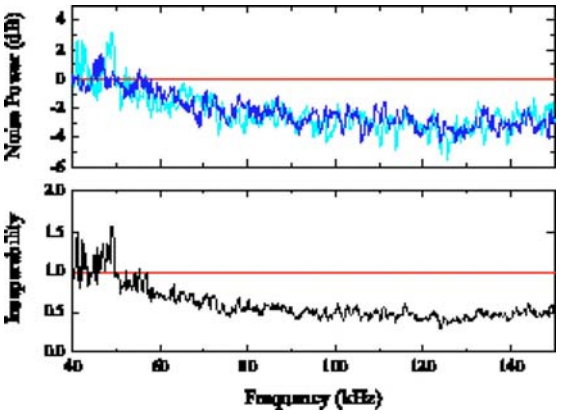

FIG. 3. Normalized noise variances from 40 kHz to 150 kHz of the ±45° vacuum modes after correction of the electronic noise and inseparability criterion for signal and idler modes. Squeezing and entanglement are observed down to 50 kHz. The resolution bandwidth is set to 3 kHz and the video bandwidth to 10 Hz.

reduce this classical excess noise. The degree of entanglement between signal and idler fields can be evaluated by the inseparability criterion developed by Duan *et al.* [17] and Simon [18]: a necessary condition for inseparability is that the half-sum of the previous squeezed variances falls below 1. This criterion is well verified in the considered frequency band, as one can observe in Fig. 2. To the best of our knowledge, our setup generates the best EPR entangled beams ever produced in the continuous variable regime. We have measured at a given noise frequency of 3.5 MHz (RBW set to 100 kHz and VBW to 300 Hz) a value of the inseparability criterion equal to 0.33 ± 0.02 [14].

Figure 3 sums up the same experimental measurements as given by Fig. 2 but now for low noise frequencies, between 40 kHz and 150 kHz. Measurements are corrected from the electronic dark noise, which is at least 4 dB below all traces. One can see that the ±45° vacuum modes are strongly squeezed: the noise variances are still reduced by 3 dB around 100 kHz and reach the shot noise limit for frequencies below 50 kHz. No significant difference is observed between the two rotated modes. The low limit frequency is well below the ones previously reported. In contrast to [8] and [9], the low-frequency squeezing is obtained with the same efficiency on both rotated modes, showing that the effect is not due to common mode rejection of excess noise but to an intrinsic absence of low-frequency noise in our setup.

We have reported in this paper the demonstration of a compact source of squeezing from 50 kHz to 10 MHz (still present above, in the bandwidth of the cavity, but not measured) with a slight increase of noise in a frequency band of 100 kHz around 1 MHz. This broadband noise reduction is likely to reduce noise in a pulsed measurement during a time window of duration T. The noise variance σ^2 of the measurement can be written

$$\sigma^2 = \int_0^{+\infty} S(\nu) T^2 \mathrm{sinc}^2(\pi \nu T) d\nu,$$

where $S(\nu)$ is the spectral noise density of the light source. Let us evaluate the improvement obtained on a measurement during a window of duration $T = 1\ \mu$s. We model our device by a shot-noise limited source below 50 kHz (the excess noise can be reduced to shot noise by a feedback loop) and squeezed by 3 dB above. In comparison with a shot-noise limited source at all frequencies, the noise variance is divided by a factor 1.7. This very simple example shows the great interest of broadband and low-frequency squeezing to improve a large class of physical measurements.

In summary, we have demonstrated significant broadband vacuum EPR entanglement and squeezing down to 50 kHz with a single OPO below threshold and without the need of optical noise cancellation technique. The degree of entanglement can be improved further by increasing the transmission escape efficiency of the OPO. Up to now, the attainable lowest frequency seems only limited by the technical noise of the laser and locking noise of the different cavities involved in our setup. The implementation of the intensity noise eater on the Nd:YAG laser—as is the case for gravitational wave detectors where lasers are expected to be shot noise limited around a few tens of Hz—should allow it to reach even lower frequencies.

Laboratoire Kastler-Brossel, of the Ecole Normale Supérieure and the Université Pierre et Marie Curie, is associated with the Centre National de la Recherche Scientifique (UMR 8552). Laboratoire Matériaux et Phénomènes Quantiques is a Fédération de Recherche (CNRS FR 2437). This work has been supported by the European Commission project QUICOV (IST-1999-13071) and ACI Photonique (Ministère de la Recherche).

[1] C. M. Caves, Phys. Rev. D **23**, 1693 (1981).
[2] P. Grangier, R. E. Slusher, B. Yurke, and A. LaPorta, Phys. Rev. Lett. **59**, 2153 (1987); in Vol. 190 of *Proceedings of the NATO Advanced Study Institute Series B: Physics* (Plenum, New York, 1988), p. 253; M. Xiao, L.A. Wu, and H. J. Kimble, Phys. Rev. Lett. **59**, 278 (1987).
[3] H. J. Kimble, Y. Levin, A. B. Matsko, K. S. Thorne, and S. P. Vyatchanin, Phys. Rev. D **65**, 022002 (2002); M. T. Jaekel and S. Reynaud, Europhys. Lett. **13**, 301 (1990); W. G. Unruh, in *Quantum Optics, Experimental Gravitation, and Measurement Theory*, edited by P. Meystre and M. O. Scully (Plenum, New York, 1982), p. 647; A. F. Pace, M. J. Collett, and D. F. Walls, Phys. Rev. A **47**, 3173 (1993).
[4] K. McKenzie, D. A. Shaddock, D. E. McClelland, B. C. Buchler, and P. K. Lam, Phys. Rev. Lett. **88**, 231102 (2002).
[5] N. Treps, N. Grosse, W. P. Bowen, C. Fabre, H.-A Bachor, and P. K. Lam, Science **301**, 940 (2003).
[6] A. C. Boccara, D. Fournier, and J. Badoz, Appl. Phys. Lett. **36**, 130 (1980).
[7] S. Feng and O. Pfister, J. Opt. B: Quantum Semiclassical Opt. **5**, 262 (2003).
[8] W. P. Bowen, R. Schnabel, N. Treps, H.-A Bachor, and P. K. Lam, J. Opt. B: Quantum Semiclassical Opt. **4**, 421 (2002).
[9] R. Schnabel, H. Vahlbruch, A. Franzen, S. Chelkowski, N. Grosse, H.-A Bachor, W.P. Bowen, P. K. Lam, and K. Danzmann, Opt. Commun. **240**, 195 (2004).
[10] *Quantum Information with Continuous Variables*, edited by S. L. Braunstein and A. K. Pati (Kluwer Academic Publishers, Dordrecht, 2003).
[11] E. J. Mason and N. C. Wong, Opt. Lett. **23**, 1733 (1998).
[12] Z. Y. Ou, S. F. Pereira, H. J. Kimble, and K. C. Peng, Phys. Rev. Lett. **68**, 3663 (1992); Y. Zhang, H. Wang, X. Li, J. Jing, C. Xie, and K. Peng, Phys. Rev. A **62**, 023813 (2000).
[13] L. Longchambon, J. Laurat, T. Coudreau, and C. Fabre, e-print quant-ph/0310036; e-print quant-ph/0311123.
[14] J. Laurat, T. Coudreau, G. Keller, N. Treps, and C. Fabre, e-print quant-ph/0410081.
[15] J. Laurat, T. Coudreau, N. Treps, A. Maître, and C. Fabre, Phys. Rev. Lett. **91**, 213601 (2003).
[16] D. A. Shaddock, M. B. Gray, and D. E. McClelland, Opt. Lett. **24**, 1499 (1999).
[17] L.-M. Duan, G. Giedke, J. I. Cirac, and P. Zoller, Phys. Rev. Lett. **84**, 2722 (2000).
[18] R. Simon, Phys. Rev. Lett. **84**, 2726 (2000).

PHYSICAL REVIEW A **67**, 032302 (2003)

Experimental investigation of continuous-variable quantum teleportation

Warwick P. Bowen,[1] Nicolas Treps,[1] Ben C. Buchler,[1] Roman Schnabel,[1] Timothy C. Ralph,[2] Hans-A. Bachor,[1] Thomas Symul,[1] and Ping Koy Lam[1]

[1]*Department of Physics, Faculty of Science, Australian National University, Canberra ACT 0200, Australia*

[2]*Department of Physics, Centre for Quantum Computer Technology, University of Queensland, St Lucia, Queensland 4072, Australia*

(Received 31 July 2002; published 10 March 2003)

We report the experimental demonstration of quantum teleportation of the quadrature amplitudes of a light field. Our experiment was stably locked for long periods, and was analyzed in terms of fidelity $\mathcal{F}$ and with signal transfer $T_q = T^+ + T^-$ and noise correlation $V_q = V^+_{\text{in}\mid\text{out}} V^-_{\text{in}\mid\text{out}}$. We observed an optimum fidelity of 0.64 ± 0.02, $T_q = 1.06 \pm 0.02$, and $V_q = 0.96 \pm 0.10$. We discuss the significance of both $T_q > 1$ and $V_q < 1$ and their relation to the teleportation no-cloning limit.

DOI: 10.1103/PhysRevA.67.032302 PACS number(s): 03.67.Hk, 03.65.Ud, 42.50.Dv, 42.65.Yj

Quantum teleportation [1] is a key part of quantum information technology both in terms of communicating [2] and processing [3] quantum information. Experimental demonstrations of teleportation have so far fallen into three main categories: teleportation of photon states [4]; of ensemble properties in liquid NMR [5]; and of optical-field states [6]. An important feature of the technique used in the optical-field state experiment of Furusawa *et al.* [6] is its high efficiency. This results in the ability to faithfully teleport arbitrary input states continuously. This is due to the in principle ability to perform the required joint measurements exactly and the technical maturity of optical-field detection. In contrast, the efficiency of single-photon experiments is presently restricted in principle due to the inability to identify all four Bell states, and also in practice by the low efficiency of single-photon production and detection.

Since the Furusawa *et al.* experiment, there have been many proposals for how quantum teleportation may be repeated using different systems [7–9]; applied to different input states [10,11]; generalized to multiparty situations [12]; and more comprehensively characterized [13,14]. Inspite of the considerable interest, to date no new experiment has been performed [15].

This paper reports the quantum teleportation of the quadrature amplitudes of a light beam. Our scheme has a number of notable differences to the previously published experiment. The input and output states are analyzed by the same homodyne detector, allowing a more consistent evaluation of their properties. Our experiment is based on a Nd:YAG (yttrium aluminum garnet) laser that produces two squeezed beams in two independently pumped optical-parametric amplifiers (OPAs). We use a more compact configuration for Alice's measurements. Finally, the encoding and decoding of the input and output signals uses a total of four independent modulators. This allows us to completely span the phase space of the input state.

We analyze our results using the fidelity $\mathcal{F}$ between the input and output states, and also with signal transfer T_q and noise correlation V_q in a manner analogous to quantum nondemolition analysis [7] (which we refer to as the T-V measure henceforth). This enables us to give a more detailed characterization of the performance of our teleporter.

Teleportation is usually described as the disembodied transportation of an *unknown quantum state* from one place (Alice) to another (Bob). In our experiment, as in Ref. [6], the teleported states are modulation sidebands of a bright optical beam. The teleportation process can be described using the field annihilation operator $\hat{a} = (\hat{X}^+ + i\hat{X}^-)/2$ where $\hat{X}^\pm = 2\alpha^\pm + \delta\hat{X}^\pm$ are the amplitude $(+)$ and phase $(-)$ quadratures of the field, $\alpha^\pm = \langle \hat{X}^\pm \rangle /2$ are the real and imaginary parts of the coherent amplitudes, and $\delta\hat{X}^\pm$ are the quadrature noise operators. Throughout this paper, the variances of these noise operators are $V^\pm = \langle \delta\hat{X}^{\pm 2} \rangle$. The fidelity can be evaluated from the overlap of the input (in) and output (out) states, and for the Gaussian states is given by

$$\mathcal{F} = 2e^{-(k^+ + k^-)} \sqrt{\frac{V^+_{\text{in}} V^-_{\text{in}}}{(V^+_{\text{in}} + V^+_{\text{out}})(V^-_{\text{in}} + V^-_{\text{out}})}}, \qquad (1)$$

where $k^\pm = \alpha^{\pm 2}_{\text{in}} (1 - g^\pm)^2 / (V^\pm_{\text{in}} + V^\pm_{\text{out}})$ and $g^\pm = \alpha^\pm_{\text{out}} / \alpha^\pm_{\text{in}}$ are the teleportation gains. For a sufficiently broad set of coherent states, the best average fidelity at unity gain without entanglement is $\mathcal{F}_{\text{class}} = 0.5$. Another interesting limit is at $\mathcal{F} = 2/3$. This limit guarantees that Bob has the best copy of the input state and is commonly referred to as the *no-cloning limit* [14]. Ideal teleportation would result in $\mathcal{F} = 1$.

Alternatively, quantum teleportation can be defined as the transfer of *quantum information* between Alice and Bob using the T-V measure. This more general definition includes cases for which only the useful quantum features of a system have been transferred. In such cases a demonstrably quantum result may be obtained even though other features of the state, for example, the state amplitude, have been distorted sufficiently to degrade fidelity. In the absence of entanglement, strict limits are placed on both the accuracy of measurement and reconstruction of an unknown state. These are the so-called two quantum duties. In contrast to fidelity, the T-V measure is state independent and therefore invariant under local symplectic operations.

Bob's reconstruction is limited by the generalized uncertainty principle of Alice's measurement $V^+_M V^-_M \geqslant 1$ [16], where $V^\pm_M$ are the measurement penalties, which holds for simultaneous measurements of conjugate quadrature ampli-

tudes. In the absence of entanglement, this places a strict limit on Bob's reconstruction accuracy. The limit can be expressed in terms of quadrature signal transfer coefficients [7], $T^{\pm}=\mathcal{R}^{\pm}_{\rm out}/\mathcal{R}^{\pm}_{\rm in}$ as

$$T_q=T^{+}+T^{-}-T^{+}T^{-}\left(1-\frac{1}{V^{+}_{\rm in}V^{-}_{\rm in}}\right)\leqslant 1 \qquad (2)$$

where $\mathcal{R}^{\pm}=\alpha^{\pm}/V^{\pm}$ are the signal-to-noise ratios. For minimum uncertainty input states ($V^{+}_{\rm in}V^{-}_{\rm in}=1$), this expression reduces to $T_q=T^{+}+T^{-}$.

Bob's reconstruction must be carried out on an optical field, the fluctuations of which obey the uncertainty principle. In the absence of entanglement, these intrinsic fluctuations remain present on any reconstructed field. Thus the amplitude and phase conditional variances, $V^{\pm}_{\rm in|\,out}=V^{\pm}_{\rm out}-|\langle\delta\hat{X}^{\pm}_{\rm in}\delta\hat{X}^{\pm}_{\rm out}\rangle|^2/V^{\pm}_{\rm in}$, which measure the noise added during the teleportation process, must satisfy $V^{+}_{\rm in|\,out}V^{-}_{\rm in|\,out}\geqslant 1$. This can be written in terms of the quadrature variances of the input and output states and the teleportation gain as

$$V_q=(V^{+}_{\rm out}-g^{+2}V^{+}_{\rm in})(V^{-}_{\rm out}-g^{-2}V^{-}_{\rm in})\geqslant 1. \qquad (3)$$

It should be noted that $(V^{+}_{\rm in|\,out}+V^{-}_{\rm in|\,out})\geqslant 2$ has also been proposed for the conditional variance limit. For cases where both quadratures are symmetric, as considered previously [7,10], both limits are equivalent. The product limit, however, is significantly more immune to asymmetry in the teleportation gain and is, therefore, preferred. The criteria of Eqs. (2) and (3) enable teleportation results to be represented on a T-V graph similar to those used to characterize quantum nondemolition experiments [17].

Both the T_q and V_q limits have independent physical significance. If Bob passes the T_q limit, this forbids any others parties from doing so, therefore, ensuring that the transfer of information to Bob is greater than to any other party. This is an ''information cloning'' limit that is particularly relevant in light of recent proposals for quantum cryptography [18]. Furthermore, if Bob passes the T_q limit at unity gain ($g^{\pm}=1$), then Bob has beaten the no-cloning limit and has $\mathcal{F}\geqslant 2/3$. Surpassing the V_q limit is a necessary prerequisite for reconstruction of nonclassical features of the input state such as squeezing. The T-V measure coincides with the teleportation no-cloning limit at unity gain when both $T_q=V_q=1$. Clearly it is desirable that the T_q and V_q limits are simultaneously exceeded. Perfect reconstruction of the input state would result in $T_q=2$ and $V_q=0$.

The laser source for our experiment was a 1.5 W monolithic nonplanar ring Nd:YAG laser at 1064 nm. Its output was split into two roughly equal power beams. One beam was mode matched into a MgO:$LiNbO_3$ frequency doubler producing 370 mW of 532 nm light. The other beam was passed through a high finesse ring cavity to reduce spectral noise. This spectrally cleaned beam, which was quantum noise limited above 6 MHz, was then used to generate the signal for teleportation; to seed a pair of MgO:$LiNbO_3$ OPAs; and to provide local oscillator beams.

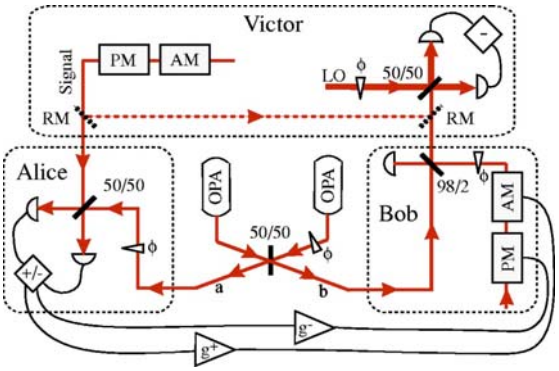

FIG. 1. A schematic diagram of the teleportation experiment. RM, removable mirror; 50/50, symmetric beam splitter; 98/2, 98% transmitting beam splitter; ϕ, phase control; A(P)M, amplitude (phase) modulators.

Our experimental setup to generate entanglement and perform teleportation is shown in Fig. 1. We produced the entanglement by combining a pair of amplitude squeezed beams with a $\pi/2$ phase shift on a 50/50 beam splitter [19]. The squeezed beams were produced by the two OPAs, each pumped with half of the 532 nm light [20]. We characterized the entanglement with the inseparability measure proposed by Duan *et al.* [21]; and obtained the result $[\langle(\hat{X}^{+}_{a}-\hat{X}^{+}_{b})^2\rangle+\langle(\hat{X}^{-}_{a}+X^{-}_{b})^2\rangle]/2=0.44\pm 0.02$, where subscripts a and b label the two entangled beams; this result is well below the inseparability limit of unity. In our situation, this value becomes equivalent to the average of the squeezed variances of the two OPAs. This corresponds to 3.6 dB of squeezing on each beams. Taking account of 16% loss in post-entanglement optics, we infer 4.8 dB of squeezing at the output of each OPA.

The teleportation experiment (Fig. 1) consisted of three parts: measurement (Alice), reconstruction (Bob), and generation and verification (Victor). At the generation stage, a beam was independently phase and amplitude modulated at 8.4 MHz. Alice then took one of the entangled beams and combined it on a 50/50 beam splitter with the input state with $\pi/2$ phase shift. The intensities of these two beams were balanced so that the sum (difference) of the photocurrents obtained through detection of the two beam splitter outputs provided a measure of the amplitude (phase) quadrature of the input state combined with the entangled beam. These photocurrents were sent electronically to Bob. Bob used them to modulate an independent laser beam that was then combined with the second entangled beam on a 98/2 beam splitter. One output of this beam splitter was Bob's reconstructed output state.

By using removable mirrors, Victor could measure the Wigner functions of both the input and output states. Assuming the states are Gaussian, Victor need only measure the two quadratures to fully characterize the input state. We achieved these measurements in a locked homodyne detector. It is interesting to note that imperfections such as inefficiency and low local oscillator power actually improve the results ob-

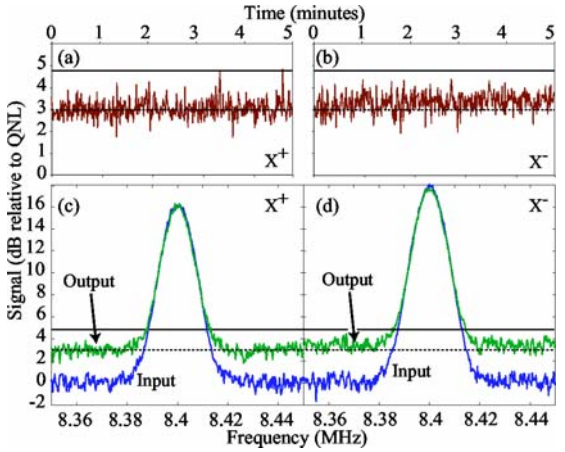

FIG. 2. The input and output states of the teleporter, as measured by Victor. (a) and (b) show the amplitude and phase noise of the output state at 8.4 MHz. (c) and (d) show the input and output of the teleporter, when probed with a signal at 8.4 MHz. In all cases, the dotted line is the no-cloning limit, while the solid line is the classical limit. All data have been corrected to account for the detection losses of Victor. Resolution bandwidth=10 kHz, video bandwidth=30 Hz.

tained by Victor. In our analysis, we corrected for these effects.

Active control of the entire experiment required ten locking loops and four temperature control loops. They ensured that the mode cleaner, frequency doubler, two OPA cavities, phases of the OPA pump beams, Alice and Bob phases, Victor homodyne detection, and the relative phase between the squeezed beams were all stably locked. A sample of the data obtained from our teleporter is shown in Fig. 2. Figures 2(a) and 2(b) show the noise of the output state as a function of time. The complete system maintained lock for long periods. The data in Figs. 2(c) and 2(d) show the measurement of the two quadratures over a 100 kHz bandwidth. Over this range the noise floor of the system was constant. The signal-to-noise-ratio was, therefore, found by comparing the peak height at 8.4 MHz to the noise at 8.35 and 8.45 MHz. Every set of teleportation data consisted of four spectra, such as those shown in Fig. 2(c) and 2(d), as well as a quantum noise calibration (not shown). Also drawn in each part of Fig. 2 are lines corresponding to the classical limit (solid line at 4.8 dB) and the no-cloning limit (dashed line at 3 dB). For this dataset, the noise floor of both quadratures lies convincingly below the classical limit and approaches very close to the no-cloning limit. Note that these limits are those calculated for an ideal lossless teleporter. The fidelity obtained for this data was $\mathcal{F}=0.64\pm0.02$.

Figure 3(d) shows the area of phase space that our experiment has probed. All points shown here satisfied $\mathcal{F}>0.5$. For the most part, our input states had nonzero coherent amplitude components, thereby allowing verification of the gains of both quadratures. One of the features of fidelity is a strong dependence on gain and signal size. For example, in the limit of a vacuum input state, the fidelity criterion will actually be

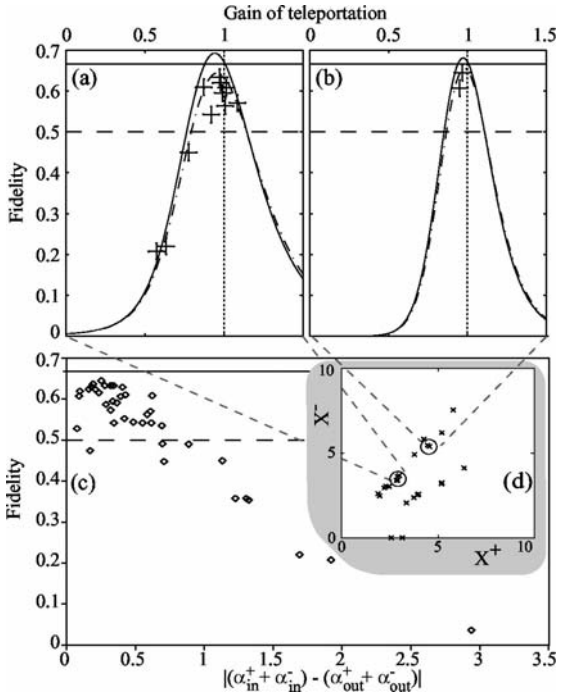

FIG. 3. Measured fidelity plotted; versus teleportation gain, g, in (a) and (b); versus coherent amplitude separation between input and output states in (c); and on phase space in (d). In (a) the input signal size was $(\alpha^+,\alpha^-)\approx(2.9,3.5)$ and in (b) $(\alpha^+,\alpha^-)\approx(4.5,5.4)$. g was calculated as the ratio of the input and output coherent amplitudes. The dashed (solid) lines show the classical (no-cloning) limits of teleportation at unity gain. The solid curves are calculated results based on available entanglement, the dot-dashed curves include the experimental asymmetric gains: for (a) $g^-=0.84g^+$ and for (b) $g^-=0.92g^+$. In (c) and (d) axes are normalized to the QNL.

satisfied perfectly by a classical teleporter (i.e., one with the entangled state replaced by two coherent states) with zero gain. The fidelity criterion, therefore, requires proof that the gain of a teleportation event is unity. A subset of our data is shown in Figs. 3(a) and 3(b). Each diagram plots fidelity as a function of teleportation gain for results with identical input states. The solid curves show the best possible performance of our system, based on our entanglement, detection efficiency, dark noise, and assuming equal gain on each quadrature. Both plots demonstrate that the highest fidelity occurs for gain less than unity. The increased fidelity is less obvious in Fig. 3(b) where the signal is approximately twice as large as that in Fig. 3(a). For small signals it is, therefore, crucial to ensure unity gain. Obtaining the correct gain setting is actually one of the more troublesome experimental details. To illustrate this point, we have plotted the dashed curves on Figs. 3(a) and 3(b) for a teleporter with asymmetric quadrature gains. Such asymmetry was not unusual in our system, and explains the variability of the results shown in Fig. 3(a). A summary of all our fidelity results is shown in Fig. 3(c) as a function of deviation from unity gain.

Analyzing teleportation results on a T-V graph has several

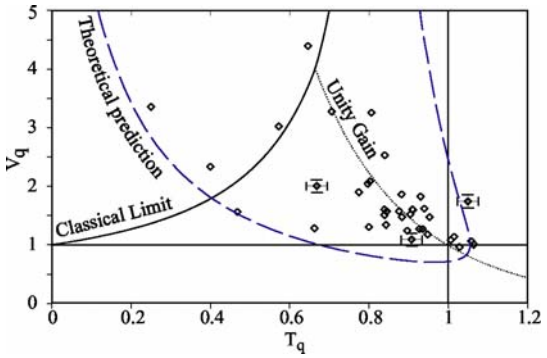

FIG. 4. *T*-*V* graph of the experimental results. The dashed theoretical curve was calculated based on the available entanglement and experimental losses. Representative error bars are shown for some points.

advantages when compared to fidelity. The *T*-*V* graph is two dimensional, and, therefore, conveys more information about the teleportation process. It tracks the quantum correlation and signal transfer in nonunity gain situations. In particular, it identifies two particularly interesting regimes that are not evident when using fidelity: the situations where the output state has minimum noise (minimum V_q), and when the input signals were transferred to the output state optimally (maximum T_q). Our *T*-*V* results are shown in Fig. 4. The classical limit curve shows the ideal achievable result as a function of gain if the entanglement was replaced with two coherent states. The unity gain curve shows the locus of points obtained at unity teleportation gain with increasing entanglement. Finally, a theoretical curve (as a function of gain) is shown for our experimental parameters. By varying our experimental conditions, particularly the gain, we have mapped out some portion of the *T*-*V* graph.

Perhaps the most striking feature of these results are the points with $T_q>1$, the best of which has $T_q=1.06\pm0.03$. Since only one party may have $T_q>1$, this shows that Bob has maximal information about the input signal and we have broken the information cloning limit. The lowest observed conditional variance product was $V_q=0.96\pm0.10$. This point also had $T_q=1.04\pm0.03$. This is the first observation of both $T_q>1$ and $V_q<1$, and with unity gain this would imply breaking of the no-cloning limit for teleportation. This particular point, however, had a fidelity of 0.63 ± 0.03. The main reason for this low fidelity is asymmetric gain, the amplitude gain was $g^+=0.92\pm0.08$, while the phase gain was $g^-=1.12\pm0.08$. Such gain errors have a dramatic impact on the measured fidelity because the output state then has a different classical amplitude ($\alpha^{\pm}$) to the input, a difference in the classical properties of the input and output states to which fidelity is very sensitive.

In conclusion, we have performed stably locked quantum teleportation of an optical field. The best fidelity, we directly observed was $\mathcal{F}=0.64\pm0.02$. The maximum two quadrature signal transfer for our apparatus was $T_q=1.06\pm0.03$. We also observed a conditional variance product of $V_q=0.96\pm0.10$ coincident with $T_q=1.04\pm0.03$. This is the first observation of both $T_q>1$ and $V_q<1$. At unity gain this would ensure violation of the no-cloning limit for teleportation. The asymmetry in our gain, however, prevented a direct measurement of $\mathcal{F}>0.67$, thereby leaving the no-cloning limit as a tantalising prospect for future experiments.

We thank the Australian Research Council for financial support and the Alexander von Humboldt foundation for supporting R.S. This work was a part of EU QIPC, Project No. IST-1999-13071 (QUICOV).

[1] C.H. Bennett *et al.*, Phys. Rev. Lett. **70**, 1895 (1993).
[2] M. Nielsen and I. Chuang, *Quantum Computation and Quantum Information* (Cambridge University Press, Cambridge, 2000).
[3] D. Gottesman and I.L. Chuang, Nature (London) **402**, 390 (1999).
[4] See, for example, D. Bouwmeester *et al.*, Nature (London) **390**, 575 (1997); D. Boschi *et al.*, Phys. Rev. Lett. **80**, 1121 (1998).
[5] M.A. Nielsen *et al.*, Nature (London) **396**, 52 (1998).
[6] A. Furusawa *et al.*, Science **282**, 706 (1998).
[7] T.C. Ralph and P.K. Lam, Phys. Rev. Lett. **81**, 5668 (1998).
[8] G. Leuchs *et al.*, J. Mod. Opt. **46**, 1927 (1999).
[9] J. Zhang and K. Peng, Phys. Rev. A **62**, 064302 (2000).
[10] R.E.S. Polkinghorne and T.C. Ralph, Phys. Rev. Lett. **83**, 2095 (1999).
[11] T. Ide *et al.*, Phys. Rev. A **65**, 012313 (2002).
[12] P. van Loock and S.L. Braunstein, Phys. Rev. Lett. **84**, 3482 (2000).
[13] T.C. Ralph *et al.*, J. Opt. B: Quantum Semiclassical Opt. **1**, 483 (1999).
[14] F. Grosshans and P. Grangier, Phys. Rev. A **64**, 010301(R) (2001).
[15] With the exception of a recent paper by Zhang *et al.*, on the same optical system used by Furusawa *et al.*, e-print quant-ph/0207076.
[16] E. Arthurs and M.S. Goodman, Phys. Rev. Lett. **60**, 2447 (1988).
[17] P. Grangier *et al.*, Nature (London) **396**, 537 (1998).
[18] F. Grosshans and P. Grangier, Phys. Rev. Lett. **88**, 057902 (2002).
[19] Z.Y. Ou *et al.*, Phys. Rev. Lett. **68**, 3663 (1992).
[20] W. Bowen *et al.*, Phys. Rev. Lett. **88**, 093601 (2002).
[21] L.-M. Duan *et al.*, Phys. Rev. Lett. **84**, 2722 (2000).

PRL 94, 050502 (2005) PHYSICAL REVIEW LETTERS week ending 11 FEBRUARY 2005

Teleportation of an Atomic Ensemble Quantum State

A. Dantan,* N. Treps, A. Bramati, and M. Pinard

Laboratoire Kastler Brossel, Université Pierre et Marie Curie, Case 74, 4 place Jussieu, 75252 Paris Cedex 05, France

(Received 30 July 2004; published 7 February 2005)

We propose a protocol to achieve high fidelity quantum state teleportation of a macroscopic atomic ensemble using a pair of quantum-correlated atomic ensembles. We show how to prepare this pair of ensembles using quasiperfect quantum state transfer processes between light and atoms. Our protocol relies on optical joint measurements of the atomic ensemble states and magnetic feedback reconstruction.

DOI: 10.1103/PhysRevLett.94.050502 PACS numbers: 42.50.Dv, 03.65.Ta, 03.67.Hk, 42.50.Ct

The realization of quantum networks involving optical fields and atomic ensembles is one of the most promising paths towards robust long distance quantum communication and information processing [1,2]. The efficient transfer of quantum states within that network is a key ingredient for a practical implementation [2]. Several continuous variable teleportation experiments with optical fields [3] have shown that continuously teleporting optical quantum states with a high efficiency was possible. On the other hand, the teleportation of a single atom or ion quantum state was demonstrated very recently [4]. In this Letter we present a direct scheme to teleport an atomic spin state in a way very similar to that used in the teleportation protocols for optical field states [5], which can hence be efficiently integrated within a light-atom quantum network, for instance.

Because of the long lifetime of their ground-state spins, atomic ensembles are good candidates to store and manipulate quantum states of light [6]. We show how to prepare the spin states via quantum state transfers with optical fields [7–9] and propose to achieve the teleportation of an atomic ensemble quantum state using an Einstein-Podolsky-Rosen- (EPR-)correlated pair of atomic ensembles. An optical joint measurement of the unknown ensemble (1) and one of the entangled ensemble (2) is then performed by Alice who sends the results to Bob. Using a suitable magnetic field Bob can reconstruct the input state on the other correlated ensemble (3). The quasi-ideal character of the atom-field quantum transfer processes allows high fidelity teleportation for easily accessible experimental parameters.

Another atomic teleportation protocol, relying on successive measurements alternating with optical displacements performed on two ensembles, was proposed by Kuzmich and Polzik [10]. However, this protocol requires several exchanges of information between Alice and Bob. Our scheme, being a direct adaptation of the teleportation protocols for light, needs two simultaneous measurements to achieve real-time quantum teleportation, and can easily be extended to other quantum communication and information protocols, such as entanglement swapping and quantum repeaters. This Letter successively describes the three steps of atomic teleportation: preparation, joint measurement, and reconstruction.

In this Letter we mainly consider cold atom ensembles, but our protocol also extends to atomic vapors. We consider three N-atom ensembles with an energy level structure in Λ [Fig. 1(a)]. We assume that they are placed inside optical cavities, for which the input-output theoretical treatment of the atom-field quantum fluctuations is well-adapted. They each interact with a coherent control field Ω_i and with a vacuum field A_i ($i = 1 - 3$). In reality, the Λ structure should be part of a larger $J \rightarrow J$ or $J \rightarrow J - 1$ transition, the two ground states being two Zeeman sublevels with $m_J = J, J - 1$, but after the preparation phase, the other levels play no role and can be safely ignored. To simplify the discussion we will therefore focus on the case of a $J = 1/2$ ground-state spin.

Preparation.—During the preparation stage Victor pumps the ensembles with the control fields so that their ground-state collective spins are aligned along the z axis: $\langle J_{zi}\rangle = N/2$. Ensemble 1 is assumed to be almost completely spin-polarized along z, with a small tilt corresponding to a nonzero coherence: $\langle J_{z1}\rangle \simeq N/2$ and $\langle J_{x1}\rangle$, $\langle J_{y1}\rangle \sim \mathcal{O}(\sqrt{N})$. This means that we consider small planar displacements of the spin in the vicinity of the north pole of the Bloch sphere. This approximation is all the more correct as the number of atoms is large. The quantum state of an ensemble is then determined by the ground-state coherence, the spin components J_x and J_y obeying a commutation relation $\langle [J_x, J_y]\rangle = i\langle J_z\rangle = iN/2$, similar to that of an harmonic oscillator. In the Gaussian approximation the atomic quantum state can then be represented by a noise ellipsoid in the (x, y) plane orthogonal to the mean spin [see Fig. 1(a)], in a manner very similar to the Fresnel representation of quantum optical field states. The atomic state is then completely characterized by the amplitude and phase of the coherence mean value, as well as its variances ΔJ_x^2 and ΔJ_y^2, which are equal to $N/4$ for a coherent spin state, for instance.

Let us suppose that the atomic state to be teleported is that of ensemble 1, prepared by Victor, unknown to Alice and Bob. With a suitable interaction Victor can prepare any Gaussian state (coherent state, squeezed state...) by an

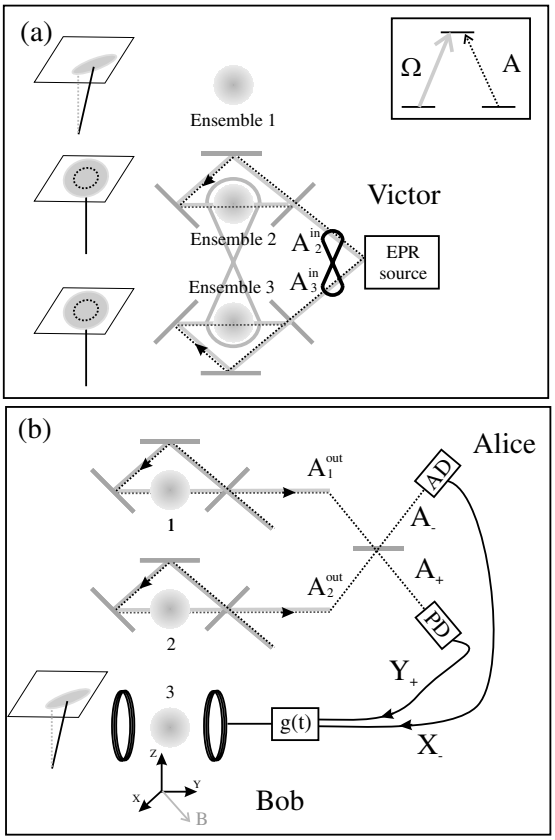

FIG. 1. Teleportation scheme: (a) *Preparation*. Insert: Λ-type level structure considered. Left: schematic atomic initial states for each ensemble (for spins 2 and 3, the dashed circle indicates the coherent spin state fluctuation distribution). (b) *Measurement and reconstruction*. Left: teleported state after reconstruction is completed. AD: amplitude detector. PD: phase detector.

adequate choice of the field state A_1^{in}, the state of which can be perfectly mapped onto the atoms. More explicitly, the coherence mean value depends on the field amplitude and phase, whereas the noise ellipsoid is given by the field quantum fluctuations. This transfer can be achieved using an electromagnetically induced transparency (EIT) (one- and two-photon resonant) or a "Raman" (large one-photon detuning, but two-photon resonant) interaction between the fields and the atoms [7,8]. In these two configurations there is little to no dissipation and the quantum fluctuations are predicted to be conserved in atom-field quantum state transfer processes. Using EPR-correlated fields Victor can also map their entanglement onto spins 2 and 3 with the same techniques [9]. Since the mean spins are parallel and equal, $J_{x2} - J_{x3}$ and $J_{y2} + J_{y3}$ are the equivalent of the usual EPR operators, satisfying $\langle [J_{x2} - J_{x3}, J_{y2} + J_{y3}] \rangle = i\langle J_{z2} - J_{z3} \rangle = 0$. We can assume without loss of generality that the fluctuations of J_{x2} and J_{x3} are correlated and those of J_{y2} and J_{y3} anticorrelated, so that the condition for their inseparability reads [11]

$$\Delta(J_{x2} - J_{x3})^2 + \Delta(J_{y2} + J_{y3})^2 < |\langle J_{z2} \rangle| + |\langle J_{z3} \rangle| = N.$$

In a symmetrical configuration the amount of atomic entanglement is given by the sum of the EPR variances (normalized to 2) [12]

$$\mathcal{I}_{2,3} = \frac{2}{N}[\Delta(J_{x2} - J_{x3})^2 + \Delta(J_{y2} + J_{y3})^2]. \qquad (1)$$

When the preparation stage is over all fields are switched off, and one disposes of an unknown atomic quantum state 1 and an EPR-correlated pair 2 and 3.

Joint measurements.—Alice then performs a simultaneous readout of ensembles 1 and 2 by rapidly switching on the control fields in cavities 1 and 2. The reverse transfer process of the preparation then takes place, and the states of spins 1 and 2 imprint in a transient manner onto the outgoing fields exiting the cavities A_1^{out} and A_2^{out}. These two fields are then mixed on a 50/50 beam splitter and Alice performs two homodyne detections of the resulting modes $A_{\pm} = (A_1^{\text{out}} \pm A_2^{\text{out}})/\sqrt{2}$ [Fig. 1(b)]. To obtain maximal information about the initial state, Alice measures the noise of two orthogonal quadratures—say $X_- = A_- + A_-^{\dagger}$ and $Y_+ = i(A_+^{\dagger} - A_+)$—and sends the results to Bob who disposes of ensemble 3. As we will show further, Bob can then reconstruct state 1 using a suitable magnetic field and achieve teleportation.

In more details, we assume an "EIT"-type interaction (one- and two-photon resonance), although a Raman interaction either with cold atoms or even with an atomic vapor would yield similar results. Alice rapidly switches the control field on in ensembles 1 and 2 at time $t = 0$. The outgoing modes can be expressed as a function of the initial atomic operators in ensembles 1 and 2 [8]

$$\begin{aligned} X_i^{\text{out}}(t) = {} & X_i^{\text{in}}(t) - \alpha J_{xi}(0) e^{-\tilde{\gamma}_0 t} \\ & - 2\eta^2 [X_i^{\text{in}}(t) - \tilde{\gamma}_0 \int_0^t e^{-\tilde{\gamma}_0 (t-s)} X_i^{\text{in}}(s) ds] \\ & + \beta [X_{\nu i}(t) - \tilde{\gamma}_0 \int_0^t e^{-\tilde{\gamma}_0 (t-s)} X_{\nu i}(s) ds], \end{aligned} \qquad (2)$$

$(i = 1, 2)$, with $\eta^2 = 2C/(1 + 2C)$, $\alpha = \eta\sqrt{8\tilde{\gamma}_0/N}$, $\beta = 2\eta/\sqrt{1 + 2C}$, C being the cooperativity parameter quantifying the collective strength of the atom-field coupling [7]. $\tilde{\gamma}_0$ represents the effective atomic decay rate in presence of the control field. This parameter depends on the cooperativity and the pumping rate due to the control field [8], and it is related to the duration of the transient optical pulse carrying the atomic state out of the cavity. η is actually related to the efficiency of the transfer [7], and is close to unity for large values of the cooperativity. $X_{\nu i}$ is a noise atomic operator accounting for noise induced by spontaneous emission and with unity white noise spectrum. X_i^{in} is

PRL **94,** 050502 (2005) PHYSICAL REVIEW LETTERS week ending 11 FEBRUARY 2005

the amplitude quadrature of the vacuum field incident on cavity i. Similar expressions hold for the phase quadratures Y_i, replacing x's, X's by y's, Y's. To derive (2) we assumed a cavity frequency bandwidth much larger than $\tilde{\gamma}_0$. In (2) the amplitude of the term proportional to $J_x(0)$ shows how the atomic state reflects on the outgoing field state. The other terms correspond to intrinsic optical field noise ($\propto X^{\text{in}}$) and added atomic noise ($\propto X_v$). The photocurrents measured by Alice can be expressed as a sum of these noise terms and the initial atomic state:

$$i_- \propto X_- \sim \text{ noise} + [J_{x1}(0) - J_{x2}(0)]e^{-\tilde{\gamma}_0 t}, \quad (3)$$

$$i_+ \propto Y_+ \sim \text{ noise} + [J_{y1}(0) + J_{y2}(0)]e^{-\tilde{\gamma}_0 t}. \quad (4)$$

By choosing the right temporal profile of her local oscillator it was shown in [8] that Alice can measure with a great efficiency the atomic states, which corresponds to the joint measurements used in the continuous variable teleportation protocols for light.

Reconstruction.—From Alice's results and his correlated ensemble 3 Bob is therefore in principle able to deduce the initial state of ensemble 1. Were we dealing with light beams, Bob could directly feed Alice's measurements to standard phase or intensity modulators to reconstruct state 1 [3,5]. The difficulty with an atomic ensemble is to physically implement the reconstruction stage. An all optical method was proposed in [10]. Another way to control the quantum fluctuations of an atomic ensemble is to use a magnetic field in order to have the spin precess in a controlled manner. Such a method was proposed to generate spin squeezing [13] and was successfully implemented recently by Geremia *et al.* to continuously monitor the atomic spin noise via feedback [14]. We propose here to use a transverse magnetic field, the components of which are proportional to Alice's homodyne detection results. Indeed, if we choose the components of the magnetic field, B_x and B_y, to be proportional to $-i_+$ and i_-, we will couple J_{x3} to i_-, and J_{y3} to i_+. Since spin 2 and 3 are initially correlated, their correlated noises will cancel leaving only spin 1 state imprinted onto that of spin 3 at the end of the reconstruction phase.

More quantitatively, the Hamiltonian corresponding to the unitary transformation that Bob performs on spin 3 is simply a $\vec{J}.\vec{B}$ coupling

$$H_B = -\lambda[B_x(t)J_{x3} + B_y(t)J_{y3}]. \quad (5)$$

The evolution equations of J_{x3} and J_{y3} are then of the form

$$\dot{J}_{x3}(t) = G(t)X_-(t), \dot{J}_{y3}(t) = G(t)Y_+(t), \quad (6)$$

in which $G(t)$ gives the electronic gain of the reconstruction process. Its temporal profile can be adjusted in order to maximize the fidelity of the reconstruction. At this point we would like to stress that choosing the right profile for this electronic gain is equivalent to choosing the right local oscillator profile in Alice's homodyne detections. We therefore choose a temporal profile in $G(t) = Ge^{-\tilde{\gamma}_0 t}$ for the gain, which we know will maximize the information that Bob gets [8]. After completion of the reconstruction, i.e., for $t \gg 1/\tilde{\gamma}_0$, the final state of J_{x3}, which we denote by J_{x3}^{out}, can be shown to be

$$J_{x3}^{\text{out}} = gJ_{x1}(0) + J_{x3}(0) - gJ_{x2}(0) + J_x^{\text{noise}} \quad (7)$$

in which $g = -G\eta/\sqrt{N\tilde{\gamma}_0}$ is the normalized gain of the teleportation protocol and J_x^{noise} is a vacuum noise operator taking into account the losses of the process. Its explicit form is not reproduced, but it is uncorrelated with the spin operators and its variance, which can be calculated from Eqs. (2) and (6), is related to the intrinsic noise added during the atom-field transfer processes: $\Delta^2 J_x^{\text{noise}} = (N/2)g^2(1 - \eta^2)/\eta^2$.

We assume for simplicity initial isotropic fluctuations for the EPR-entangled ensembles, i.e., $\Delta J_{xi}^2 = \Delta J_{yi}^2 = (N/4)\cosh(2r)$ $(i = 2, 3)$, and symmetrical correlations $\langle \delta J_{x2} \delta J_{x3} \rangle = -\langle \delta J_{y2} \delta J_{y3} \rangle = (N/4)\sinh(2r)$. With these notations the inseparability criterion value (1) is then given by $\mathcal{I}_{2,3} = 2e^{-2r}$, which is 0 for perfect EPR entanglement and 2 for no entanglement. The normalized variance of J_{x3} after reconstruction is then

$$V_{x3}^{\text{out}} = g^2 V_{x1} + 2g^2 \frac{1 - \eta^2}{\eta^2} + (1 + g^2)\cosh(2r) - 2g\sinh(2r), \quad (8)$$

with an identical expression for the variance of J_{y3}. Note that, if the gain is set to 0, one retrieves the fact that the fluctuations of spin 3 are not modified: $V_{x3}^{\text{out}} = \cosh(2r) = V_{x3}$. Setting a *unity gain* ($g = 1$), the variances of the equivalent input noises $N_\alpha^{\text{out}} \equiv V_{\alpha 3}^{\text{out}} - g^2 V_{\alpha 1}$ $(\alpha = x, y)$ [15] are related to the EPR entanglement and the losses

$$N_{x,y}^{\text{out}} = 2e^{-2r} + 2\frac{1 - \eta^2}{\eta^2}. \quad (9)$$

For high entanglement ($r \gg 1$) and negligible losses ($\eta \sim 1$) the equivalent input noises go to 0, which means that the spin 1 state has indeed been fully teleported to spin 3.

At this point we can make a few comments. First, this result is very similar to that of light beam teleportation protocols [3,5,15,16] and shows that the input noise variances go down to 0 if Alice and Bob share perfectly entangled ensembles ($r = \infty$) and in the absence of losses ($\eta = 1$). In absence of entanglement ($r = 0$), $N_x^{\text{out}} = N_y^{\text{out}} = 2$, one retrieves the fact that two units of vacuum noise are added for the measurement and the reconstruction in the protocol. A good criterion to estimate the quality of the teleportation is provided by the product of the equivalent input noise variances $V_q \equiv \sqrt{N_x^{\text{out}} N_y^{\text{out}}}$ [16]. In the absence of losses the classical limit of 2 is beaten as soon as one disposes of entanglement. The equivalent input noises being independent of the input state our teleporta-

tion protocol is unconditional, and the various measures used in light teleportation protocols [3,5,15,16] to assess the success of the teleportation are valid. Of course, for a fixed value of N, the state to be teleported has to satisfy $\langle J_{x1}\rangle, \langle J_{y1}\rangle \sim \mathcal{O}(\sqrt{N})$, else the fidelity decreases. However, teleporting larger coherences can always be achieved by increasing N.

Second, we have assumed that the measurement and the feedback times are negligible with respect to the ground-state spin lifetime, so that ensemble 3 does not evolve before the reconstruction. This approximation is fairly reasonable since the ground-state lifetime for cold atoms or paraffin-coated cells is at least of the order of several milliseconds or even up to the second [10].

Third, the intrinsic noise ($\propto 1/C$), that is, the noise which does not come from the detector quantum inefficiency or electronic noise, is expected to be rather small, thanks to the cooperative behavior of the atoms in the cavity—C can easily be made of the order of 100–1000 using low finesse cavities. This should ensure losses at the percent level and, therefore, a good teleportation. High-Q cavities are not required because the atom-field coupling is enhanced by the collective atomic behavior ($C \propto N$). Bad cavities are actually preferable since the cavity bandwidth has to be much larger than the atomic spectrum width $\tilde{\gamma}_0$.

It is also interesting to look at the physical meaning of the magnetic reconstruction. The unity gain condition $g = 1$ actually translates into the very intuitive condition that the rotation angle of spin 3 during reconstruction in a time $(2\tilde{\gamma}_0)^{-1}$ should be equal to the relative spin fluctuations: $\theta = \omega_L/(2\tilde{\gamma}_0) = 1/\sqrt{N}$, where ω_L is the Larmor frequency. This condition also gives us the order of magnitude of the magnetic field necessary to perform the reconstruction. For an interaction with $N = 10^6$ cesium atoms on the D_2 line, a gyromagnetic factor of 450 kHz/G and $\tilde{\gamma}_0 = (2\pi)225$ kHz, the amplitude of the magnetic field is about 1 mG.

Last, in order to check the quality of the teleportation, Victor can simply perform a readout of ensemble 3 with the same technique previously used by Alice and compare the output state with the input state that he had prepared. Another way to check that this teleportation scheme is successful would be for Bob not to reconstruct the atomic state, but instead, to perform an optical readout of ensemble 3 and use both his homodyne detection results and Alice's results to deduce the input state. However, in this scheme, the atomic state of 1 is never effectively teleported to ensemble 3. The spin 1 state is actually teleported to the outgoing field A_3^{out}, realizing atom-to-field teleportation.

A straightforward but nonetheless important application of our protocol for quantum communication is *atomic entanglement swapping*: if ensemble 1 in the previous scheme was initially quantum-correlated with another ensemble 0, the previous teleportation scheme ensures that ensembles 0 and 3 are entangled at the end of the process. This is of importance for the realization of quantum networks in which quantum repeaters can ensure good quality transmission of the quantum information over long distances [2].

*Electronic address: dantan@spectro.jussieu.fr

[1] M. Nielsen and I. Chuang, *Quantum Computation and Quantum Information* (Cambridge University Press, Cambridge, England, 2000).

[2] L. M. Duan, J. I. Cirac, P. Zoller, and E. S. Polzik, Phys. Rev. Lett. **85**, 5643 (2000); L. M. Duan *et al.*, Nature (London) **414**, 413 (2001).

[3] A. Furusawa *et al.*, Science **282**, 706 (1998); W. P. Bowen *et al.*, Phys. Rev. A **67**, 032302 (2003); T. C. Zhang *et al.*, Phys. Rev. A **67**, 033802 (2003).

[4] M. Riebe *et al.*, Nature (London) **429**, 734 (2004); M. D. Barrett *et al.*, Nature (London) **429**, 737 (2004).

[5] S. L. Braunstein and H. J. Kimble, Phys. Rev. Lett. **80**, 869 (1998).

[6] M. D. Lukin, Rev. Mod. Phys. **75**, 457 (2003).

[7] A. Dantan *et al.*, Phys. Rev. A **67**, 045801 (2003).

[8] A. Dantan and M. Pinard, Phys. Rev. A **69**, 043810 (2004).

[9] A. Dantan, A. Bramati, and M. Pinard, Europhys. Lett. **67**, 881 (2004).

[10] A. Kuzmich and E. S. Polzik, Phys. Rev. Lett. **85**, 5639 (2000).

[11] L. M. Duan *et al.*, Phys. Rev. Lett. **84**, 2722 (2000); R. Simon, Phys. Rev. Lett. **84**, 2726 (2000).

[12] G. Giedke *et al.*, Phys. Rev. Lett. **91**, 107901 (2003).

[13] L. K. Thomsen, S. Mancini, and H. M. Wiseman, Phys. Rev. A **65**, 061801 (2002).

[14] J. M. Geremia, J. K. Stockton, and H. Mabuchi, Science **304**, 270 (2004).

[15] T. C Ralph and P. K. Lam, Phys. Rev. Lett. **81**, 5668 (1998); F. Grosshans and P. Grangier, Phys. Rev. A **64**, 010301 (2001).

[16] W. P. Bowen *et al.*, IEEE J. Sel. Top. Quantum Electron. **9**, 1519 (2003).

Mesure de polarisation

Article 8, reproduit en page 94

Stokes-operator-squeezed continuous-variable polarization states

R. Schnabel, W. P. Bowen, N. Treps, T.C. Ralph, H.-A. Bachor et P.K. Lam

Phys. Rev. A 67, 012316

Abstract : We investigate nonclassical Stokes-operator variances in continuous-wave polarization-squeezed laser light generated from one and two optical parametric amplifiers. A general expression of how Stokes-operator variances decompose into two-mode quadrature operator variances is given. Stokes parameter variance spectra for four different polarization-squeezed states have been measured and compared with a coherent state. Our measurement results are visualized by three-dimensional Stokes-operator noise volumes mapped on the quantum Poincaré sphere. We quantitatively compare the channel capacity of the different continuous-variable polarization states for communication protocols. It is shown that squeezed polarization states provide 33% higher channel capacities than the optimum coherent beam protocol.

Article 9, reproduit en page 105

Experimental demonstration of continuous variable polarization entanglement

W.P. Bowen, N. Treps, R. Schnabel et P.K. Lam

Phys. Rev. Lett. 89, 253601 (2002)

Abstract : We report the experimental transformation of quadrature entanglement between two optical beams into continuous variable polarization entanglement.We extend the inseparability criterion proposed by Duan et al. [Phys. Rev. Lett. 84, 2722 (2000)] to polarization states and use it to quantify the entanglement.We propose an elaboration utilizing two quadrature entangled pairs for which all three Stokes operators between a pair of beams are entangled.

PHYSICAL REVIEW A **67**, 012316 (2003)

Stokes-operator-squeezed continuous-variable polarization states

Roman Schnabel,[1,2] Warwick P. Bowen,[1] Nicolas Treps,[1] Timothy C. Ralph,[3] Hans-A. Bachor,[1] and Ping Koy Lam[1]
[1]*Department of Physics, Faculty of Science, Australian National University, Canberra ACT 0200, Australia*
[2]*Albert-Einstein-Institut, Max-Planck-Institut für Gravitationsphysik, 30167 Hannover, Germany*
[3]*Department of Physics, Centre for Lasers, University of Queensland, St. Lucia, Queensland QLD 4072, Australia*
(Received 13 August 2002; published 28 January 2003)

We investigate nonclassical Stokes-operator variances in continuous-wave polarization-squeezed laser light generated from one and two optical parametric amplifiers. A general expression of how Stokes-operator variances decompose into two-mode quadrature operator variances is given. Stokes parameter variance spectra for four different polarization-squeezed states have been measured and compared with a coherent state. Our measurement results are visualized by three-dimensional Stokes-operator noise volumes mapped on the quantum Poincaré sphere. We quantitatively compare the channel capacity of the different continuous-variable polarization states for communication protocols. It is shown that squeezed polarization states provide 33% higher channel capacities than the optimum coherent beam protocol.

DOI: 10.1103/PhysRevA.67.012316 PACS number(s): 03.67.−a, 42.50.Dv, 42.65.Yj, 03.65.−w

I. INTRODUCTION

The quantum properties of the polarization of continuous-wave light are of increasing interest since they offer new opportunities for communicating quantum information with light and for transferring quantum information from atoms to photons and vice versa. In the single photon regime, the quantum polarization states have been vigorously studied, theoretically and experimentally, with investigations of fundamental problems of quantum mechanics, such as Bell's inequality [1,2], and of potential applications such as quantum cryptography [3,4]. In comparison, continuous-variable quantum polarization states have received little attention. Recently, however, due to their apparent usefulness to quantum communication schemes, interest in them has been growing and a number of theoretical papers have been published [5–14].

Continuous-variable quantum polarization states can be carried by a bright laser beam, providing high-bandwidth capabilities and, therefore, faster signal transfer rates than single-photon systems. In addition, several proposals have been made for quantum networks that consist of spatially separated nodes of atoms, whose spin states enable the storage and processing of information, connected by optical quantum communication channels [15–17]. Mapping of quantum states from photonic to atomic media is a crucial element in these networks. For continuous-variable polarization states, this mapping has been experimentally demonstrated [18]. Very recently, entanglement was experimentally demonstrated for optical continuous-variable polarization states [19].

Several methods for generating continuous-variable polarization squeezed states have been proposed, most using nonlinearity provided by Kerr-like media and optical solitons [8,11,14]. The two experimental demonstrations previous to our work reported here and in Ref. [20], however, were achieved by combining a dim quadrature squeezed beam with a bright coherent beam on a polarizing beam splitter [22,23]. In both cases, only the properties of the state relevant to the experimental outcome were characterized. The full characterization of a continuous-variable polarization state requires measurements of the fluctuations in both the orientation, and the length of the Stokes vector on a Poincaré sphere.

In this paper, we present the complete experimental characterization of the Stokes-vector fluctuations for four different quantum polarization states. We make use of ideas recently published by Korolkova *et al.* [14]. Their concept of squeezing more than one Stokes-operator of a laser beam and a simple scheme to measure the Stokes-operator variances are realized. Our results given in Ref. [20] are extended and discussed in more detail. Experimental data from polarization-squeezed states generated from a single quadrature squeezed beam and from two quadrature squeezed beams are compared.

The outline of this paper is as follows. We present a description of the theory involved in our experiments. The well-known Schwinger bosonic representation allows the decomposition of any spinlike operator into a pair of mode operators of the quantum harmonic oscillator [21]. In this paper, we are interested in the variances of these operators and present a decomposition for the Stokes-operators variances; our decomposition is general within the commonly used linearization approach. In the experimental section, we characterize the polarization fluctuations of a single amplitude squeezed beam from an optical parametric amplifier (OPA). It can be seen that only the fluctuations of the Stokes vector length are below that of a coherent beam (i.e., squeezed). Grangier *et al.* [22] and Sørensen *et al.* [23] converted this to squeezing of the Stokes vector orientation by combining the quadrature squeezed beam with a much brighter coherent beam on a polarizing beam splitter. We experimentally generate this situation and indeed show that the Stokes vector orientation is squeezed. This result is compared with measurements on polarization states generated from two quadrature squeezed beams. Two bright amplitude or phase squeezed beams from two independent OPAs are overlapped on a polarizing beam splitter [14,20] demonstrating ''pancakelike'' and ''cigarlike'' uncertainty volumes on the Poincaré sphere for phase and amplitude squeezed input beams, respectively. Both the orientation and the length of the Stokes vector were squeezed for the cigarlike

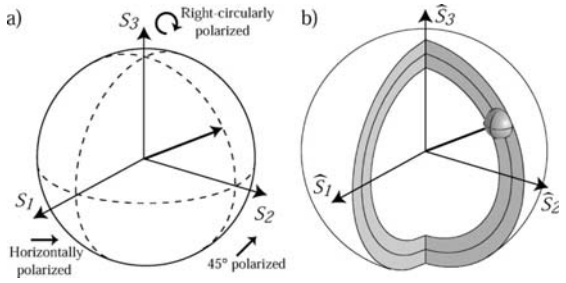

FIG. 1. Diagram of (a) classical and (b) quantum Stokes vectors mapped on a Poincaré sphere; the ball at the end of the quantum vector visualizes the quantum noise in $\hat{S}_1$, $\hat{S}_2$, and $\hat{S}_3$; and the nonzero quantum sphere thickness visualizes the quantum noise in $\hat{S}_0$.

uncertainty volume. In the final section, several schemes for encoding information on continuous-variable polarization states of light are discussed. The conventional fiber-optic communication protocol is compared with the optimized coherent beam and squeezed beam protocols. We show that the channel capacity of the cigarlike polarization-squeezed states exceeds the channel capacity of coherent states, quadrature squeezed states, and all other polarization-squeezed states.

II. THEORETICAL BACKGROUND

The polarization state of a light beam in classical optics can be visualized as a Stokes vector on a Poincaré sphere (Fig. 1) and is determined by the four Stokes parameters [24]: S_0 represents the average beam intensity whereas S_1, S_2, and S_3 characterize its polarization and form a Cartesian axes system. If the Stokes vector points in the direction of S_1, S_2, or S_3 the polarized part of the beam is horizontally, linearly at 45°, or right-circularly polarized, respectively. Two beams are said to be opposite in polarization and do not interfere if their Stokes vectors point in opposite directions. The quantity $S=(S_1^2+S_2^2+S_3^2)^{1/2}$ is the radius of the classical Poincaré sphere and describes the average intensity of the polarized part of the radiation. The fraction S/S_0 $(0<S/S_0<1)$ is called the degree of polarization. For quasimonochromatic laser light that is almost completely polarized S_0 is a redundant parameter, completely determined by the other three parameters ($S_0=S$ in classical optics). All four Stokes parameters are accessible from the simple experiments shown in Fig. 2.

An equivalent representation of polarization states of light is given by the four elements of the coherence matrix (Jones matrix). The relations between these elements and the Stokes parameters can be found in Ref. [25]. In contrast to the coherence matrix elements, the Stokes parameters are observables and, therefore, can be associated with Hermitian operators. Following Refs. [26,27], we define the quantum-mechanical analog of the classical Stokes parameters for pure states in the commonly used notation:

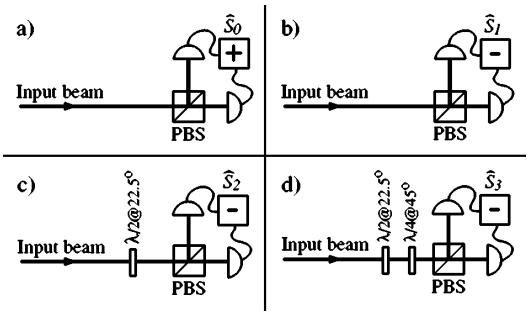

FIG. 2. Apparatus required to measure each of the Stokes parameters. PBS, polarizing beam splitter; λ/2 and λ/4, half- and quarter-wave plates, respectively, the plus and minus signs imply that an electrical sum or difference has been taken.

$$\begin{aligned}\hat{S}_0&=\hat{a}_H^\dagger\hat{a}_H+\hat{a}_V^\dagger\hat{a}_V,\\ \hat{S}_1&=\hat{a}_H^\dagger\hat{a}_H-\hat{a}_V^\dagger\hat{a}_V,\\ \hat{S}_2&=\hat{a}_H^\dagger\hat{a}_V e^{i\theta}+\hat{a}_V^\dagger\hat{a}_H e^{-i\theta},\\ \hat{S}_3&=i\hat{a}_V^\dagger\hat{a}_H e^{-i\theta}-i\hat{a}_H^\dagger\hat{a}_V e^{i\theta},\end{aligned} \tag{1}$$

where the subscripts H and V label the horizontal and vertical polarization modes, respectively, θ is the phase shift between these modes, and the $\hat{a}_{H,V}$ and $\hat{a}_{H,V}^\dagger$ are annihilation and creation operators for the electromagnetic field in frequency space [28].

The commutation relations of the annihilation and creation operators

$$[\hat{a}_k,\hat{a}_l^\dagger]=\delta_{kl}, \quad \text{with} \quad k,l\in\{H,V\}, \tag{2}$$

directly result in Stokes-operator commutation relations

$$[\hat{S}_1,\hat{S}_2]=2i\hat{S}_3, \quad [\hat{S}_2,\hat{S}_3]=2i\hat{S}_1, \quad [\hat{S}_3,\hat{S}_1]=2i\hat{S}_2. \tag{3}$$

Apart from the normalization factor, these relations are identical to the commutation relations of the Pauli spin matrices. In fact, the three Stokes parameters in Eq. (3) and the three Pauli spin matrices both generate the special unitary group of symmetry transformations SU(2) of Lie algebra [29]. Since this group obeys the same algebra as the three-dimensional rotation group, distances in three dimensions are invariant. Accordingly, the operator $\hat{S}_0$ is also invariant and commutes with the other three Stokes-operators ($[\hat{S}_0,\hat{S}_j]=0$, with $j=1,2,3$). The noncommutability of the Stokes-operators $\hat{S}_1$, $\hat{S}_2$, and $\hat{S}_3$ precludes the simultaneous exact measurement of their physical quantities. As a direct consequence of Eq. (3), the Stokes-operator mean values $\langle\hat{S}_j\rangle$ and their variances $V_j=\langle\hat{S}_j^2\rangle-\langle\hat{S}_j\rangle^2$ are restricted by the uncertainty relations [26]

$$V_1V_2\geq|\langle\hat{S}_3\rangle|^2, \quad V_2V_3\geq|\langle\hat{S}_1\rangle|^2, \quad V_3V_1\geq|\langle\hat{S}_2\rangle|^2. \tag{4}$$

In general, this results in nonzero variances in the individual Stokes parameters as well as in the radius of the Poincaré sphere [see Fig. 1(b)]. The quantum noise in the Stokes parameters even affects the definitions of the degree of polarization [5,11] and the Poincaré sphere radius. It can be shown from Eqs. (1) and (2) that the quantum Poincaré sphere radius is different from its classical analog, $\langle \hat{S} \rangle = \langle \hat{S}_0^2 + 2\hat{S}_0 \rangle^{1/2}$.

Recently, it has been shown that the Stokes-operator variances may be obtained from the frequency spectrum of the electrical output currents of the setups shown in Fig. 2 [14]. To calculate the Stokes-operator variances, we use the linearized formalism here. The creation and annihilation operators are expressed as sums of real classical amplitudes $\alpha_{H,V}$ and quantum noise operators $\delta\hat{a}_{H,V}$ [30],

$$\hat{a}_{H,V} = \alpha_{H,V} + \delta\hat{a}_{H,V}. \tag{5}$$

The operators in Eq. (5) are non-Hermitian and therefore nonphysical. To express the Stokes-operators of Eq. (1) in terms of Hermitian operators, we define the generalized quadrature quantum noise operators $\delta\hat{X}_{H,V}(\xi)$,

$$\delta\hat{X}_{H,V}(\xi) = \delta\hat{a}_{H,V}^{\dagger} e^{i\xi} + \delta\hat{a}_{H,V} e^{-i\xi}, \tag{6}$$

$$\delta\hat{X}_{H,V}(\xi = 0) = \delta\hat{X}_{H,V}^{+} = \delta\hat{a}_{H,V}^{\dagger} + \delta\hat{a}_{H,V}, \tag{7}$$

$$\delta\hat{X}_{H,V}(\xi = \pi/2) = \delta\hat{X}_{H,V}^{-} i(\delta\hat{a}_{H,V}^{\dagger} - \delta\hat{a}_{H,V}). \tag{8}$$

ξ is the phase of the quantum-mechanical oscillator and $\delta\hat{X}_{H,V}^{+}$ and $\delta\hat{X}_{H,V}^{-}$ are the amplitude quadrature noise operator and the phase quadrature noise operator, respectively.

If the variances of the noise operators are much smaller than the coherent amplitudes, then a first-order approximation of the noise operators is appropriate. This yields the Stokes-operator mean values

$$\begin{aligned} \langle \hat{S}_0 \rangle &= \alpha_H^2 + \alpha_V^2 = \langle \hat{n} \rangle, \\ \langle \hat{S}_1 \rangle &= \alpha_H^2 - \alpha_V^2, \\ \langle \hat{S}_2 \rangle &= 2\alpha_H \alpha_V \cos\theta, \\ \langle \hat{S}_3 \rangle &= 2\alpha_H \alpha_V \sin\theta. \end{aligned} \tag{9}$$

These expressions are identical to the Stokes parameters in classical optics. Here, $\langle \hat{n} \rangle$ is the expectation value of the photon number operator. For a coherent, beam the expectation value and variance of $\hat{n}$ have the same magnitude, this magnitude equals the conventional shot-noise level. The variances of the Stokes parameters are given by

$$\begin{aligned} V_0 &= \alpha_H^2 \langle (\delta\hat{X}_H^{+})^2 \rangle + \alpha_V^2 \langle (\delta\hat{X}_V^{+})^2 \rangle + 2\alpha_H \alpha_V \langle \delta\hat{X}_H^{+} \delta\hat{X}_V^{+} \rangle, \\ V_1 &= \alpha_H^2 \langle (\delta\hat{X}_H^{+})^2 \rangle + \alpha_V^2 \langle (\delta\hat{X}_V^{+})^2 \rangle - 2\alpha_H \alpha_V \langle \delta\hat{X}_H^{+} \delta\hat{X}_V^{+} \rangle, \\ V_2(\theta) &= \alpha_H^2 \langle (\delta\hat{X}_V(-\theta))^2 \rangle + \alpha_V^2 \langle (\delta\hat{X}_H(\theta))^2 \rangle, \\ &\quad + 2\alpha_H \alpha_V \langle \delta\hat{X}_V(-\theta)\, \delta\hat{X}_H(\theta) \rangle, \\ V_3(\theta) &= V_2\left(\theta - \frac{\pi}{2}\right). \end{aligned} \tag{10}$$

It can be seen from Eqs. (10) that the variances of Stokes-operators can be expressed in terms of the variances of quadrature operators of two-modes. The polarization-squeezed state can then be defined in a straightforward manner. The variances of the noise operators in the above equation are normalized to one for a coherent beam. Therefore, the variances of the Stokes parameters of a coherent beam are all equal to the shotnoise of the beam. For this reason a Stokes parameter is said to be squeezed if its variance falls below the shot-noise of an equal-power coherent beam. Although, the decomposition to the *H*, *V*-polarization axis of Eqs. (10) is independent of the actual procedure of generating a polarization-squeezed beam, it becomes clear that two overlapped quadrature squeezed beams can produce a single polarization squeezed beam. If two beams in the horizontal and vertical polarization modes having uncorrelated quantum noise are used, then Eqs. (10) can be rewritten as

$$\begin{aligned} V_0 &= V_1 = \alpha_H^2 \langle (\delta\hat{X}_H^{+})^2 \rangle + \alpha_V^2 \langle (\delta\hat{X}_V^{+})^2 \rangle, \\ V_2(\theta) &= \cos^2\theta [\alpha_V^2 \langle (\delta\hat{X}_H^{+})^2 \rangle + \alpha_H^2 \langle (\delta\hat{X}_V^{+})^2 \rangle] \\ &\quad + \sin^2\theta [\alpha_V^2 \langle (\delta\hat{X}_H^{-})^2 \rangle + \alpha_H^2 \langle (\delta\hat{X}_V^{-})^2 \rangle], \\ V_3(\theta) &= V_2\left(\theta - \frac{\pi}{2}\right). \end{aligned} \tag{11}$$

Here, we choose the amplitude and the phase quadrature noise operators to express the variances. This corresponds to our actual experimental setup, where either amplitude or the phase quadratures were squeezed. It can be seen from Eqs. (11) that in a polarization-squeezed beam generated from two amplitude squeezed beams $\hat{S}_0$ and two additional Stokes parameters can in theory be perfectly squeezed while the fourth is antisqueezed if specific angles of $\theta = 0$ or $\theta = \pi/2$ are used. By utilizing only one squeezed beam it is not possible to simultaneously squeeze any two of $\hat{S}_1$, $\hat{S}_2$, and $\hat{S}_3$ by more than 3 dB below shot noise ($V_i + V_j \geqslant \langle \hat{n} \rangle$, with $i,j \in \{1,2,3; i \neq j\}$).

III. EXPERIMENT

Prior to our work presented here and in Ref. [20], polarization squeezed states were generated by combining a strong coherent beam with a single weak-amplitude squeezed beam [22,18]. In both of those experiments, the variance of only one Stokes parameter was determined, and therefore, the polarization state was not fully characterized. In this paper, we experimentally characterize the mean and variance of all four Stokes-operators for these states. We extend the work to polarization-squeezed states produced from two amplitude

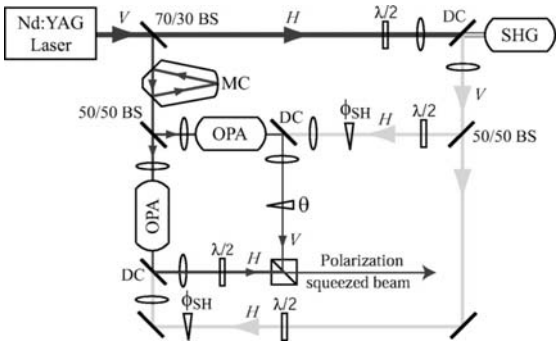

FIG. 3. Schematic of the polarization squeezing experiment. MC, mode cleaner; BS, beam splitter; DC, dichroic beam splitter; λ/2, half-wave plate; ϕ_{SH}, phase shift between 532 nm and 1064 nm light at the OPAs; θ, phase shift between quadrature squeezed beams; PBS, polarizing beam splitter; *H*, horizontal polarization mode; *V*, vertical polarization mode.

or phase squeezed beams. Figure 3 shows our experimental setup.

A. Generation of quadrature squeezed light

We produced the two quadrature squeezed beams required for this experiment in a pair of OPAs. Each OPA was an optical resonator consisting of a hemilithic MgO:$LiNbO_3$ crystal and an output coupler. The reflectivities of the output coupler were 96% and 6% for the fundamental (1064 nm) and the second harmonic (532 nm) laser modes, respectively. Each OPA was pumped with single-mode 532-nm light generated by a 1.5 W Nd:YAG nonplanar ring laser and frequency doubled in a second-harmonic generator (SHG). The SHG was of identical structure to the OPAs but with 92% reflectivity at 1064 nm. The OPAs were seeded with 1064-nm light after spectral filtering in a modecleaner. The refractive indices of the MgO:$LiNbO_3$ crystals in each resonator was modulated with an rf field, this provided error signals on the reflected seed power that were used to lock their lengths. The modulation also resulted in a phase modulation on the output beams from the SHG and each OPA. The coherent amplitude of each OPAs output was a deamplified or amplified version of the seed coherent amplitude; the level of amplification was dependent on the phase difference between pump and seed (ϕ_{SH}). Therefore, the second-harmonic pump phase modulation resulted in a modulation of the amplification of the OPAs. Error signals could be extracted from this effect, enabling the relative phase between pump and seed to be locked. Locking to deamplification or amplification provided an amplitude or phase squeezed output, respectively. Typical measured variance spectra of the two locked quadrature squeezed beams are shown in Fig. 4. Since the squeezed states were carried by bright laser beams of $\approx$1 mW, the noise reduction was degraded at lower frequencies due to the laser relaxation oscillation. At higher frequencies, the squeezed spectrum was limited by the bandwidth of the OPAs.

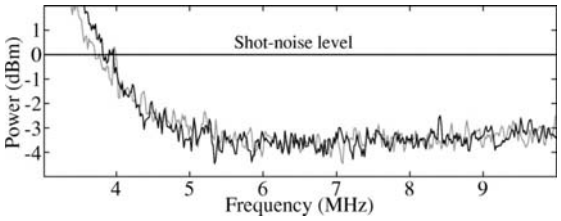

FIG. 4. Typical measured variance spectra of the two locked bright quadrature squeezed beams.

Past experiments requiring two quadrature squeezed beams commonly used a single ring resonator with two outputs [31]; with two independent OPAs the necessary intracavity pump power is halved, this reduces the degradation of squeezing due to Green-induced infrared absorption [32].

B. Measuring the Stokes operators

Instantaneous values of the Stokes-operators of all polarization states analyzed in this paper were obtained with the apparatus shown in Fig. 2. The uncertainty relations of Eqs. (4) dictate that $\hat{S}_1$, $\hat{S}_2$, and $\hat{S}_3$ cannot, in general, be measured simultaneously. The beam under interrogation was split on a polarizing beam splitter and the two outputs were detected on a pair of high quantum efficiency photodiodes with 30 MHz bandwidth; the resulting photocurrents were added and subtracted to yield photocurrents containing the instantaneous values of $\hat{S}_0$ and $\hat{S}_1$. To measure $\hat{S}_2$, the polarization of the beam was rotated by 45° with a half-wave plate before the polarizing beam splitter and the detected photocurrents were subtracted. To measure $\hat{S}_3$, the polarization of the beam was again rotated by 45° with a half-wave plate and a quarter-wave plate was introduced before the polarizing beam splitter such that a horizontally polarized input beam became right-circularly polarized. Again the detected photocurrents were subtracted. The expectation value of each Stokes-operator was equal to the dc output of the detection device and the variance was obtained by passing the output photocurrent into a Hewlett-Packard E4405B spectrum analyzer. Every polarization state interrogated in this work had a total power $\langle \hat{S}_0 \rangle$ of roughly 2 mW.

An accurate shot-noise level was required to determine whether any given Stokes-operator was squeezed. This was measured by operating a single OPA without the second-harmonic pump. The seed power was adjusted so that the output power was equal to that of the beam being interrogated. In this configuration, the detection setup for $\hat{S}_2$ [see Fig. 2(c)] functions exactly as a homodyne detector measuring vacuum noise scaled by the OPA output power, the variance of which is the shot noise. Throughout each experimental run the power was monitored and was always within 2% of the power of the coherent calibration beam. This led to a conservative error in our frequency spectra of ± 0.05 dB.

The Stokes-operator variances reported in this paper were taken over the range from 3 to 10 MHz. The dark noise of the detection apparatus was always more than 4 dB below the measured traces and was taken into account. Each dis-

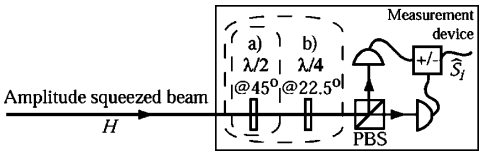

FIG. 5. Apparatus used to produce and analyze a single amplitude squeezed beam. Optics in (a) and (b) were included to measure the variance and the expectation value of $\hat{S}_2$ and $\hat{S}_3$, respectively.

played trace is the average of three measurement results normalized to the shot noise and smoothed over the resolution bandwidth of the spectrum analyzer which was set to 300 kHz. The video bandwidth of the spectrum analyzer was set to 300 Hz.

As is the case for all continuous-variable quantum optical experiments, the efficiency of the Stokes-operator measurements was critical. The overall detection efficiency of the interrogated beams was 76%. The loss came primarily from three sources: loss in escape from the OPAs (14%), detector inefficiency (7%), and loss in optics (5%). In the experiment, where a squeezed beam was overlapped with a coherent beam, additional loss was incurred due to poor mode matching between the beams and the detection efficiency was 71%. Depolarizing effects are thought to be another significant source of loss for some polarization squeezing proposals [5]. In our scheme, the nonlinear processes (OPAs) are separated from the polarization manipulation (wave plates and polarizing beam splitters), and depolarizing effects are insignificant.

C. Quantum polarization states from a single squeezed beam

We first characterize the polarization state of a single bright amplitude squeezed beam provided by one of our OPAs, as shown in Fig. 5. The squeezed beam was horizontally polarized, resulting in Stokes-operator expectation values of $\langle\hat{S}_0\rangle=\langle\hat{S}_1\rangle=|\alpha_H|^2$ and $\langle\hat{S}_2\rangle=\langle\hat{S}_3\rangle=0$. The variance spectra of the operators were measured and are displayed in Fig. 6. The variances of S0 and S1 were squeezed. This result is quite obvious since the laser beam used was amplitude squeezed and impinged on a single detector in this detector setup. Therefore, both the measurements performed equated a measurement of the amplitude quadrature variance. For the measurements of $\hat{S}_2$ and $\hat{S}_3$, the beam intensity was divided equally between the two detectors. The electronic subtraction yielded vacuum noise scaled by the beam intensity, thus both variance measurements were at the shot-noise level. It is apparent from these measurements that only the length of the Stokes vector, is well determined; the orientation is just as uncertain as it would be for a coherent state.

To obtain squeezing of the orientation of the Stokes vector, Grangier *et al.* [22] and Sørensen *et al.* [23] overlapped a dim quadrature squeezed beam with a bright orthogonally polarized coherent beam. We consider this situation next (as shown in Fig. 7). Since two beams are now involved, the relative phase θ becomes important. A dc and an rf error signal, both dependent on θ, were extracted from the Stokes-operator measurement device. Together, these error signals

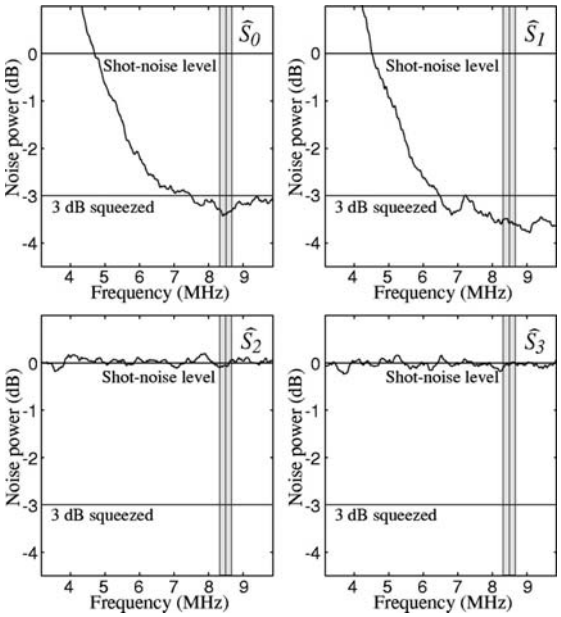

FIG. 6. Measured variance spectra of quantum noise on $\hat{S}_0$, $\hat{S}_1$, $\hat{S}_2$, and $\hat{S}_3$ for a single bright amplitude squeezed beam; normalized to shot noise. The shaded region was used to construct the Poincaré sphere representation in Fig. 12(b).

allowed us to lock θ to either 0 or $\pi/2$ rad in all of the following experiments. We mixed a bright horizontally polarized coherent beam with a dim vertically polarized amplitude squeezed beam. Since the horizontally polarized beam was much more intense than the vertically polarized beam, the Stokes-operator expectation values became $\langle\hat{S}_0\rangle\approx\langle\hat{S}_1\rangle\approx|\alpha_H|^2$ and $\langle\hat{S}_2\rangle\approx\langle\hat{S}_3\rangle=0$. The Stokes-operator variances obtained for this polarization state are shown in Fig. 8, here $\hat{S}_2$ is antisqueezed and $\hat{S}_3$ is squeezed. The variances of $\hat{S}_0$ and $\hat{S}_1$ were slightly above the shot-noise level because of residual noise from our laser resonant relaxation oscillation. The experiment carried out with θ locked to 0 rad is not shown, in this case, the measured variances of $\hat{S}_2$ and $\hat{S}_3$ were swapped. In fact, the Stokes vector was still pointing along $\hat{S}_1$ but the quantum noise was rotated on the Poincaré sphere [see Fig. 13(b)].

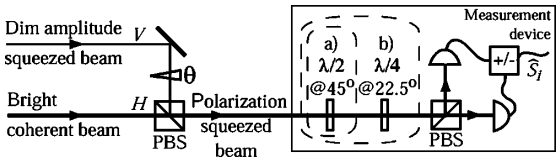

FIG. 7. Apparatus used to produce and analyze the polarization squeezed beam produced by overlapping a dim quadrature squeezed beam with a bright coherent beam. Optics in (a) and (b) were included to measure the variance and the expectation value of $\hat{S}_2$ and $\hat{S}_3$, respectively.

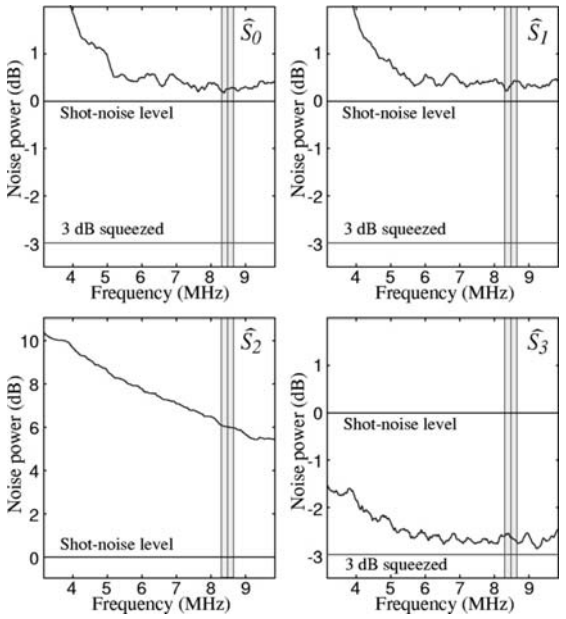

FIG. 8. Measured variance spectra of quantum noise on $\hat{S}_0$, $\hat{S}_1$, $\hat{S}_2$, and $\hat{S}_3$ for a vacuum amplitude squeezed and a bright coherent input beams; normalized to shot noise. The shaded region was used to construct the Poincaré sphere representation in Fig. 12(c).

D. Quantum polarization states from two quadrature squeezed beams

The two experiments described in Sec. III C demonstrated how it is possible to squeeze the length and orientation of the Stokes vector. In this section, we demonstrate that it is possible to do both simultaneously. The two quadrature squeezed beams produced in our OPAs were combined with orthogonal polarization on a polarizing beam splitter [14] as shown in Fig. 9. This produced an output beam with Stokes-parameter variances as given by Eqs. (11). Both input beams had equal power ($\alpha_H = \alpha_V = \alpha/\sqrt{2}$) and both were squeezed in the same quadrature. The Stokes parameters and their variances were again determined as shown in Fig. 2. The relative phase between the quadrature squeezed input beams θ was locked to $\pi/2$ rads producing a right-circularly polarized beam with Stokes parameter means of $\langle \hat{S}_1 \rangle = \langle \hat{S}_2 \rangle = 0$ and $\langle \hat{S}_0 \rangle = \langle \hat{S}_3 \rangle = |\alpha|^2$.

First, both OPA pump beams were phase locked to amplification, this produced two phase squeezed beams. Figure 10 shows the measurement results obtained; $\hat{S}_0$, $\hat{S}_1$, and $\hat{S}_3$ were all anti-squeezed and $\hat{S}_2$ was squeezed throughout the range of the measurement. The optimum noise reduction of $\hat{S}_2$ was 2.8 dB below shot noise and was observed at 4.8 MHz. Our OPAs are particularly sensitive to phase noise coupling in from the MgO:LiNbO$_3$ crystals. We attribute the structure in the frequency spectra of $\hat{S}_2$ and the poorer degree of squeezing observed here, to this. Apart from this structure, these results are very similar to those produced by a single

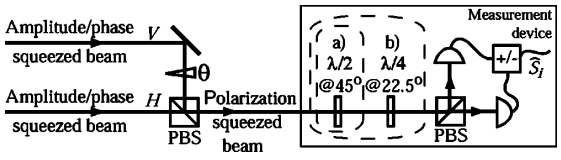

FIG. 9. Apparatus used to produce and analyze the beam produced by combining two quadrature squeezed beams. Optics in (a) and (b) were included to measure the variance and the expectation value of $\hat{S}_2$ and $\hat{S}_3$, respectively.

squeezed beam and a coherent beam; the orientation of the Stokes vector is squeezed. However, here the uncertainty in the length of the Stokes vector is greater than for a coherent state so the polarization state, although produced from two quadrature squeezed beams, is actually less certain.

Figure 11 shows the measurement results obtained with the OPAs locked to deamplification. Therefore, both OPAs provided amplitude squeezed beams. Again, we interrogated the combined beams and found $\hat{S}_0$, $\hat{S}_1$, and $\hat{S}_3$ all to be squeezed from 4.5 MHz to the limit of our measurement, 10 MHz. $\hat{S}_2$ was antisqueezed throughout the range of the measurement. Between 7.2 MHz and 9.6 MHz $\hat{S}_0$, $\hat{S}_1$, and $\hat{S}_3$ were all more than 3 dB below shot noise. The squeezing of $\hat{S}_0$ and $\hat{S}_3$ was degraded at low frequency due to our lasers resonant relaxation oscillation. Since this noise was correlated, it is canceled in the variance of $\hat{S}_1$. The maximum squeezing of $\hat{S}_0$ and $\hat{S}_2$ was 3.8 dB and 3.5 dB, respectively,

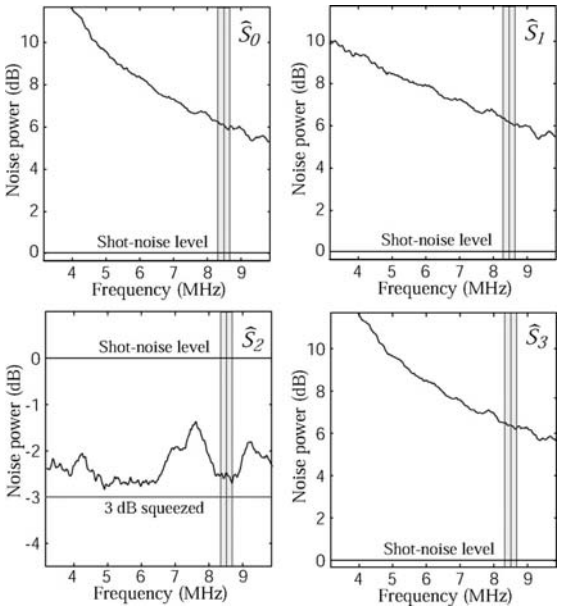

FIG. 10. Measured variance spectra of quantum noise on $\hat{S}_0$, $\hat{S}_1$, $\hat{S}_2$, and $\hat{S}_3$ for two locked phase squeezed input beams; normalized to shot noise. The shaded region was used to construct the Poincaré sphere representation in Fig. 12(d).

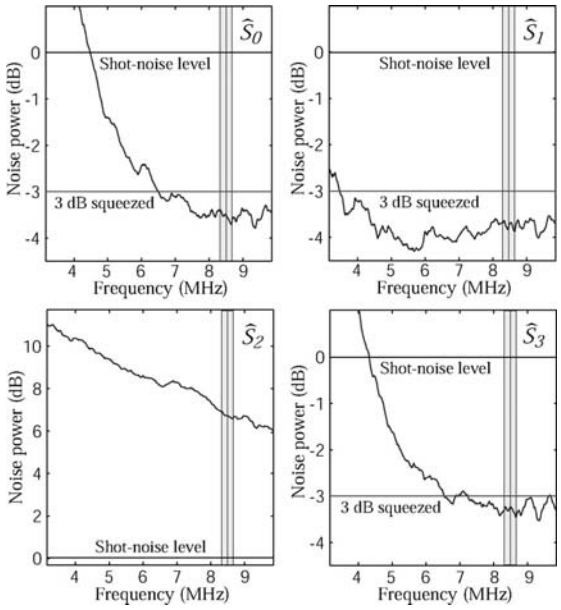

FIG. 11. Measured variance spectra of quantum noise on $\hat{S}_0$, $\hat{S}_1$, $\hat{S}_2$, and $\hat{S}_3$ for two locked amplitude squeezed input beams; normalized to shot noise. The shaded region was used to construct the Poincaré sphere representation in Fig. 12(e).

and was observed at 9.3 MHz. The maximum squeezing of $\hat{S}_1$ was 4.3 dB at 5.7 MHz. The repetitive structure at 4, 5, 6, 7, 8, and 9 MHz was caused by electrical pickup in our SHG resonator emitted from a separate experiment operating in the laboratory. In this case both the orientation and the length of the Stokes vector were squeezed.

Finally, we point out that the variances of $\hat{S}_1$ in Figs. 8, 10, and 11 were all squeezed at frequencies down to 3 MHz and even below, whereas Fig. 4 shows a clear degradation below 4 MHz. This improved performance is due to electrical noise cancellation of correlated laser relaxation oscillation noise. This noise is effectively reduced by taking the difference of the two photo currents in our detector setup to measure V_1.

IV. VISUALIZATION OF QUANTUM CORRELATIONS IN CONTINUOUS-VARIABLE POLARIZATION STATES

In this section, measured quantum correlations in polarization states at 8.5 MHz are visualized. Based on the theoretical formalism in Sec. II continuous-variable polarization states can be characterized by the measurement of Stokes-operator expectation values and variances using the setup shown in Fig. 2. Our noise measurement results at 8.5 MHz on five different states are summarized in Fig. 12. The noise characteristics of the Stokes parameters are mapped onto the coordinate system of the Poincaré sphere, assuming Gaussian noise statistics. Given this assumption, the standard deviation contour surfaces shown here provide an accurate representation of the states three-dimensional noise distribution.

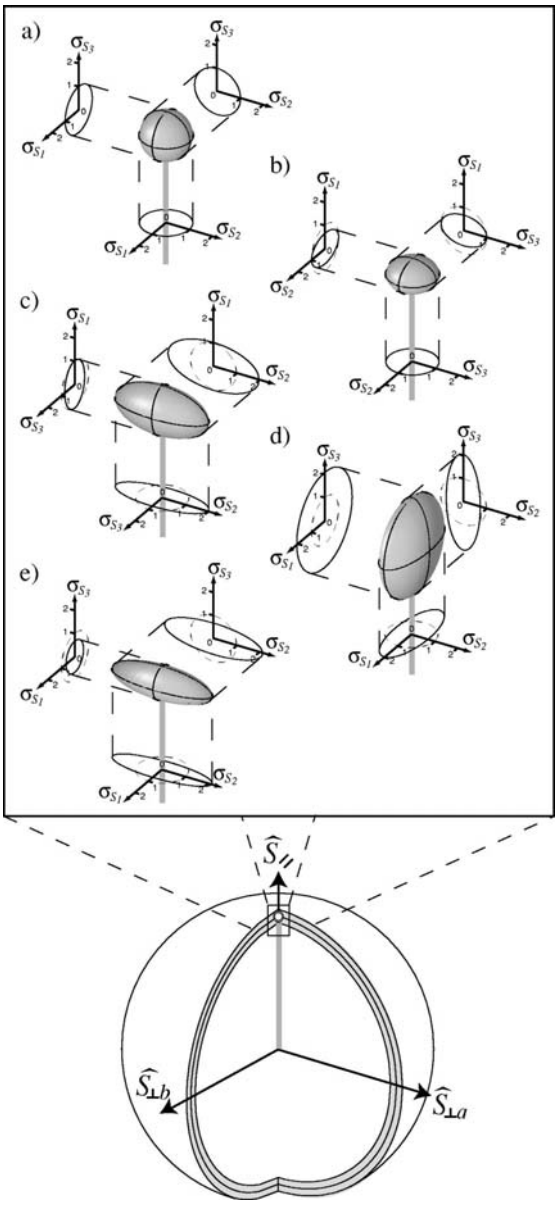

FIG. 12. Measured quantum polarization noise at 8.5 MHz from different combinations of input beams. (a) Single coherent beam, (b) coherent beam and squeezed vacuum, (c) bright squeezed beam, (d) two phase squeezed beams, and (e) two amplitude squeezed beams. The surface of the ellipsoids defines the standard deviation of the noise normalized to shot noise ($\sigma_{S_i}=\sqrt{V_i}$). $\hat{S}_{\parallel}$ denotes the Stokes operator along the Stokes vector.

The quantum polarization noise of a coherent state forms a sphere of noise as portrayed in Fig. 12(a). The noise volumes (b)–(e) visualizes the measurements on a single bright amplitude squeezed beam, on the combination of a vacuum amplitude squeezed beam and a bright coherent beam, on two

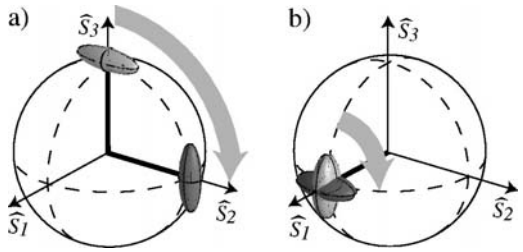

FIG. 13. Visualization of measured quantum noise and measured Stokes vectors of four polarization states mapped onto the Poincaré sphere. The states were generated from (a) two bright amplitude squeezed inputs and (b) a bright coherent beam and a amplitude squeezed vacuum. The rotation in (a) and also in (b) was achieved by a $\theta=\pi/2$ phase shift or an additionally introduced $\lambda/4$ wave plate.

locked phase squeezed input beams and on two locked amplitude squeezed beams, respectively. In all cases, the Stokes-operator noise volume describes the end position of the Stokes vector pointing upwards. In (b) and (c) the Stokes vectors are parallel to the direction of S_1, in (d) and (e) parallel to the direction of S_3, since we used horizontally and right-circularly polarized light, respectively. However, there was no fundamental bias in the orientation of the quantum Stokes vector in our experiment. By varying the angle of an additional half-wave plate in the polarization-squeezed beam or by varying θ, any orientation may be achieved. In fact, as mentioned earlier, our experiments were also carried out with θ locked to 0 rad. This had the effect of rotating the Stokes vector and its quantum noise by $\pi/2$ around $\hat{S}_1$. Nearly identical results were obtained but on alternative Stokes parameters. Figure 13 a) shows Poincaré sphere representations of this rotation for the polarization states produced by two amplitude squeezed beams. In Fig. 13(b), the combination of a amplitude squeezed vacuum and a bright coherent beam exemplifies that different orientations of the noise volume can be generated using appropriate combination of wave plates.

V. CHANNEL CAPACITY OF POLARIZATION SQUEEZED BEAMS

The reduced level of fluctuations in polarization-squeezed light can be used to improve the channel capacity of communication protocols. Let us consider information encoded on the sidebands of a bandwidth-limited single spatial mode laser beam. We assume that only direct detection is employed, or in other words, that phase sensitive techniques such as homodyne measurement are not available. This is not an artificial constraint since phase-sensitive techniques are technically difficult to implement and are rarely utilized in conventional optical communications systems.

An upper bound to the amount of information that can be carried by a bandwidth-limited additive white Gaussian noise channel is given by the Shannon capacity C [33] in bits per dimension,

$$C=\frac{1}{2}\log_2(1+R). \tag{12}$$

R is the signal-to-noise ratio of the channel and is given by the ratio of the spectral variance of the signal modulation V_s and the noise spectral variance V_n,

$$R=\frac{V_s}{V_n}. \tag{13}$$

We wish to compare the channel capacities achieveable with pure coherent and squeezed states for a given average photon number in the sidebands $\bar{n}$, where

$$\bar{n}=\langle \delta\hat{a}_H^\dagger \delta\hat{a}_H+\delta\hat{a}_V^\dagger \delta\hat{a}_V\rangle \tag{14}$$

and

$$\langle \delta\hat{a}^\dagger \delta\hat{a}\rangle=\frac{1}{4}(V_n^+ + V_n^- -2+V_s^+ + V_s^-). \tag{15}$$

$\bar{n}$ takes into account both sideband photons entailed by squeezing of the quantum noise and by signal modulation. The superscripts $+$ and $-$ label the amplitude and the phase quadrature, respectively. Note that without squeezing and signal modulation, the number of sideband photons is equal to zero. An overview of quantum noise limited channel capacities may be found in Refs. [34,35].

First, let us consider strategies which might be employed with a coherent light beam. In conventional optical communication systems, the polarization degrees of freedom are ignored completely and information is encoded only on $\hat{S}_0$ as intensity fluctuations. Taking $\alpha_V=0$, the variance of the Stokes-operator $\hat{S}_0$ is given by $V_0=\alpha_H^2(V_{n,H}^+ + V_{s,H}^+)$ in accordance with Eq. (11). For this one-dimensional coherent channel, $V_{n,H}^+=\langle|\delta X_H^+|^2\rangle=1$ and, therefore, $R=V_{s,H}^+$. It can be shown from Eqs. (14) and (15) that for this arrangement, the average photon number per bandwidth per second is $\bar{n}=\frac{1}{4}V_{s,H}^+$ providing a photon resource limited Shannon capacity of

$$C_{\mathrm{coh}}^i=\frac{1}{2}\log_2(1+4\bar{n}), \tag{16}$$

as a function of $\bar{n}$. This is a nonoptimal strategy, however. Examining Eqs. (3) and (9) we see that it is possible to choose an arrangement, for which two of the Stokes operators commute and so can be measured simultaneously. Indeed, it is easy to show that such simultaneous measurements can be made using only linear optics and direct detection. In particular, let us assume that $\alpha_H=\alpha_V$ such that $\hat{S}_2$ and $\hat{S}_3$ commute, and use $\hat{S}_2$ and $\hat{S}_3$ as two independent information channels. Then $\hat{S}_2=\hat{S}_0$ and the information in both dimensions can be simultaneously extracted by subtracting and adding the photocurrents of the same pair of detectors. Assuming equal signal-to-noise ratios, $R_2=R_3$, we find that $V_{s,2}=V_{s,3}=2\bar{n}$, and the channel capacity may be written

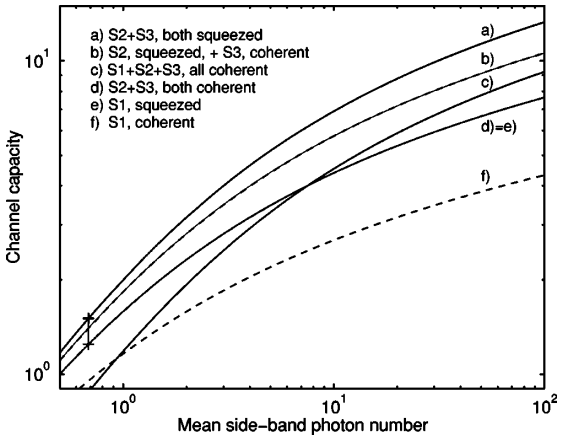

FIG. 14. Calculated channel capacities for various continuous-variable polarization states. The channel's dimension and the channel's quantum noise performance is varied. The cross in the upper curve marks the channel capacity, which can be achieved using the polarization-squeezed state in Fig. 11 and is compared with the optimum coherent state channel capacity (lower cross).

$$C_{\mathrm{coh}}^{ii}=\frac{1}{2}\log_2(1+R_2)+\frac{1}{2}\log_2(1+R_3)=\log_2(1+2\bar{n}). \tag{17}$$

This channel capacity is always greater than that of Eq. (16) and for large $\bar{n}$ is 100% greater.

For sufficiently high $\bar{n}$ a further improvement in channel capacity can be achieved. Consider placing signals on all three Stokes-operators. Because of the noncommutation of $\hat{S}_1$ with $\hat{S}_2$ and $\hat{S}_3$, it is not possible to read out all three signals without a measurement penalty. Suppose the receiver adopts the following strategy: divide the beam on a beamsplitter with transmitivity ϵ and then measure $\hat{S}_1$ on the reflected output and $\hat{S}_2$ and $\hat{S}_3$ on the other output. Division of the beam will reduce the measured signal-to-noise ratios due to the injection of quantum noise at the beamsplitter such as $R_1=(1-\epsilon)V_{s,1}$, $R_2=\epsilon V_{s,2}$, and $R_3=\epsilon V_{s,3}$. We find that for large $\bar{n}$ an optimum is reached with $\epsilon=2/3$ and the signal photon number in each Stokes parameter being $\bar{n}_1=\bar{n}_2=\bar{n}_3=\bar{n}/3$. Hence the channel capacity is

$$C_{\mathrm{coh}}^{\mathrm{iii}}=\frac{1}{2}\log_2(1+R_1)+\frac{1}{2}\log_2(1+R_2)+\frac{1}{2}\log_2(1+R_3)$$
$$=\frac{1}{2}\log_2\left(1+\frac{4}{9}\bar{n}\right)+\log_2\left(1+\frac{8}{9}\bar{n}\right). \tag{18}$$

This capacity beats that of Eq. (17) for $\bar{n}>7.56$. In summary, the optimum coherent channel capacity is given by Eq. (18) for average photon numbers $\bar{n}>7.56$ and by Eq. (17) for lower values, see Fig. 14 curves traces *c* and *d*.

Now let us examine the effect of polarization squeezing on the channel capacity. Consider, first, the simple case of intensity modulation on a single squeezed beam, which is equivalent to using a squeezed beam in the first coherent case considered [case (i)]. The channel capacity can be maximized by optimizing the fraction of photons that are introduced by squeezing the quantum noise and the residual fraction of photons, which actually carries the signal. For large photon numbers we find a proportioning of 0.5. For an average photon number of 1, just one-third of that photon should be used to reduce the quantum noise. The maximum channel capacity for a one-dimensional squeezed channel is found to be

$$C_{1\mathrm{sqz}}^{\mathrm{i}}=\log_2(1+2\bar{n}), \tag{19}$$

which was previously given in Ref. [34]. This capacity beats only the corresponding coherent state. It is as efficient as the two-dimensional coherent channel, but less efficient than the three-dimensional coherent one for large photon numbers.

Consider now a polarization-squeezed beam that is produced from a minimum uncertainty squeezed beam and a coherent beam, as in Sec. III C. Suppose, as in case ii, that $\hat{S}_2$ and $\hat{S}_3$ commute and arrange such that $\hat{S}_2$ has fluctuations at the quantum noise level, while $\hat{S}_3$ is optimally squeezed. Again signals are encoded on $\hat{S}_2$ and $\hat{S}_3$. The channel capacity can be maximized by adjusting the relative signal sizes on the two Stokes-operators for fixed average photon number as a function of the squeezing. Here, one-third of the photons is used to squeeze and two-third is split equally for the two dimensions. The resultant maximum channel capacity is

$$C_{1\mathrm{sqz}}^{\mathrm{ii}}=\frac{3}{2}\log_2\left(1+\frac{4}{3}\bar{n}\right). \tag{20}$$

This always beats all three coherent state cases considered here, but in the limit of large $\bar{n}$ the advantage is minimal since the scaling with photon number is the same as that of $C_{\mathrm{coh}}^{\mathrm{iii}}$ in Eq. (18).

If the polarization-squeezed beam is produced from two amplitude squeezed beams as in Sec. III D, the enhancement becomes more significant. Suppose again that $\hat{S}_2$ and $\hat{S}_3$ commute but now that both are optimally squeezed. Again encoding on $\hat{S}_2$ and $\hat{S}_3$, and varying the signal strength as a function of squeezing to maximize the channel capacity for a given $\bar{n}$. The maximum is reached when the photons are used to squeeze the noise and transport information in equal shares. The channel capacity for this arrangement is given by

$$C_{2\mathrm{sqz}}^{\mathrm{ii}}=2\log_2(1+\bar{n}), \tag{21}$$

which for large $\bar{n}$ is 33% greater than both the optimum coherent scheme and the scheme using a single quadrature squeezed beam. No further improvement of the channel capacity can be obtained by encoding the information on three Stokes parameters, as in case (iii). Optimization of the beam splitter reflectivity results in the already considered two-dimensional arrangement. This is not a surprising result since the third Stokes parameter is antisqueezed. Figure 14 summarizes our results.

Finally, we assess the channel capacities that could, in principle, be achieved using the polarization-squeezed state generated in our experiment from two amplitude squeezed beams. The polarization squeezing achieved in Fig. 11 implies that, in the frequency range of 8–10 MHz, 0.17 sideband photons per bandwidth per second were present in each of the two dimensions. This is an optimum quantum resource to transmit 0.68 sideband photons. Signals sufficiently high above detector dark noise would achieve a channel capacity that is around 21% greater than the ideal channel capacity achievable from a coherent beam with the same average sideband photon number (see crosses in Fig. 14).

VI. CONCLUSION

The field of quantum communication and computation is receiving much attention. The continuous-variable polarization states investigated here are one of the most promising candidates for carrying the information in a quantum network. In this paper, we have characterized the nonclassical properties of these states on the basis of the Stokes-operators and their variances. Different classes of polarization-squeezed states have been generated and experimentally characterized. We compared the coherent polarization state in Fig. 12(a) with squeezed polarization states generated from a single amplitude squeezed beam as in Fig. 12(c) and from two amplitude squeezed beams as in Fig. 12(e), and proved that squeezing of better than 3 dB of three Stokes parameters ($\hat{S}_0$, $\hat{S}_1$, and $\hat{S}_3$) simultaneously is possible only in the latter case. We have theoretically analyzed the channel capacity for several communication protocols using continuous-variable polarization states. For a given average photon number $\overline{n}$, we found the polarization state produced from two quadrature squeezed states can provide a 33% greater channel capacity than both the optimum coherent scheme and the scheme using a single quadrature squeezed beam.

ACKNOWLEDGMENTS

We acknowledge the Alexander von Humboldt foundation for support of R. Schnabel; the Australian Research Council for financial support. This work is a part of EU QIPC Project No. IST-1999-13071 (QUICOV).

[1] J.S. Bell, *Speakable and Unspeakable in Quantum Mechanics* (Cambridge University Press, Cambridge, London, 1988).
[2] J.F. Clauser and A. Shimony, Rep. Prog. Phys. **41**, 1881 (1978); A. Aspect, P. Grangier, and G. Roger, Phys. Rev. Lett. **49**, 91 (1982).
[3] S. Wiesner, SIGACT News **15**, 78 (1983); C.H. Bennett and G. Brassard, in *Proceedings of IEEE International Conference on Computers, Systems and Signal Processing, Bangalore, India, 1984*, (IEEE, New York, 1984), pp. 175–179; C.H. Bennett, Phys. Rev. Lett. **68**, 3121 (1992); A.K. Ekert, *ibid.* **67**, 661 (1991).
[4] W.T. Buttler, R.J. Hughes, P.G. Kwiat, G.G. Luther, G.L. Morgan, J.E. Nordholt, C.G. Peterson, and C.M. Simmons, Phys. Rev. A **57**, 2379 (1998); H. Zbinden, H. Bechmann-Pasquinacci, N. Gisin, and G. Ribordy, Appl. Phys. B: Lasers Opt. **67**, 743 (1998).
[5] G.S. Agarwal and R.R. Puri, Phys. Rev. A **40**, 5179 (1989).
[6] A.S. Chirkin, A.A. Orlov, and D.Y. Parashchuk, Quantum Electron. **23**, 870 (1993).
[7] V.P. Karasev and A.V. Masalov, Opt. Spectrosc. **74**, 551 (1993).
[8] N.V. Korolkova and A.S. Chirkin, J. Mod. Opt. **43**, 869 (1996).
[9] A.S. Chirkin, A.P. Alodjants, and S.M. Arakelian, Opt. Spectrosc. **82**, 919 (1997).
[10] P.A. Bushev, V.P. Karassiov, A.V. Masalov, and A.A. Putilin, Opt. Spectrosc. **91**, 526 (2001).
[11] A.P. Alodjants, S.M. Arakelian, and A.S. Chirkin, Appl. Phys. B: Lasers Opt. **66**, 53 (1998).
[12] A.P. Alodjants, A.Y. Leksin, A.V. Prokhorov, and S.M. Arakelian, Laser Phys. **12**, 247 (2002).
[13] T.C. Ralph, W.J. Munro, and R.E.S. Polkinghorne, Phys. Rev. Lett. **85**, 2035 (2000).
[14] N. Korolkova, G. Leuchs, R. Loudon, T.C. Ralph, and Ch. Silberhorn, Phys. Rev. A **65**, 052306 (2002).
[15] D.P. DiVincenzo, Science **270**, 255 (1995).
[16] J.I. Cirac and P. Zoller, Phys. Rev. Lett. **74**, 4091 (1995).
[17] A. Kuzmich and E.S. Polzik, Phys. Rev. Lett. **85**, 5639 (2000).
[18] J. Hald, J.L. Sørensen, C. Schori, and E.S. Polzik, Phys. Rev. Lett. **83**, 1319 (1999).
[19] W.P. Bowen, N. Treps, R. Schnabel, and P.K. Lam, Phys. Rev. Lett. **89**, 253601 (2002).
[20] W.P. Bowen, R. Schnabel, H.-A. Bachor, and P.K. Lam, Phys. Rev. Lett. **88**, 093601 (2002).
[21] J. Schwinger, U. S. Atomic Energy Commission Report No. NYO-3071 (unpublished); in *Quantum Theory of Angular Momentum*, edited by L.C. Biedenharn and H. van Dam (Academic, New York, 1965).
[22] P. Grangier, R.E. Slusher, B. Yurke, and A. LaPorta, Phys. Rev. Lett. **59**, 2153 (1987).
[23] J.L. Sørensen, J. Hald, and E.S. Polzik, Phys. Rev. Lett. **80**, 3487 (1998).
[24] G.G. Stokes, Trans. Cambridge Philos. Soc. **9**, 399 (1852).
[25] L. Mandel and E. Wolf, *Optical Coherence and Quantum Optics* (Cambridge University Press, Cambridge, London, 1995).
[26] J.M. Jauch and F. Rohrlich, *The Theory of Photons and Electrons*, 2nd ed. (Springer, Berlin, 1976).
[27] B.A. Robson, *The Theory of Polarization Phenomena* (Clarendon, Oxford, 1974).
[28] Here, we have excluded the phase difference θ from the mode operators to illustrate the link to our experiment more clearly.
[29] See, for example, M. Kaku, *Quantum Field Theory* (Oxford University Press, New York, 1993).
[30] D.F. Walls and G.J. Milburn, *Quantum Optics* (Springer, Berlin, 1995).

[31] See, for example, Z.Y. Ou, S.F. Pereira, H.J. Kimble, and K.C. Peng, Phys. Rev. Lett. **68**, 3663 (1992).
[32] Y. Furukawa, K. Kitamura, A. Alexandrovski, R.K. Route, M.M. Fejer, and G. Foulon, Appl. Phys. Lett. **78**, 1970 (2001).
[33] C.E. Shannon, Bell Syst. Tech. J. **27**, 623 (1948).
[34] Y. Yamamoto and H.A. Haus, Rev. Mod. Phys. **58**, 1001 (1986).
[35] C.M. Caves and P.D. Drummond, Rev. Mod. Phys. **66**, 481 (1994).

VOLUME 89, NUMBER 25 PHYSICAL REVIEW LETTERS 16 DECEMBER 2002

Experimental Demonstration of Continuous Variable Polarization Entanglement

Warwick P. Bowen, Nicolas Treps, Roman Schnabel, and Ping Koy Lam
Department of Physics, Faculty of Science, Australian National University, ACT 0200, Australia
(Received 13 March 2002; published 4 December 2002)

We report the experimental transformation of quadrature entanglement between two optical beams into continuous variable polarization entanglement. We extend the inseparability criterion proposed by Duan *et al.* [Phys. Rev. Lett. **84**, 2722 (2000)] to polarization states and use it to quantify the entanglement. We propose an elaboration utilizing two quadrature entangled pairs for which all three Stokes operators between a pair of beams are entangled.

DOI: 10.1103/PhysRevLett.89.253601 PACS numbers: 42.50.Dv, 03.67.Hk, 42.65.Yj

The polarization state of light has been extensively studied in the quantum mechanical regime of single (or few) photons. The demonstration of entanglement of the polarization of pairs of photons has been of particular interest. This entanglement has facilitated the study of many interesting quantum phenomena such as Bell's inequality [1]. Comparatively, research on continuous variable quantum polarization states has been cursory. Recently, however, interest in the field has increased due to the demonstration of transfer of continuous variable quantum optical polarization states to the spin state of atomic ensembles [2]; and to its potential for local oscillator-free continuous variable quantum communication networks. A number of theoretical papers have now been published [3,4], of particular interest is the work of Korolkova *et al.* [5] which introduces the new concept of continuous variable polarization entanglement, and proposes methods for its generation and characterization. Previous to the work presented here, however, only the squeezing of polarization states had been experimentally demonstrated [2,6,7].

In this paper we report the experimental transformation of the commonly studied and well understood entanglement between the phase and amplitude quadratures of two beams (quadrature entanglement) [8] onto a polarization basis. Quadrature entanglement can be characterized using the inseparability criterion proposed by Duan *et al.* [9]. We generalize this criterion to an arbitrary pair of observables and apply it to the Stokes operators that define quantum polarization states. We experimentally generate entanglement of Stokes operators between a pair of beams, satisfying both the inseparability criterion, and the product of conditional variances which is a signature of the EPR paradox [10]. Interacting this entanglement with a pair of distant atomic ensembles could entangle the atomic spin states. We also analyze the polarization state generated by combining two quadrature entangled pairs. We show that if the quadrature entanglement is strong enough to beat a bound $\sqrt{3}$ times lower than that for the inseparability criterion, then all three Stokes operators can be simultaneously entangled.

The polarization state of a light beam can be described as a Stokes vector on a Poincaré sphere and is determined by the four Stokes operators [11]: $\hat{S}_0$ represents the beam intensity whereas $\hat{S}_1$, $\hat{S}_2$, and $\hat{S}_3$ characterize its polarization and form a Cartesian axis system. If the Stokes vector points in the direction of $\hat{S}_1$, $\hat{S}_2$, or $\hat{S}_3$, the polarized part of the beam is horizontally, linearly at 45°, or right-circularly polarized, respectively. Quasimonochromatic laser light is almost completely polarized, in this case $\hat{S}_0$ is a redundant parameter, determined by the other three operators. All four Stokes operators can be measured with simple experiments [5]. Following [11] we expand the Stokes operators in terms of the annihilation $\hat{a}$ and creation $\hat{a}^\dagger$ operators of the constituent horizontally (subscript H) and vertically (subscript V) polarized modes

$$\begin{aligned} \hat{S}_0 &= \hat{a}_H^\dagger \hat{a}_H + \hat{a}_V^\dagger \hat{a}_V, & \hat{S}_2 &= \hat{a}_H^\dagger \hat{a}_V e^{i\theta} + \hat{a}_V^\dagger \hat{a}_H e^{-i\theta}, \\ \hat{S}_1 &= \hat{a}_H^\dagger \hat{a}_H - \hat{a}_V^\dagger \hat{a}_V, & \hat{S}_3 &= i\hat{a}_V^\dagger \hat{a}_H e^{-i\theta} - i\hat{a}_H^\dagger \hat{a}_V e^{i\theta}, \end{aligned} \tag{1}$$

where θ is the phase difference between the H, V-polarization modes. Equations (1) are an example of the well-known bosonic representation of angular momentum type operators in terms of a pair of quantum harmonic oscillators introduced by Schwinger [12]. The commutation relations of the annihilation and creation operators $[\hat{a}_k, \hat{a}_l^\dagger] = \delta_{kl}$ with $k, l \in \{H, V\}$ directly result in Stokes operator commutation relations, $[\hat{S}_i, \hat{S}_j] = 2i\hat{S}_k$, where $i, j, k = 1, 2, 3$ are cyclically interchangeable. These commutation relations dictate uncertainty relations, which indicate that entanglement is possible between the Stokes operators of two beams, we term this continuous variables polarization entanglement. Three observables are involved, compared to two for quadrature entanglement, and the entanglement between two of them relies on the mean value of the third. To provide a proper definition of this entanglement, we have chosen to extend the inseparability criterion proposed by Duan *et al.* [9]. The inseparability criterion characterizes the separability of, and therefore the entanglement

between, the amplitude $\hat{X}^+$ and phase $\hat{X}^-$ quadratures of a pair of optical beams (denoted throughout by the subscripts x and y) with Gaussian noise statistics. These quadrature operators are observables and can be obtained from the annihilation and creation operators, $\hat{X}^+ = \hat{a} + \hat{a}^\dagger$, $\hat{X}^- = i(\hat{a}^\dagger - \hat{a})$. In this paper we restrict ourselves to the symmetric situation where all experimental outcomes are independent of exchange of beams x and y, in this case the inseparability criterion can be written as

$$\Delta^2_{x\pm y}\hat{X}^+ + \Delta^2_{x\pm y}\hat{X}^- < 4. \tag{2}$$

Throughout this paper $\Delta^2\hat{O} = \langle \delta\hat{O}^2\rangle$ where $\hat{O} = \langle\hat{O}\rangle + \delta\hat{O}$. $\Delta^2_{x\pm y}\hat{O}$ is the smaller of the sum and difference variances of the operator $\hat{O}$ between beams x and y, $\Delta^2_{x\pm y}\hat{O} = \min\langle(\delta\hat{O}_x \pm \delta\hat{O}_y)^2\rangle$. Note that for physically realistic entanglement between two observables, one observable must be correlated, and the other anticorrelated between subsystems x and y. The minimization utilized in calculating $\Delta^2_{x\pm y}\hat{O}$ selects the relevant sign for each observable. The measure in Eq. (2) relies explicitly on the uncertainty relation between the amplitude and phase quadrature operators. Given the general Heisenberg uncertainty relation $\Delta^2\hat{A}\Delta^2\hat{B} \geq |\langle\delta\hat{A}\delta\hat{B}\rangle|^2 = |[\delta\hat{A}, \delta\hat{B}]|^2/4 + |\langle\delta\hat{A}\delta\hat{B} + \delta\hat{B}\delta\hat{A}\rangle|^2/4$ [13] it can be generalized to any pair of observables $\hat{A}$, $\hat{B}$. Unlike the commutation relation $|[\delta\hat{A}, \delta\hat{B}]|$, the correlation function $|\langle\delta\hat{A}\delta\hat{B} + \delta\hat{B}\delta\hat{A}\rangle|$ is state dependant. In this work we assume it to be zero and arrive at the sufficient condition for inseparability

$$\Delta^2_{x\pm y}\hat{A} + \Delta^2_{x\pm y}\hat{B} < 2|[\delta\hat{A}, \delta\hat{B}]|. \tag{3}$$

To allow direct analysis of our experimental results, we define the degree of inseparability $I(\hat{A}, \hat{B})$, normalized such that $I(\hat{A}, \hat{B}) < 1$ guarantees the state is inseparable

$$I(\hat{A}, \hat{B}) = \frac{\Delta^2_{x\pm y}\hat{A} + \Delta^2_{x\pm y}\hat{B}}{2|[\delta\hat{A}, \delta\hat{B}]|}. \tag{4}$$

An arbitrary pair of polarization modes may be constructed by combining horizontally and vertically polarized modes on a pair of polarizing beam splitters. In the symmetric situation, which this paper is restricted to, the horizontally (vertically) polarized input beams must be interchangeable; therefore, their expectation values and variances must be the same ($\alpha_H = \langle\hat{a}_{H,x}\rangle = \langle\hat{a}_{H,y}\rangle$, $\alpha_V = \langle\hat{a}_{V,x}\rangle = \langle\hat{a}_{V,y}\rangle$, $\Delta^2\hat{X}^\pm_H = \Delta^2\hat{X}^\pm_{H,x} = \Delta^2\hat{X}^\pm_{H,y}$, $\Delta^2\hat{X}^\pm_V = \Delta^2\hat{X}^\pm_{V,x} = \Delta^2\hat{X}^\pm_{V,y}$), and the relative phase between horizontally and vertically polarized modes for subsytems x and y must be related by $\theta = \theta_x = \pm\theta_y + m\pi$ where m is an integer. Given these assumptions it is possible to calculate $I(\hat{S}_i, \hat{S}_j)$ from Eqs. (1). We choose to simplify the situation further, providing results that may be directly related to our experiment. We assume that the horizontal and vertical inputs are not correlated, and that each input beam does not exhibit internal amplitude/phase quadrature correlations. Finally, we assume that the vertically polarized input modes are bright ($\alpha_V^2 \gg 1$) so that second order terms are negligible. The denominators of Eq. (4) for the three possible combinations of Stokes operators are then found to be

$$\begin{aligned} |[\delta\hat{S}_1\delta, \hat{S}_2]| &= 4\alpha_H\alpha_V \sin\theta, \\ |[\delta\hat{S}_1, \delta\hat{S}_3]| &= 4\alpha_H\alpha_V \cos\theta, \\ |[\delta\hat{S}_2, \delta\hat{S}_3]| &= 2|\alpha_H^2 - \alpha_V^2|. \end{aligned} \tag{5}$$

In our experiment the phase θ between the horizontally and vertically polarized input modes was controlled to be $\pi/2$, in this situation $|[\delta\hat{S}_1, \delta\hat{S}_3]| = 0$ which means that using the inseparability criterion of Eq. (4) it is impossible to verify entanglement between $\hat{S}_1$ and $\hat{S}_3$. On the other hand $|[\delta\hat{S}_1, \delta\hat{S}_2]|$ and $|[\delta\hat{S}_2, \delta\hat{S}_3]|$ both have finite values and therefore the potential for entanglement. We experimentally determined $I(\hat{S}_1, \hat{S}_2)$ and $I(\hat{S}_2, \hat{S}_3)$ from measurements of α_V, α_H, and $\Delta^2_{x\pm y}\hat{S}_i$.

The experimental transformation between quadrature and polarization entanglement demonstrated here becomes clearer if $\Delta^2_{x\pm y}\hat{S}_i$ are expressed in terms of quadrature operators. Assuming that $\alpha_H^2 \ll \alpha_V^2$ we find from Eqs. (1) that $\Delta^2_{x\pm y}\hat{S}_1 = \alpha_V^2\Delta^2_{x\pm y}\hat{X}^+_V$, $\Delta^2_{x\pm y}\hat{S}_2 = \alpha_V^2\Delta^2_{x\pm y}\hat{X}^-_H$, and $\Delta^2_{x\pm y}\hat{S}_3 = \alpha_V^2\Delta^2_{x\pm y}\hat{X}^+_H$. $I(\hat{S}_1, \hat{S}_2)$ and $I(\hat{S}_2, \hat{S}_3)$ can then be written

$$I(\hat{S}_1, \hat{S}_2) = \frac{\alpha_V}{\alpha_H}\left(\frac{\Delta^2_{x\pm y}\hat{X}^+_V + \Delta^2_{x\pm y}\hat{X}^-_H}{8}\right), \tag{6}$$

$$I(\hat{S}_2, \hat{S}_3) = \left(1 + \frac{\alpha_H^2}{\alpha_V^2}\right)\left(\frac{\Delta^2_{x\pm y}\hat{X}^+_H + \Delta^2_{x\pm y}\hat{X}^-_H}{4}\right). \tag{7}$$

Equation (6) shows that as α_V/α_H increases the level of correlation required for $I(\hat{S}_1, \hat{S}_2)$ to fall below unity and therefore to demonstrate inseparability quickly becomes experimentally unachievable. In particular, if the horizontal inputs are vacuum states $I(\hat{S}_1, \hat{S}_2)$ becomes infinite and verification of entanglement is not possible. In contrast, Eq. (7) shows that in this situation $I(\hat{S}_2, \hat{S}_3)$ becomes identical to the criterion for quadrature entanglement [Eq. (2)] between the two horizontally polarized inputs. Therefore, quadrature entanglement between the horizontally polarized inputs is transformed to polarization entanglement between $\hat{S}_2$ and $\hat{S}_3$. In the following section we experimentally demonstrate this transformation. The asymmetry of these results arises because the Stokes vector of the output mode of each polarizing beam splitter is aligned almost exactly along $\hat{S}_1$ (since $\alpha_H \gg \alpha_V$). This creates an asymmetry in the commutation relations and a corresponding bias in the uncertainty relations that define the inseparability criteria.

In our experiment two equal power 1064 nm amplitude squeezed beams were produced in a pair of spatially separated optical parametric amplifiers (OPAs). The

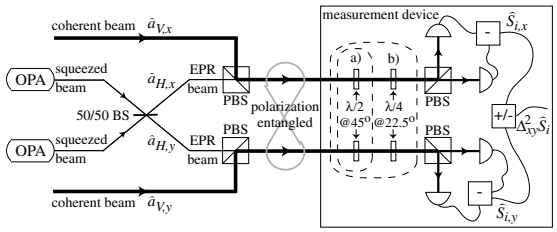

FIG. 1. Experimental production and characterization of continuous variable polarization entanglement. The optics within (a) are included to measure $\hat{S}_2$, and those within (b) to measure $\hat{S}_3$. (P)BS: (polarizing) beam splitter.

OPAs were optical resonators constructed from hemilithic MgO:$LiNbO_3$ crystals and output couplers and are described in detail in Ref. [7]. We combined the squeezed beams with $\pi/2$ phase shift on a 50/50 beam splitter with interference efficiency of 97.8%. The output beams exhibited the conventional quadrature entanglement [8]. We modematched each entangled beam into a homodyne detector that provided amplitude or phase quadrature measurements and characterized the entanglement with the inseparability measure given in Eq. (2). We obtained the result $I(\hat{X}^+, \hat{X}^-) = (\Delta^2_{x\pm y}\hat{X}^+ + \Delta^2_{x\pm y}\hat{X}^-)/4 = 0.44$, which is well below unity. We also determined the product of conditional variances between the beams ($\min_g[\langle(\delta\hat{X}^+_x + g\delta\hat{X}^+_y)^2\rangle\langle(\delta\hat{X}^-_x - g\delta\hat{X}^-_y)^2\rangle] < 1$), which was propose by Reid and Drummond [10] as a signature of the EPR paradox. We observed a value of 0.58 which is also well below unity.

We transformed the entanglement onto a polarization basis by combining each entangled beam (horizontally polarized) with a much more intense vertically polarized coherent beam ($\alpha^2_V = 30\alpha^2_H$) with measured modematching efficiency for both of 91% (see Fig. 1). The relative phase between the horizontal and vertical input modes θ was controlled to be $\pi/2$. The two resultant beams were polarization entangled. We verified this entanglement by measuring correlations of the Stokes operators between the beams.

Each beam was split on a polarizing beam splitter and the two outputs were detected on a pair of high quantum efficiency photodiodes. Dependent on the inclusion of wave plates before the polarizing beam splitter, the difference photocurrent between the two photodiodes yielded instantaneous values for $\hat{S}_1$, $\hat{S}_2$, or $\hat{S}_3$ (see Fig. 1). The variance of the unity gain electronic sum or subtraction of the Stokes operator measurements between the polarization entangled beams was obtained in a spectrum analyzer that had a resolution bandwidth of 300 kHz and video bandwidth of 300 Hz. This resulted in values for $\Delta^2_{x\pm y}\hat{S}_i$. All of the presented results were taken over the sideband frequency range from 2 to 10 MHz and are the average of ten consecutive traces. Every trace was more than 4.5 dB above the measurement dark noise which was taken into account. We determined α^2_V directly by blocking the horizontal modes and measuring the power spectrum of the subtraction between the two homodynes, this also gave α^2_H since the ratio α^2_V/α^2_H was measured to equal 30.

Figure 2 shows our experimental measurements of $I(\hat{S}_1, \hat{S}_2)$ and $I(\hat{S}_2, \hat{S}_3)$. The dashed lines indicate the results a pair of coherent beams would produce. Both traces are below this line throughout almost the entire measurement range; this is an indication that the light is in a nonclassical state. At low frequencies both traces were degraded by noise introduced by the relaxation oscillation of our laser. $I(\hat{S}_2, \hat{S}_3)$ shows polarization entanglement, however as expected $I(\hat{S}_1, \hat{S}_2)$ is far above unity. The best entanglement was observed at 6.8 MHz with $I(\hat{S}_2, \hat{S}_3) = 0.49$ which is well below unity.

By electronically adding or subtracting the Stokes operator measurements with a gain g chosen to minimize the resulting variance we observed a signature of the EPR paradox for polarization states. In this case the product of the conditional variances of $\hat{S}_2$ and $\hat{S}_3$ from one beam after utilizing information gained through measurement of the other must be less than the Heisenberg uncertainty product ($\min_g[\langle(\delta\hat{S}_{2,x} \pm g\delta\hat{S}_{2,y})^2\rangle\langle(\delta\hat{S}_{3,x} \pm g\delta\hat{S}_{3,y})^2\rangle] < |[\delta\hat{S}_2, \delta\hat{S}_3]|^2/4$). We observed a conditional variance product of $0.77|[\delta\hat{S}_2, \delta\hat{S}_3]|^2/4$.

Polarization entanglement has more degrees of freedom than quadrature entanglement because three observables, rather than two, are involved. In the following section we consider the continuous variable situation most analogous to single photon polarization entanglement where the correlation is independent of the basis of measurement, and demonstrate theoretically that all three Stokes operators can be simultaneously entangled. We extend the work of Ref. [5], and arrange the entanglement such that Eqs.. (5) are equal and the mean value of the

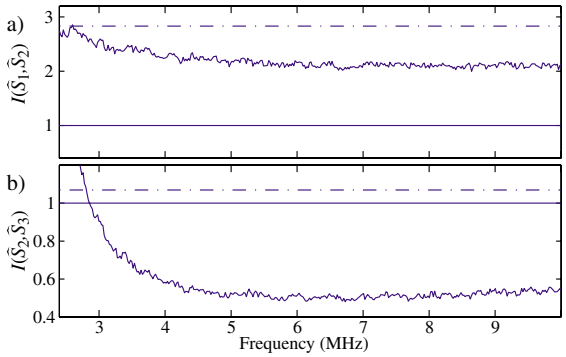

FIG. 2 (color online). Experimental measurement of (a) $I(\hat{S}_1, \hat{S}_2)$ and (b) $I(\hat{S}_2, \hat{S}_3)$, values below unity indicate entanglement. The dashed line is the corresponding measurement inferred between two coherent beams.

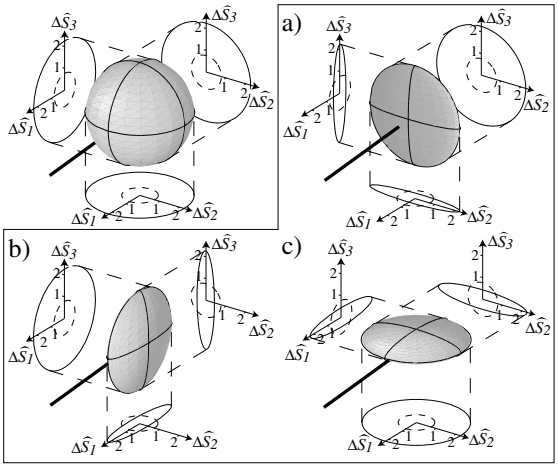

FIG. 3. Calculated polarization entanglement produced from four pure quadrature squeezed beams with squeezed quadrature variances of 0.1; axes normalized to 1 for a coherent state. The top left figure represents the knowledge of beam y before any measurement of beam x. (a), (b), and (c) represent the conditional knowledge of beam y given measurements of $\hat{S}_1$, $\hat{S}_2$, and $\hat{S}_3$, respectively, on beam x. If the conditional knowledge is better than the dashed circles the state is entangled.

three Stokes operators are the same ($|\langle \hat{S}_i \rangle| = \alpha^2$). This leads to $\alpha_V^2 = [(\sqrt{3}-1)/2]\alpha^2$, $\alpha_H^2 = [(\sqrt{3}+1)/2]\alpha^2$, $\theta_x = \pi/4 + n_x\pi/2$, and $\theta_y = \pi/4 + n_y\pi/2$, where n_x and n_y are integers. We assume that the two horizontally polarized inputs, and the two vertically polarized inputs, are quadrature entangled with the same degree of correlation such that $\Delta^2_{x\pm y}\hat{X}^{\pm}_H = \Delta^2_{x\pm y}\hat{X}^{\pm}_V = \Delta^2_{x\pm y}\hat{X}$. In this configuration, Eqs. (5) become $|\langle \delta\hat{S}_i \delta\hat{S}_j \rangle| = \alpha^2$, for all $i \neq j$. To simultaneously minimize all three degrees of Stokes operator inseparability $[I(\hat{S}_i, \hat{S}_j)]$ it is necessary that $\theta_x = -\theta_y + n\pi$. After making this assumption we find that $\Delta^2_{x+y}\hat{S}_i = \sqrt{3}\alpha^2\Delta^2_{x\pm y}\hat{X}$ for all i. Hence, in this situation $I(\hat{S}_i, \hat{S}_j)$ are all identical, and the entanglement is equivalent between any two Stokes operators. The condition for entanglement can then be expressed as a simple criterion on the quadrature entanglement between the input beams

$$I(\hat{S}_i, \hat{S}_j) < 1 \Longleftrightarrow I(\hat{X}^+, \hat{X}^-) < 1/\sqrt{3}, \tag{8}$$

where $I(\hat{X}^+, \hat{X}^-) = I(\hat{X}^+_H, \hat{X}^-_H) = I(\hat{X}^+_V, \hat{X}^-_V)$. The factor of $1/\sqrt{3}$ arises from the projection of the quadrature properties onto a polarization basis in which the Stokes vector is pointing at equal angle $[\cos^{-1}(1/\sqrt{3})]$ from all three Stokes operator axes. In principle it is possible to have all three Stokes operators perfectly entangled. In other word, ideally the measurement of any Stokes operator of one of the beams could allow the exact prediction of that Stokes operator from the other beam (see Fig. 3). The experimental production of such a field is a straightforward extension of the experiment reported here, given the availability of four independent squeezed beams. Maximal single photon polarization entanglement enables tests of Bells inequality [1]. It has recently been shown that continuous variable polarization entanglement of the form discussed above can also exhibit Bell-like correlations [4]. This entanglement resource would also enable the demonstration of maximal continuous variable polarization teleportation.

To conclude, we have presented the first generation of continuous variable polarization entanglement. The scheme presented transforms the well-understood quadrature entanglement to a polarization basis. The two Stokes operators orthogonal to the Stokes vectors of the polarization entangled beams easily fulfill a generalized version of the inseparability criterion proposed by Duan *et al.*. We have also demonstrated that in the limiting case of our experimental configuration where $\alpha_V^2 \gg 1$ and $\alpha_H^2 = 0$ it is not possible to verify entanglement between any other pair of Stokes operators. Finally, we have shown that using four squeezed beams it is possible for all three Stokes operators to be perfectly entangled, although with a bound $\sqrt{3}$ times lower (stronger) than that for quadrature entanglement.

This work was supported by the Australian Research Council and is part of the EU QIPC Project, No. IST-1999-13071 (QUICOV). R. S. acknowledges the Alexander von Humboldt Foundation for support. We are grateful of H. A. Bachor and T. C. Ralph for invaluable discussion.

[1] A. Aspect *et al.*, Phys. Rev. Lett. **49**, 91 (1982).
[2] J. Hald *et al.*, Phys. Rev. Lett. **83**, 1319 (1999); B. Julsgaard *et al.*, Nature (London) **413**, 400 (2001).
[3] N. V. Korolkova and A. S. Chirkin, J. Mod. Opt. **43**, 869 (1996); A. S. Chirkin *et al.*, Kvant. Elektron. Mosk. **20**, 999 (1993); A. P. Alodjants *et al.*, Appl. Phys. B **66**, 53 (1998).
[4] T. C. Ralph *et al.*, Phys. Rev. Lett. **85**, 2035 (2000).
[5] N. V. Korolkova *et al.*, Phys. Rev. A **65**, 052306 (2002).
[6] P. Grangier *et al.*, Phys. Rev. Lett. **59**, 2153 (1987).
[7] W. P. Bowen *et al.*, Phys. Rev. Lett.**88**, 093601 (2002).
[8] Z. Y. Ou *et al.*, Phys. Rev. Lett. **68**, 3663 (1992).
[9] L-M. Duan *et al.*, Phys. Rev. Lett. **84**, 2722 (2000).
[10] M. D. Reid and P. D. Drummond, Phys. Rev. Lett. **60**, 2731 (1988).
[11] J. M. Jauch and F. Rohrlich, *The Theory of Photons and Electrons* (Springer, Berlin, 1976), 2nd ed.; B. A. Robson, *The Theory of Polarization Phenomena* (Clarendon, Oxford, 1974).
[12] J. Schwinger, in *Quantum Theory of Angular Momentum*, edited by L. C. Biedenharn and H. van Dam (Academic Press, New York, 1965), pp. 229–279.
[13] H. A. Haus, *Electromagnetic Noise and Quantum Optical Measurements* (Springer, Berlin, 2000).

Le nano positionnement

Article 10, reproduit en page 111

Surpassing the standard quantum limit for high sensitivity measurements in optical images using non classical light

N. Treps, U. Andersen, B. Buchler, P. K. Lam, A. Maître, H.-A. Bachor, C. Fabre
Phys. Rev. Lett. 88, 203601 (2002)

Abstract : Using continuous wave superposition of spatial modes, we demonstrate experimentally displacement measurement of a light beam below the standard quantum limit. Multimode squeezed light is obtained by mixing a vacuum squeezed beam and a coherent beam that are spatially orthogonal. Although the resultant beam is not squeezed, it is shown to have strong internal spatial correlations. We show that the position of such a light beam can be measured using a split detector with an increased precision compared to a classical beam. This method can be used to improve the sensitivity of small displacement measurements.

Article 11, reproduit en page 115

A Quantum Laser Pointer

N. Treps, N. Grosse, W. P. Bowen, C. Fabre, H.-A. Bachor, and P. K. Lam
Science Aug 15 2003 : 940-943

Abstract : The measurement sensitivity of the pointing direction of a laser beam is ultimately limited by the quantum nature of light. To reduce this limit, we have experimentally produced a quantum laser pointer, a beam of light whose direction is measured with a precision greater than that possible for a usual laser beam. The laser pointer is generated by combining three different beams in three orthogonal transverse modes, two of them in a squeezed-vacuum state and one in an intense coherent field. The result provides a demonstration of multichannel spatial squeezing, along with its application to the improvement of beam positioning sensitivity and, more generally, to imaging.

Article 12, reproduit en page 119

Quantum measurements of spatial conjugate variables : Displacement and tilt of a Gaussian beam

V. Delaubert, N. Treps, C.C. Harb, P.K. Lam and H.-A. Bachor
Optics Letters 31 1537-1539 (2006)

Abstract : We consider the problem of measurement of optical transverse profile parameters and their conjugate variable. Using multimode analysis, we introduce the concept of detection noise modes. For Gaussian beams, displacement and tilt are a pair of transverse-profile conjugate variables. We experimentally demonstrate the optimal encoding and detection of these variables

with a spatial homodyning scheme. Using higher-order spatial mode squeezing, we show the sub-shot-noise measurements for the displacement and tilt of a Gaussian beam.

Article 13, reproduit en page 122

Tools for multi-mode quantum information : modulation, detection and squeezing of spatial laser modes

M.Lassen, V.Delaubert, C.C.Harb, P.K.Lam, N.Treps, P.Buchhave, C.Fabre, and H-A.Bachor

Soumis à Phys. Rev. Lett.

Abstract : We present here all the required tools for continuous variable parallel quantum information protocols based on multi-mode quantum correlations and entanglement. We describe our ability to encode and detect quantum information with high efficiency. We experimentally demonstrate the generation of spatial correlations or optical squeezing in higher order transverse Hermite-Gauss modes. The higher order mode squeezing is achieved by the mode selective tuning of the phase matching condition and the cavity resonance condition of the nonlinear $\chi^{(2)}$ optical parametric amplification.

Article 14, reproduit en page 127

Continuous-Variable Spatial Entanglement for Bright Optical Beams

M.T.L. Hsu, W.P. Bowen, N. Treps and P.K. Lam

Phys. Rev. A 72, 013802 (2005)

Abstract : A light beam is said to be position squeezed if its position can be determined to an accuracy beyond the standard quantum limit. We identify the position and momentum observables for bright optical beams and show that position and momentum entanglement can be generated by interfering two position, or momentum, squeezed beams on a beam splitter. The position and momentum measurements of these beams can be performed using a homodyne detector with local oscillator of an appropriate transverse beam profile. We compare this form of spatial entanglement with split detection-based spatial entanglement.

Article 15, reproduit en page 134

Optical storage of high density information beyond the diffraction limit : a quantum study

V. Delaubert, N. Treps, G. Bo and C. Fabre

Phys. Rev. A 73, 013820 (2006)

Abstract : We propose an optical readout scheme allowing a proof of principle of information extraction below the diffraction limit. This technique, which could lead to improvement in data readout density onto optical disks, is independent from the wavelength and numerical aperture of the reading apparatus, and involves a multipixel array detector. Furthermore, we show how to use nonclassical light in order to perform a bit discrimination beyond the quantum noise limit.

VOLUME 88, NUMBER 20 PHYSICAL REVIEW LETTERS 20 MAY 2002

Surpassing the Standard Quantum Limit for Optical Imaging Using Nonclassical Multimode Light

N. Treps,[1,2] U. Andersen,[2,3] B. Buchler,[2] P. K. Lam,[2] A. Maître,[1] H.-A. Bachor,[2] and C. Fabre[1]

[1]*Laboratoire Kastler Brossel, Université Pierre et Marie Curie, case 74, 75252 Paris cedex 05, France*

[2]*Department of Physics, Faculty of Science, Australian National University, Canberra ACT 0200, Australia*

[3]*Department of Physics, Technical University of Denmark, DK-2800 Kongens Lyngby, Denmark*

(Received 18 January 2002; published 3 May 2002)

Using continuous wave superposition of spatial modes, we demonstrate experimentally displacement measurement of a light beam below the standard quantum limit. Multimode squeezed light is obtained by mixing a vacuum squeezed beam and a coherent beam that are spatially orthogonal. Although the resultant beam is not squeezed, it is shown to have strong internal spatial correlations. We show that the position of such a light beam can be measured using a split detector with an increased precision compared to a classical beam. This method can be used to improve the sensitivity of small displacement measurements.

DOI: 10.1103/PhysRevLett.88.203601 PACS numbers: 42.50.Dv, 42.30.–d, 42.50.Lc

It has long been known that optical measurements are ultimately limited in their sensitivity by quantum noise, or shot noise, of the light. For more than a decade the usage of nonclassical light has provided ways of improving the sensitivity beyond this standard quantum limit [1]. For example, squeezed light has been used to improve interferometric [2] and absorption [3] measurements. However, these improvements can be applied only to signals that correspond to the time modulation of light, as they rely on the temporal quality of the light. On the other hand, many applications require spatial measurement of light. While improvements for spatial applications based on nonclassical light have been proposed theoretically [4,5], no experimental demonstration has yet been shown to work with continuous wave light. The challenge is to create strong spatial correlations within a laser beam, rather than the temporal correlation typically found in nonclassical light sources [6]. While some experiments involving sub-Poissonian vertical cavity surface admitting lasers operating in a transverse multimode regime exhibited a nonrandom spatial distribution of the quantum noise [7], no spatial correlation was observed within the produced beam. Here we present the first successful experimental demonstration of a spatially ordered light source and a measurement of the spatial modulation of a laser beam position to below the standard quantum limit in the continuous wave regime.

This experimental work builds on theoretical work done on nonclassical multimode states of light [8]. Such states display strong spatial correlations, and their productions have been the subject of extensive studies in recent years [9]. In particular, the process of parametric down conversion in a nonlinear optical medium has been extensively studied, as it produces "twin photons" which are quantum correlated both temporally and spatially. Such strong spatial quantum correlations in the plane perpendicular to the direction of propagation are produced in spontaneous down conversion [10] and in multimode transverse optical parametric oscillators [11]. Nevertheless, to our knowledge, there has been no experimental demonstration of quantum correlations with a multimode transverse light in the continuous wave regime.

Precision optical imaging using CCD cameras or photodetector arrays is required in many areas of science, ranging from astronomy to biology. Ultimately, the performance of optical imaging technology is limited by quantum mechanical effects. Of particular importance, as far as applications are concerned, is the measurement of image displacements, for example, the position of a laser beam. Techniques that rely on determining the position of a laser spot include atomic force microscopy [12], measurement of very small absorption coefficients via the mirage effect [13], and observation of the motion of single molecules [14]. These measurements are usually performed as shown in Fig. 1. The beam is incident on a split detector that delivers two currents proportional to the light intensity integrated over the two halves ($x < 0$ and $x > 0$) of the image plane. If the beam is initially centered on the detector, the mean value of the photocurrent difference is directly proportional to the relative displacement d of the beam with respect to the detector. With a classical, shot

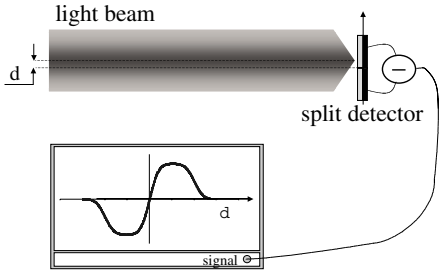

FIG. 1. Measurement of the displacement of a light beam. A split detector measures the intensities of the two halves of the image plane. When the beam is nearly centered, the difference between these intensities gives a signal that is proportional to the beam displacement d.

noise limited laser source, the smallest displacement that can be measured (with a signal-to-noise ratio of one) is shown to be [4]

$$d_{\mathrm{SQL}} = \frac{\sqrt{N}}{2I(0)}. \tag{1}$$

Here N is the total number of photons recorded by the two detectors during the measurement time, and $I(0)$ is the local density of photons (photons per unit transverse length) at the position of the boundary between the two detectors. For a TEM_{00} Gaussian beam with radius w_0, the minimum measurable displacement is found to be

$$d_{\mathrm{SQL}} = \sqrt{\frac{\pi}{8}}\,\frac{w_0}{\sqrt{N}}. \tag{2}$$

For maximum focusing of the Gaussian beam, $w_0 = \lambda$, and we obtain $d_{\mathrm{SQL}} \approx \lambda/\sqrt{N}$, which is the absolute minimum displacement of a physical system that can be measured with classical beams [12]. Equation (2) shows that a more powerful laser, or a longer measurement time, gives increased measurement precision. However, in many applications these alternatives are simply not practical. In the case of atomic force microscopy, for example, excessive laser power ultimately leads to radiation pressure noise [15]. For biological applications, large laser power may damage the samples under investigation and an increased integration time leads to loss of bandwidth. This is the motivation for looking for alternative methods of increasing measurement precision.

The limit of Eq. (2) can be surpassed only using multimode nonclassical light. Let us consider a beam of light with an electric field distribution given by $E(x)$. We can build an orthonormal basis of the transverse plane $\{u_i\}$ such that $u_0 = E(x)/\,\|E(x)\|$ is the first vector; u_1 is a "flipped" mode, given by $-u_0(x)$ for $x < 0$ and $u_0(x)$ for $x > 0$ (see Fig. 2); and the other modes are chosen in order to form a basis. In this basis, the mean field of our light lies only in the first mode u_0 but, *a priori,* all of the modes contribute to the quantum noise. In order to determine the relevant modes of our measurement, we consider the interference quantities between two modes on each half of the split detector:

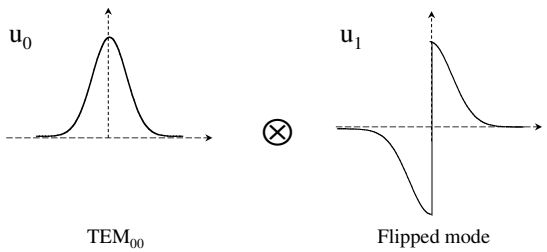

FIG. 2. Electric field profile of the two constituent modes used to form the nonclassical multimode beam.

$$I_{x<0}(u_i, u_j) = \int_{-\infty}^{0} u_i^*(x)u_j(x)\,dx\,,$$
$$I_{x>0}(u_i, u_j) = \int_{0}^{+\infty} u_i^*(x)u_j(x)\,dx\,. \tag{3}$$

Then the interference quantities relevant for a total measurement (sum of the two photodetectors) and a differential measurement (difference of the two photodetectors) can be written as follows:

$$I_{\mathrm{sum}}(u_i u_j) = I_{x<0}(u_i, u_j) + I_{x>0}(u_i, u_j)\,,$$
$$I_{\mathrm{diff}}(u_i u_j) = I_{x<0}(u_i, u_j) - I_{x>0}(u_i, u_j)\,. \tag{4}$$

One can then show that for any transverse mode u_i,

$$I_{\mathrm{sum}}(u_i u_1) = I_{\mathrm{diff}}(u_i u_0)\,. \tag{5}$$

Since all u_i, for $i \geq 2$, are orthonormal to u_1 [i.e., $I_{\mathrm{sum}}(u_i u_1) = 0$], Eq. (5) demonstrates that these modes have a zero overlap integral with u_0 in a differential measurement. It can then be shown that only u_1, which has a nonzero overlap integral with u_0, has to be considered along with u_0 in the noise calculation [4,16].

We note that the modes u_0 and u_1 have perfect interference visibility as shown by their complete overlap integral for the differential measurement, i.e., $I_{\mathrm{diff}}(u_0 u_1) = 1$. In this regard, the measurement is analogous to a perfect homodyne measurement with a beam splitter. The two modes are equivalent to the two input beams of a beam splitter and the two halves of the multimode beam are equivalent to the two outputs. Therefore, similar to a homodyne measurement, the noise on the differential measurement is completely canceled when the flipped mode is occupied by a perfect squeezed vacuum, with the squeezed quadrature in phase with the coherent field of the $u_0(x)$ mode. Conversely, the same result is also obtained when the mode profiles of the squeezed and the coherent fields are interchanged. In order to avoid the effect of losses, we have chosen a squeezed vacuum mode $u_0(x)$. We would like to stress that this simplified explanation can be applied only because we have conveniently identified the two relevant transverse modes of the measurement. However, contrary to a homodyne measurement, the entire measurement is performed using a single beam. Furthermore, a more general analysis is not limited to only two-mode beams.

The experimental setup is shown in Fig. 3. A stable Nd:YAG 700 mW laser provides a cw single mode beam at 1064 nm. A part of this beam is sent to a locked $\mathrm{MgO{:}LiNbO_3}$ frequency doubling cavity. The 532 nm output of the frequency doubler is used to pump a degenerate optical parametric amplifier (OPA) that produces a stable 10 μW squeezed beam in the TEM_{00} mode at 1064 nm. The noise reduction of the OPA output is measured to be 3.5 dB. Details of this squeezing system may be found in [17]. The flipped mode, $u_1(x)$, is produced by sending the remaining part of the initial 1064 nm laser beam through

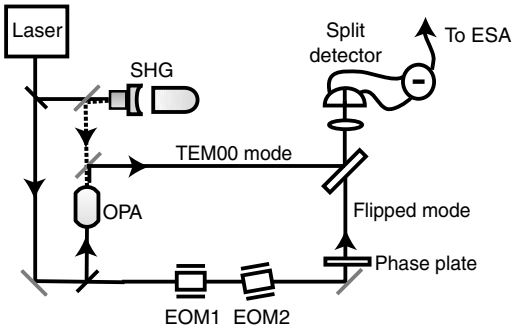

FIG. 3. Scheme of the experimental setup. SHG: second harmonic generator; OPA: optical parametric amplifier; EOM: electrooptic modulator; and ESA: electronic spectrum analyzer. The dashed lines correspond to light at 532 nm, and the solid line to the light at 1064 nm. The TEM00 mode is produced by the OPA and is a squeezed vacuum, the flipped mode is a coherent state.

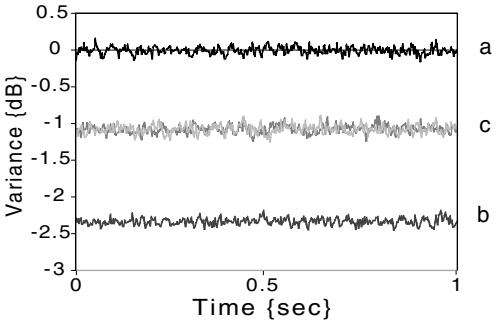

FIG. 4. Noise spectral density at 4.5 MHz of the photocurrents as a function of time (resolution bandwidth 100 kHz). (a) Sum of the two photocurrents. (b) Difference between the photocurrents. (c) Noise on each detector.

a specially designed phase plate. This phase plate consists of two birefringent half-wave plates, one rotated by 90° with respect to the other, forming the two halves $x < 0$ and $x > 0$ of the transverse plane. These elements introduce a phase shift of 180° between the field amplitudes of the two halves. The squeezed output from the OPA is required to be superimposed onto the flipped mode with minimal loss. This is achieved by using a beam splitter that reflects 92% of the squeezed state and transmits 8% of the coherent state. The reflected output is then sent to a quadrant InGaAs detector (EPITAXX 505Q) with quantum efficiency greater than 90%. Only two of the four quadrants, of dimensions 500 μm $\times$ 500 μm each and with a dead zone between the pixels of 25 μm, are used in this experiment. A lens of focal length 30 mm is used to image the phase plate on the detector plane and to counteract the diffraction of the flipped mode, which undergoes an abrupt phase change and therefore contains high spatial frequency components.

Figure 4 shows the different noise levels monitored as a function of time when the relative phase between the coherent state and the squeezed state is chosen for maximum noise reduction. Because of the high stability of the various servoloops in the experimental setup, the actively locked operation of the setup can be kept for hours. The noise measured on the sum of the two halves (Fig. 4a), i.e., on the total beam, coincides with the shot noise level for the conditions of this experiment, as expected from the coherent beam, which is not affected by the presence of a squeezed vacuum in an orthogonal mode. The noise measured on each individual half (Fig. 4c) is reduced by 1.08 $\pm$ 0.06 dB below the quantum noise limit. The fact that the intensity noise on each half of the beam is below the quantum noise limit, whereas the whole beam is at shot noise, shows the strong nonclassical characteristic of this multimode beam. This is corroborated by the experimental data of Fig. 4b, which give the noise on the intensity difference between the two halves at 2.34 $\pm$ 0.05 dB below the quantum limit. The results suggest that the beam is made of two strongly quantum correlated parts, indicating that a significant amount of spatial correlation has been created among the photons. With the measured noise reduction in the squeezed vacuum and a perfect setup (i.e., a perfect phase plate and a perfect mode matching between the two transverse modes), one would expect 2.5 $\pm$ 0.2 dB of noise reduction on the difference between the two pixels. This demonstration is, to our knowledge, the first experiment in which spatial quantum effects have ever been observed in a bright beam of light.

This spatial noise correlation can now be used to improve the precision of displacement measurements in the image plane. For practical reasons, we have chosen to induce the displacement only in the coherent mode, before the mixing on the beam splitter. However this displacement is of the order of the nanometer, which is several orders of magnitude smaller that the relevant precision for the mode matching of the two transverse modes, and the theoretical prediction for the measurements is the same as if the displacement were done on the total beam. In order to produce a small controllable beam displacement in the frequency range of the previous measurements, we use two electro-optic modulators (EOMs) driven at 4.5 MHz. Figure 3 shows that EOM2 is slightly tilted with respect to the propagation of the light beam. When a voltage is applied across EOM2, a change in refractive index is induced and the transmitted beam experiences a parallel transverse displacement measured at about 3 nm/V. We introduce a modulation at 4.5 MHz as signal for our displacement measurement which can be easily distinguished from the low frequency beam displacements induced by mechanical or acoustic vibrations. Apart from the parallel displacement, EOM2 will also introduce an unwanted phase modulation on the transmitted beam which is detrimental to our measurement. EOM1 of Fig. 3 is therefore used to compensate for this introduced phase modulation. When

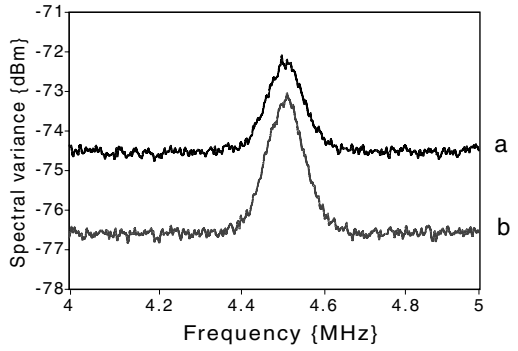

FIG. 5. Noise spectrum of the photocurrent difference in the presence of an oscillating displacement of amplitude 2.9 Å and frequency 4.5 MHz (resolution bandwidth: 100 kHz). (a) Using a coherent state of light. (b) Using the two-mode non classical state of light. This curve is obtained by averaging the signal over 10 successive traces.

correct gains are chosen for both modulators, the transmitted beam will not have any phase or amplitude modulation and is left only with pure transverse displacement modulation. Figure 5 shows the differential signal monitored by a spectrum analyzer when the light beam undergoes a displacement modulation with an amplitude of 2.9 Å. With a resolution bandwidth of 100 kHz, our setup recorded a modulation peak in the Fourier spectrum. Figure 5a shows the trace when vacuum instead of the squeezed vacuum is used in mode $u_0(x)$. Thus this noise floor gives the standard quantum limit in such a displacement measurement. The signal-to-noise ratio (SNR) of this measurement is 0.68. When the two-mode nonclassical beam is utilized in the measurement (Fig. 5b), we obtain a SNR of 1.20. This gives an improvement of the displacement measurement sensitivity by a factor of 1.7. The result is in agreement with the theoretical value calculated with the noise reduction reported in the previous paragraph. Similar measurements have been performed with a 10 kHz resolution bandwidth (and therefore a longer measurement time) and the results show the same improvement of the SNR.

Our results demonstrate that multimode nonclassical states of light can be utilized to improve the optical measurement of small displacements. The noise floor of displacement measurements can actually be reduced to below the standard quantum limit. Of particular relevance are the potential usage of multimode squeezed light in atomic force microscopy and biological microscopy. Though our experimental demonstration is restricted to one-dimensional displacement measurements, it can be extended to two-dimensional displacement measurements with more complex forms of multimodal nonclassical light.

We would like to thank L. Lugiato and M. Kolobov for many enlightening discussions and CSIRO, Sydney, for the manufacturing of the special phase plate. This work is funded by the European Project No. IST-2000-26019 "Quantum images," the Centre National de la Recherche Scientifique, and the Australian Research Council.

[1] H-A Bachor, *A Guide to Experiments in Quantum Optics* (Wiley-VCH, Weinheim, 1998).
[2] M. Xiao, L. A. Wu, and H. J. Kimble, Phys. Rev. Lett. **59**, 278 (1987); P. Grangier *et al.,* Phys. Rev. Lett. **59**, 19 (1987).
[3] E. Polzik, J. Carri, and H. J. Kimble, Appl. Phys. B **55**, 279 (1992); F. Marin, A. Bramati, V. Jost, and E. Giacobino, Opt. Commun. **140**, 146 (1997).
[4] C. Fabre, J. B. Fouet, and A. Maître, Opt. Lett. **25**, 76–78 (1999).
[5] Seng-Tiong Ho, P. Kumar, and J. H. Shapiro, Phys. Rev. A **37**, 2017 (1988).
[6] M. Kolobov and C. Fabre, Phys. Rev. Lett. **85**, 3789 (2000).
[7] J. P. Poizat, T. Chang, and P. Grangier, Phys. Rev. A **61**, 043807 (2000); J. P. Hermier *et al.,* IEEE J. Quantum Electron. **37**, 87 (2001).
[8] L. A. Lugiato, A. Gatti, and H. Wiedemann, in *Quantum Fluctuations,* Proceedings of the Les Houches Summer School (North-Holland, Amsterdam, 1997), p. 431.
[9] M. I. Kolobov, Rev. Mod. Phys. **71**, 1539 (1999).
[10] A. Joobeur *et al.,* Phys. Rev. A **53**, 4360 (1996).
[11] L. A. Lugiato and I. Marzoli, Phys. Rev. A **52**, 4886 (1995); I. Marzoli, A. Gatti, and L. A. Lugiato, Phys. Rev. Lett. **78**, 2092 (1997).
[12] C. A. J. Putman *et al.,* J. Appl. Phys. **72**, 6 (1992).
[13] C. Boccara, D. Fournier, and J. Badoz, Appl. Phys. Lett. **36**, 130 (1980).
[14] H. Kojima *et al.,* Biophys. J. **73**, 2012 (1997).
[15] D. P. E. Smith, Rev. Sci. Instrum. **66**, 3191 (1995).
[16] V. Delaubert *et al.* [J. Opt. A (to be published)].
[17] B. C. Buchler *et al.,* Phys. Rev. A **65**, 011803(R) (2002).

Table 3. L-Phe as starting material. Concentrations: 500 μmol Phe, 8.5 mmol $Mg(OH)_2$,1 mmol $FeSO_4$, 1 mmol $NiSO_4$, and 3 mmol Na_2S; 1 bar CO charged after 0, 4, 20, and 44 hours.

Time (hours)	pH	Phe-Phe (D) LL + DD (μmol)	Phe-Phe (D) DL + LD (μmol	Urea (F) LL + DD (μmol)	Urea (F) DL + LD (μmol)	Hydantoin (E) all isomers (μmol)
0.5	9.5	4	—	4	—	—
1	9.5	5	—	5	—	—
2	9.4	18	—	7	—	—
4	9.4	20	—	9	—	2
20	9.5	29	—	11	—	4
44	9.9	32	2	15	1	7
120	9.7	29	8	18	5	14

We previously considered two possibilities as activated α-amino acid: an *N*-carboxy-amino acid anhydride or an oxazolidinone (*1*). We now tentatively favor the *N*-carboxy-amino acid anhydride, because so far in the reaction of Phe to Phe-Phe we have not detected *N*-formyl-Phe-Phe. *N*-carboxy-amino acid anhydrides are well known to form peptides in aqueous systems through *N*-carbamoyl peptides (*3*). In the experiments starting with L-Phe, we confirmed our previous finding (*1*) of a racemization of the α-amino acid. We suggest that this racemization occurs at the hydantoin stage, which agrees with previous work (*4*), whereas the *N*-carboxy-amino acid anhydride is refractory to racemization (*3*).

Our findings establish the catabolic segment of a peptide cycle. Both the anabolic and the catabolic segments of the peptide cycle are driven by energy coupling with a net conversion of CO to CO_2. The mechanisms of both energy couplings are analogous, proceeding through analogous five-membered rings (*N*-carboxy-amino acid anhydride or imide, respectively). This conversion is an oxidation reaction. The corresponding oxidizing agent is seen in the colloidal system $(Fe^{II},Ni^{II})S$-CO, which is present in great excess. Its reduction may proceed stoichiometrically or catalytically with H^+ and/or CO as terminal oxidant. The redox energy driving the peptide cycle is converted into group activation energy in (B) and (E). The redox energy flow is normally inhibited, but it is here catalyzed by the peptide cycle. This is the mark of a metabolism.

Our results are compatible with the theory of a chemoautotrophic origin of life (*5*, *6*) in the presence of CO-laden volcanic exhalations. For the heterotrophic origin of life in a prebiotic broth, it has been suggested that hydantoin derivatives of α-amino acids (not of peptides) formed by dehydrating ring closure of *N*-carbamoyl-amino acids and led to prebiotic peptides and to the emergence of an Ur-hydantoinase (*7*). According to our results, hydantoins are not precursors for the synthesis of peptides but rather are intermediates in the breakdown of peptides. This is yet another example of the differences between these two theories.

The anabolic and catabolic segments of the peptide cycle operate simultaneously and under exactly the same conditions. This means that in a primordial metabolism the constituents of the peptide cycle exist under steady-state conditions. In extant organisms, peptides or proteins are synthesized as well as degraded. This is a precondition for metabolic control and for preventing the cellular metabolism from being choked by peptides. We suggest that the primordial peptide cycle may have continued to function until after the onset of cellularization.

Because the constituents of the primordial peptide cycle are continuously formed and degraded, they form a dynamic chemical library that scans the space of structural possibilities. This library may well have been self-selecting, because the constituents may be differentially stabilized by bonding as ligands to transition-metal centers, and early evolution may be seen as proceeding by positive ligand feedback into the catalytic transition-metal centers of the metabolism.

The new CO-driven peptide degradation may be used for a one-pot sequencing of peptides or proteins (at least their N-terminal segments). The reaction may also be used for converting a mixture of α-amino acids into a chemical library for screening.

The hydantoin derivative resulting from a glycylpeptide is related to the imidazol ring of uric acid. This opens a surprise connection between the origin of peptides and a possible origin of purines, which by extension would support the notion of a coevolution of peptides (proteins) and nucleic acids. The demonstrated hydrolysis of the hydantoin derivative with (Fe,Ni)S may be seen as the evolutionary precursor of the reaction of hydantoinase, a metal-dependent enzyme (*4*). The demonstrated hydrolysis of the urea derivative with (Fe,Ni)S may be seen as the evolutionary precursor of the reaction of the Ni-enzyme urease (*8*). If this notion is correct, these enzymes and their metal dependence may well be extant echoes from the distant past of life.

References and Notes

1. C. Huber, G. Wächtershäuser, *Science* **281**, 670 (1998).
2. Materials and methods are available as supporting material on *Science* Online.
3. H. R. Kricheldorf, α-*Aminoacid-N-Carboxy Anhydrides and Related Heterocycles: Syntheses, Properties, Peptide Synthesis, Polymerization* (Springer Verlag, Berlin, 1987).
4. C. Syldatk *et al.*, *Appl. Microbiol. Biotechnol.* **51**, 293 (1999).
5. G. Wächtershäuser, *Microbiol. Rev.* **52**, 452 (1988).
6. C. Huber, G. Wächtershäuser, *Science* **276**, 245 (1997).
7. J. Taillades *et al.*, *Origins Life Evol. Biosph.* **28**, 61 (1998).
8. E. Jabri *et al.*, *Science* **268**, 998 (1995).
9. This work was funded by Deutsche Forschungsgemeinschaft (WA-983/1-4). We thank A. Bacher for providing the laboratory facilities for carrying out this work and for continued support, B. Cordes for HPLC-MS, and M. Schulte-Bockholt for laboratory assistance.

Supporting Online Material
www.sciencemag.org/cgi/content/full/301/5635/938/DC1
Materials and Methods
Figs. S1 and S2

6 May 2003; accepted 1 July 2003

A Quantum Laser Pointer

Nicolas Treps,[1,2]* Nicolai Grosse,[1] Warwick P. Bowen,[1] Claude Fabre,[2] Hans-A. Bachor,[1] Ping Koy Lam[1]

The measurement sensitivity of the pointing direction of a laser beam is ultimately limited by the quantum nature of light. To reduce this limit, we have experimentally produced a quantum laser pointer, a beam of light whose direction is measured with a precision greater than that possible for a usual laser beam. The laser pointer is generated by combining three different beams in three orthogonal transverse modes, two of them in a squeezed-vacuum state and one in an intense coherent field. The result provides a demonstration of multichannel spatial squeezing, along with its application to the improvement of beam positioning sensitivity and, more generally, to imaging.

Measuring the pointing direction of a laser beam is one of the most direct, practical, and sensitive applications of light. It is used to detect with high sensitivity various weak physical effects such as spatial electro-optical or magneto-optical variations, refractive index gradients, the motion of single macromolecules, or the displacements of cantile-

vers in surface microscopes (*1*). On the other hand, this type of measurement, done at the quantum level, is one of the simplest systems for the study of the quantum properties of optical imaging (*2*). We demonstrated experimentally the limit to position measurements imposed by the quantum aspects of a usual laser beam, in which the photons are randomly distributed within the transverse plane. We showed how this standard quantum limit can be reduced using nonclassical light with specially designed spatial quantum correlations in both spatial coordinates (x and y), which allows a cancellation of the quantum noise in the position measurement. This device, termed a "quantum laser pointer," may be used to improve the sensitivity of a wide range of optical instruments. This is also a demonstration of a multichannel nonclassical beam of light: The photons are spatially ordered in the two transverse dimensions.

The most commonly used device to measure the position of the center of a beam of light is a split detector, that is, a detector with two or more separated areas. The difference between the photocurrents delivered by these areas is proportional to the displacement of the beam relative to the detector. Because we wanted to measure the two coordinates of the beam's center, we used a quadrant detector (Fig. 1). The two currents

$$I_x = (I_a + I_b) - (I_c + I_d),$$
$$I_y = (I_a + I_c) - (I_b + I_d) \qquad (1)$$

(where I_a, I_b, I_c, and I_d designate measurements in each quadrant) are proportional, respectively, to the horizontal and vertical position of the laser beam in the small displacement regime.

Instead of the average position of the beam, which is difficult to measure because of low-frequency vibrations and air index fluctuations, we considered and measured oscillations of the beam position with ultrasmall amplitude d_{mod} at high temporal frequencies Ω ($\Omega > 1$ Mhz). The ultimate limit of the position measurement is given by quantum mechanics: The noise in the measurement arising from the random arrival time of the photons on the detector is responsible for a lower limit to the amplitude d that can be measured with a coherent beam (i.e., a perfect usual laser beam) and corresponds to a signal-to-noise ratio equal to 1 (*3*). This quantum noise, or shot noise, limit is given, in the case of a TEM_{00} (transverse electromagnetic) beam, by

$$d_{QNL} \approx \sqrt{\frac{\pi}{8}} \frac{w_0}{\sqrt{N}} \qquad (2)$$

where w_0 is the waist of the Gaussian beam and N is the number of photons detected per measurement time interval Δt. To demonstrate this limit experimentally, we first measured the quantum noise $n(\Omega)$ with no modulation, using standard quantum optics techniques (*4*), and then added a very small modulation of the beam position $d(\Omega)$. The recorded signal contains both the actual displacement signal and the quantum noise. This noise can be reduced by averaging the traces over a long time, but at the expense of fast response time. We therefore chose a fixed integration time, Δt. We can be sure, with a reasonable degree of confidence, that the signal is due to an actual beam oscillation, rather than to a large fluctuation of the background noise, when the total signal—displacement and noise—is larger than the quantum noise alone. For example, we can choose as the smallest detectable amplitude that value for which the two traces differ by 3 standard deviations.

To determine the oscillation amplitude at a defined analysis frequency Ω, we used a spectrum analyzer, which demodulates the signal and measures the power spectral density. It displays the value for $n(\Omega)^2 + d(\Omega)^2$ on a logarithmic *dB* scale (Fig. 2A). We chose as the detection time $\Delta t = 10$ μs and set the resolution bandwidth (RBW) and video bandwidth (VBW) of the spectrum ana-

[1]Australian Research Council Centre of Excellence for Quantum-Atom Optics, the Australian National University, Canberra ACT 0200, Australia. [2]Laboratoire Kastler Brossel, Université Pierre et Marie Curie, case 74, 75252 Paris cedex 05, France.

*To whom correspondence should be addressed. E-mail: nicolas.treps@spectro.jussieu.fr

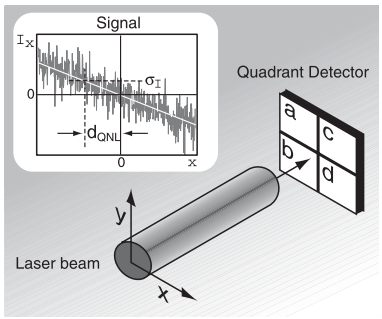

Fig. 1. Measurement of laser beam direction. A laser beam is incident on a quadrant detector. Simple arithmetic operations are performed on the four photo currents to produce signals I_x and I_y, which are proportional to the displacement in the horizontal and vertical axes, respectively. An example signal for I_x is plotted. The standard deviation of the signal σ_I defines the quantum noise limited displacement d_{QNL}.

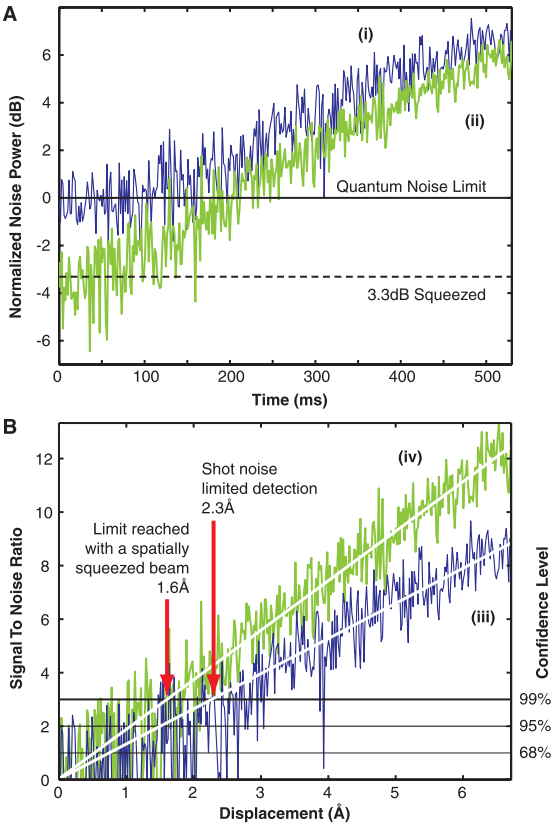

Fig. 2. (**A**) Measurement of horizontal displacement signal ramped up in time, with (i) coherent beams and (ii) spatially squeezed beams. Both radio-frequency spectrum analyzer traces are the averages of 20 runs with VBW = RBW = 1 kHz. The observed noise reduction of the squeezed beams measurement is 3.3 ± 0.2 dB. (**B**) Data from (A) processed to show signal-to-noise improvement (left vertical axis) plotted against the inferred displacement. Traces (iii) and (iv) show the results from data (i) and (ii), respectively. The squeezing translates into an increase in displacement sensitivity. Choosing a 99% confidence level (right vertical axis), the smallest displacement detectable improved from 2.3 to 1.6 Å.

lyzer to 1 kHz. We used a mirror mounted on a piezo-electric transducer to perform the oscillation. The modulation amplitude d_{mod} was slowly increased over time. The upper curve corresponds to the measurement performed with a coherent state and is the best measurement that can be achieved with classical means. The lower curve corresponds to the same measurement but with the nonclassical beam, called a "spatially squeezed" beam, that we produced as described below. The signal differs from the background noise for a modulation amplitude, which is greater for the coherent beam than for the spatially squeezed beam. In Fig. 2B, the same data are normalized to the respective noise levels, both for a usual laser and for a spatially squeezed beam. The vertical axis is now the difference between the measured signal and the noise with no displacement, and the traces for the coherent and the spatially squeezed beams are superimposed. In the case of the spatially squeezed light, the average of the signal trace crosses the threshold of confidence, set here at 3 standard deviations, for a smaller oscillation amplitude. We found a corresponding oscillation amplitude of 1.6 Å and an improvement by a factor of 1.5 compared with the standard quantum noise limit. Because both traces increase linearly with d_{mod}, this result is independent of the choice of confidence level. Most important, we have achieved such an improvement for two simultaneous measurements performed on the beam, namely the oscillation amplitudes in two orthogonal directions.

Let us consider a beam incident and centered on a quadrant detector. As in (3), we describe the electric field operator by

$$\hat{E}(x, y) = \sum_i \hat{a}_i u_i(x, y) \qquad (3)$$

where (x, y) are the transverse coordinates, $[u_i]$ is a complete basis of transverse modes, and $\hat{a}_i$ is the corresponding annihilation operator. Because the displacement to be measured is very small compared with the diameter of the beam, the noise on the signals I_x and I_y of Eq. 1 can be calculated when the beam is exactly centered, that is, when

$$\langle \int_{x<0} \hat{E}^\dagger \hat{E}\, dxdy \rangle = \langle \int_{x>0} \hat{E}^\dagger \hat{E}\, dxdy \rangle \text{ and}$$

$$\langle \int_{y<0} \hat{E}^\dagger \hat{E}\, dxdy \rangle = \langle \int_{y>0} \hat{E}^\dagger \hat{E}\, dxdy \rangle \qquad (4)$$

We chose the transverse modes basis such that the first transverse mode u_0 has the shape of the input beam, $u_0(x,y) = \langle \hat{E}(x,y) \rangle / \|E(x,y)\|$. Then we defined two "flipped modes," u_1 and u_2, such that $u_1(x,y) = -u_0(x,y)$ for $x < 0$, $u_1(x,y) = u_0(x,y)$ for $x > 0$, $u_2(x,y) = -u_0(x,y)$ for $y < 0$, and $u_2(x,y) = u_0(x,y)$ for $y > 0$. The important point is that Eq. 4 ensures that u_0, u_1, and u_2 are orthonormal and hence can actually be the beginning of a transverse-mode basis. It can be shown that the noise in the horizontal and vertical measurements arises only from the noise of u_1 and u_2, respectively (*5*). Hence, both measurements can be improved if and only if both modes are vacuum-squeezed states. These considerations show that to improve simultaneously two independent measurements on a light beam, it is necessary to use a multimode transverse beam containing two squeezed states in the mode u_1 and u_2, that is, a true spatially multimode squeezed beam (*6*). This analysis can be extended to an arbitrary number of independent measurements, each measurement being a channel in an information theory point of view: To improve an *n*-channel measurement beyond the standard quantum limit, one needs to use *n* squeezed states in appropriate modes. This bears a strong similarity to the quantum study of superresolution (*7*).

To construct our quantum laser pointer, three beams are necessary, two in squeezed-vacuum states and the third in an intense coherent state. These three beams have to be mixed, avoiding any losses for at least the two squeezed beams, because that would destroy the squeezing. In our setup (Fig. 3), the two highly squeezed beams (about 4 dB) are produced by two optical parametric amplifiers (OPAs) (*8*) driven by one laser. We chose an unusual spatial mode distribution: The transverse mode u_0 (corresponding to the bright coherent state) is the horizontally flipped mode of a TEM_{00} mode. Hence, the first squeezed beam (u_1) is in the TEM_{00} mode and the second squeezed beam (u_2) is in a "doubly flipped" TEM_{00} mode, as shown in the phase distribution maps in Fig. 3. The transverse modes are produced with optical wave plates made from birefringent half wave plates that were assembled at the appropriate $\pi/2$ angle. We used either two singly flipped wave plates or a four-quadrant wave plate. The mixing is achieved with a ring optical cavity. The TEM_{00} squeezed beam can be transmitted with nearly 100% efficiency in the case of an impedance-matched cavity. Because we chose a transversally nondegenerate cavity, the other squeezed beam, which is in a transverse mode orthogonal to the TEM_{00} mode, is reflected at the output mirror of the cavity and then perfectly mixed with the first squeezed beam. The cavity had a finesse of around 35, and we measured an efficiency of >95% for the transmitted beam and >94% for the reflected beam. The limit in efficiency came essentially from the imperfections of the OPA beam shape compared with a TEM_{00} mode. This technique for mixing the two beams

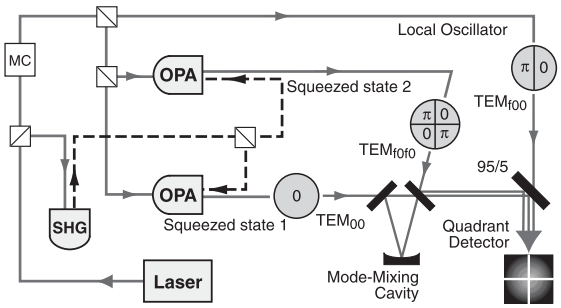

Fig. 3. Schematic of the experiment. SHG, second harmonic generator; OPA, optical parametric amplifier; MC, mode cleaner; 95/5, beam splitter with 95% reflectivity; TEM_{00}, squeezed TEM_{00} mode used for improving the horizontal measurement; TEM_{f0f0}, squeezed TEM_{f0f0} mode used for improving the vertical measurement; TEM_{f00}, coherent TEM_{f00} mode used as a local oscillator. Dotted lines, 532 nm light; solid lines, 1064 nm light.

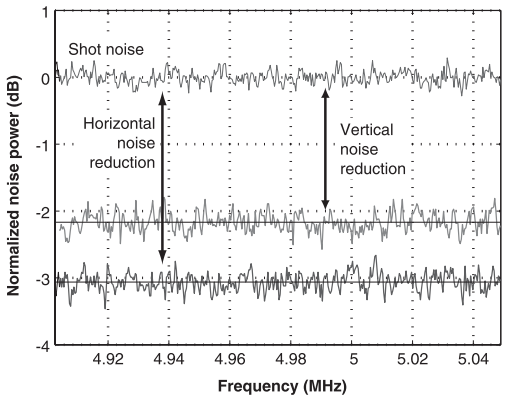

Fig. 4. Measured spectra showing the noise reductions in both horizontal and vertical measurements. The top trace corresponds to the quantum noise limit (QNL), whereas the two lower ones correspond to the noise in the vertical and the horizontal measurements done with a spatially squeezed beam. The noise spectra are normalized to 0 dB = QNL.

had, to our knowledge, never been implemented before and can be extended to a wide range of applications. In particular, it can be used to mix any two orthogonal transverse modes. Finally, the resulting beam is mixed with the coherent beam on a 95%/5% beam splitter as in (*5*).

The experiment was performed in a fully locked configuration, stable for at least 10 minutes. The detection was performed with a quadrant detector, each of the quadrants having a high quantum efficiency (more than 90%), and the corresponding electronic amplifiers were optimized to ensure their exact balance (*9*). The four individual photocurrents were combined to measure the quantities I_x and I_y of Eq. 1. A spectrum analyzer was used to perform the demodulation and obtain the detection at 4.3 MHz. A first experiment, without any modulation, showed the amount of noise reduction we could obtain (Fig. 4). We achieved simultaneously 3.05 ± 0.1 dB of horizontal noise reduction and 2.0 ± 0.1 dB of vertical noise reduction. The configuration used here is scalable, and it is possible to increase the number of independent modes with a slight variation of the layout. From a quantum information point of view, each transverse mode is an independent communication channel, and the usual quantum communication proposals can be extended to the multichannel configuration (*10*, *11*). This same beam of light was used to perform the displacement measurement described above.

Our experiment can be considered with equal interest from different points of view. On the fundamental side, it is now possible to experimentally mix several nonclassical beams in orthogonal transverse modes, thereby producing multimode spatially squeezed beams. This ability is of major importance in the field of quantum imaging. On the quantum information side, this experiment opens the way to the use of multimode light in the parallel processing of quantum information. Finally, this experiment clearly demonstrates the practical applicability of spatial squeezing to displacement measurements. As a major advance, this experiment overcomes most of the technical obstacles. In particular, we can avoid losses in the mixing of the transverse modes.

Our technique can be used to improve the measurement of a displacement induced by interaction with a physical system, as discussed in (*12*), even if this interaction introduces losses. Indeed, it will be possible to mix the coherent state with the squeezed states after the interaction, and without losses. Real applications will follow after the production of easy-to-use, efficient sources of squeezed light.

References and Notes

1. Tim J. Senden, *Current Opinion in Colloid and Interface Science* **6**, 95 (2001).
2. L. A. Lugiato, A. Gatti, E. Brambilla, *J. Opt. B Quantum Semiclass. Opt.* **4**, S176 (2002).
3. C. Fabre, J. B. Fouet, A. Maître, *Optics Letters* **25**, 76 (1999).
4. H.-A. Bachor, *A Guide to Experiments in Quantum Optics* (Wiley-VCH, Weinheim, Germany, 1998).
5. N. Treps *et al.*, *Phys. Rev. Letters* **88**, 203601 (2002).
6. M. I. Kolobov, *Rev. Mod. Phys.* **71**, 1539 (1999).
7. M. I. Kolobov, C. Fabre, *Phys. Rev. Lett.* **85**, 3789 (2000).
8. W. P. Bowen, R. Schnabel, H.-A. Bachor, P. K. Lam, *Phys. Rev. Lett.* **88**, 093601 (2002).
9. M. Martinelli *et al.*, *Phys. Rev. A* **67**, 023808 (2003).
10. I. V. Sokolov, M. I. Kolobov, A. Gatti, L. A. Lugiato, *Opt. Comm.* **193**, 174 (2001).
11. I. V. Sokolov, internal communication within the European Network on Quantum Imaging (QUANTIM) on the possibility of multimode dense coding.
12. C. Boccara, D. Fournier, J. Badoz, *Appl. Phys. Lett.* **36**, 130 (1980).

13. This work was carried out as part of the Australian Research Council Centre of Excellence Program. It was funded by the Australian Research Council and supported by the Laboratoire Kastler Brossel as part of QUANTIM, contract IST-2000-26019. We thank the Commonwealth Scientific and Industrial Research Organisation (Lindfield, Australia) for the precise making of the wave plates; B.C. Buchler and R. Schnabel for their valuable contributions, in particular to the design, construction, and optimization of the two OPAs; and A. Maître for invaluable discussions.

6 May 2003; accepted 9 July 2003

Electrical Manipulation of Magnetization Reversal in a Ferromagnetic Semiconductor

D. Chiba,[1] M. Yamanouchi,[1] F. Matsukura,[1] H. Ohno[1,2]*

We report electrical manipulation of magnetization processes in a ferromagnetic semiconductor, in which low-density carriers are responsible for the ferromagnetic interaction. The coercive force H_C at which magnetization reversal occurs can be manipulated by modifying the carrier density through application of electric fields in a gated structure. Electrically assisted magnetization reversal, as well as electrical demagnetization, has been demonstrated through the effect. This electrical manipulation offers a functionality not previously accessible in magnetic materials and may become useful for reversing magnetization of nanoscale bits for ultrahigh-density information storage.

Magnetization reversal is a fundamental process for writing information, or bits, onto magnetic materials used in data storage, and is generally done by applying magnetic fields locally to the magnetic material. In order to realize higher data density per unit area, the magnetic energy density of the material has to be increased to make the nanometer-scale magnetic bits stable against thermal fluctuations, which at its limit pushes the required magnetic fields for writing too high to generate. Manipulation of magnetization reversal by other means has thus become an important challenge for magnetic information storage (*1*–*5*). We show that electrical manipulation of the magnetization processes is possible in a semiconducting ferromagnetic material and demonstrate electrically assisted magnetization reversal, as well as electrical demagnetization.

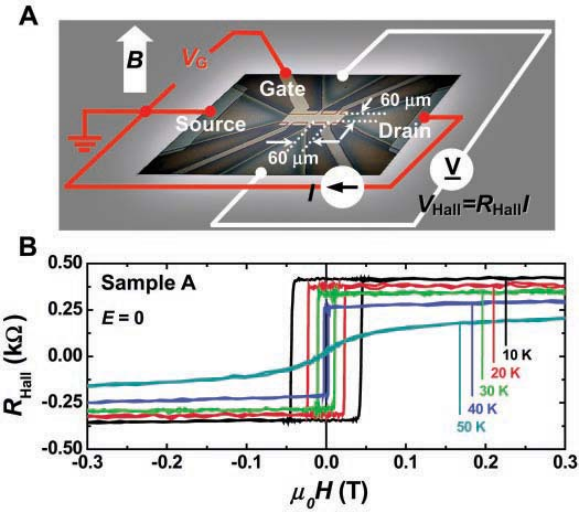

Fig. 1. (**A**) Hall bar–shaped field effect transistor having a ferromagnetic semiconductor (In,Mn)As channel. To probe the magnetization M of the channel, Hall resistance $R_{Hall} = V_{Hall}/I$ proportional to the channel magnetization is measured. (**B**) Temperature dependence of R_{Hall} ($\propto M$) versus magnetic field $\mu_0 H$ curves with square-shaped hysteresis up to temperatures below 50 K in sample A. Sample A has a ferromagnetic transition temperature of 52 K. No electric field is applied ($E = 0$). Magnetic field sweep rate is 3.7 mT/min.

May 15, 2006 / Vol. 31, No. 10 / OPTICS LETTERS 1537

Quantum measurements of spatial conjugate variables: displacement and tilt of a Gaussian beam

Vincent Delaubert

Australian Research Council Centre of Excellence for Quantum-Atom Optics, The Australian National University, Canberra ACT 0200, Australia, and Laboratoire Kastler Brossel, 4 Place Jussieu, Case 74, Paris 75252 Cedex 05, France

Nicolas Treps

Laboratoire Kastler Brossel, 4 Place Jussieu, Case 74, Paris 75252 Cedex 05, France

Charles C. Harb, Ping Koy Lam, and Hans-A. Bachor

Australian Research Council Centre of Excellence for Quantum-Atom Optics, The Australian National University, Canberra ACT 0200, Australia

Received November 28, 2005; revised February 23, 2006; accepted March 6, 2006; posted March 9, 2006 (Doc. ID 66257)

We consider the problem of measurement of optical transverse profile parameters and their conjugate variable. Using multimode analysis, we introduce the concept of detection noise modes. For Gaussian beams, displacement and tilt are a pair of transverse-profile conjugate variables. We experimentally demonstrate the optimal encoding and detection of these variables with a spatial homodyning scheme. Using higher-order spatial mode squeezing, we show the sub-shot-noise measurements for the displacement and tilt of a Gaussian beam. © 2006 Optical Society of America

OCIS code: 270.6570.

Quantum information protocols rely on the use of conjugated variables of a physical system for information encoding. For single-mode continuous-variable systems, there are only a very limited number of choices for such conjugate-variable pairs. Phase and amplitude quadrature measurements with a balanced homodyne detector or polarization Stokes parameter measurements using polarization discriminating detectors[1,2] are the common conjugate variables used experimentally.

By not restricting ourselves to single-mode analysis, we can use the ability of a laser beam to transmit high multimode information by extending these protocols to the transverse spatial domain. The transverse profile of the beam is then described by a set of orthonormal modes that potentially allows a parallel treatment of information. Recently this parallel processing scheme was used in single-photon experiments to extend q-bits to q-dits using modes with higher angular momentum.[3,4]

Such an improvement requires perfect matching of the detection system to the spatial information contained in the light beam. Indeed, we have shown that a single detector extracts information from only one specific transverse mode of the beam.[5] We call this mode the noise mode of detection since it is the only mode contributing to the measurement noise. As a consequence, information encoded in any other mode orthogonal to the detection noise mode is undetected. Moreover, noise modes of detection are the transverse spatial modes whose modulation in magnitude is transferred perfectly to the detected output as a photocurrent.

The use of classical resources sets a lower bound on detection performance that is called the quantum noise limit (QNL) and arises from the random time arrival of photons on the detector. In the case of displacement measurement of a laser beam, the transverse displacement d_{QNL} of a TEM_{00} laser beam corresponding to a signal-to-noise ratio (SNR) of 1 is given by $d_{\mathrm{QNL}}=w_0/2\sqrt{N}$, where w_0 is the waist of the beam and N is its total number of photons in the interval $\tau=1/\mathrm{RBW}$, where RBW is the resolution bandwidth.[6] Note that the ability to resolve signal relative to noise can be further improved by averaging with the spectrum analyzer, by reducing the video bandwidth (VBW) and thus increasing the number of photons detected in the measurement interval, if the system has enough stability. For a 100 μm waist, 1 mW of power at a wavelength of $\lambda=1$ μm, with RBW=100 kHz and VBW=100 Hz, the quantum noise limit is, for instance, given by $d_{\mathrm{QNL}}=0.2$ nm, and the minimum measurable transverse displacement is $d_{\mathrm{min}}=7$ pm.

To achieve a measurement sensitivity beyond the QNL, it is a necessary and sufficient condition to fill the noise mode of detection with squeezed light.[5] As required by commutation relations, a measurement of the conjugate variable shows excess noise above the QNL.

In this Letter we first explain how spatial information can be encoded onto a beam and how optimized measurement of spatial properties of a beam can be achieved classically. As an example, we use the displacement and tilt of a Gaussian laser beam[7] (which are two spatial conjugate variables) to show the quantitative results of SNR measurements that surpass the quantum noise limit.

Encoding information in the transverse plane of a laser beam can be achieved by modulating any of its scalar parameters p around a mean value p_0. This parameter can correspond to any deformation of the transverse profile, such as displacement and tilt, which are properties that are easy to visualize and to

0146-9592/06/101537-3/$15.00

1538 OPTICS LETTERS / Vol. 31, No. 10 / May 15, 2006

use in practice. In the simple case of a TEM_{00} mode, the parameterized beam can then be written in the general form by considering the first-order Taylor expansion for small modulations $(p-p_0)/p_0 \ll 1$:

$$u_{00}(p) \approx u_{00}(p_0) + (p-p_0)\frac{\partial(u_{00})}{\partial p}, \quad (1)$$

where u_{ij} denote the TEM_{ij} Hermite–Gauss modes and $u_{ij}(p)$ denotes the same mode that experienced the modification induced by p. Specifically, a transversely displaced and tilted beam along the x direction is given by

$$u_{00}(d) = u_{00} + d\frac{\partial(u_{00})}{\partial x} = u_{00} + \frac{d}{w}u_{10}, \quad (2)$$

$$u_{00}(\theta) = u_{00} + \theta\frac{\partial(u_{00})}{\partial \theta} = u_{00} + i\frac{\pi\theta w}{\lambda}u_{10}, \quad (3)$$

where d, θ, and w are the displacement, tilt, and waist diameter of the beam in the plane of observation, respectively.[7] Equations (2) and (3) show that small displacement information of a Gaussian beam is encoded in the amplitude quadrature of the copropagating TEM_{10} mode, while small tilt modulation is directly coupled to the phase quadrature of the TEM_{10} mode.

To extract this spatial information out of the modulated beam, let us consider the example of homodyne detection. This device selects the particular mode of the incoming beam, which is matched to the local oscillator transverse profile. Thus, the detection noise mode is the one imposed by the local oscillator. By changing the transverse distribution and phase of the local oscillator, Φ_{LO}, one can, at will, tune the noise mode of detection to any spatial information of the incoming beam. In addition, by squeezing the noise mode of the incoming beam, one can improve the measurement sensitivity. This apparatus, which we call a spatial homodyne detector, is therefore a perfect tool for multimode quantum information processing.

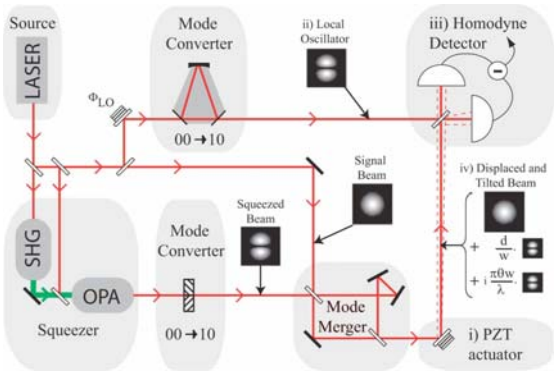

Fig. 1. (Color online) Schematic diagram of the experiment for optimal displacement and tilt measurements with a spatial homodyne detector. A TEM_{00} mode, which is displaced and tilted using a PZT actuator (i), is mode matched to the TEM_{10} local oscillator (ii) of a balanced homodyne detector (iii). The TEM_{10} local oscillator selects the quadratures amplitude of the TEM_{10} component of the input beam that contains the small displacement and tilt information of the incident TEM_{00} beam (iv).

In the case of small displacement and tilt measurement, a homodyne detector with a TEM_{10} local oscillator can measure the TEM_{10} component of an incoming beam with up to 100% efficiency. Hence, the detector precisely matches the displacement and tilt conjugate observables of a TEM_{00} incident beam. A TEM_{10} spatial homodyne detector, as shown in Fig. 1, is in this sense an optimal small displacement and tilt detector. Note that this scheme is not only 25% more efficient than the conventional split detector for measuring a displacement,[8] it is also sensitive to tilt, which is not accessible in the plane of a split detector.

As the TEM_{10} mode is the noise mode of the spatial homodyne detector, we can experimentally improve the detection sensitivity by filling the TEM_{10} mode of the input beam with squeezed light. This nonclassical beam is produced with an optical parametric amplifier (OPA) that emits a very low power (pW) 3.6 dB squeezed TEM_{00} mode at 1064 nm (note that a ring cavity—not represented in Fig. 1—spatially filters the laser beam to a pure TEM_{00} mode that is used as the main TEM_{00} mode and produces a shot-noise-limited beam for frequencies greater than 1 MHz that is used to seed the OPA). A phase mask converts the low-power squeezed beam into a TEM_{10} mode, with an efficiency of 80%,[9] which brings the squeezing level in the TEM_{10} down to 2 dB. This squeezed TEM_{10} beam is combined (with less than 5% losses) with the main bright TEM_{00} beam by means of a modified Mach–Zehnder interferometer.[6] This beam interacts with a piezoelectric (PZT) actuator that induces simultaneously displacement and tilt at RF frequencies (4 MHz). Note that the relative amounts of tilt and displacement are fixed here by the characteristics of the actuator. This beam is analyzed with a homodyne detector whose TEM_{10} local oscillator beam is produced via a misaligned ring cavity that is resonant for the TEM_{10} mode. Note that mode matching between these two beams is achieved in a preliminary step by measuring a fringe visibility of 97% between the bright TEM_{00} mode and the TEM_{00} mode generated when the cavity is locked on resonance for the TEM_{00} mode instead of the TEM_{10} mode.

The experimental results obtained with the spectrum analyzer in zero-span mode at 4 MHz when the TEM_{10} local oscillator phase is scanned and locked for displacement ($\phi_{LO}=0$) and tilt ($\phi_{LO}=\pi/2$) measurement are presented in Figs. 2(a) and 2(b), respectively. Note that, without the use of squeezed light, the displacement modulation is masked by quantum noise. Improvement of the SNR for displacement measurement beyond the quantum noise limit is achieved when the squeezed quadrature of the TEM_{10} mode is in phase with the displacement measurement quadrature (i.e., in phase with the incoming TEM_{00} mode). Since we are dealing with conjugated variables, improving displacement mea-

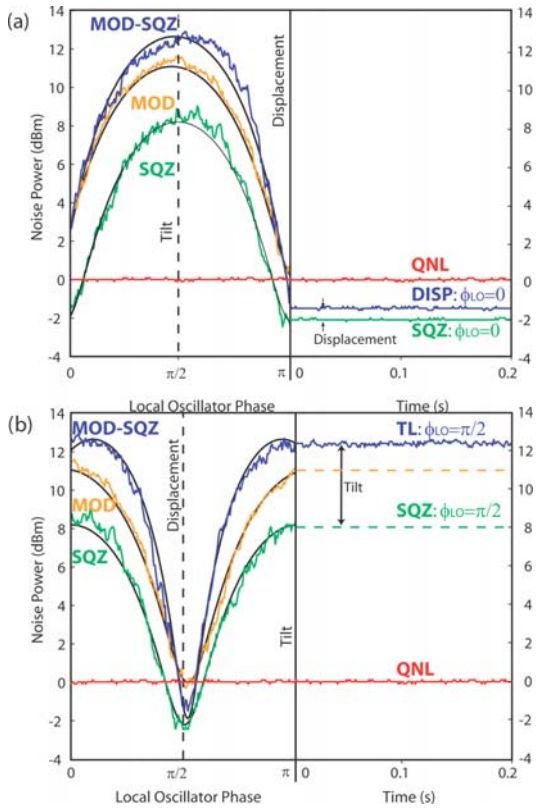

Fig. 2. (Color online) Demonstration of sub-shot-noise measurements of (a) displacement and (b) tilt modulations using the spatial homodyne detector. The figures show an example where there was 90% of tilt and only 10% of displacement modulations. The left-hand side of each part shows the scanning of local oscillator phase ϕ_{LO} that successively accesses the pure displacement (at $\phi_{LO}=0$ and π) to pure tilt (at $\phi_{LO}=\pi/2$ and $3\pi/2$) information of the beam. SQZ, quadrature noise of squeezed light with 2 dB of squeezing and 8 dB of antisqueezing on the TEM_{10} mode but without any modulation signal. MOD, measured modulation with coherent light. MOD-SQZ, measured modulation with squeezed light. The right-hand side of each figure part shows the locked local oscillator phase corresponding to the (a) displacement or (b) tilt measurement. SQZ, at $\phi_{LO}=0$ is the squeezed noise level 2 dB below the shot noise and at $\phi_{LO}=\pi/2$ is 8 dB of antisqueezing noise. DISP, MOD-SQZ curve locked to $\phi_{LO}=0$ for displacement measurement. TL, MOD-SQZ curve locked to $\phi_{LO}=\pi/2$ for tilt measurement. Displacement measurement is improved by the 2 dB of squeezing, while the tilt measurement is degraded by the 8 dB of antisqueezing.

surement degrades the tilt measurement of the same beam, as required by the antisqueezing of the other quadrature. Displacement measurement is improved by the 2 dB of squeezing, whereas the tilt measurement is degraded by the 8 dB of antisqueezing. Theoretical curves calculated with 2 dB of noise reduction and 90% of tilt modulation and 10% of displacement modulation [smooth curves in Fig. 2(a)] are in very good agreement with the experimental data. In our experiment, we have a TEM_{00} waist size of $w_0=106$ μm in the PZT plane, a power of 170 μW, RBW=100 kHz, and VBW=100 Hz, corresponding to a QNL of $d_{QNL}=0.6$ nm. The measured displacement lies 0.5 dB above the squeezed noise floor, yielding a displacement modulation 0.08 times larger than the QNL. As the modulation has a square dependence on the displacement d, we get $d_{exp}=\sqrt{0.08}d_{QNL}=0.15$ nm. This would correspond to a trace 0.3 dB above the QNL and cannot therefore be clearly resolved without squeezed light. The ratio between the displacement and tilt modulation can be inferred from the theoretical fit in Fig. 2, giving a measured tilt of 0.13 μrad.

We have demonstrated a technique for encoding and extracting continuous-wave quantum information on multiple co-propagating optical modes. We use spatial modulation as a practical technique to couple two transverse modes and have devised a detection system whose noise mode perfectly matches beam position and momentum variables, which are a pair of conjugate transverse variables.

This work shows that in principle a large set of orthogonal multimode information is accessible. We can already simultaneously encode and detect information in the x and y directions,[10] which corresponds to simultaneous use of TEM_{10} and TEM_{01} modes. Possible extension of this approach to array detectors and higher-order spatial modes will be investigated. This technique, demonstrated here in the context of quantum imaging, leads to feasible parallel quantum information processing.

We thank Claude Fabre, Magnus Hsu, Warwick Bowen, and Nicolai Grosse for stimulating discussions, and Shane Grieves for technical support. This work was made possible by the support of the Australian Research Council Centre of Excellence program. V. Delaubert's e-mail address is vincent.delaubert@anu.edu.au.

References

1. W. P. Bowen, R. Schnabel, H.-A. Bachor, and P. K. Lam, Phys. Rev. Lett. **88**, 093601 (2002).
2. N. Korolkova, G. Leuchs, R. Loudon, T. C. Ralph, and C. Silberhorn, Phys. Rev. A **65**, 052306 (2002).
3. A. Mair, A. Vaziri, G. Weihs, and A. Zeilinger, Nature **412**, 3123 (2001).
4. N. K. Langford, R. B. Dalton, M. D. Harvey, J. L. O'Brien, G. J. Pryde, A. Gilchrist, S. D. Bartlett, and A. G. White, Phys. Rev. Lett. **93**, 053601 (2004).
5. N. Treps, V. Delaubert, A. Maître, J. M. Courty, and C. Fabre, Phys. Rev. A **71**, 013820 (2005).
6. N. Treps, N. Grosse, W. P. Bowen, M. T. L. Hsu, A. Maître, C. Fabre, H.-A. Bachor, and P. K. Lam, J. Opt. B: Quantum Semiclassical Opt. **6**, S664 (2004).
7. M. T. L. Hsu, W. P. Bowen, N. Treps, and P. K. Lam, Phys. Rev. A **72**, 013802 (2005).
8. M. T. L. Hsu, V. Delaubert, P. K. Lam, and W. P. Bowen, J. Opt. B: Quantum Semiclassical Opt. **6**, 495 (2004).
9. V. Delaubert, D. A. Shaddock, P. K. Lam, B. C. Buchler, H.-A. Bachor, and D. E. McClelland, J. Opt. A, Pure Appl. Opt. **4**, 393 (2002).
10. N. Treps, N. Grosse, W. P. Bowen, A. Maître, C. Fabre, H.-A. Bachor, and P. K. Lam, Science **301**, 940 (2003).

Tools for Multi-mode Quantum Information: Modulation, Detection and Spatial Quantum Correlations

M.Lassen[1,2], V.Delaubert[1,3], H-A.Bachor [1],* P.K.Lam[1], N.Treps[3], P.Buchhave [2], C.Fabre[3], and C.C.Harb [1,41]

[1] *The Australian National University, ACQOA, Canberra ACT 0200, Australia*
[2] *Department of Physics, DTU, Building 309, 2800 Lyngby, Denmark*
[3] *Laboratoire Kastler Brossel, 4 place Jussieu, case 74, Paris 75252 Cedex 05, France*
[4] *School of Information Technology and Electrical Engineering, University College, The University of New South Wales, Canberra, ACT, 2600.*

(Dated: July 7, 2006)

We present here all the required tools for continuous variable parallel quantum information protocols based on multi-mode quantum correlations and entanglement. We describe our ability to encode and detect quantum information with high efficiency. We experimentally demonstrate the generation of spatial correlations or optical squeezing in higher order transverse Hermite-Gauss modes. The higher order mode squeezing is achieved by the mode selective tuning of the phase matching condition and the cavity resonance condition of the nonlinear $\chi^{(2)}$ optical parametric amplification.

PACS numbers: 42.50.-p; 03.67.a; 42.50.Dv

Optical quantum communication and information processing is developing rapidly [1]. Both single photons and continuous wave laser beams (CW) are being used, already enabling the generation, transmission and detection of quantum correlations. One of the advantages of CW optical techniques is that close to perfect modulation and detection schemes are available, which is a requirement for the effective use of squeezed and entangled light [2–5] for applications such as sensing and gravitational-wave detection [6], quantum communication [7], cryptography [8–10] and quantum logic.

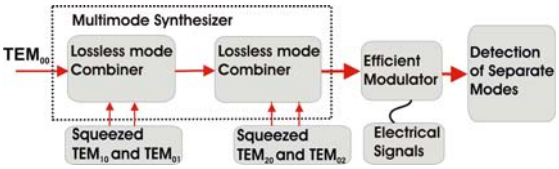

FIG. 1: A multi-mode optical system for quantum communication and information processing.

The aim of our research is to explore how a single laser beam can be used to carry multiple quantum information encoded in orthogonal modes. Conventionally, the information is encoded on the two quadratures of a single mode TEM_{00} laser beam [11, 12], where each quadrature contains a spectrum of modulations as well as quantum correlations. However, it is possible to use the transverse spatial modes to carry additional information and entanglement. Restricting ourselves to variations along one dimension of the transverse plane, x, we will denote the higher order Hermite-Gauss (H-G) modes TEM_{n0}, with spatial mode function $u_n(x)$. The first H-G modes are directly related to small spatial variations of a Gaussian beam [13]. The real and imaginary parts of the TEM_{10} mode represent changes in tilt, $\delta\theta$, and transverse position, δd, of a TEM_{00} beam [14], whereas the real and imaginary parts of the TEM_{20} mode are related to a waist size mismatch, δw, and a waist position mismatch along the propagation axis, δz. The following equation quantifies these relationships:

$$E(x) = A_0\left[u_0(x) + \left(\frac{\delta d}{w_0} + i\frac{\pi w_0 2\delta\theta}{\lambda}\right)u_1(x) + \frac{\sqrt{2}\delta w}{w_0}u_2(x) + i\frac{\delta z\pi\lambda}{w_0^2}\left(u_0(x)+u_2(x)\right)\right], \quad (1)$$

where A_0 is the amplitude, w_0 is the waist and λ is the wavelength.

We can synthesize a multi-mode laser beam which combines the TEM_{00} mode with the higher order transverse modes TEM_{01}, TEM_{10}, TEM_{02} and TEM_{20} [14, 15]. Each mode contains two quadratures and can be squeezed. It is possible to address each mode individually and to encode signals via efficient spatial modulators. We can also transfer modulation from one mode to another. Such a multi-mode system can provide advantages in regard to the complexity of the protocols [16] and allows the parallel transfer of quantum information. This is complementary to single photon systems designed to transmit more than q-bits or q-dits [17, 18].

The key requirements for the CW multi-mode information system is our availability of simple and fully efficient modulation and detection of quantum information of a laser beam and our ability to generate and combine higher order modes selectively with high efficiency. We can preform information encoding using mechanical or electro-optic spatial modulators directly into the transverse orthogonal modes. These devices are simple and can have close to perfect efficiencies [14, 15]. The detection of these modes requires special attention. Conventional spatial detectors, such as split detectors or diode

*Electronic address: Hans.Bachor@anu.edu.au

arrays, are simple but provide only limited efficiency notably because of their geometry. For example, the best theoretical efficiency of a split detector for displacement measurements is only 64% [19]. In contrast, spatial homodyne detectors, with a local oscillator (LO) beam that is mode matched to the higher order mode under investigation can achieve, in theory, perfect detection efficiency. We have shown efficiency values of more than 96% in ref. [14, 20]. This combination of modulation, detection and combination of higher order modes means that we have all the tools for encoding and readout of spatial quantum information. The crucial component missing until now was the selective and efficient generation of quantum correlations or squeezing in higher order transverse modes. In this paper we fill this technology gap by demonstrating an experimental technique for selectively generating the required squeezed spatial modes. We exploit the subtle physics of phase matching in type I second order ($\chi^{(2)}$) nonlinear processes to select the individual transverse modes and to squeeze the modes.

The nonlinear interaction in second harmonic generation (SHG) and optical parametric amplification (OPA) are reciprocal. We analyze the mode up-conversion of a single pass SHG to optimize the performance of our OPA. The SHG process combines two fundamental photons from the pump beam to generate one second harmonic (SH) photon with twice the energy. The transverse profile of the SH mode therefore corresponds to the decomposition of the square of the fundamental pump mode profile into the SH basis. In the general case, the generated SH field is hence composed of several components. These components are all even since the TEM_{n0} pump squared profile is necessarily even. $2n$ is their highest order as the squared TEM_{n0} profile does not project onto higher order modes. The normalized profile of the generated SH field for a TEM_{n0} pump can thus be written as: $\mathcal{E}_n(x) = \sum_{i=1}^{n} \Gamma_{ni} v_{2i}(x)$, where v_{2i} denotes the even SH modes and $\Gamma_{ni} = \int_{-\infty}^{\infty} \frac{u_n^2(x)}{\alpha_n} v_{2i}(x)dx$ describes the spatial mode overlap between the squared pump and the SHG modes in the transverse plane, where u_n denotes the fundamental modes and $\alpha_n^2 = \int_{-\infty}^{\infty} u_n^4(r)dx$ corresponds to the normalization of the squared pump.

The common case of using a TEM_{00} mode for the pump yields $\Gamma_{00} = 1$ and corresponds to a perfect spatial overlap as the profile of the generated SH mode is also a TEM_{00} mode. For non TEM_{00} pump modes, the overlap coefficients calculated for a TEM_{10} pump are given by $\Gamma_{10} = 0.58$ and $\Gamma_{12} = 0.82$, for a TEM_{20} mode pump $\Gamma_{20} = 0.47$, $\Gamma_{22} = 0.44$ and $\Gamma_{24} = 0.77$. The presence of several non zero coefficients implies that for all cases, except a TEM_{00} pump mode, the generated profiles do not correspond to the pump intensity distribution.

In order to test this simple mode overlap model for second order nonlinear interaction, we pump a single pass SHG experiment with a TEM_{n0} pump mode, the experimental setup is shown in Fig. 2 a). We use a lithium niobate crystal ($MgO:LiNbO_3$) in a type I second order (χ^2) nonlinear interaction [21]. The TEM_{n0} pump mode, wavelength of 1064 nm produced by a diode-pumped NPRO Nd:YAG laser, is generated by misaligning a ring cavity, designed to prevent any transverse mode degeneracy and locked to the resonance of the TEM_{n0} mode. The locking of the cavities is achieved by using the Pound-Drever-Hall method [22]. This mode converting device delivers a pure transverse TEM_{n0} output mode, which is then focused into the crystal such that $z_R = l/2$, where z_R is the beam Rayleigh range and l is the crystal length. A dichroic mirror, DM, is used to filter out the fundamental pump field, and the SH profile is detected with a CCD camera in the far field using an imaging lens.

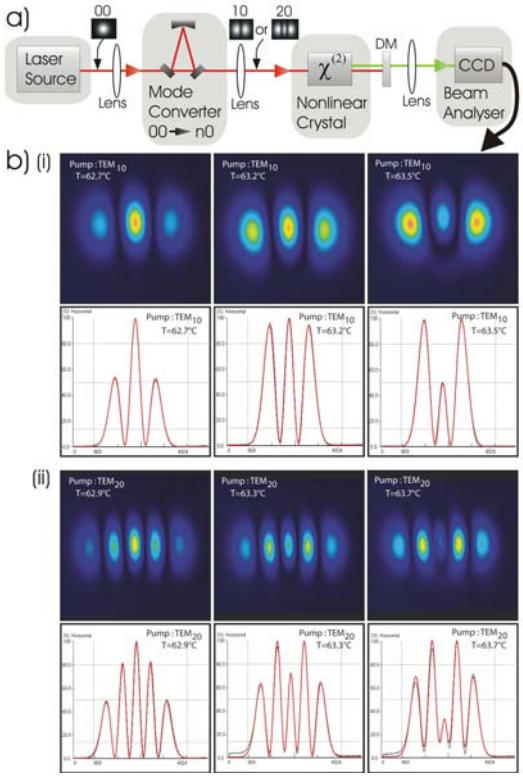

FIG. 2: a) Scheme for single pass SHG measurement. b) SH profiles generated in the crystal far field for three phase matching temperatures. (i) TEM_{10} and (ii) TEM_{20} pump mode. The cross-section traces contain both the data and theory fits.

The generated SH profiles, normalized to their maximum, are presented for different crystal temperatures in Fig. 2 b)(i) and b)(ii) for a TEM_{10} and TEM_{20} pump mode, respectively. It is clearly observed that the spatial distribution of the SH field varies strongly with the phase matching temperature of the nonlinear interaction. In the case of a TEM_{10} pump the SH field can be converted from a predominantly TEM_{00} mode to a predominantly TEM_{20} profile. Tuning the crystal temperature

allows reproducible control over the coefficients of the linear combination between the TEM_{00} and TEM_{20} modes. Similarly, for the TEM_{20} pump mode we find that the SH field is a crystal temperature dependant linear combination of the TEM_{00}, TEM_{20} and TEM_{40} modes. This is in good agreement with the calculated overlap coefficients.

This phenomenon can be explained if we consider the propagation of the H-G modes. The H-G modes have different Gouy phase shifts [23], and consequently not all of the SH components are simultaneously phase matched with the pump along the length of the crystal. Since the birefringence of lithium niobate is highly temperature dependant, phase matching for each mode occurs at different crystal temperatures. Allowing small variations of the coefficients given in the mode overlap integral to account for the mode selectivity and including phase shifts between each component to account for the Gouy phase shift accumulated during the propagation, we see an excellent agreement between the theoretical prediction and the experiment, as shown by the cross-section traces in Fig. 2. This proves that transverse mode coupling can be fully described by our simple mode-overlap model and that no coupling with other modes need to be considered.

Since the first generation of squeezed states by parametric down conversion by Wu *et al.* in 1986 [24], OPAs have proven to reliably produce up to 6 dB of squeezing [25] and down to sub-kHz frequencies [6], but have been limited to TEM_{00} mode operation. The use of such a system to generate squeezing in higher order H-G modes has to date not been demonstrated.

As discussed previous the ideal profile of the pump beam should match the square of the seed beam. Although generating such a complicated multi-mode pump beam is in principle possible by using holograms [26] or using a spatial light modulator, we chose to simply use the TEM_{00} green mode delivered by the laser at the cost of reduced parametric interaction. Also the mode-mismatch between the SH TEM_{00} pump mode and fundamental TEM_{n0} seed modes leads to nonlinear losses and noise, which will degrade or even destroy the non-classical correlations. It is therefore very important to mode-match the SH TEM_{00} pump mode with the fundamental TEM_{n0} seed mode of the OPA cavity. In order to achieve better mode-matching with a non-optimal pump we use the effect of mode selective phase matching to tune the OPA cavity to a specific mode. Perfect phase-matching temperature is measured at approximately 63.2^0 Celsius. In order to generate TEM_{n0} squeezing with a non-optimal TEM_{00} SH pump mode, we change the temperature of the nonlinear crystal to approximately 62.8^0 Celsius. We find that the nonlinear interaction is increase with respect to case of perfect mode-matching temperature, this is due to better spatial overlap between the SH pump and seed modes. From Fig. 2b)(i) and b)(ii) can it be seen that the multi-mode SH pump mode is mainly a TEM_{00} mode and therefore the spatial overlap between the non-optimal TEM_{00} SH pump mode and the TEM_{n0} seed mode is increased.

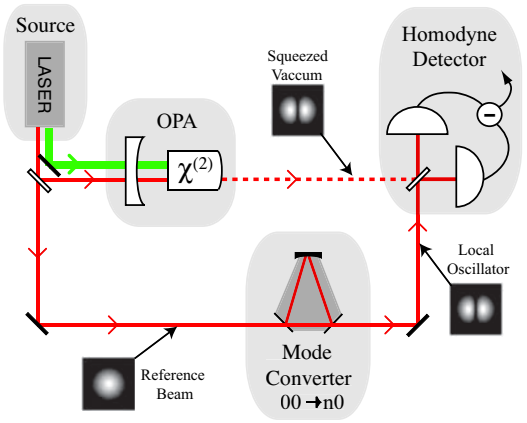

FIG. 3: Experimental setup to generate TEM_{n0} transverse mode squeezing. An OPA is seeded with a infrared misaligned TEM_{00} beam. The cavity is then locked to the TEM_{n0} mode and pumped with a SH TEM_{00} beam. The TEM_{n0} squeezed beam thereby produced is analyzed using spatial homodyne detection, whose TEM_{n0} LO is created from a misaligned ring cavity. Transverse beam profiles are represented in the case of TEM_{10} mode squeezing.

A schematic diagram of our experimental setup to generate higher order squeezing with non-optimal pump is presented in Fig. 3. The figure shows an hemilithic OPA with a near-concentric cavity design, the nonlinear crystal is a lithium niobate ($MgO:LiNbO_3$) crystal. All the technical details about the operation of the OPA can be found in ref. [27]

The measured squeezing in the three first H-G modes is shown in Fig. 4 with a resolution bandwidth of 300 kHz and a video bandwidth of 300 Hz at a detection frequency of 4.5 MHz. All traces are normalized to the quantum noise level (QNL), which is given by trace ii) and is measured by blocking the squeezed beam before the homodyne detector. Traces i) and iii) are obtained by scanning the LO phase and locking to the squeezed amplitude quadrature. The squeezing and anti-squeezing values are corrected for electronic noise, which is measured about -9 dB below the QNL. We measured -4.0 ± 0.1 dB of squeezing and $+8.5 \pm 0.1$ dB of anti-squeezing for the TEM_{00}, -2.6 ± 0.1 dB of squeezing and $+5.4 \pm 0.1$ dB of anti-squeezing for the TEM_{10} and -1.5 ± 0.1 dB of squeezing and $+2.7 \pm 0.1$ dB of anti-squeezing for the TEM_{20}.

The detection efficiency of our experiment is affected by different kind of losses. The efficiency of photodetection and propagation through the optics is recorded as $\eta_{prop} = 0.90 \pm 0.06$. The homodyne efficiency is measured to be $\eta_{hd}(TEM_{00}) = 0.98 \pm 0.02$, $\eta_{hd}(TEM_{10}) = 0.95 \pm 0.02$ and $\eta_{hd}(TEM_{20}) = 0.91 \pm 0.02$ for the different modes. This mode dependance is due to the larger spatial extension and stronger aperturing of the higher order modes by the optics. The induced losses

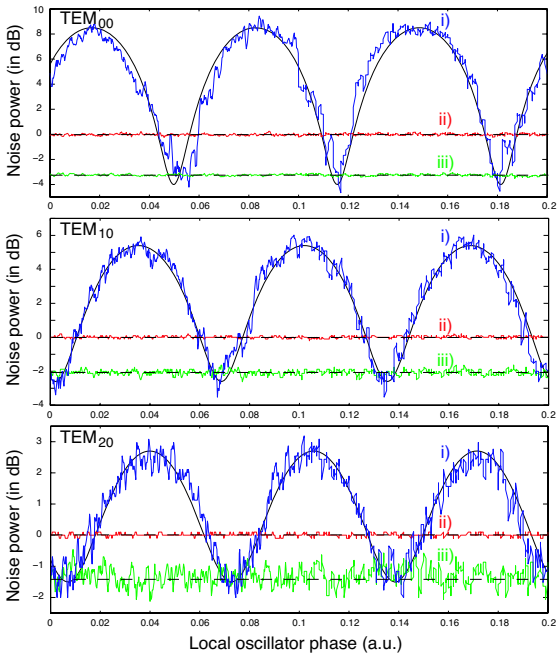

FIG. 4: Experimental squeezing traces for a) TEM_{00}, b) TEM_{10} and c) TEM_{20} recorded by homodyne detection. The different traces are i) Scan of the relative phase between the LO and the squeezed beam. ii) The quantum noise limit. iii) Locked to the squeezed amplitude quadrature.

due to non-optimal pump mode limit us presently to noise suppressions of -2.6 dB and -1.5 dB for the TEM_{10} and TEM_{20} mode. However, we can infer about -7 dB and -5 dB of noise suppression inside the OPO. This is similar to the degree of squeezing observed in conventional CW quantum information experiments, future refinements will allow us to increase the observed squeezing.

To our knowledge this is the first demonstration of higher order transverse mode squeezing. Temperature dependent phase matching of spatial modes is shown in a single pass SHG experiment. It shows that mode coupling between different transverse modes is possible in a second order type I nonlinear interaction, and that the ratio and phase between the generated SH components can be adjusted continuously via crystal temperature. This is the key effect for coupling the higher order modes using nonlinear interactions such as SHG or OPA. We combine all this to show the generation of squeezed light in the TEM_{10} and TEM_{20} H-G modes. We believe that using an optimal pump mode the output field of the OPA can in principle be squeezed in an arbitrary higher order H-G mode.

Our experiments have demonstrated all the necessary tools for multi-mode parallel quantum information. The encoding of quantum information is direct and efficient since the higher order modes contain information that is directly linked to the position, momentum, size and focussing of a TEM_{00} mode. The detection with spatial homodyne detection is very efficient. These important result opens the way for quantum information processing with continuous variables in the transverse plane using the basis of H-G modes. The technology for multiple squeezers driven by one laser is available [28] and we can now consider the synthesis of multi-mode beams with at least 5 orthogonal modes, each with a pair of commuting variables. We can now envision a procedure to generate entangled beams and test information protocols that are based on parallel mode processing. These experiments complement the work on quantum imaging which aims at generating multi-mode spatial quantum information in one device and to transmit, amplify and process spatial quantum correlations [29, 30].

We would like to thank Magnus Hsu, Gabriel Hétet, and Oliver Glöckl for many useful discussions. This work was supported by the Australian Research Council Centre of Excellence scheme. ML is supported by the Danish Technical Research Council (STVF Project No. 26-03-0304).

[1] European Commission. *Quantum Information processing and communication in Europe, http://www.cordis.lu/ist/fet/qipc.htm.* Luxembourg, Italy, 2005.
[2] Z.Y. Ou *et al. Phys. Rev. Lett.*, 68:3663, 1992.
[3] Ch. Silberhorn *et al. Phys. Rev. Lett.*, 86(19):4267, 2001.
[4] C. Schori *et al. Phys. Rev. A*, 66:033802, 2002.
[5] W.P. Bowen *et al. Phys. Rev. A*, 69:012304, 2004.
[6] K. McKenzie *et al. Phys. Rev. Lett.*, 93(16):161105, 2004.
[7] A. Furusawa *et al. Science*, 282(5389):706, 1998.
[8] F. Grosshans *et al. Nature*, 421(6920):238, 2003.
[9] C. Weedbrook *et al. Phys. Rev. Lett.*, 93(17):1705041–4, 2004.
[10] S. Lorenz *et al. Appl. Phys. B*, B79(3):273, 2004.
[11] H-A. Bachor and T.C. Ralph. *A guide to experiments in quantum optics.* Wiley, Berlin, 2004.
[12] S.L. Braunstein *et al. Rev. Mod. Phys.*, 77:513, 2005.
[13] H. Kogelnik. Polytechnic Press, 1964.
[14] V. Delaubert *et al. Opt. Lett.*, Doc. ID66257, 2006.
[15] N. Treps *et al. Science*, 301:940, 2004.
[16] C.M. Caves and P.D. Drummond. *Rev. Mod. Phys.*, 66(2):481, 1994.
[17] A. Zeilinger. *Science.*, 289(5478):405, 2000.
[18] N.K. Langford *et al. Rev. Rev. Lett.*, 93(5):053601–1, 2004.
[19] M.T.L Hsu *et al. J. of Opt. B*, 6:495, 2004.
[20] H-A. Bachor *et al. J. of Mod. Opt.*, 53(5-6):597, 2006.
[21] R.W. Boyd. *Nonlinear Optics.* Academic Press, San

Diego, 1992.
[22] R.W.P. Drever *et al. Appl. Phys. B*, B31(2):97–105, 1983.
[23] A.E. Siegman. *Lasers*. University Science, Mill Valley California, 1986.
[24] L.A. Wu *et al. Phys. Rev. Lett.*, 57(20):2520, 1986.
[25] P.K. Lam *et al. J. of Opt. B*, 1(4):469–474, 1999.
[26] A. Vaziri *et al. J. of Opt. B*, 4(2):S47–S51, 2002.
[27] M. Lassen *et al. J. of the Euro Opt. Soc.-RP.*, 1(1), 2006.
[28] N. Takei *et al. Phys. Rev. A.*, 72:042304–1, 2005.
[29] C. Schwob *et al. Appl. Phys. B*, 66(6):685–699, 1998.
[30] S. Gigan *et al. J. of Mod. Opt.*, 53(5):809–820, 2006.

PHYSICAL REVIEW A **72**, 013802 (2005)

Continuous-variable spatial entanglement for bright optical beams

Magnus T. L. Hsu,[1] Warwick P. Bowen,[1,*] Nicolas Treps,[2] and Ping Koy Lam[1,†]
[1]*Australian Centre for Quantum-Atom Optics, Department of Physics, Australian National University, ACT 0200, Australia*
[2]*Laboratoire Kastler Brossel, Université Pierre et Marie Curie, Case 74, 75252 Paris cedex 05, France*
(Received 24 January 2005; published 5 July 2005)

A light beam is said to be position squeezed if its position can be determined to an accuracy beyond the standard quantum limit. We identify the position and momentum observables for bright optical beams and show that position and momentum entanglement can be generated by interfering two position, or momentum, squeezed beams on a beam splitter. The position and momentum measurements of these beams can be performed using a homodyne detector with local oscillator of an appropriate transverse beam profile. We compare this form of spatial entanglement with split detection-based spatial entanglement.

DOI: 10.1103/PhysRevA.72.013802 PACS number(s): 42.50.Dv, 42.30.−d

I. INTRODUCTION

The concept of entanglement was first proposed by Einstein, Podolsky, and Rosen in a seminal paper in 1935 [1]. The original Einstein-Podolsky-Rosen (EPR) entanglement, as discussed in the paper, involved the position and momentum of a pair of particles. In this paper, we draw an analogy between the original EPR entanglement and the position and momentum $(x-p)$ entanglement of bright optical beams.

Entanglement has been reported in various manifestations. For continuous wave (cw) optical beams, these include, quadrature [2,3] and polarization [4] entanglement. Spatial forms of entanglement, although well studied in the single photon regime, have not been studied significantly in the continuous wave regime. Such forms of entanglement are interesting as they span a potentially infinite Hilbert space. Spatial EPR entanglement [5] has wide-ranging applications from two-photon quantum imaging [6,7] to holographic teleportation [8,9] and interferometric faint phase object quantum imaging [10].

Current studies are focused on $x-p$ entanglement for the few photons regime. Howell *et al.* [11] observed near and far-field quantum correlation, corresponding to the position and momentum observables of photon pairs. Gatti *et al.* [12] have also discussed the spatial EPR aspects in the photons pairs emitted from an optical parametric oscillator below threshold. Other forms of spatial entanglement which are related to image correlation have also been investigated. A scheme to produce spatially entangled images between the signal and idler fields from an optical parametric amplifier has been proposed by Gatti *et al.* [13–15]. Their work was extended to the macroscopic domain by observing the spatial correlation between the detected signal and idler intensities, generated via the parametric down conversion process [16].

Our proposal considers the possibility of entangling the position and momentum of a free propagating beam of light, as opposed to the entanglement of local areas of images, considered in previous proposals. Our scheme is based on the concept of position squeezed beams where we have shown that we have to squeeze the transverse mode corresponding to the first order derivative of the mean field in order to generate the position squeezed beam [17]. Similarly to the generation of quadrature entangled beams, the position squeezed beams are combined on a beam splitter to generate x-p entangled beams. We also propose to generate spatial entanglement for split detection, utilizing spatial squeezed beams reported by Treps *et al.* [18–20]. This form of spatial entanglement has applications in quantum imaging systems.

By considering the relevant modal decomposition of displaced and tilted fields, we arrive at general expressions for the position and momentum of an optical beam. We then limit ourselves to the regime of small displacements and tilts. This is the relevant regime for observing quantum optical phenomena, since for large displacements (tilts) the overlap between displaced (tilted) and nondisplaced (nontilted) beams approaches zero and hence they become perfectly distinguishable even in a classical sense. Applying this restriction, we show that as expected the position and momentum of an optical field are Fourier transform related. We then consider the specific case of a beam with TEM_{00} mode shape. TEM_{00} beams have the unique feature of satisfying the position-momentum uncertainty relation in the equality, and therefore represent an ideal starting point for the generation of spatial entanglement. We explicitly show that the position and momentum observables derived in this paper for a TEM_{00} beam are conjugate observables which obey the Heisenberg commutation relation. We then propose a scheme to produce x-p entanglement for TEM_{00} optical beams. Finally, we consider spatial squeezed beams for split detectors and show that it is also possible to generate spatial entanglement with such beams.

II. POSITION-MOMENTUM ENTANGLEMENT

A. Definitions—Classical treatment

Let us consider an optical beam with an x- and y-symmetric transverse intensity profile propagating along the z axis. Since the axes of symmetries remain well defined

*Present address: Quantum Optics Group, MC 12-33, Norman Bridge Laboratory of Physics, California Institute of Technology, Pasadena, CA 91125, USA.
†Email address: ping.lam@anu.edu.au

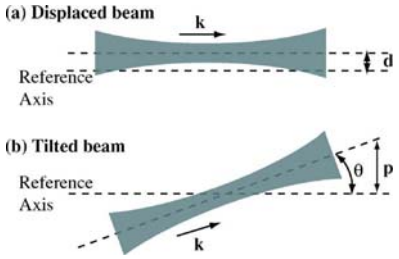

FIG. 1. (Color online) (a) Beam displacement d, and (b) beam tilt by angle θ, from a reference axis.

during propagation, we can relate the beam position relative to these axes. To simplify our analysis we henceforth assume without loss of generality, a one-dimensional beam displacement, d, from the reference x axis [see Fig. 1(a)]. We denote the electric field profile of the beam by $E(x)$. For a displaced beam, the electric field profile is given by

$$E_d(x) = E(x) + d\frac{\partial E(x)}{\partial x} + \frac{d^2}{2}\frac{\partial^2 E(x)}{\partial x^2} + \cdots . \tag{1}$$

In the regime where displacement is much smaller than the beam size, we can utilize the linearized approximation where only the zeroth and first order terms are significant. We see from this expression that the zeroth order term is not dependent on d, and that the displacement is directly proportional to the derivative of the field amplitude $\partial E(x)/\partial x$ [17].

The transverse beam momentum p on the other hand, can be obtained from the transverse component of the wave number of the beam, $p = k \sin\theta$, where $k = 2\pi/\lambda$ and the beam tilt is θ. This beam tilt is defined with respect to a pivot point at the beam waist, as shown in Fig. 1(b).

The electric field profile for a tilted beam with untilted electric field profile $E(x)$ and wavelength λ is given by

$$E_\theta(x) = \exp\left[\frac{i2\pi x \sin\theta}{\lambda}\right] E(x\cos\theta). \tag{2}$$

We can again simplify Eq. (2) by taking the zeroth and first order Taylor expansion terms to get a transverse beam momentum of $p \approx k\theta$. In the case of small displacement or tilt, we therefore obtain a pair of equations

$$E_d(x) \approx E(x) + d\frac{\partial E(x)}{\partial x}, \tag{3}$$

$$E_p(x) \approx E(x) + p\ ixE(x). \tag{4}$$

Equations (3) and (4) give the field parameters that relate to the displacement and tilt of a beam. For freely propagating optical modes, the Fourier transform of the derivative of the electric field, $\mathcal{F}[\partial E(x)/\partial x]$, is of the form $ixE(x)$. Hence the Fourier transform of displacement is tilt.

In the case of a single photon, the position and momentum are defined by considering the spatial probability density of the photon, given by $|E(x)|^2/I$, where $I = \int |E(x)|^2 dx$ is the normalization factor. The mean position obtained from an ensemble of measurements on single photons is then given by $\langle x\rangle = (1/I)\int x|E(x)|^2 dx$. The momentum of the photon is defined by the spatial probability density of the photon in the far-field, or equivalently by taking the Fourier transform of $\langle x\rangle$. These definitions are consistent with our definitions of position and momentum for bright optical modes.

B. TEM$_{pq}$ basis

In theory, spatial entanglement can be generated for fields with any arbitrary transverse mode shape. However, as with other forms of continuous-variable entanglement, the efficacy of protocols to generate entanglement is highest if the initial states are minimum uncertainty. For position and momentum variables, the minimum uncertainty states are those which satisfy the Heisenberg uncertainty relation $\Delta^2\hat{x}\Delta^2\hat{p} \geqslant \hbar$, in the equality. This equality is only satisfied by states with Gaussian transverse distributions [21], therefore we limit our analysis to that of TEM$_{00}$ modes.

A field of frequency ω can be represented by the positive frequency part of the mean electric field $\mathcal{E}^+ e^{i\omega t}$. We are interested in the transverse information of the beam described fully by the slowly varying field envelope $\mathcal{E}^+$. We express this field in terms of the TEM$_{pq}$ modes. For a measurement performed in an exposure time T, the mean field for a displaced TEM$_{00}$ beam can be written as

$$\mathcal{E}_d^+(x) = i\sqrt{\frac{\hbar\omega}{2\epsilon_0 cT}}\sqrt{N}\left[u_0(x) + \frac{d}{w_0}u_1(x)\right], \tag{5}$$

where the first term indicates that the power of the displaced beam is in the TEM$_{00}$ mode while the second term gives the displacement signal contained in the amplitude of the TEM$_{10}$ mode component. The corresponding mean field for a tilted TEM$_{00}$ beam can be written as

$$\mathcal{E}_p^+(x) = i\sqrt{\frac{\hbar\omega}{2\epsilon_0 cT}}\sqrt{N}\left[u_0(x) + \frac{iw_0 p}{2}u_1(x)\right], \tag{6}$$

where the second term describes the beam momentum signal, contained in the $\pi/2$ phase-shifted TEM$_{10}$ mode component.

C. Definitions—Quantum treatment

We now introduce a quantum mechanical representation of the beam by taking into account the quantum noise of optical modes. We can write the positive frequency part of the electric field operator in terms of photon annihilation operators $\hat{a}$. The field operator is given by

$$\hat{\mathcal{E}}_{\text{in}}^+ = i\sqrt{\frac{\hbar\omega}{2\epsilon_0 cT}}\sum_{n=0}^{\infty}\hat{a}_n u_n(x), \tag{7}$$

where $u_n(x)$ are the transverse beam amplitude functions for the TEM$_{pq}$ modes and $\hat{a}_n$ are the corresponding annihilation operators. $\hat{a}_n$ is normally written in the form of $\hat{a}_n = \langle\hat{a}_n\rangle + \delta\hat{a}_n$, where $\langle\hat{a}_n\rangle$ describes the coherent amplitude part and $\delta\hat{a}_n$ is the quantum noise operator.

In the small displacement and tilt regime, the TEM$_{00}$ and TEM$_{10}$ modes are the most significant [17], with the TEM$_{10}$ mode contributing to the displacement and tilt signals. We

can rewrite the electric field operator for mean number of photons N as

$$\hat{\mathcal{E}}_{in}^{+} = i\sqrt{\frac{\hbar\omega}{2\epsilon_0 cT}}\left[\sqrt{N}u_0(x) + \frac{\delta\hat{X}_{a_0}^{+} + i\delta\hat{X}_{a_0}^{-}}{2} + \sum_{n=1}^{\infty}\left(\frac{\hat{X}_{a_i}^{+} + i\hat{X}_{a_i}^{-}}{2}\right)u_i(x)\right], \tag{8}$$

where the annihilation operator is now written in terms of the amplitude $\hat{X}_a^+$ and phase $\hat{X}_a^-$ quadrature operators.

The displacement and tilt of a TEM_{00} beam is given by the amplitude and phase of the $u_1(x)$ mode in Eqs. (5) and (6), respectively. We can, therefore, write the beam position and momentum operators as

$$\hat{x} = \frac{w_0}{2\sqrt{N}}\hat{X}_{a_1}^{+}, \tag{9}$$

$$\hat{p} = \frac{1}{w_0\sqrt{N}}\hat{X}_{a_1}^{-}. \tag{10}$$

D. Commutation relation

Two observables corresponding to the position and momentum of a TEM_{00} beam have been defined. We have shown that the position and momentum observables correspond to near- and far-field measurements of the beam, respectively. Hence we expect from Eqs. (9) and (10) that the position and momentum observables do not commute. Indeed, the commutation relation between the two quadratures of the TEM_{10} mode is $[\hat{X}_{a_1}^{+},\hat{X}_{a_1}^{-}]=2i$. This leads to the commutation relation between the position and momentum observables of an optical beam with N photons

$$[\hat{x},\hat{p}] = \frac{i}{N}. \tag{11}$$

This commutation relation is similar to the position-momentum commutation relation for a single photon, aside from the $1/N$ factor. The $1/N$ factor is related to the precision with which one can measure beam position and momentum. Rewriting the Heisenberg inequality using the commutation relation gives

$$\Delta^2\hat{x}\Delta^2\hat{p} \geq \frac{1}{4N}. \tag{12}$$

The position measurement of a coherent optical beam gives a signal which scales with N. The associated quantum noise of the position measurement scales with $\sqrt{N}$. Hence the positioning sensitivity of a coherent beam scales as $\sqrt{N}$ [17,18]. The same consideration applied to the sensitivity of beam momentum measurement shows an equivalent dependence of $\sqrt{N}$. This validates the factor of N in the Heisenberg inequality and the commutation relation for a cw optical beam.

As an aside, it is interesting to consider the implications of the Heisenberg inequality of Eq. (12) on recent discussions of ghost imaging in discrete variable quantum optics [22–24]. In ghost imaging, the spatial resolution of an imaging system is enhanced using a pair of correlated fields. One field passes through the object, and object information is then retrieved through spatially resolved photon coincidences between the two fields. At first glance, the results of Bennink *et al.* [22,23], and Gatti *et al.* [24] appear contradictory. According to Bennink *et al.* the position-momentum uncertainty relation sets an ultimate resolution limit which can only be surpassed using entangled fields; while Gatti *et al.* show that thermal fields can achieve the same resolution as entangled fields for large N. We see from Eq. (12) that these statements are not mutually incompatible. For small N the position and momentum of the beams, and therefore also the imaging resolution, are highly uncertain; however, as N becomes large the uncertainty product $\Delta^2\hat{x}\Delta^2\hat{p}$ approaches zero, so that even without quantum resources x and p can be known simultaneously with arbitrary precision.

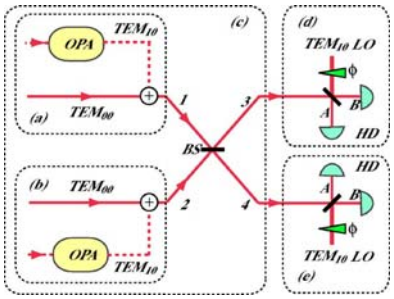

FIG. 2. (Color online) Scheme for generating position-momentum entanglement for continuous wave TEM_{00} optical beams. OPA: optical parametric amplifiers for the generation of squeezed light, BS: 50:50 beam splitter, HD: homodyne detectors, LO: local oscillator beams, and ϕ: phase of local oscillator beam.

E. Entanglement scheme

We have shown that the position and momentum observables of cw TEM_{00} optical beams satisfy the Heisenberg commutation relation. Consequently, EPR entanglement for the position and momentum of TEM_{00} beams is possible. Experimentally, the usual quadrature entanglement is generated by mixing two amplitude squeezed beams on a 50:50 beamsplitter. The same idea can be applied to generate EPR x-p entanglement, by using position squeezed beams [17]. Our scheme to produce x-p entanglement between two cw TEM_{00} optical beams is shown in Fig. 2. The position squeezed beams in Figs. 2(a) and 2(b) are generated via the in-phase combination of a vacuum squeezed TEM_{10} beam with a coherent TEM_{00} beam. Such a beam combination can be achieved experimentally, for example, using an optical cavity or a beam-splitter [20]. The result of the combination is a position squeezed beam. To generate entanglement, we consider beams with zero mean position and momentum, but we are interested in the quantum noise of the position and momentum of the beam. With this assumption, the electric field operators for the two input beams at the beam splitter are given by

$$\hat{\mathcal{E}}_1^+ = i\sqrt{\frac{\hbar\omega}{2\epsilon_0 cT}}\left(\sqrt{N}u_0(x) + \sum_{n=0}^{\infty}\delta\hat{a}_n u_n(x)\right) \tag{13}$$

$$\hat{\mathcal{E}}_2^+ = i\sqrt{\frac{\hbar\omega}{2\epsilon_0 cT}}\left(\sqrt{N}u_0(x) + \sum_{n=0}^{\infty}\delta\hat{b}_n u_n(x)\right) \tag{14}$$

where in both equations, the first bracketed term describes the coherent amplitude of the TEM_{00} beam. The second bracketed terms describe the quantum fluctuations present in all modes. For position squeezed states, only the TEM_{10} mode is occupied by a vacuum squeezed mode. All other modes are occupied by vacuum fluctuations. It is also assumed that the number of photons in each of the two beams, during the measurement window, is equal to N. The two position squeezed beams (1,2) are combined in-phase on a 50:50 beam splitter (BS) in Fig. 2(c).

The usual input-output relations of a beam splitter apply. The electric field operators describing the two output fields from the beam splitter are given by $\hat{\mathcal{E}}_3 = (\hat{\mathcal{E}}_1 + \hat{\mathcal{E}}_2)/\sqrt{2}$ and $\hat{\mathcal{E}}_4 = (\hat{\mathcal{E}}_1 - \hat{\mathcal{E}}_2)/\sqrt{2}$. To demonstrate the existence of entanglement, we seek quantum correlation and anticorrelation between the position and momentum quantum noise operators. The position operators corresponding to beams 3 and 4 are given, respectively, by

$$\delta\hat{x}_3 = \frac{w_0}{2\sqrt{2}\sqrt{N}}(\delta\hat{X}_{a_1}^+ + \delta\hat{X}_{b_1}^-) = \frac{1}{\sqrt{2}}\left(\delta\hat{x}_a + \frac{w_0^2}{2}\delta\hat{p}_b\right), \tag{15}$$

$$\delta\hat{x}_4 = \frac{w_0}{2\sqrt{2}\sqrt{N}}(\delta\hat{X}_{a_1}^+ - \delta\hat{X}_{b_1}^-) = \frac{1}{\sqrt{2}}\left(\delta\hat{x}_a - \frac{w_0^2}{2}\delta\hat{p}_b\right). \tag{16}$$

The momentum operators corresponding to the photocurrent difference for beams 3 and 4 are given by

$$\delta\hat{p}_3 = \frac{1}{w_0\sqrt{2}\sqrt{N}}(\delta\hat{X}_{a_1}^- + \delta\hat{X}_{b_1}^+) = \frac{1}{\sqrt{2}}\left(\delta\hat{p}_a + \frac{2}{w_0^2}\delta\hat{x}_b\right), \tag{17}$$

$$\delta\hat{p}_4 = \frac{1}{w_0\sqrt{2}\sqrt{N}}(\delta\hat{X}_{a_1}^- - \delta\hat{X}_{b_1}^+) = \frac{1}{\sqrt{2}}\left(\delta\hat{p}_a - \frac{2}{w_0^2}\delta\hat{x}_b\right). \tag{18}$$

In our case where the two input beams are position squeezed, the sign difference between the position noise operators in Eqs. (15) and (16) as well as that between the momentum noise operators in Eqs. (17) and (18) are signatures of correlation and anticorrelation for $\delta\hat{x}$ and $\delta\hat{p}$.

F. Inseparability criterion

Many criterions exist to characterize entanglement, for example, the *inseparability criterion* [25] and the *EPR criterion* [26]. We have adopted the *inseparability criterion* to characterize position-momentum entanglement. For states with Gaussian noise statistics, Duan *et al.* [25] have shown that the *inseparability criterion* is a necessary and sufficient criterion for EPR entanglement.

In the case where two beams are perfectly interchangeable and have symmetrical fluctuations in the amplitude and phase quadratures, the *inseparability criterion* has been generalized and normalized to a product form given by [4,27–31]

$$\mathcal{I}(\hat{x},\hat{p}) = \frac{\langle(\hat{x}_3 + \hat{x}_4)^2\rangle\langle(\hat{p}_3 - \hat{p}_4)^2\rangle}{|[\hat{x},\hat{p}]|^2} \tag{19}$$

for any pair of conjugate observables $\hat{x}$ and $\hat{p}$, and a pair of beams denoted by the subscripts 3 and 4. For states which are inseparable, $\mathcal{I}(\delta\hat{x},\delta\hat{p}) < 1$. By using observables $\delta\hat{x}$ and $\delta\hat{p}$ from Eqs. (15)–(18) as well as the commutation relation of Eq. (11) the inseparability criterion for beams 3 and 4 is given by

$$\mathcal{I}(\delta\hat{x},\delta\hat{p}) = \frac{16N^2}{\omega_0^4}\langle(\delta\hat{x}_{a_1}^+)^2\rangle\langle(\delta\hat{x}_{b_1}^+)^2\rangle = \langle(\delta\hat{X}_{a_1}^+)^2\rangle\langle(\delta\hat{X}_{b_1}^+)^2\rangle < 1, \tag{20}$$

where we have assumed that the TEM_{10} modes of beams 1 and 2 are amplitude squeezed [i.e., $\langle(\delta\hat{X}_{a_1}^+)^2\rangle < 1$ and $\langle(\delta\hat{X}_{b_1}^+)^2\rangle < 1$].

Thus we have demonstrated that continuous-variable EPR entanglement between the position and momentum observables of two cw beams can be achieved.

G. Detection scheme

Reference [17] has shown that the optimum small displacement measurement is homodyne detection with a TEM_{10} local oscillator beam [see Fig. 2(d)]. When the input beam is centered with respect to the TEM_{10} local oscillator beam, no power is contained in the TEM_{10} mode. Due to the orthogonality of Hermite-Gauss modes, the TEM_{10} local oscillator only detects the TEM_{10} vacuum noise component. As the input beam is displaced, power is coupled into the TEM_{10} mode. This coupled power interferes with the TEM_{10} local oscillator beam, causing a change in photocurrent observed at the output of the homodyne detector. Thus the difference photocurrent of the TEM_{10} homodyne detector is given by [17]

$$\hat{n}_-^d = \frac{2\sqrt{N}\sqrt{N_{\mathrm{LO}}}}{w_0}\hat{x}, \tag{21}$$

where N_{LO} and N are the total number of photons in the local oscillator and displaced beams, respectively, with $N_{\mathrm{LO}} \gg N$. The linearized approximation is utilized, where second order terms in $\delta\hat{a}$ are neglected since $N \gg |\langle\delta\hat{a}_n^2\rangle|$ for all n.

In order to measure momentum, one could use a lens to Fourier transform to the far-field plane, where the beam is then measured using the TEM_{10} homodyning scheme. However, we have shown that the position and momentum of a TEM_{00} beam differs by the phase of the TEM_{10} mode component. Indeed for a tilted TEM_{00} beam, the TEM_{10} mode component is $\pi/2$ phase shifted relative to the TEM_{00} mode component. Consequently the phase quadrature of the TEM_{10} mode has to be interrogated. This can be achieved by utiliz-

ing a TEM_{10} local oscillator beam with a $\pi/2$ phase difference relative to the TEM_{10} mode component of the TEM_{00} beam. The resulting photocurrent difference between the two homodyning detectors, for $N_{LO} \gg N$, is given by

$$\hat{n}_-^p = w_0 \sqrt{N} \sqrt{N_{LO}} \hat{p}. \tag{22}$$

III. SPATIAL ENTANGLEMENT FOR SPLIT DETECTION

The entanglement presented in the previous section is analogous to x-p entanglement in the single photon regime. However, the choice of the mean field mode is restricted to the TEM_{00} mode. This limits the richness of a spatial variable and thus excludes the possibility of generating an infinite Hilbert space. To exploit the properties of spatial variables, we now consider more traditional forms of spatial squeezing. Consequently, we study the possibility of generating spatial entanglement for array detection devices, based on spatial squeezed beams.

A. Spatial squeezing

Spatial squeezing was first introduced by Kolobov [32]. The generation of spatial squeezed beams for split and array detectors was experimentally demonstrated by Treps *et al.* [18–20]. A one-dimensional spatial squeezed beam has a spatially ordered distribution, where there exists correlation between the photon numbers in both transverse halves of the beam. A displacement signal applied to this beam can thus be measured to beyond the QNL.

We consider a beam of normalized transverse amplitude function $v_0(x)$ incident on a split detector. The noise of split detection has been shown to be due to the flipped mode [33], given by

$$v_1(x) = \begin{cases} v_0(x) & \text{for } x > 0, \\ -v_0(x) & \text{for } x < 0. \end{cases}$$

When the field is centered at the split-detector, such that the mean value of the measurement is zero, the flipped mode is thus orthogonal to the mean field mode. In this instance, modes $v_i(x)$ (for $i > 1$) can be derived to complete the modal basis. The electric field operator written in this new modal basis is given by

$$\hat{\mathcal{E}}^+ = i \sqrt{\frac{\hbar\omega}{2\epsilon_0 c T}} \left[\sqrt{N} v_0(x) + \sum_{n=0}^{\infty} \delta\hat{c}_n v_n(x) \right], \tag{23}$$

where the first term describes the coherent excitation of the beam in the $v_0(x)$ mode and N is the total number of photons in the beam. It has been shown that the corresponding photon number difference operator for split detection is given by [17]

$$\hat{n}_-^{(+)} = \sqrt{N} \delta \hat{X}_{c_0}^+. \tag{24}$$

The beam is spatially squeezed if the state of the flipped mode is vacuum squeezed and in phase with the mean field mode [see Figs. 3(a) and 3(b)].

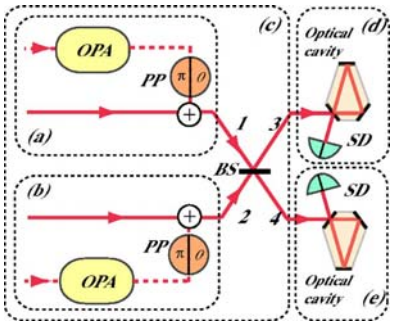

FIG. 3. (Color online) Scheme for generating spatial entanglement for TEM_{00} continuous wave light beams. OPA: optical parametric amplifiers for generating squeezed beams, PP: phase plates for producing flipped modes, and BS: 50:50 beam splitter.

B. Spatial homodyne

Since split detection is commonly used as a detection device for beam position, one would naturally consider taking the Fourier transform of a spatial squeezed beam to obtain the conjugate observable for the beam. However, we have shown that split detection does not correspond exactly to beam position measurement. Thus the Fourier plane of the spatial squeezed beam does not provide the conjugate observable. More practically, the flipped mode is not mode-shape invariant under Fourier transformation. In the far-field, each odd-ordered mode component of the flipped mode obtains a $(2n+1)\pi$ Gouy phase difference, compared to the near-field. Thus the mode shape in the far-field is no longer a flipped mode. Consequently, far- and near-field measurements of a spatial squeezed beam will not give the conjugate observables.

However, we can find the conjugate observables of a spatial squeezed beam by drawing an analogy to standard homodyne detection. In split detection, the equivalent local oscillator mode is the mean field $v_0(x)$ mode. The mode under interrogation by the split detector is the flipped mode $v_1(x)$. In the case of homodyne detection, the phase of the local oscillator beam is varied to measure the conjugate observables (i.e., amplitude and phase quadratures) of the input beam. Adapting this concept to the split detector, the conjugate observables for the spatial squeezed beam is thus the amplitude and phase quadratures of the flipped mode, while the mode shape of the flipped mode remains unaltered. This is further verified upon inspection of Eq. (24).

Our scheme to perform a phase measurement of the flipped mode is shown in Fig. 3(d). In our scheme we assume that the mean field is a TEM_{00} mode. Note that in principle, this analysis could be performed for any mode shape. The coherent TEM_{00} mode component provides a phase reference for the flipped mode, analogous to that of a local oscillator beam in homodyne detection. Thus the phase quadrature of the flipped mode can be accessed by applying a $\pi/2$ phase shift between the TEM_{00} mode and the flipped mode noise component. Experimentally, this is achievable using an optical cavity. When the cavity is nonresonant for the $v_0(x)$ and $v_1(x)$ modes it will reflect off the two modes, in phase, onto

the split detector. This will give a measurement of the amplitude quadrature of the flipped mode. However, the cavity can be tuned to be partially resonant on the $v_0(x)$ mode while reflecting the flipped mode. A $\pi/2$ phase difference can then be introduced between the reflected $v_0(x)$ and $v_1(x)$ modes, giving a measurement of the phase quadrature of the flipped mode. The corresponding photon number difference operator is

$$\hat{n}_-^{(-)} = \sqrt{N}\delta\hat{X}_{c_0}^-, \tag{25}$$

which is the orthogonal quadrature of the spatial squeezed beam. The photon number operators corresponding to the two measurements in Eqs. (24) and (25) are conjugate observables and satisfy the commutation relation $[\hat{n}_-^{(+)},\hat{n}_-^{(-)}] = 2iN$.

It is important to realize that the number of photons N in Eqs. (24) and (25) are only approximately equal. This is due to the fact that partial power in the TEM_{00} mode is transmitted by the cavity, when the cavity is partially resonant on the TEM_{00} mode. Although it is possible to implement a scheme that conserves the total number of photons at detection (e.g., losslessly separating the mean field and flipped modes and recombining them with a phase difference), we would like to emphasize that our scheme is more simple and intuitive, as well as being valid when N is large.

C. Entanglement scheme

In order to generate spatial entanglement for split detection, two spatial squeezed beams labeled 1 and 2 are combined on a 50:50 beam splitter, as shown in Fig. 3(c).

The electric field operators for the two input spatial squeezed beams at the beam splitter are described in a form identical to that of Eq. (23). The annihilation operators of the electric field operators for input beams 1 and 2 are labeled by $\hat{c}_n$ and $\hat{d}_n$, respectively. By following a similar procedure as before, the photon number difference operator for output beams 3 and 4 from the beam splitter are calculated.

For the amplitude quadrature measurement, the addition of the difference photocurrent between beams 3 and 4 yields

$$\hat{n}_{3-}^{(+)} + \hat{n}_{4-}^{(+)} = \sqrt{N}(\delta\hat{X}_{c_0}^+ + \delta\hat{X}_{d_0}^+). \tag{26}$$

For the phase quadrature measurement, the subtraction of the difference photocurrent between beams 3 and 4 gives

$$\hat{n}_{3-}^{(-)} - \hat{n}_{4-}^{(-)} = \sqrt{N}(\delta\hat{X}_{d_0}^+ - \delta\hat{X}_{c_0}^+). \tag{27}$$

To verify spatial entanglement, the *inseparability criterion* is utilized. The substitution of Eqs. (26) and (27) and the commutation relation between the photon number difference operators into the generalized form of the *inseparability criterion* gives

$$\mathcal{I}(\delta\hat{n}_-^{(+)}, \delta\hat{n}_-^{(-)}) = \frac{N\left(V_{c_0}^2 + 2V_{c_0}V_{d_0} + V_{d_0}^2\right)}{4N} < 1, \tag{28}$$

where $V_{c_0} = \langle(\delta\hat{X}_{c_0}^+)^2\rangle$ and $V_{d_0} = \langle(\delta\hat{X}_{d_0}^+)^2\rangle$ are the variances for the flipped mode component of the spatial squeezed beams 1 and 2. The inseparability criterion is satisfied for amplitude squeezed flipped modes $V_{c_0} < 1$ and $V_{d_0} < 1$.

We have proposed a scheme to generate spatial entanglement for split detection using spatial squeezed beams. Spatial squeezing has been defined for any linear measurement performed with an array detector [34]. Similarly, spatial entanglement corresponding to any linear measurement can be obtained. For an infinite span array detector with infinitesimally small pixels, it is thus possible to generate multimode spatial entanglement, increasing the Hilbert space to being infinite-dimensional.

IV. CONCLUSION

We have identified the position and momentum of a TEM_{00} optical beam. By showing that $\hat{x}$ and $\hat{p}$ are conjugate observables that satisfy the Heisenberg commutation relation, a continuous variable x-p entanglement scheme is proposed. This proposed entanglement, as considered by EPR [1], was characterized using a generalized form of the *inseparability criterion*.

We further explored a form of spatial entanglement which has applications in quantum imaging. The detection schemes for quantum imaging are typically array detectors. In this paper, we considered the split detector. We utilized the one-dimensional spatial squeezing work of Treps *et al.* [18] and proposed a spatial homodyning scheme for the spatial squeezed beam. By identifying the conjugate observables for the spatial squeezed beam as the amplitude and phase quadratures of the flipped mode, we showed that split detection-based spatial entanglement can be obtained.

ACKNOWLEDGMENTS

We would like to thank Vincent Delaubert and Hans-A. Bachor for fruitful discussions. This work was supported by the Australian Research Council Centre of Excellence Programme. The Laboratoire Kastler-Brossel of the Ecole Normale Superieure and Université Pierre et Marie Curie are associated via CNRS.

[1] A. Einstein, B. Podolsky, and N. Rosen, Phys. Rev. **47**, 777 (1935).
[2] Ch. Silberhorn, P. K. Lam, O. Weiss, F. König, N. Korolkova, and G. Leuchs, Phys. Rev. Lett. **86**, 4267 (2001).
[3] Z. Y. Ou, S. F. Pereira, H. J. Kimble, and K. C. Peng, Phys. Rev. Lett. **68**, 3667 (1992).
[4] W. P. Bowen, N. Treps, R. Schnabel, and P. K. Lam, Phys. Rev. Lett. **89**, 253601 (2002).
[5] L. A. Lugiato, A. Gatti, and E. Brambilla, J. Opt. B: Quantum Semiclassical Opt. **4**, S176 (2002).

[6] A. F. Abouraddy, B. E. A. Saleh, A. V. Sergienko, and M. C. Teich, Phys. Rev. Lett. **87**, 123602 (2001).
[7] T. B. Pittman, Y. H. Shih, D. V. Strekalov, and A. V. Sergienko, Phys. Rev. A **52**, R3429 (1995).
[8] A. F. Abouraddy, B. E. A. Saleh, A. V. Sergienko, and M. C. Teich, Opt. Express **9**, 498 (2001).
[9] I. V. Sokolov, M. I. Kolobov, A. Gatti, and L. A. Lugiato, Opt. Commun. **193**, 175 (2001).
[10] I. V. Sokolov, J. Opt. B: Quantum Semiclassical Opt. **2**, 179 (2000).
[11] J. C. Howell, R. S. Bennink, S. J. Bentley, and R. W. Boyd, Phys. Rev. Lett. **92**, 210403 (2004).
[12] A. Gatti and L. A. Lugiato, Phys. Rev. A **52**, 1675 (1995).
[13] A. Gatti, E. Brambilla, L. A. Lugiato, and M. I. Kolobov, Phys. Rev. Lett. **83**, 1763 (1999).
[14] A. Gatti, E. Brambilla, L. A. Lugiato, and M. I. Kolobov, J. Opt. B: Quantum Semiclassical Opt. **2**, 196 (2000).
[15] A. Gatti, L. A. Lugiato, K. I. Petsas, and I. Marzoli, Europhys. Lett. **46**, 461 (1999).
[16] A. Gatti, E. Brambilla, and L. A. Lugiato, Phys. Rev. Lett. **90**, 133603 (2003).
[17] M. T. L. Hsu, V. Delaubert, P. K. Lam, and W. P. Bowen, J. Opt. B: Quantum Semiclassical Opt. **6**, 495 (2004).
[18] N. Treps, U. Andersen, B. Buchler, P. K. Lam, A. Maître, H.-A. Bachor, and C. Fabre, Phys. Rev. Lett. **88**, 203601 (2002).
[19] N. Treps, N. Grosse, W. P. Bowen, C. Fabre, H.-A. Bachor, and P. K. Lam, Science **301**, 940 (2003).
[20] N. Treps, N. Grosse, W. P. Bowen, M. T. L. Hsu, A. Maître, C. Fabre, H.-A. Bachor, and P. K. Lam, J. Opt. B: Quantum Semiclassical Opt. **6**, S664 (2004).
[21] D. J. Griffiths, *Introduction to Quantum Mechanics* (Prentice-Hall, Eaglewood Cliffs, NJ, 1995).
[22] R. S. Bennink, S. J. Bentley, R. W. Boyd, and J. C. Howell, Phys. Rev. Lett. **92**, 033601 (2004).
[23] R. S. Bennink, S. J. Bentley, and R. W. Boyd, Phys. Rev. Lett. **89**, 113601 (2002).
[24] A. Gatti, E. Brambilla, M. Bache, and L. A. Lugiato, Phys. Rev. Lett. **93**, 093602 (2004).
[25] L.-M. Duan, G. Giedke, J. I. Cirac, and P. Zoller, Phys. Rev. Lett. **84**, 2722 (2000).
[26] M. D. Reid and P. D. Drummond, Phys. Rev. Lett. **60**, 2731 (1988)
[27] W. P. Bowen, N. Treps, R. Schnabel, and P. K. Lam, Phys. Rev. Lett. **89**, 253601 (2002).
[28] W. P. Bowen, R. Schnabel, P. K. Lam, and T. C. Ralph, Phys. Rev. Lett. **90**, 043601 (2003).
[29] W. P. Bowen, R. Schnabel, P. K. Lam, and T. C. Ralph, Phys. Rev. A **69**, 012304 (2004).
[30] S. Tan, Phys. Rev. A **60**, 2752 (1999).
[31] S. Mancini, V. Giovannetti, D. Vitali, and P. Tombesi, Phys. Rev. Lett. **88**, 120401 (2002).
[32] M. I. Kolobov, Rev. Mod. Phys. **71**, 1539 (1999).
[33] C. Fabre, J. B. Fouet, and A. Maître, Opt. Lett. **76**, 76 (2000).
[34] N. Treps, V. Delaubert, A. Maître, J. M. Courty, and C. Fabre, e-print quant-ph/0407246.

PHYSICAL REVIEW A **73**, 013820 (2006)

Optical storage of high-density information beyond the diffraction limit: A quantum study

V. Delaubert,[1] N. Treps,[1] G. Bo,[2] and C. Fabre[1]
[1]*Laboratoire Kastler Brossel, UPMC, Case 74, 4 Place Jussieu, 75252 Paris Cedex 05, France*
[2]*Laboratoire Pierre Aigrain, Ecole Normale Supérieure, 24 rue Lhomond, 75231 Paris Cedex 05, France*
(Received 13 September 2005; revised manuscript received 28 November 2005; published 27 January 2006)

We propose an optical readout scheme allowing a proof of principle of information extraction below the diffraction limit. This technique, which could lead to improvement in data readout density onto optical disks, is independent from the wavelength and numerical aperture of the reading apparatus, and involves a multipixel array detector. Furthermore, we show how to use nonclassical light in order to perform a bit discrimination beyond the quantum noise limit.

DOI: 10.1103/PhysRevA.73.013820 PACS number(s): 42.50.Dv, 42.30.Va, 42.30.Wb

I. INTRODUCTION

The reconstruction of an object from its image beyond the diffraction limit, typically of the order of the wavelength, is a hot field of research, though a very old one, as Bethe already dealt with the theory of diffraction by subwavelength holes in 1944, to the best of our knowledge [1]. More recently, a theory has been developed to be applied to the optical storage problem, in order to study the influence of very small variations of pit width or depth relative to the wavelength [1–6]. To date, only a few super-resolution techniques [7] include a quantum treatment of the noise in the measurement, but to our knowledge, none has been applied to the optical data storage problem.

Optical disks are now reaching their third generation, and have improved their data capacity from 0.65 Gbytes for compact disks (using a wavelength of 780 nm), to 4.7 Gbytes for DVDs ($\lambda = 650$ nm), and eventually to 25 GB for the Blu-Ray disks (using a wavelength of 405 nm). In addition to new coding techniques, this has been achieved by reducing the spot size of the diffraction-limited focused laser beam onto the disk, involving higher numerical apertures and shorter wavelengths.

Several further developments are now in progress, such as the use of volume holography, 266 nm reading lasers, immersion lenses, near field systems, multidepths pits [8], or information encoding on angle positions of asymmetrical pits [9]. These new techniques rely on a bit discrimination using small variations of the measured signals. Therefore, the noise is an important issue, and ultimately, quantum noise will be the limiting factor.

In this paper, we investigate an alternative and complementary way to increase the capacity of optical storage, involving the retrieval of information encoded on a scale smaller than the wavelength of the optical reading device. We investigate a way to optimize the detection of subwavelength structures using multipixel array. With an attempt to a full treatment of the optical disk problem being far too complex, we have chosen to illustrate our proposal on a very simple example, leaving aside most technical constraints and complications, but still involving all the essence of the overall problem.

We first explain how the use of an array detector can lead to an improvement of the detection and distinction of subwavelength structures present in the focal spot of a laser beam. We then focus on information extraction from an optical disk with a simple but illustrative example, considering that only a few bits are burnt on the dimensions of the focal spot of the reading laser, and show how the information is encoded from the disk to the light beam, propagated to the detector, and finally detected. We explain the gain configuration of the array detector that has to be chosen in order to improve the signal-to-noise ratio of the detection. Moreover, as quantum noise is experimentally accessible, and will be a limiting factor for further improvements, we perform a quantum calculation of the noise in the detection process. Indeed, we present how this detection can be optimized to perform simultaneous measurements below the quantum noise limit, using nonclassical light.

II. PROPOSED SCHEME FOR BIT SEQUENCE RECOGNITION IN OPTICAL DISKS

We propose an optical readout scheme shown in Fig. 1 allowing information extraction from optical disks beyond the diffraction limit, based on the multipixel detection. Bits, coded as pits and holes on the optical disk, induce phase flips in the electric field transverse profile of the incident beam at reflection. The reflected beam is imaged in the far field of the disk plane, where the detector stands. In the far field, the phase profile induced by the disk is converted into an intensity profile, that the multipixel detectors can, at least partly, reconstruct.

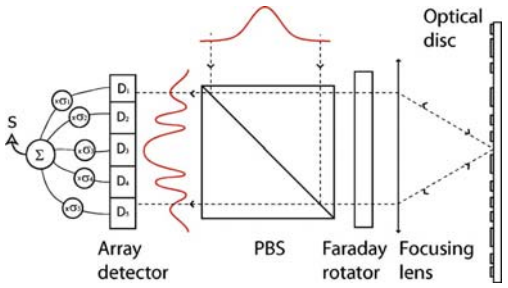

FIG. 1. (Color online) Scheme for information extraction from optical disks, using an array detector.

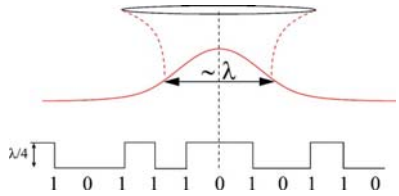

FIG. 2. (Color online) Example of a bit sequence on an optical disk. The spacing between the bits is smaller than the wavelength, the minimum waist of the incident laser beam being of the order of λ. A hole depth of λ/4 insures a π phase shift between fields reflected on a pit and a hole.

Taking into account that a lot of *a priori* information is available—i.e., only a finite number of intensity profiles is possible—we propose to use a detector with a limited number of pixels D_k whose gains can independently be varied depending on which bit sequence one wants to detect. The signal is then given by

$$S = \sum_k \sigma_k N_k, \tag{1}$$

where N_k is the mean photon number detected on pixel D_k, and σ_k is the electronic gain of the same pixel. Ideally, to each bit sequence present on the disk corresponds a set of gains chosen so that the value of the measurement is zero, thus canceling noise from the mean field. Measuring the signal for a given time interval T around the centered position of a bit sequence in the focal spot, and testing, in parallel, all the predefine sets of gain in the remaining time, allows us to deduce which bit sequence is present on the disk.

We will first show that this improvement in a density of information encoded on an optical disk is already possible using classical resources. Moreover, as the measurement is made around a zero mean value, the classical noise is mostly canceled. Hence, we reach regimes where the quantum noise can be the limiting factor. We will demonstrate how to perform measurements beyond the quantum noise limit, using previous results on quantum noise analysis in multipixel detection developed in Ref. [10].

III. ENCODING INFORMATION FROM A DISK ONTO A LIGHT BEAM

We have explained the general principle of readingout subwavelength bit sequences encoded on an optical disk, and now focus on the information transfer from the optical disk to the laser beam, through an illustrative example.

Let us recall that bits are encoded by pits and holes on the disk surface: a step change from hole to pit (or either from pit to hole) encodes bit 1, whereas no depth change on the surface encodes bit 0, as represented in Fig. 2. A hole depth of λ/4 ensures a π phase shift between the fields reflected by a pit and a hole. In this section, we compute the incident field distribution on the optical disk affected by the presence of a bit sequence in the focal spot, and finally analyze the intensity back reflected in the far field, in the detection plane, as sketched in Fig. 1.

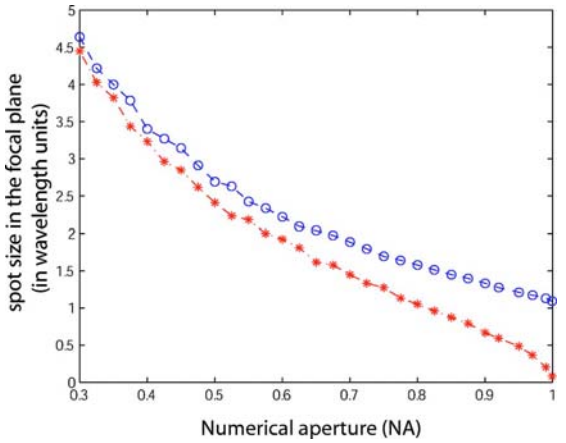

FIG. 3. (Color online) Evolution of the focused spot size of an incident plane wave with the numerical aperture (for λ=780 nm in air medium). The spot size is limited to the order of the wavelength in the nonparaxial case (○), whereas it goes to zero for very high numerical apertures in the paraxial case (∗).

A. Beam focalization

Current optical disk readout devices involve a linearly polarized beam strongly focused on the disk surface to point out details whose size is of the order of the laser wavelength. The numerical aperture (NA) of the focusing lens can be large (0.47 for CDs, 0.6 for DVDs, and 0.85 for BLU RAY disks), and the exact calculation of the field cannot be done in the paraxial and scalar approximation. Thus, the vectorial theory of diffraction has to be taken into account.

The structure of the electromagnetic field in the focal plane of a strongly focused beam has been investigated for decades now [11], as its applications include areas such as microscopy, laser microfabrication, micromanipulation, and optical storage [12–19].

In our case of interest, we can restrict the field calculation to the focal plane, which is the disk plane. Thus Richards and Wolf integrals [20], that are not suitable for a general propagation of the field, but which can provide the field profile in the focal plane for any type of polarization of the incoming beam as long as the focusing length is much larger than the wavelength, can be used to achieve this calculation. These integrals have already been used in many publications dealing with tight focusing processes [21–28]. As highlighted in these references, the importance of the vectorial aspect of the field can easily be understood when a linearly polarized beam is strongly focused, as the polarization of the wave after the lens is not perpendicular to the propagation axis anymore and has thus components along this axis. In order to estimate the limit of validity of the paraxial approximation, we computed focused spot sizes of linearly polarized beams in the focal plane for different numerical apertures, first in the paraxial approximation, and then calculated with Richards and Wolf integrals. The results are compared in Fig. 3 for an incident plane wave in an air medium with λ=780 nm, where the spot size is defined as the diameter

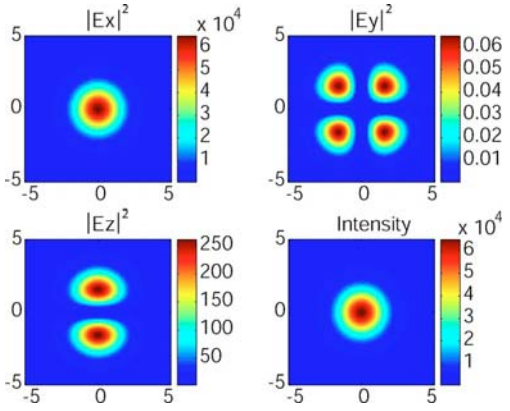

FIG. 4. (Color online) Norm of the different field components and resultant intensity in the focal plane with a linearly polarized incident field along the x axis, focused with a 0.47 numerical aperture.

which contains 86% of the focused energy, as in Ref. [29]. We see that when the numerical aperture exceeds 0.6, a good prediction requires a nonparaxial treatment. Moreover, whereas there is no theoretical limit to focalization in the paraxial case, we see that nonparaxial effects prevent us to reach a waist smaller than the order of the wavelength. Note that this limit is not fundamental and can be overcome by modifying the polarization of the incoming beam. Quabis and co-workers have indeed managed to reduce the spot area to about 0.1 λ^2 using an incident radially polarized doughnut beam [21,24].

As our aim is to present a demonstration of principle and not a full treatment of the optical disk problem, the following calculations will be done using the physical parameters of the actual compact disks ($\lambda=780$ nm and NA=0.47, corresponding to a focalization angle of 27° in air medium). In this case, the paraxial and scalar approximations are still valid. Indeed, Fig. 4, giving the transverse profile of the three field components and the resultant intensity in the focal plane using the former parameters, shows that although the field is not strictly linearly polarized as foreseen before, $E_y \ll E_z \ll E_x$, and we can thus consider that only E_x is different from zero with a good approximation. Note that the exact expression would not intrinsically change the problem, as our scheme can be adapted to any field profile discrimination.

B. Reflection onto the disk

In order to compute the reflected field, we simply assume that bumps and holes are generated in such a way that they induce a π phase shift between them at reflection on the field profile. Note that the holes' depth is usually $\lambda/4$, but precise calculations would be required to give the exact shape of the pits, as they are supposed to be burnt below the wavelength size, and as the field penetration in those holes is not trivial [4–6]. As we have shown that only one vectorial component of the field was relevant in the focal plane, we can directly apply this phase shift to the amplitude profile of this component.

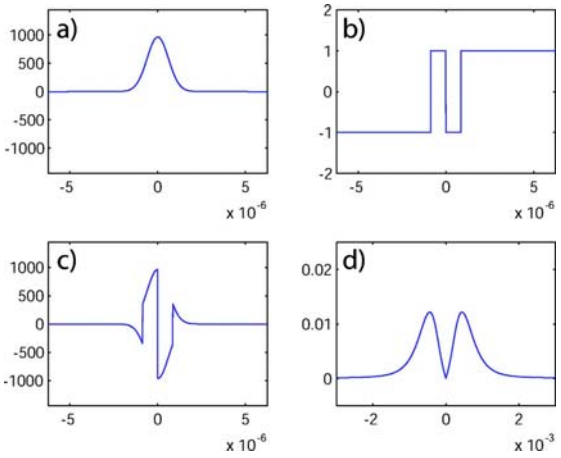

FIG. 5. (Color online) Modifications of the transverse amplitude field profile trough propagation, in the case of a 111 bit sequence in the focal spot: (a) incoming beam profile; (b) 111 bit sequence; (c) corresponding reflected field in the disk plane; (d) far field profile in the detector plane.

We first envision a scheme with only three bits in the focal spot, which means that 2^3 different bit sequences, i.e., a byte, have to be distinguished from each other, using the information extracted from the reflected field. Note that we neglect the influence of other bits in the neighborhood. A more complete calculation involving this effect with more bits will be considered in a further approach.

The amplitude profiles obtained when the incident beam is centered on a bit of the CD are presented on Fig. 5, for a particular bit sequence. Note that we have chosen the space between two bits on the disk equal to the waist size of the reading beam. The first three curves, respectively, show the field amplitude profile incident on the disk, an example of a bit sequence, and the corresponding profile just after reflection onto the disk. We see that binary information is encoded from bumps and holes on the CD to phase flips in the reflected field.

C. Back propagation to the detector plane

In order to extract the information encoded in the transverse amplitude profile of the beam, the field has to be back propagated to the detector plane. A circulator, composed of a polarizing beam splitter and a Faraday rotator, ensures that the linearly polarized reflected beam reaches the array detector, as shown in Fig. 1. Assuming that the detector is positioned just behind the lens plane, the expression of the detected field is given by the far field of the disk plane, apertured by the diameter of the focusing lens. As the focal length and the diameter of the lens are large compared to the wavelength, we use the Rayleigh Sommerfeld integral to compute the field in the lens plane [30]. As an example, the calculated far field profile when the bit sequence 111 is present in the focal spot is shown on the fourth graph of Fig. 5.

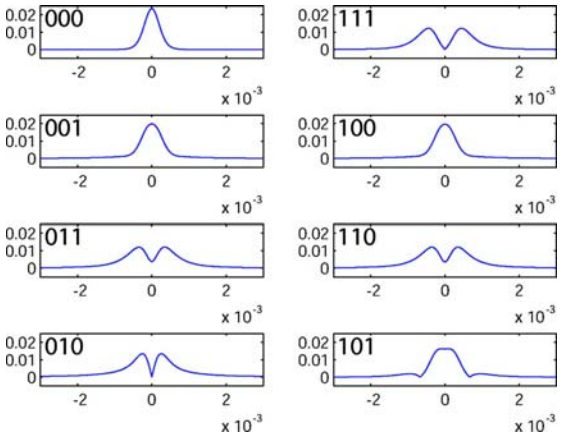

FIG. 6. (Color online) Field profiles in the array detector plane, for each of the 8 bit sequence configuration. Note that they are clearly distinguishable, except for the bit sequences 100 and 001, and 011 and 110, which have the same profile because of the symmetry of the bit sequence relative to the position of the incident laser beam.

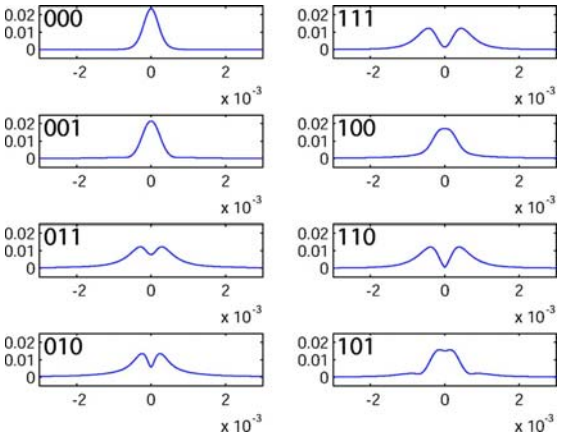

FIG. 7. (Color online) Field profiles in the array detector plane, for each of the 8 bit sequence configuration, when the position of the disk has been shifted of $w_0/6$ relative to the incident beam. The profile degeneracy for 100 and 001, and 011 and 110 is raised. Note that the other profiles have experienced a much smaller shape modification between the two positions of the disk.

The presence of the lens provides a limited aperture for the beam and cuts the high spatial frequencies of the field, which can be a source of information loss, as the difference between each bit sequence can rely on those high frequencies. However, we will see that enough information remains in the low frequency part of the spatial spectrum, so that the 8 bits can be distinguished. This is due to the fact that we have in this problem a lot of *a priori* information on the possible configurations to distinguish.

We see in Fig. 6 that, with the physical parameters used in compact disk readout devices, 6 over 8 profiles in the detector plane are still different enough to be distinguished. At this stage, we are nevertheless unable to discriminate between symmetric configurations, because they give rise to the same far field profile. Therefore, 100 and 001, and 110 and 011, cannot be distinguished. Note that this problem can be solved thanks to the rotation of the disk. Indeed, an asymmetry is created when the position of the disk relative to the laser beam is shifted, thus modifying differently the two previously indistinguishable profiles. As shown in Fig. 7, where the far field profiles are represented after a shift of $w_0/6$ in the position of the disk, the degeneracy has been removed. Moreover, it is important to note that the other profiles experience a small shape modification. This redundant information is very useful in order to remove ambiguities while the disk is rotating.

IV. INFORMATION EXTRACTION FOR BIT SEQUENCE RECOGNITION

In this section, we describe the detection, present some illustrative results, and the way they can be used to increase the readout precision of information encoded on optical disks. We show here that a pixellized detector with a very small number of pixels is enough to distinguish between the 8 bit sequences. Note that for technical and computing time reasons, it is not realistic to use a charge-coupled device (CCD) camera to record the reflected images, as such cameras cannot yet combine good quantum efficiency and high speed.

A. Detected profiles

For simplicity reasons, we limit our calculation to a 5 pixels array detector $D_1,\ldots,D_5$, each of whom has an electronic gain $\sigma_1,\ldots,\sigma_5$, as shown in Fig. 8 The size of each detector has been chosen without a systematic optimi-

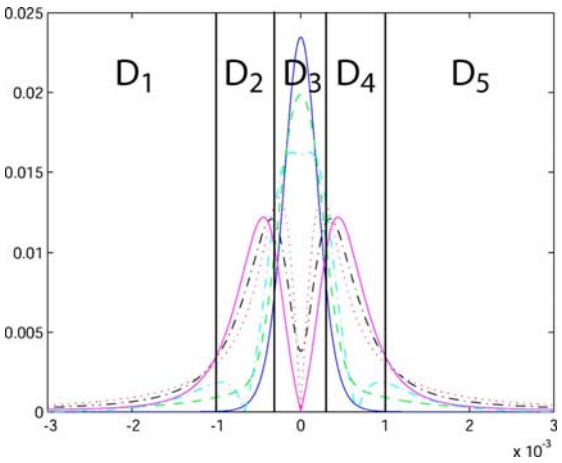

FIG. 8. (Color online) Far field profiles for each bit configuration, and array detector geometry. The 5 detectors $D_1,\ldots,D_5$ have electronic gains $\sigma_1(i),\ldots,\sigma_5,\ldots,(i)$ according to the bit sequence i which is present in the focal spot.

zation, which will be done in a further approach. Gain values are adapted to detect a mean signal equal to zero for each bit configuration present in the focal spot, in order to cancel the common mode classical noise present in the mean field [10]. It means that for each bit sequence i, gains are chosen to satisfy the following relation:

$$\sum_{k=1}^{5} \sigma_k(i) N_k(i) = 0, \tag{2}$$

where $N_k(i)$ is the mean photon number detected on pixel D_k when bit i is present in the focal spot on the disk

$$N_k(i) = \int_{D_k} n_i(x) dx, \tag{3}$$

where $n_i(x)$ is the number of photons incident on the array detector, at position x, when the bit sequence i is present in the focal spot.

As all profiles are symmetrical when the incident beam is centered on a bit, we have set $\sigma_1 = \sigma_5$ and $\sigma_2 = \sigma_4$. In addition, we have chosen $\sigma_3 = -\sigma_1/2$. Using these relations and Eq. (2), we compute gain values adapted to the recognition of each bit sequence. Note that the calculation of each gain configuration requires *a priori* information on the far field profiles, or at least an experimental calibration using a well-known sample.

Now that these gain configurations are set, we can investigate for a bit sequence on the optical disk.

B. Classical results

The expression of the detected signal $S_i(j)$ is given by

$$S_i(j) = \sum_{k=1}^{5} \sigma_k(j) N_k(i), \tag{4}$$

where i refers to the bit sequence effectively present in the focal spot, and j to the gain set adapted to the detection of the bit sequence j. It merely corresponds to the intensity weighted by the electronic gains. Note that for $i=j$—and only in this case if the detector is well chosen—the mean value of the signal $S_i(i)$ is equal to zero, according to Eq. (2). All possible values of $S_i(j)$ are presented for a total number of incident photons $N_{inc}=25$, in Table I where i is read vertically, and corresponds to the bit sequence on the disk, whereas j is read horizontally and refers to the gain set adapted to the detection of bit j. In order not to have redundant information, we have gathered results corresponding to identical far field profiles. A zero value is obtained for only one gain configuration, allowing an identification of the bit sequence present in the focal spot.

The reading process to determine which bit sequence is lit on the disk follows these few steps: the time dependent intensity is first measured on each of the five detectors with all electronic gains set to 1; these intensities are integrated for a time T; the signal is then calculated, using the different gain configurations j; the bit sequence effectively present in the focal spot is determined by the only signal yielding a zero value. Note that the second step just corresponds to the N_k measurements. The integration time T is chosen as the time interval during which the signal leads to the determination of a unique bit sequence. The third step corresponds to the simple calculation of a line in Table I. This can be done in parallel thanks to the speed of data processing on dedicated processors, and the reading rate will thus not be affected compared to current devices. Finally, note that the last step requires a good choice of the parameters in order to be able to distinguish all bit sequences. It means that the noise level has to be smaller than the difference between the two closest values from 0, in order to get a zero mean value for only one bit sequence. Indeed, there must be no overlap between the expectation values when we take into account the noise and thus the uncertainty relative to each measurement. Note that using the zero value as the discriminating factor could be combined with the use of all the calculated values, as each line of Table I is distinct. We just need to know how to weight each data point according to the noise related to its obtention.

TABLE I. Detected signals $S_i(j)$ where i is read vertically and corresponds to the bit sequence on the disk, whereas j is read horizontally and refers to the gain set adapted to the detection of bit j. A zero value means that the tested gain configuration is adapted to the bit sequence.

	000	001/100	010	011/110	101	111
000	0	−34	−204	−254	−77	−303
001/100	15	0	−76	−99	−19	−121
010	23	20	0	−6	16	−13
011/110	24	22	5	0	19	−5
101	19	11	−36	−50	0	−63
111	24	23	9	5	20	0

V. NOISE CALCULATION

A. The shot noise limit

To include the noise in our calculation, we separate classical and quantum noise contributions. The classical noise comprises residual noise of the laser diode, mechanical, and thermal vibrations. The major part of this noise is directly proportional to the signal, i.e., to the number of detected photons. For a detection of the total number of photons N_{inc} in the whole beam during the integration time of the detector, the classical noise contribution $\sqrt{\langle \delta N_{inc}^2 \rangle}$ would thus be written as

$$\sqrt{\langle \delta N_{inc}^2 \rangle} = \beta N_{inc}, \tag{5}$$

where β is a constant factor. And the individual noise variable $\delta N_i(k)$ arising from detection on pixel D_k is given by

$$\delta N_i(k) = \frac{N_i(k)}{N_{inc}} \delta N_{inc}. \tag{6}$$

Using Eqs. (4)–(6) a simple calculation yields the variance of the signal arising from the classical noise

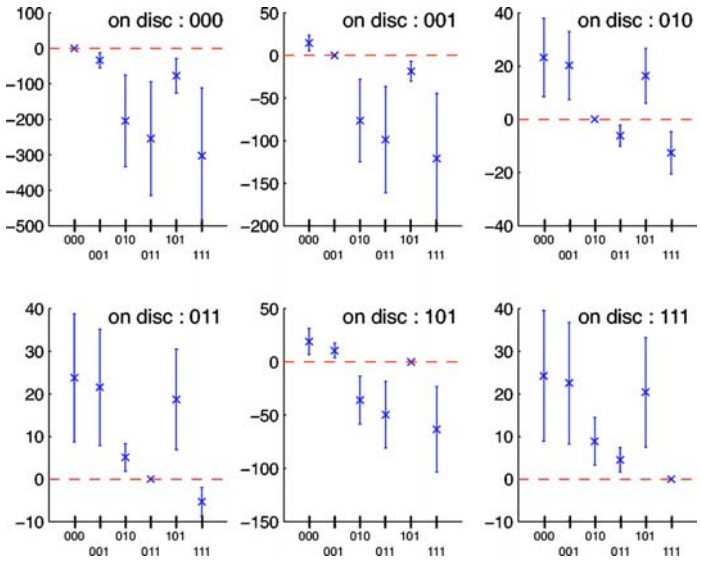

FIG. 9. (Color online) Classical noise (10 dB of excess noise) represented as error bars, for $\lambda = 0.78\ \mu$m, NA=0.47, and 25 detected photons. Each inset corresponds to the 6 signals obtained for the different gain configurations, when one particular bit sequence is present in the focal spot. Each bit sequence present in the focal spot can be clearly identified as only one gain configuration can give a zero value for each inset.

$$\langle \delta \hat{S}_i^2(j) \rangle_{Cl} = \frac{BS_i^2(j)}{N_{inc}}, \tag{7}$$

where the constant $B = N_{inc}\beta^2$ is the classical noise factor, and is chosen so that, when $B=1$ and when all the intensity is detected by one detector, the classical noise term is equal to the shot noise term. Note that classical noise does not deteriorate measurements having a zero mean value. For this reason, we have chosen to discriminate bit sequences by choosing gains such as $S_i(i)=0$, as mentioned earlier.

The calculation of the quantum contribution requires the use of quantum field operators, describing the quantum fluctuations in all transverse modes of the field. By changing the gain configuration of the array detector, not only the signal $S_i(j)$ is modified, but also the related quantum noise denoted $\langle \delta \hat{S}_i^2(j) \rangle_{Qu}$, as different gain configurations are sensitive to noise in different modes of the field. We have shown in Ref. [10] that for a multipixel detection of an optical image, the measurement noise arises from only one mode component of the field, referred to as the *detection mode*, or *noise mode* [31,32]. The expression of the quantum noise is then

$$\langle \delta \hat{S}_i^2(j) \rangle_{Qu} = f_{i,j}^2 N_{inc} \langle \delta \hat{X}_{w_{i,j}}^2 \rangle, \tag{8}$$

where $\delta \hat{X}_{w_{i,j}}$ is the quantum noise contribution of the noise-mode $w_{i,j}(x)$ which is defined for one set of gain j, when the bit sequence i is present in the focal spot, as

$$w_{i,j}(x) = \frac{\sigma_k(j) n_i(x)}{f_{i,j}}, \quad \forall\, x \in D_k \tag{9}$$

and where $f_{i,j}$ is a normalization factor, which expression is

$$f_{i,j}^2 = \frac{\sum_{k=1}^{5} \sigma_k^2(j) N_k(i) dx}{N_{inc}}. \tag{10}$$

The noise mode corresponds in fact to the incident field profile weighted by the gains. The shot noise level corresponds to $\langle \delta \hat{X}_{w_{i,j}}^2 \rangle = 1$.

The variance of the signal can eventually be written as

$$\langle \delta \hat{S}_i^2(j) \rangle = f_{i,j}^2 N_{inc} \langle \delta \hat{X}_{w_{i,j}}^2 \rangle + \frac{BS_i^2(j)}{N_{inc}}. \tag{11}$$

We have first represented the classical noise with an excess noise of 10 dB, as error bars for each result $S_i(j)$, in Fig. 9. We have chosen a representation with a number of detected photons of only 25. Each of the six insets refers to the measurement obtained for a particular bit sequence in the focal spot. The six data points and associated error bars refer to the results obtained when the six gain configurations are tested. One inset thus corresponds to one line in Table I. We can see that with this choice of parameters, the bit sequence effectively present in the focal spot can be determined without ambiguity by the only zero value. The sequence corresponds to the one for which the gains were optimized. We see that the bit sequence discrimination can be achieved even with a very low number of photons. The relative immunity to classical noise of our scheme arises from the fact that measurements are performed around a zero mean value. Thus, given this limit in the minimum necessary photon number and the flux of photons one can calculate the maximum data rate, which is found to be 2×10^7 Mbits/s (this estimation takes into account an integration time T corresponding to $\frac{1}{10}$ of the delay between the readout process of two adjacent bits with a 1 mW laser). This very high value shows that classical noise should not be a limit for data rates in such a scheme.

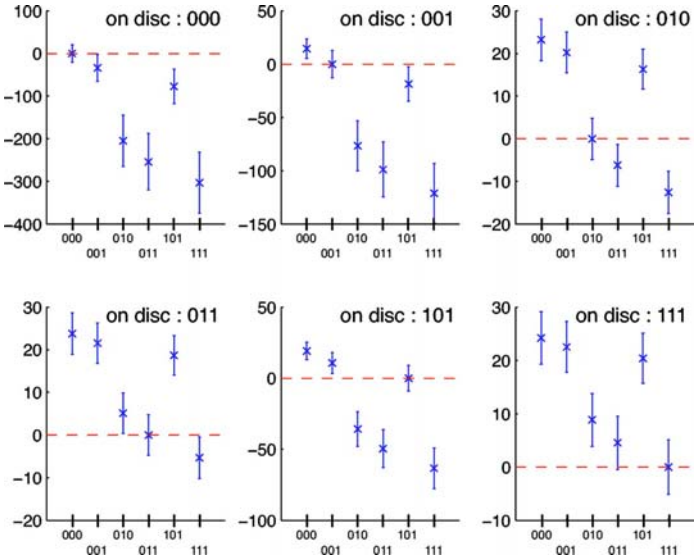

FIG. 10. (Color online) Shot noise represented as error bars, for $\lambda=0.78\ \mu$m, NA $=0.47,25$ detected photons. Some bit sequences cannot be determined without ambiguity because of the noise level.

The effect of quantum noise is very small, but becomes a limiting factor for such a small number of detected photons, or for a large number of bits encoded on the disk in the wavelength size. In order to see independently the effect of each contribution to the noise, we have thus represented in Fig. 10 the shot noise also for 25 detected photons, appearing as the threshold under which it is impossible to distinguish bit sequences because of the quantum noise. Note that for the represented case, the shot noise is the most important contribution, and that it prevents a bit sequence discrimination, as a zero value for the signal can be obtained for several gain configurations in the same inset.

B. Beyond the shot noise limit

When the shot noise is the limiting factor, nonclassical light can be used to perform measurements beyond the quantum noise limit. We have shown in Ref. [10] that squeezing the noise mode of the incident field was a necessary and sufficient condition to a perfect measurement. What we are interested in is improving the measurements that yield a zero value, which are obtained when the gain configuration matches the bit sequence in the focal spot, as $S_i(i)=0$. Using Eq. (11), we see that $w_{i,i}$ has to be squeezed. As no information on the bit present in the focal spot is available before the measurement, in order to improve simultaneously all the bit sequence detections, the six noise modes have to be squeezed at the same time in the incident field. These six transverse modes are not necessarily orthogonal, but one can show that squeezing the subspace that can generate all of them is enough to induce the same amount of squeezing.

The quantum noise with 10 dB of squeezing on the subspace generated by the $w_{i,i}$ is represented as error bars in Fig.

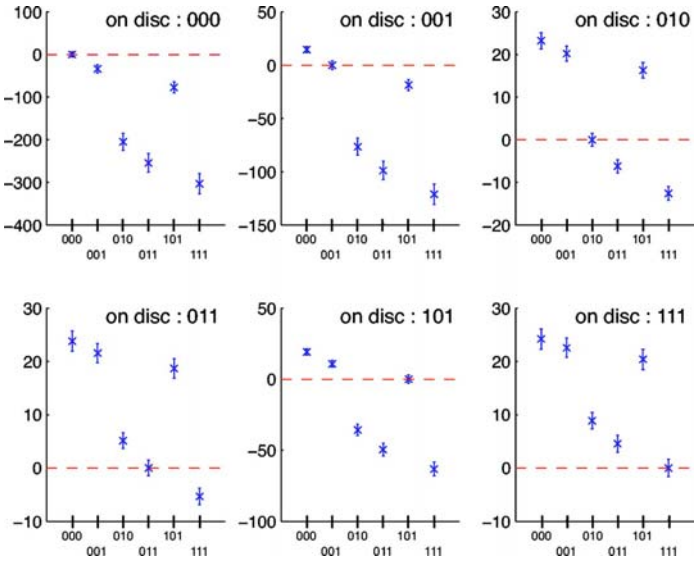

FIG. 11. (Color online) Quantum detection noise represented as error bars, for $\lambda=0.78\ \mu$m, NA$=0.47,25$ detected photons and -10 dB of simultaneous squeezing for all the flipped modes. The ambiguity in the presence of shot noise has been removed and each bit sequence can be identified.

11. The noise of each noise-mode $w_{i,j}$ is computed using its overlap integrals with the generator modes of the squeezed subspace, assuming that all modes orthogonal to the squeezed subspace are filled with coherent noise. In this case, the effect of squeezing, reducing the quantum noise on the measurements, and especially on the measurement for which the gains have been optimized, is enough to discriminate bit sequences that were masked by quantum noise.

VI. CONCLUSION

We have proposed a way of information extraction from optical disks, based on a multipixel detection. We have first demonstrated, using only classical resources, that this detection could allow large data storage capacity, by burning several bits in the spot size of the reading laser. We have presented a proof of principle through a simple example which will be refined in further studies. We have also shown that in shot noise limited measurements, using squeezed light in appropriate modes of the incident laser beam can lead to improvement in bit sequence discrimination.

The next steps are to study in detail how to extract the redundant information when the disk is spinning, and to systematically optimize the number of bits in the focal spot, the number and size of pixels in the array detector. Such a regime involving a large number of bits in the focal spot will ultimately be limited by the shot noise, and will require the quantum noise calculations presented in this paper.

ACKNOWLEDGMENTS

We thank Magnus Hsu, Ping Koy Lam and Hans Bachor for fruitful discussions. Laboratoire Kastler Brossel, of the Ecole Normale Superieure and University Pierre et Marie Curie, is associated to CNRS. This work has been supported by the European Union in the frame of the QUANTIM network (Contract No. IST 2000-26019).

[1] H. A. Bethe, Phys. Rev. **7**, 66 (1944); **8**, 163 (1944).
[2] D. S. Marx and P. Psaltis, J. Opt. Soc. Am. A **14**, 1268 (1997).
[3] D. S. Marx and P. Psaltis, Appl. Opt. **36**, 6434 (1997).
[4] X. Wang, J. Mason, M. Latta, T. C. Strand, D. S. Marx, and P. Psaltis, J. Opt. Soc. Am. A **18**, 565 (2001).
[5] W.-C. Liu and M. W. Kowarz, Appl. Opt. **38**, 3787 (1999).
[6] J. M. Brok and H. P. Urbach, J. Opt. Soc. Am. A **20**, 256 (2003).
[7] I. Sokolov and M. Kolobov, Opt. Lett. **29**, 703 (2004).
[8] M. T. L. Hsu, W. P. Bowen, V. Delaubert, C. Fabre, H.-A. Bachor, and P. K. Lam (unpublished).
[9] P. Török (unpublished).
[10] N. Treps, V. Delaubert, A. Maître, J. M. Courty, and C. Fabre, Phys. Rev. A **71**, 013820 (2005).
[11] A. G. van Nie, Philips Res. Rep. **19**, 378 (1964); **19**, 394 (1964).
[12] M. Lax, W. H. Louisell, and W. B. McKnight, Phys. Rev. A **11**, 1365 (1975).
[13] S. R. Seshadri, J. Opt. Soc. Am. A **19**, 2134 (2002), and references therein.
[14] A. Ciattoni, B. Crosignani, and P. Di Porto, Opt. Commun. **177**, 9 (2000).
[15] Q. Cao and X. Deng, J. Opt. Soc. Am. A **15**, 1144 (1998).
[16] B. T. Landesman and H. H. Barrett, J. Opt. Soc. Am. A **5**, 1610 (1988).
[17] G. Rodriguez-Morales and S. Chavez-Cerda, Opt. Lett. **5**, 430 (2004).
[18] Z. Ulanowski and I. K. Ludlow, Opt. Lett. **25**, 1792 (2000).
[19] T. A. Nieminen, H. Rubinsztein-Dunlop, and N. R. Heckenberg (unpublished).
[20] B. Richards and E. Wolf, Proc. R. Soc. London, Ser. A **253**, 359 (1959).
[21] S. Quabis, R. Dorn, M. Eberler, O. Glöckl, and G. Leuchs, Appl. Phys. B **72**, 109 (2001).
[22] L. Novotny, R. D. Grober, and K. Karrai, Opt. Lett. **26**, 789 (2001).
[23] R. Dorn, S. Quabis, and G. Leuchs, Phys. Rev. Lett. **91**, 233901 (2003).
[24] S. Quabis, R. Dorn, M. Eberler, O. Glöckl, and G. Leuchs, Opt. Commun. **179**, 1 (2000).
[25] C. J. R. Sheppard, J. Opt. Soc. Am. A **18**, 1579 (2001).
[26] P. Török, P. Varga, Z. Laczik, and G. R. Booker, J. Opt. Soc. Am. A **12**, 325 (1995).
[27] K. S. Youngworth and T. G. Brown, Opt. Express **7**, 77 (2000).
[28] Q. Zhan and J. R. Leger, Opt. Express **10**, 324 (2002).
[29] A. E. Siegman, *Lasers* (University Science, Mill Valley, CA, 1986).
[30] M. Born and E. Wolf, *Principle of Optics* (Cambridge University Press, 1959).
[31] V. Delaubert, N. Treps, C. C. Harb, P. K. Lam, and H.-A. Bachor e-print arxiv/ quant-ph/0512151
[32] N. Treps, N. Grosse, W. P. Bowen, M. T. L. Hsu, A. Maître, C. Fabre, H.-A. Bachor, and P. K. Lam, J. Opt. B: Quantum Semiclassical Opt. **6**, S664 (2004).

Le tout multimode : les cavités dégénérées

Article 16, reproduit en page 144

Image transmission through a stable paraxial cavity

S. Gigan, L. Lopez, N. Treps, A. Maître, and C. Fabre
Phys. Rev. A **72** 023804 (2005)

Abstract : We study the transmission of a monochromatic "image" through a paraxial cavity. Using the formalism of self-transform functions, we show that a transverse degenerate cavity transmits the self-transform part of the image, with respect to the field transformation over one round-trip of the cavity. This formalism gives insight into the understanding of the behavior of a transverse degenerate cavity, complementary to the transverse mode picture. An experiment of image transmission through a hemiconfocal cavity shows the interest of this approach.

Article 17, reproduit en page 154

Experimental study of the spatial distribution of quantum correlations in a confocal optical parametric oscillator

M. Martinelli, N.Treps, S. Ducci, S. Gigan, A. Maître et C. Fabre
Phys. Rev. A 67, 023808 (2003)

Abstract : We study experimentally the spatial distribution of quantum noise in the twin beams produced by a type-II optical parametric oscillator operating in a confocal cavity above threshold. The measured intensity correlations are at the same time below the standard quantum limit and not uniformly distributed inside the beams. We show that this feature is an unambiguous evidence for the multimode and nonclassical character of the quantum state generated by the device.

Article 18, reproduit en page 163

Multimode squeezing properties of a confocal optical parametric oscillator : Beyond the thin-crystal approximation

L. Lopez, S. Gigan, N. Treps, A. Maître, C. Fabre, and A. Gatti
Phys. Rev. A 72, 013806 (2005)

Abstract : Up to now, transverse quantum effects usually labeled as "quantum imaging" effects which are generated by nonlinear devices inserted in resonant optical cavities have been calculated using the "thin-crystal approximation," i.e., taking into account the effect of diffraction only inside the empty part of the cavity, and neglecting its effect in the nonlinear propagation inside the nonlinear crystal. We introduce in the present paper a theoretical method which is not restricted by this approximation. It allows us in particular to treat configurations closer to the actual experimental ones, where the crystal length is comparable to the Rayleigh length of the

cavity mode. We use this method in the case of the confocal optical parametric oscillator, where the thin-crystal approximation predicts perfect squeezing on any area of the transverse plane, whatever its size and shape. We find that there exists in this case a "coherence length" which gives the minimum size of a detector on which perfect squeezing can be observed, and which gives therefore a limit to the improvement of optical resolution that can be obtained using such devices.

Article 19, reproduit en page 173

Noiseless Optical Amplification of Images using transverse degenerate OPOs

L. Lopez, N. Treps, C. Fabre and A. Maître

En préparation

Abstract :

PHYSICAL REVIEW A **72**, 023804 (2005)

Image transmission through a stable paraxial cavity

Sylvain Gigan,* Laurent Lopez, Nicolas Treps, Agnès Maître, and Claude Fabre
Laboratoire Kastler-Brossel, Université Pierre et Marie Curie, Case 74, 75252 Paris cedex 05, France
(Received 25 February 2005; published 5 August 2005)

We study the transmission of a monochromatic "image" through a paraxial cavity. Using the formalism of self-transform functions, we show that a transverse degenerate cavity transmits the self-transform part of the image, with respect to the field transformation over one round-trip of the cavity. This formalism gives insight into the understanding of the behavior of a transverse degenerate cavity, complementary to the transverse mode picture. An experiment of image transmission through a hemiconfocal cavity shows the interest of this approach.

DOI: 10.1103/PhysRevA.72.023804 PACS number(s): 42.60.Da, 42.30.Va, 42.30.Lr

I. INTRODUCTION

Image transmission and propagation in a paraxial system, using optical devices such as lenses and mirrors, is a well known and extensively studied problem [1]. The free propagation of a field changes its transverse distribution, but in some planes such as conjugate planes or Fourier planes, one gets simple transformations of the image. On the other hand, transmission through a cavity has a drastic effect on the transverse distribution of the field, as one must take into account the transverse characteristics and the resonances of the cavities. Optical cavities have also been studied extensively for a long time, starting with the Fabry-Perot resonator, then to the laser [2], and they are commonly used as temporal frequency filters. Less known are their spatial frequency filter properties. An optical cavity is associated with an eigenmode basis—i.e., a family of modes (like TEM_{pq} Hermite Gaussian modes) which superimpose onto themselves after a round-trip inside the cavity. This basis depends on the geometrical characteristics of the cavity (length, curvature of the mirrors, etc.). Only eigenmodes can be transmitted through the cavity at resonance, and the cavity acts both as a spatial filter and frequency filter. This mode selection property of cavities, which does not exist in free propagation, is well known in the longitudinal domain for frequency filtering. However, the general transverse effect of a cavity on an image has, to the authors' knowledge, never been carefully investigated. Whereas the transmission of an image through a cavity which is only resonant for one transverse mode is well known to be completely destructive for this image, some particular cavities called transverse degenerate cavities can partially transmit an image in a way that we will present in the present paper.

We will show that it is possible to model the effect of any cavity on an image by a general operator, which acts as a nonunitary transformation on the field. This formalism appears to be very general and of broad interest not only in optics [3] but in physics in general [4]. Indeed, we will show how it is possible to produce specific states such as a self-Fourier transform state of a physical system.

This work is part of a more general study of quantum effects in optical images [5,6] and more precisely of noiseless parametric image amplification [7,8], performed in the continuous-wave regime. In order to have a significant parametric gain with a low-power laser, we need resonant optical cavities, operating in the regenerative amplifier regime, below, but close to, the oscillation threshold [9]. As a first step, we therefore need to precisely assess the imaging properties of an empty optical cavity. This study turns out to be interesting in itself and might also be useful for other experiments.

We begin this paper by recalling in Sec. II some useful features of paraxial propagation of an image and of degenerate cavities. Following some pioneering work [10,11], we develop in Sec. III a formalism to understand the transmission of an image through a paraxial cavity and link it to the formalism of cyclic transforms. In Sec. IV, we show simulations and experimental results of image transmission through a simple degenerate cavity: the hemiconfocal cavity.

II. *ABCD* CAVITY ROUND-TRIP MATRIX TRANSFORMS

All the theory developed in this paper will be performed within the paraxial approximation. We consider a monochromatic electromagnetic field $E(\vec{r},t)$ at frequency ω, linearly polarized along a vector $\vec{u}$ and propagating along a direction z of space. The position in the transverse plane will be represented by the vector $\vec{r}=x\vec{i}+y\vec{j}$. The electric field is supposed stationary and can be written in a given transverse plane as

$$\vec{E}(\vec{r},t) = \mathrm{Re}[E(\vec{r})e^{-i\omega t}\vec{u}], \tag{1}$$

where $\vec{u}$ is the polarization unit vector. The local intensity in this plane is then

$$I(\vec{r}) = \frac{1}{2}\epsilon_0 c E(\vec{r})E^*(\vec{r}). \tag{2}$$

The input image considered all along this paper is defined by a given transverse repartition of the complex transverse field $E_{in}(\vec{r})$ in an input plane z_{in}. We suppose that its extension is finite around the optical axis and that its transverse variations are such that this image propagates within the

*Electronic address: gigan@spectro.jussieu.fr

paraxial approximation. We will consider both intensity images and "field" images—i.e., not only the transverse intensity distribution of the field, but also the amplitude distribution itself.

A. Image propagation in a paraxial system

The field $E(\vec{r})$ is propagating through an optical system along the z axis. An input-output relation of the form can be written

$$E_{out}(\vec{r}) = \mathcal{T}[E_{in}(\vec{r})], \tag{3}$$

where $E_{in}(\vec{r})$ and $E_{in}(\vec{r})$ are the fields just before and just after the optical system and $\mathcal{T}$ is the transformation of the field associated with the optical system. If the system is only a linear paraxial system (made of lenses or curved mirrors, but without diaphragms), the propagation properties of the system are described by its Gauss matrix T (often called $ABCD$ matrix) which is written

$$T = \begin{pmatrix} A & B \\ C & D \end{pmatrix}. \tag{4}$$

All the properties of the system can be inferred from the values of the coefficients A, B, C, and D and of the total optical length L of the system (responsible for a phase factor which is not included in the $ABCD$ coefficients). We will assume that the index of refraction is the same at the input and output of the system. As a consequence, we have $\det(T)=AD-BC=1$. In particular, the transformation $\mathcal{T}$ of the field can be derived from the Huygens-Fresnel equation in free space in the case $B \neq 0$ [2]:

$$\begin{aligned} \mathcal{T}:E(\vec{r}_1) \rightarrow E(\vec{r}_2) \\ = -e^{ikL}\frac{i}{B\lambda}\int\int d^2\vec{r}_1 E(\vec{r}_1) \\ \times \exp\left[-i\frac{\pi}{B\lambda}(A\vec{r}_1^2 - 2\vec{r}_1\vec{r}_2 + D\vec{r}_2^2)\right]. \end{aligned} \tag{5}$$

If $B=0$, the Gauss matrix can be written

$$T = \begin{pmatrix} M & 0 \\ C & \dfrac{1}{M} \end{pmatrix}.$$

In this case the field in the output plane is given by

$$\mathcal{T}:E(\vec{r}_1) \rightarrow E(\vec{r}_2) = -e^{ikL}ME(M\vec{r}_1)e^{ikCM\vec{r}_2^2/2}. \tag{6}$$

In terms of imaging, a conjugate plane corresponds to a transformation for which one retrieves the input image within a magnification factor M. From Eqs. (5) and (6), the following can be inferred.

(i) If $B=0$, one retrieves the intensity image but not the amplitude [there is a phase curvature coming from the term $e^{ikCM\vec{r}_2^2/2}$ of Eq. (6)]. We will call such a transform an "intensity-conjugate transform," (ICT).

(ii) If $B=0$ and $C=0$, one retrieves the amplitude image (and the intensity image of course). We will call such a transform an "amplitude-conjugate transform" (ACT). This transform is sometimes also called a near-field (NF) transform.

Another interesting transformation is the one for which one obtains the spatial Fourier transform of the image. Still from Eqs. (5) and (6), one sees the following.

(i) If $A=0$, one obtains the Fourier transform for the field, within a curvature phase term corresponding to the factor $e^{-i\pi D\vec{r}_2^2/B\lambda}$ of Eq. (5). This factor does not affect the intensity distribution. We will call this transformation a "intensity Fourier transform" (IFT).

(ii) If $A=0$ and $D=0$, one obtains a perfect spatial Fourier transform for the amplitude field. We will call this transformation an "amplitude Fourier transform" (AFT). It is sometimes called a far-field (FF) transform.

It is straightforward to see that a $2f$-$2f$ system (a lens of focal distance f placed in between two free propagation of length $2f$) performs an ICT and that a f-f system performs an AFT. A simple implementation of an ACT would be a system of two lenses of focal distance f separated by a distance $2f$, preceded and followed by a distance f (i.e., two successive f-f systems). When designing an optical system, is it important to note that if one combines intensity transformations (or any combination of amplitude and intensity transformation), the final result is in general not anymore a simple transformation of the field (even its intensity profile) due to the phase factors. Whereas successive iterations of the AFT and ACT perform AFT or ACT, this is not the case for the IFT and ICT.

Let us recall a few obvious facts, which will be nonetheless useful to understand the rest of the discussion. Two length scales have to be considered for the optical system length L: the "rough length," important to understand propagation (diffraction) effects, and the "exact length," which must be known on the scale of λ, necessary to determine the exact phase of the field.

B. Transverse degeneracy of a resonator

For simplicity purposes, all our discussion about cavities will be restricted to the case of linear optical cavities with two spherical mirrors. Its extension of the discussion to more complex cases (ring cavity, cylindrical mirrors, etc.) is straightforward. We also assume that the transverse extension of the field is not limited by the size of the mirrors. In this simple case the cavity is fully described by its round-trip Gauss matrix T_{cav}, starting from a given reference plane.

We consider here only geometrically stable cavities ($|A+D|<2$). In this case, the eigenmodes of the device are the Hermite-Gauss (HG) modes adapted to the cavity, i.e., having a wave front coinciding with the mirror surfaces. The normalized transverse electric field in the TEM_{mn}-mode basis is given by

$$\begin{aligned} A_{mn}(\vec{r},z) = C_{mn}\frac{1}{w(z)}H_m\left(\frac{\sqrt{2}x}{w(z)}\right) \\ \times H_n\left(\frac{\sqrt{2}y}{w(z)}\right)e^{ik[r^2/2q(z)]}e^{-i(n+m+1)\arctan(z/z_R)}e^{ikz}, \end{aligned} \tag{7}$$

where

$$C_{mn} = \frac{1}{\sqrt{\pi 2^{m+n-1} m! n!}},$$

$$z_R = \frac{\pi w_0}{\lambda},$$

$$q(z) = z - i z_R,$$

$$w(z) = w_0 \sqrt{1 + \left(\frac{z}{z_R}\right)^2},$$

$$\Psi(z) = (n + m + 1)\arctan\left(\frac{z}{z_R}\right). \tag{8}$$

w_0 is the waist of the TEM_{00} mode of the cavity taken in its focal plane, of coordinate $z=0$, and q is the complex radius of curvature. It is important to note that q is independent from m and n, and only depends on the position and size of the waist. Finally, $\Psi(z)$, the Gouy phase shift, will play a major role in this discussion.

Let us note the mirror positions z_1 and z_2 and the total length of the cavity, $L=z_2-z_1$. The resonant cavity eigenmodes will be the HG modes A_{mn} having a total round-trip phase shift equal to $2p'\pi$, with p' integer. If the input field has a fixed wavelength λ, this will occur only for a comb of cavity length values $L_{mnp'}$ given by

$$L_{mnp'} = \frac{\lambda}{2}\left(p' + (n + m + 1)\frac{\alpha}{2\pi}\right), \tag{9}$$

where

$$\alpha = 2\left[\arctan\left(\frac{z_2}{z_R}\right) - \arctan\left(\frac{z_1}{z_R}\right)\right] \tag{10}$$

is the Gouy phase shift accumulated by the TEM_{00} mode along one cavity round-trip. It is related to the cavity Gauss matrix T_{cav} eigenvalues μ_{12} by the relation

$$\mu_{1,2} = e^{\pm i\alpha}. \tag{11}$$

This simple relation has been shown in [12] for a linear cavity with two curved mirrors. We give in the Appendix a demonstration of this result valid for any stable paraxial cavity.

A cavity is called "transverse degenerate" when for a given frequency and cavity length, several transverse modes are simultaneously resonant. From Eq. (9), we can see the following.

(i) There is a natural degeneracy for HG modes giving the same value to $s=m+n$, related to the cylindrical symmetry of the device. We will not consider this natural degeneracy any longer and call s the transverse mode order and p the longitudinal mode order.

(ii) The cavity is transverse degenerate when α is a rational fraction of 2π. Let us write $\alpha/2\pi$ as an irreducible fraction

$$\alpha = 2\pi\frac{K}{N}[2\pi], \tag{12}$$

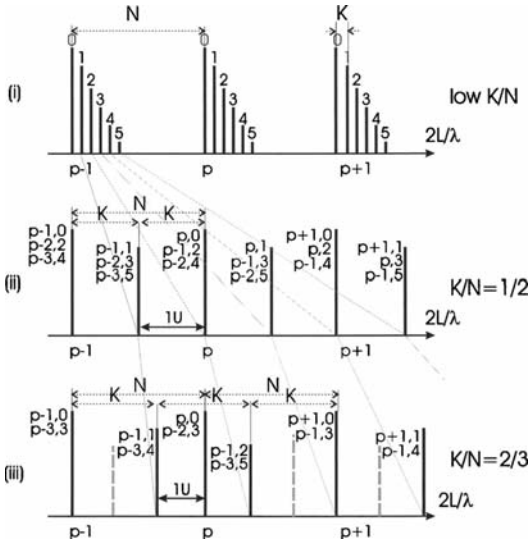

FIG. 1. Partial transverse and longitudinal comb in three configurations. (i) Low K/N cavity, (ii) cavity with $K/N=1/2$, for instance confocal, and (iii) cavity with $K/N=2/3$. K and N are integers. For (ii) and (iii) we indicated besides each peak the first possible modes (p,s). For simplicity, we represented in (iii) the peaks corresponding to other combs on a grey dashed line.

with K, N integers and $0<K/N<1$. K/N is called the *degeneracy order of the cavity* [12].

As the degeneracy order is the remainder part of the total Gouy phase shift over one turn of the cavity, we conclude that there exists an infinite number of cavity configurations with the same degeneracy order. Furthermore, the rational fraction ensemble being dense in $\mathbb{R}$, transverse degenerate cavities compose a dense ensemble among all the possible cavities.

Let us first consider the comb of cavity resonant lengths (see Fig. 1). Rewriting Eq. (9) as

$$L_{sp} = \frac{\lambda}{2N}[Np + K(s + 1)]. \tag{13}$$

where p is an integer. One sees that whereas the free spectral range of the cavity for longitudinal modes (p periodicity) remains equal to the usual value $\lambda/2$, the natural unit to describe the comb is $\lambda/2N$. N and K appear than as the steps, in this natural unit, for the longitudinal comb (when fixing s) and for the transverse comb (when fixing p). Within a free spectral range, there exist N lengths for which the teeth of the comb coincide, allowing us to define N *families* of modes.

Let us now consider the cavity in terms of rays optics. Equation (11) implies that a paraxial cavity with a degeneracy order K/N verifies [12,13]

$$(T_{cav})^N = \begin{pmatrix} A & B \\ C & D \end{pmatrix}^N = \begin{pmatrix} 1 & 0 \\ 0 & 1 \end{pmatrix} = I_2, \tag{14}$$

where I_2 is the identity matrix of size 2×2. This relation

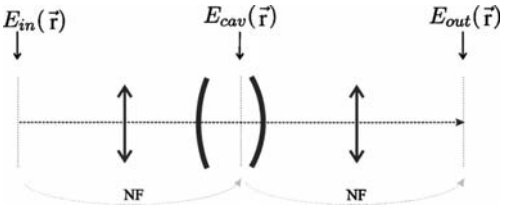

FIG. 2. Scheme of the transmission of an image through a cavity. A real near field (ACT) is performed from the input image to the inside of the cavity—with lenses and the input mirror—and another one is performed from that plane to the imaging system.

means that *any* incoming ray will retrace back onto itself after N round-trips, forming a closed trajectory, or *orbit*. The total phase accumulated on such an orbit is $2K\pi$ [as can be seen in Eq. (11)].

Up to now, only perfect Fabry-Perot resonators have been considered. If one consider a cavity with a given finesse $\mathcal{F} \simeq 2\pi/\gamma$ where γ is the energy loss coefficient over one round-trip, supposed small, then $\mathcal{F}/2\pi$ is the mean number of round-trips of energy in the cavity before it escapes. As a consequence, for a given finesse and a cavity with a degeneracy order of K/N, we have to compare $\mathcal{F}$ to N. If the finesse is low (i.e., $\mathcal{F} \ll N$), then light will escape before retracing its path and the previous discussion is not relevant. In the rest of the discussion we will then stay in the high-finesse limit ($\mathcal{F} \gg N$).

We now have all the tools necessary to study the propagation of a paraxial image in a stable resonant cavity.

III. IMAGE TRANSMISSION THROUGH A PARAXIAL STABLE CAVITY

We will consider for simplicity an impedance-matched cavity, where the input and output mirrors have the same reflectivity and no other losses exist in the cavity, so that at exact resonance a mode is transmitted with an efficiency equal to unity. As shown on Fig. 2, we define the input image as the transverse field configuration $E_{in}(\vec{r})$ at a chosen plane before the cavity. We want to image it on a detection plane after the cavity. After propagation along a first paraxial system corresponding to an ACT of magnification equal to 1, $E_{in}(\vec{r})$ is transformed into its near field at a given reference plane inside the cavity (position z_{ref}). After propagation along a second identical paraxial system, a new near field (output image) is obtained with unity magnification after the cavity on a detection plane [a charge-coupled device (CCD), for instance]. As the three planes are perfectly imaged on each other, we will use the same notation $\vec{r}$ for these three transverse coordinates and we will omit the z coordinate.

Let $a_{m,n}$ be the projection of the image on the mode $A_{m,n}$ of the cavity:

$$a_{m,n} = \int E_{in}(\vec{r}) A^{*}_{m,n}(\vec{r}) d^2\vec{r}. \tag{15}$$

We can write E_{in} as

$$E_{in}(\vec{r}) = \sum_{m,n} a_{m,n} A_{m,n}(\vec{r}). \tag{16}$$

The effect of the cavity on the image can be understood as a complex transmission $t_{m,n}$ on each mode $A_{m,n}$, depending on the length and geometry of the cavity. The output image will then be written as

$$E_{out}(\vec{r}) = \sum_{m,n} t_{m,n} a_{m,n} A_{m,n}(\vec{r}). \tag{17}$$

A. Single-mode cavity

Let us consider a single-mode cavity having a length L chosen so that only the TEM_{00} resonates. The transmission function of the cavity is

$$t_{m,n} = \delta_{m0}\delta_{n0}, \tag{18}$$

and the output image is:

$$E_{out}(\vec{r},t) = \sum_{m,n} t_{m,n} a_{m,n} A_{m,n}(\vec{r}) = a_{0,0} A_{0,0}(\vec{r}). \tag{19}$$

All the transverse information about the input image E_{in} is then lost when passing through the cavity. In such a single-mode cavity, the Gouy phase shift $\alpha/2\pi$ is not a rational fraction, so that whatever N, $T^N_{cav} \neq I_2$. In terms of geometrical optics, this means that no ray (except the ray on the optical axis) ever retraces its path on itself. This is the usual understanding of the effect of a cavity on an image, where the image is completely destroyed.

In general the precise length of the resonator is controlled through a piezoelectric transducer. If the single-mode cavity length is scanned over one free spectral range, every Laguerre-Gauss cavity eigenmode will be transmitted one after the other. The intensity field averaged over time on a CCD will be, at a given transverse position,

$$\langle I_{out}(\vec{r}) \rangle \propto \sum_{m,n} |a_{m,n}|^2 |A_{m,n}(\vec{r})|^2. \tag{20}$$

Each mode is transmitted at a different moment and does not interfere with the others. As a consequence we obtain the sum of the intensity into each TEM_{pq} mode of the image, and not the image since $\Sigma_{m,n}|a_{m,n}|^2|A_{m,n}(\vec{r})|^2 \neq |\Sigma_{m,n} a_{m,n} A_{mn}(\vec{r})|^2$. This means that, even scanned, a single-mode cavity does not transmit correctly an image.

B. Planar cavity

It is important to study the planar cavity, since it is both widely used experimentally and often taken as a model cavity in theoretical works. Let us consider a planar cavity of length L. The Gauss matrix is

$$\begin{pmatrix} A & B \\ C & D \end{pmatrix} = \begin{pmatrix} 1 & 2L \\ 0 & 1 \end{pmatrix}. \tag{21}$$

It does not fulfill condition (14) for any N value and is therefore not degenerate. Strictly speaking, the planar cavity is not a paraxial cavity, even for rays making a small angle β with

the cavity axis, which escape from the axis after a great number of reflections. As a consequence, there is no Gaussian basis adapted to this cavity. The planar cavity eigenmodes are the tilted plane waves $e^{ik(\beta_1 x+\beta_2 y)}$, which are *not degenerate* since they resonate for different lengths: $L=p\lambda/2(1+\beta_1^2/2+\beta_2^2/2)$. For a given length the cavity selects a cone of plane waves with a given value of $\beta_1^2+\beta_2^2$. The planar cavity is therefore *not* an imaging cavity. However, given a detail size, if the finesse is low enough and the cavity short enough for the diffraction to be negligible, then the image can be roughly transmitted. This study is again outside the scope of this paper.

C. Totally degenerate cavity

Let us now consider a completely degenerate paraxial cavity, in which all the transverse modes are resonant for the same cavity length. As a consequence the transmission function of this cavity brought to resonance is

$$t_{m,n}=1 \tag{22}$$

and the output field will be

$$E_{out}(\vec{r})=\sum_{m,n} t_{m,n}a_{m,n}A_{m,n}(\vec{r})=E_{in}(\vec{r}). \tag{23}$$

Its Gauss matrix is $T_{cav}=I_2$; its degeneracy order is 1: *every* input ray will retrace its path after a single round-trip. A completely degenerate cavity can be called self-imaging. Examples of self imaging cavities have been described in [13].

D. Cavity of degeneracy order K/N

Let us now study the propagation of an image through a transverse degenerate cavity with degeneracy order K/N. We will use a formalism of self-transform function, which we introduce in the next subsection.

1. Cyclic transforms

Some functions are there own Fourier transform. They verify

$$\tilde{f}(u)=f(u), \tag{24}$$

where the Fourier transform $\tilde{f}$ is defined by

$$\tilde{f}(u)=\int_{-\infty}^{+\infty} f(x)e^{2\pi iux}dx. \tag{25}$$

Two well-known examples are the Gaussian functions $f(x)=\alpha e^{-\pi x^2}$ and the infinite Dirac comb $f(x)=\Sigma_n \delta(x-n)$. These functions are called self-Fourier functions (SFF's). Caola [14] showed that for any function $g(x)$, then f, defined as

$$f(x)=g(x)+g(-x)+\tilde{g}(x)+\tilde{g}(-x), \tag{26}$$

is a SFF. Lohmann and Mendlovic [15] showed later that this construction method for a SFF [Eq. (26)] is not only sufficient but necessary. Any SFF $f(x)$ can be generated through Eq. (26) from another function $g(x)$. Lipson [4] remarked that such distributions should exist in the middle of a confocal resonator. Lohmann and Mendlovic [3] also studied how such states could be used to enhance the resolution in imaging.

It is straightforward to generalize this approach to an N-cyclic transform. A transform $\mathcal{T}_C$ is said to be N-cyclic if applied N times to *any* function F one gets the initial function

$$\mathcal{T}_C^N[F(x)]=F(x).$$

Let $\mathcal{T}$ be any transform. A function F_S will be a self-transform function of $\mathcal{T}$ if

$$\mathcal{T}[F_S(x)]=F_S(x).$$

Given $\mathcal{T}_C$ an N-cyclic transform and $g(x)$ a function, it has been shown in [15] that $F_S(x)$, defined as

$$F_S(x)=g(x)+\mathcal{T}_C[g(x)]+\mathcal{T}_C^2[g(x)]+\cdots+\mathcal{T}_C^{N-1}[g(x)], \tag{27}$$

is a self-transform function of $\mathcal{T}_C$ and that any self-transform function F_S of $\mathcal{T}_C$ can be generated in this manner (take $g=F_S/N$, for instance). The Fourier transform is 4-cyclic. Other cyclic transforms and associated self-transform functions are studied in [4,16,17].

We will show here that degenerate cavities produce such self-transform functions from an input image through a transformation similar to Eq. (27).

2. Image propagation through a K/N degenerate cavity

Let us consider a resonator cavity with order of degeneracy K/N. Let γ be the (low) intensity losses over one round trip on the mirrors. For an impedance-matched cavity without internal losses, the losses are identical in the two mirrors, meaning that the amplitude transmission of one mirror is $t=\sqrt{\gamma/2}$. For a cavity at resonance, we have

$$\mathcal{T}_{cav}^N[E_{in}(\vec{r})]=E_{in}(\vec{r}), \tag{28}$$

since after N turns the field comes back onto itself. It means we can view $\mathcal{T}_{cav}$ as a N-cyclic transform on the intensity.

The output field at resonance will be

$$E_{out}(\vec{r})=t^2\sum_{n=0}^{\infty}[(1-t^2)\mathcal{T}_{cav}]^n E_{in}(\vec{r}), \tag{29}$$

the factor $(1-t^2)$ taking into account the double reflection of the field at each round-trip. Using the fact that $\mathcal{T}_{cav}^N[E_{in}(\vec{r})]=E_{in}(\vec{r})$, we can finally rewrite the output field as

$$E_{out}(\vec{r})=\frac{t^2}{1-(1-t^2)^N}\sum_{n=0}^{N-1}(1-t^2)^n\mathcal{T}_{cav}^n[E_{in}(\vec{r})]. \tag{30}$$

In the high-finesse limit ($\mathcal{F}\gg N$) $(1-t^2)^n\simeq 1-nt^2\simeq 1$ for $n\leqslant N$, so that

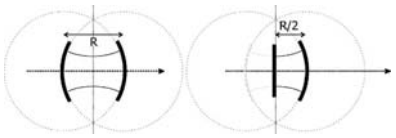

FIG. 3. The confocal cavity (left) has a symmetry plane. Placing a plane mirror in this plane gives us the hemiconfocal cavity (right).

$$E_{out}(\vec{r}) \simeq \frac{1}{N}\sum_{n=0}^{N-1} \mathcal{T}_{cav}^{n}[E_{in}(\vec{r})]. \tag{31}$$

The output image is thus the self-transform field for N-cyclic transform $\mathcal{T}_{cav}$, constructed from the input image through the method of Eq. (27).

Let us finally note that most of this discussion can be extended to more complex cavities, provided $\mathcal{T}_{cav}$ is a cyclic transform and that the present formalism holds for single-mode or totally degenerate cavities: in the former case it means that a self-transform function for a noncyclic transform is just a cavity mode; in the latter case the transform is just the identity, and of course any field is a self-transform for identity.

IV. HEMICONFOCAL CAVITY

We will now illustrate this formalism by considering in more detail a particular cavity, the hemiconfocal cavity, which is made of a plane mirror and a curved mirror R of radius of curvature R separated by a distance $L=R/2$ (see Fig. 3), which has already been studied in terms of beam trajectories [18]. We have studied this kind of cavity both theoretically and experimentally in the framework of our experimental investigations of the cw amplification of images in a cavity [19].

A. Theoretical study

It is straightforward to show that the round-trip Gouy phase shift α is equal to $\pi/2$ for a hemiconfocal cavity, so that its degeneracy order is 1/4: there are four distinct families of transverse modes, depending on the value $p+q$ modulo 4. The round-trip Gauss matrix, starting from the plane mirror, is

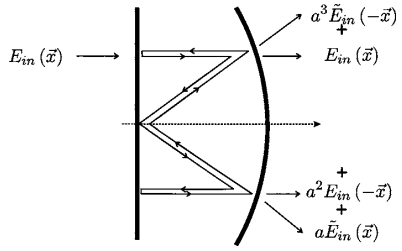

FIG. 4. Ray trajectory picture in the hemiconfocal cavity.

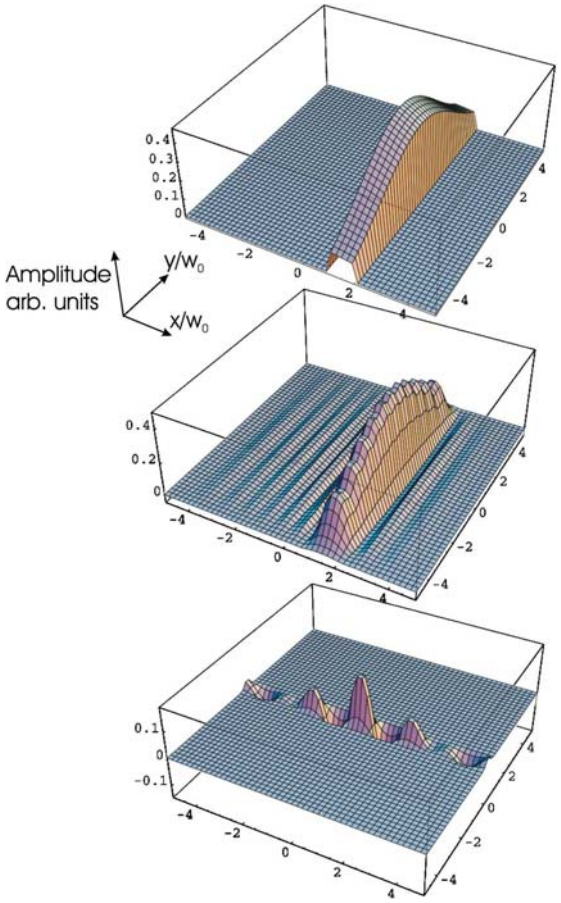

FIG. 5. (Color online) Input image: infinite slit intercepting a large Gaussian mode (top), projection on the first 400 modes of the cavity (middle), and spatial Fourier transform (bottom). The transverse unit is scaled to the waist w_0 of the cavity.

$$T_{cav} = \begin{pmatrix} 0 & \frac{R}{2} \\ -\frac{2}{R} & 0 \end{pmatrix}, \tag{32}$$

so that

$$T_{cav}^{2} = \begin{pmatrix} -1 & 0 \\ 0 & -1 \end{pmatrix}, \quad T_{cav}^{4} = \begin{pmatrix} 1 & 0 \\ 0 & 1 \end{pmatrix}. \tag{33}$$

So two round-trips give the opposite of the identity (symmetry with respect to the cavity axis), which is the Gauss matrix of the confocal cavity, and four round-trips give the identity, as expected for a cavity with degeneracy order 1/4.

T_{cav} is the transformation of an f-f system and is an exact AFT transform:

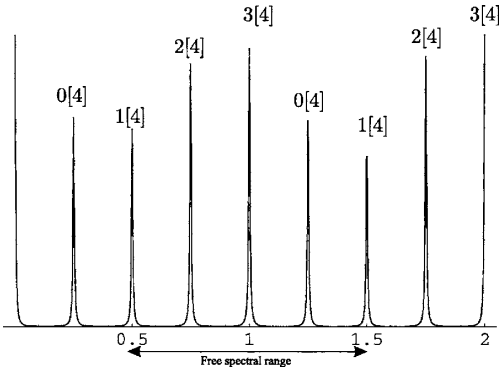

FIG. 6. Simulation of the transmissions peaks of the cavity for the slit of Fig. 9, for a finesse $\mathcal{F}=500$.

$$\mathcal{T}_{cav}:E(\vec{r}_1)\rightarrow -e^{ikL}\frac{2i}{R\lambda}\int\int \mathrm{d}^2\vec{r}_1 E(\vec{r}_1)\exp\left[-i\frac{4\pi}{\lambda R}\vec{r}_1\vec{r}_2\right]. \tag{34}$$

It is equal to the two-dimensional (2D) spatial Fourier transform of the form

$$\tilde{u}(\vec{y})=\frac{2}{\lambda R}\int u(\vec{r})e^{-i(4\pi/\lambda R)\vec{y}\vec{r}}d^2\vec{r} \tag{35}$$

multiplied by a phase factor $a=ie^{ikL}$, which depends on the exact length of the cavity. It must verify $a^4=1$ at resonance, so that $a=1$, i, -1 or $-i$.

If $E_{in}(\vec{r})$ is the input image, then the output field is (see Fig. 4)

$$E(\vec{r})=\frac{1}{4}[E_{in}(\vec{r})+a^2E_{in}(-\vec{r})]+a[\tilde{E}_{in}(\vec{r})+a^2\tilde{E}_{in}(-\vec{r})]. \tag{36}$$

In terms of imaging, a is the phase between then even-odd parts of the field and its spatial Fourier transform, and a^2 gives the parity of the output image. Each value of a corresponds to a given family of modes—more precisely,

$$\begin{aligned} a=1 &\rightarrow \text{modes } m+n=0[4],\\ a=i &\rightarrow \text{modes } m+n=1[4],\\ a=-1 &\rightarrow \text{modes } m+n=2[4],\\ a=-i &\rightarrow \text{modes } m+n=3[4]. \end{aligned} \tag{37}$$

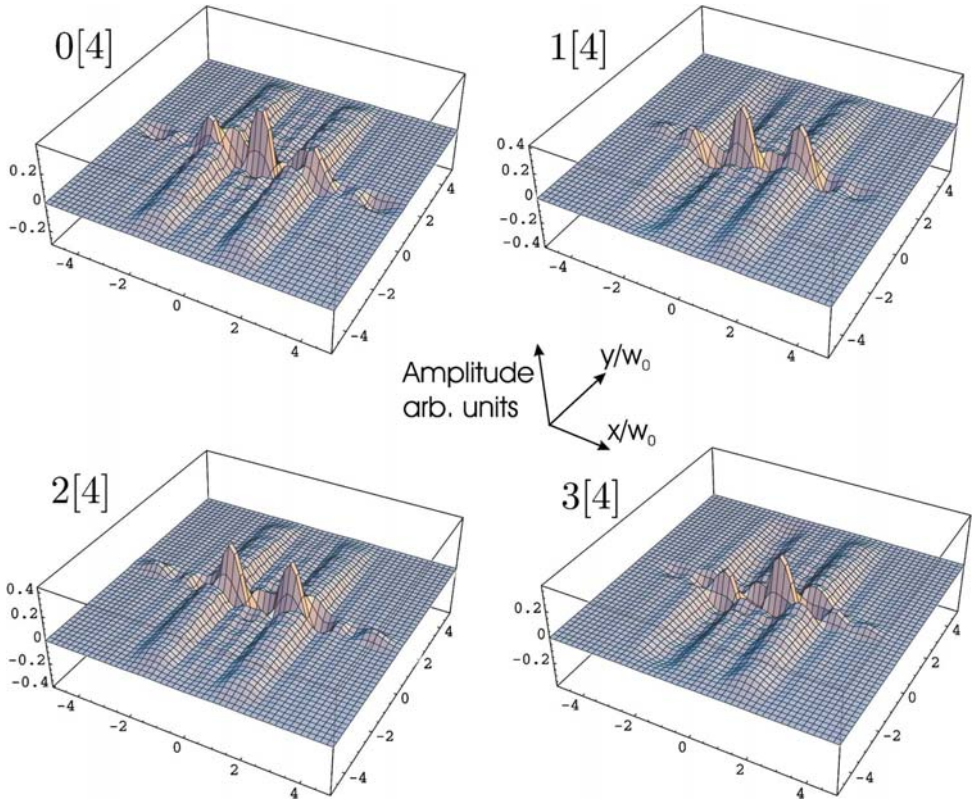

FIG. 7. (Color online) Theoretical transmission (amplitude) of the slit by the hemiconfocal cavity, for every mode family $m+n=i[4]$. The transverse unit is scaled to the waist w_0 of the cavity.

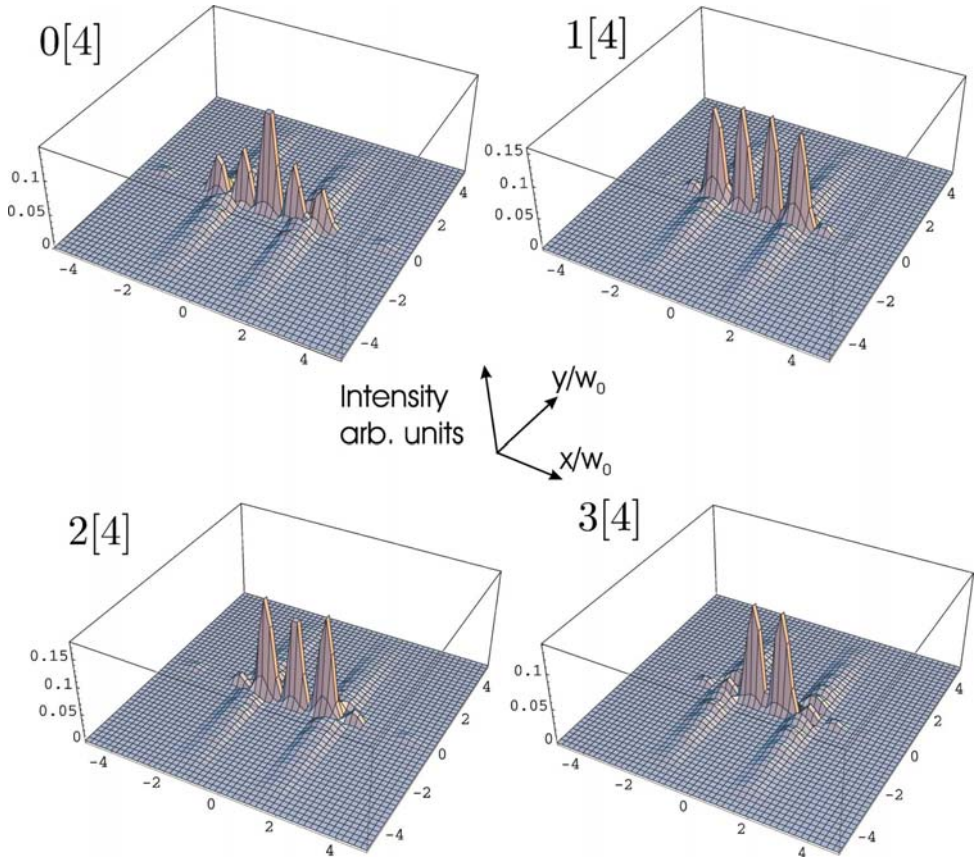

FIG. 8. (Color online) Theoretical transmission (in intensity) of the slit by the hemiconfocal cavity, for every mode family $m+n=i[4]$. The transverse unit is scaled to the waist w_0 of the cavity.

For example, the hemiconfocal cavity tuned on the $m+n=0[4]$ family will transmit the sum of the even part of the image and of the even part of its Fourier transform.

B. Numerical simulation

We will now give results of a numerical simulation in a simple experimental configuration: in order to create the input image E_{in}, a large Gaussian TEM_{00} mode is intercepted by a single infinite slit of width w_0, shifted from the optical axis by $1.5w_0$, which is imaged (near field) onto the reference plane (z_{ref}) of the cavity. Without the slit, the input TEM_{00} mode has in the reference plane a size equal to 3 times the waist of the TEM_{00} cavity eigenmode. We study the transmission of this input image through the cavity at the near-field detection plane. We represented in Fig. 5 the input image, its decomposition over the first 400 TEM_{pq} modes (with $0<p, q<20$), and its spatial Fourier transform. Limiting the decomposition of the image to only ~400 modes is equivalent to cutting high-order spatial frequencies and, therefore, takes into account the limited transverse size of the optics.

Figure 6 gives the expected transmission peak as a function of cavity length and displays the four families of modes in a given free spectral range. The height of each peak is proportional to the intensity of the image projection on the family of mode. For instance, a symmetric field will have no intensity on the 1[4] and 3[4] families.

Figure 7 gives the amplitude of the transmitted field for each family of modes, calculated from the transmission of the 400 first TEM_{mn} modes. For each family, one easily recognizes the even or odd part of the image (two slits) and the Fourier transform along the axis perpendicular to the slits.

The expected intensity image is represented in Fig. 8 for each family. One observes that the Fourier transform is much more intense that the transmitted image, even though Eq. (36) shows that there is as much energy in the Fourier transform than in the image. In the present case, the Fourier transform is much more concentrated than the image, which is the reason why the local intensity is higher. As the parity information on the field disappears when looking at the intensity, it is difficult to infer from it which resonance is involved. An indication can come from the intensity on the optical axis, which is always zero for an antisymmetric output. One can note that if we add the amplitude fields corresponding to the resonances $m+n=j[4]$ and $m+n=j+2[4]$, the two terms corresponding to the Fourier transform vanish. One only gets

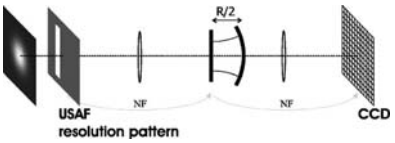

FIG. 9. Schematic representation of the experimental setup.

the even or odd part of the image, which corresponds to the action on the image of a confocal cavity. It is interesting to note that no combination of modes transmit only the Fourier transform of the image.

An interesting question is to know which information is lost in the transmission through the cavity, since one only transmits a quarter of the input intensity. By looking at the transmitted image, it seems that no information is really lost, except in areas where the image and its Fourier transform overlap. But here we have some *a priori* information on the image that we have sent and we know which part of the output is the image and which part is the Fourier transform. In more general cases, the information we lose is the knowledge about whether what we observe is the image or the Fourier transform, as well as half the image (since the parity is fixed by the geometry of the cavity, only half the output image is relevant to reconstruct it). Therefore, for a given resonance, this cavity not only cuts 75% of the modes; it also destroys 75% of the information.

As a conclusion, the transmission through the cavity transforms the input image into its its self-transform function corresponding to the round-trip transform of the hemiconfocal cavity. One may notice that for the resonance $m+n=0$[4], a self-Fourier image—i.e., a SFF field—is obtained.

C. Experimental demonstration

For practical reasons, we had to use a hemiconfocal cavity in our experimental setup designed to study parametric image amplification in optical cavities (see Fig. 9). We placed a USAF (U.S. Air Force) resolution target on the path of a TEM_{00} mode produced by a Nd:YAG laser and imaged it onto the plane mirror of a hemiconfocal cavity, of length 50 mm, servolocked on a resonance peak. The size of the TEM_{00} mode inside the cavity was 3 times larger than the eigenmode waist of the cavity. The finesse of the cavity was about 600. The plane mirror of the cavity was then imaged on a CCD camera. The experimental transmitted images, together with the corresponding objects, are represented in Fig. 10. The size of the TEM_{00} cavity mode is roughly equal to the width of the transmitted slit in the second line. One notices that each output image is symmetric, the center of symmetry being the axis of the cavity. It is possible to recognize on the transmitted images the symmetrized input image and the patterns at the center corresponding to the Fourier transform of the input. For a slit it is well known that its Fourier transform is the sinc-squared diffraction pattern, perpendicular to the slit. This kind of pattern can be recognized in the upper two images of the figure. In the last image the symmetrized "2" is somewhat truncated by the limited field of view imposed by the size of the illuminating TEM_{00} mode,

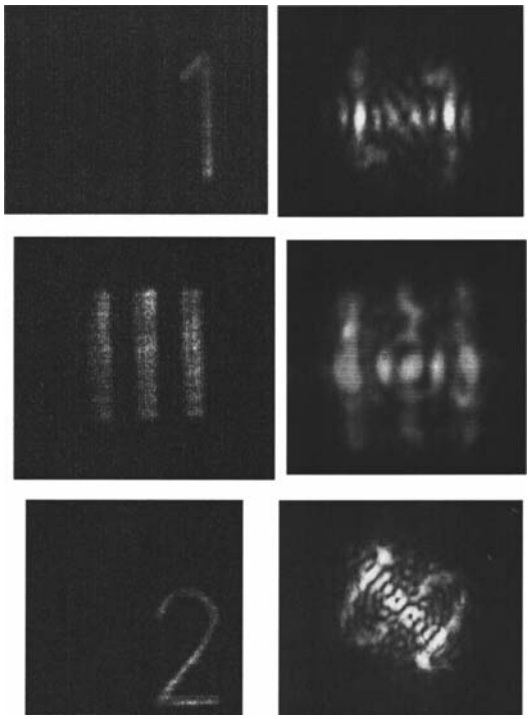

FIG. 10. Image on the resolution target (left) and its transmission through the hemiconfocal cavity (right).

whereas the diffraction pattern has the general shape of the Fourier transform of the slit formed by the main bar of the "2," tilted at 45°, plus a more complex shape corresponding to the Fourier transform of the remaining part of the image.

V. CONCLUSION

In summary, this paper has studied in a general way the problem of image transmission through a paraxial cavity, characterized by its round-trip ($ABCD$) matrix, the eigenvalues of which give the round-trip Gouy phase shift and, therefore, the order of the transverse degeneracy of the cavity. We have shown that the formalism of self-transform functions, already applied in optics but never to cavities, was very useful to understand how an image is transmitted through a degenerate cavity: at resonance the cavity transmits the self-transform part of the input field. We have then focused our attention on the hemiconfocal cavity, which performs a spatial Fourier transform over one round-trip, and shown that it transmits the self-Fourier part of the image. This property was demonstrated experimentally on various shapes of input images. Furthermore, we have shown that a transverse degenerate cavity is a very convenient way to produce a self-transform field from any input field—for instance, in the case of the hemiconfocal cavity a field which is its own Fourier transform (i.e., its own far field).

From a more practical point of view, transverse degenerate cavities can be useful for imaging purposes. For example,

they are necessary for intracavity cw parametric amplification of images. The observation of cw image amplification with low pump powers will be reported in a forthcoming publication [19]. These experimental results open the way to the observation of specific quantum aspects of imaging which have been predicted to occur in such devices, such as noiseless phase-sensitive amplification, local squeezing, or spatial entanglement.

ACKNOWLEDGMENTS

Laboratoire Kastler-Brossel, of the Ecole Normale Supérieure and the Université Pierre et Marie Curie, is associated with the Centre National de la Recherche Scientifique. This work was supported by the European Commission in the framework of the QUANTIM project (Grant No. IST-2000-26019).

APPENDIX: EIGENVECTORS AND GOUY PHASE OF A CAVITY

Let A, B, C, and D be the coefficients of the cavity round-trip Gauss matrix T_{cav}, starting from any plane. Given that $AD-BC=1$, the eigenvalues of this Gauss are

$$\mu_{1,2} = e^{\pm i \arccos[(A+D)/2]}. \tag{A1}$$

They are simply related to the matrix trace $A+D$ and, as expected, independent of the reference plane one choses in the cavity to calculate the Gauss matrix. Let us now consider the fundamental Gaussian mode of the cavity, $E(r) = E(0)e^{-ikr^2/2q}$, where q is the complex radius of curvature. Using the propagation relation (5), one easily computes that, on axis, it becomes, after one round-trip,

$$E'(0) = E(0)e^{ikL}\frac{1}{B/q + A}. \tag{A2}$$

The round-trip Gouy phase shift α for this mode is therefore

$$\alpha = \mathrm{Arg}\left[\frac{1}{B/q + A}\right]. \tag{A3}$$

On the other hand, after one round-trip in the cavity, the complex radius of curvature becomes $(A_q+B)/(C_q+d)$, but since it is an eigenmode of the cavity, q must verify

$$q = \frac{Aq + B}{Cq + d}, \tag{A4}$$

from which one deduces

$$A + \frac{B}{q} = \frac{D + A}{2} + i\sqrt{1 - (A + D)^2/4}. \tag{A5}$$

From Eq. (A3), one then find that $\alpha=\arccos[(A+D)/2]$, and therefore using Eq. (A1) one retrieves relation (11).

[1] M. Born and E. Wolf, *Principles of Optics*, 7th ed. (Cambridge University Press, Cambridge, England, 1999).
[2] A. E. Siegman, *Lasers* (University Science Books, Mill Valley, CA, 1986).
[3] A. Lohmann and D. Mendlovic, Appl. Opt. **33**, 153 (1994).
[4] S. G. Lipson, J. Opt. Soc. Am. A **10** (9), 2088 (1993).
[5] M. I. Kolobov and L. A. Lugiato, Phys. Rev. A **52**, 4930 (1995).
[6] M. Kolobov, Rev. Mod. Phys. **71**, 1539 (1999).
[7] Sang-Kyung Choi, Michael Vasilyev, and Prem Kumar, Phys. Rev. Lett. **83**, 1938 (1999).
[8] Fabrice Devaux and Eric Lantz, Phys. Rev. Lett. **85**, 2308 (2000).
[9] Z. Y. Ou, S. F. Pereira, and H. J. Kimble, Phys. Rev. Lett. **70**, 3239 (1993).
[10] H. M. Ozaktas and D. Mendlovic, Opt. Lett. **19**, 1678 (1994).
[11] H. M. Ozatkas and D. Mendlovic, J. Opt. Soc. Am. A **12**, 743 (1995).
[12] J. Dingjan, Ph.D. thesis, Leiden University, 2003.
[13] J. A. Arnaud, Appl. Opt. **8**, 189 (1969).
[14] M. J. Caola, J. Phys. A **24**, L1143 (1991).
[15] A. Lohmann and D. Mendlovic, J. Opt. Soc. Am. A **9**, 2009 (1992).
[16] K. Patorski, Prog. Opt. **28**, 3 (1989).
[17] A. Lohmann and D. Mendlovic, Opt. Commun. **93**, 25 (1992).
[18] Y. F. Chen, C. H. Jiang, Y. P. Lan, and K. F. Huang, Phys. Rev. A **69**, 053807 (2004).
[19] S. Gigan, L. Lopez, V. Delaubert, N. Treps, C. Fabre, and A. Maitre, e-print quant-ph/0502116.

PHYSICAL REVIEW A **67**, 023808 (2003)

Experimental study of the spatial distribution of quantum correlations in a confocal optical parametric oscillator

M. Martinelli,* N. Treps, S. Ducci,† S. Gigan, A. Maître,† and C. Fabre
Laboratoire Kastler Brossel, Université Pierre et Marie Curie, case 74, 75252 Paris cedex 05, France
(Received 16 September 2002; published 13 February 2003)

We study experimentally the spatial distribution of quantum noise in the twin beams produced by a type-II optical parametric oscillator operating in a confocal cavity above threshold. The measured intensity correlations are at the same time below the standard quantum limit and not uniformly distributed inside the beams. We show that this feature is an unambiguous evidence for the multimode and nonclassical character of the quantum state generated by the device.

DOI: 10.1103/PhysRevA.67.023808 PACS number(s): 42.50.Dv, 42.65.Yj, 42.30.−d, 42.50.Lc

I. INTRODUCTION

To date, almost all the experiments investigating the quantum properties of the states of light produced by optical parametric oscillators (OPOs) have been performed through the measurement of the *total intensity* of the generated fields, obtained by integrating on the detector the whole wave-front intensity distribution. Such measurements have put in evidence the squeezed vacuum character of the output of a degenerate OPO below threshold [1], the quantum intensity correlations between the signal and idler beams (twin beams) [2], and the bright squeezing of the output of an optical parametric amplifier (OPA) [3] and of the pump beam reflected by an OPO [4].

In the past years, the interest has turned to the spatial aspects of quantum fluctuations, in particular, because they open new perspectives in the quantum information field: spatial features offer the possibility of parallel processing and multichannel operation, each part in a transverse section of a beam playing the role of a channel. The concepts of temporal squeezing and correlations of light beams as a whole have been extended to spatiotemporal properties for the local quantum fluctuations in the plane perpendicular to the propagation: squeezing of the temporal fluctuations inside a small part of the transverse plane, or temporal quantum correlations between different transverse areas of the beam are some of the manifestations of the transverse quantum properties of light. It has been shown that, in order to obtain strong spatial quantum effects, one needs to use *multimode nonclassical states of light*, in contrast to the single-mode operation of the experiments quoted above. It has also been shown that such nonclassical multimode states can be used to improve the optical resolution [5] and to measure small transverse displacements of a light beam below the standard quantum limit [6,7].

Our investigations of the spatial distribution of multimode states of light produced by OPOs are related to the pioneer studies of the stochastic spatial noise performed in gas lasers [8], and more recently in semiconductor lasers (diode lasers and vertical cavity surface emitting lasers [VCSELs]) [9], for which the spatial distribution of the quantum fluctuations of the output beam has been studied and interpreted in terms of a superposition of several Hermite-Gauss modes. They must also be connected to the studies of spatial quantum effects for the photons generated by spontaneous parametric down-conversion, at the photon counting level, for example, to the recent demonstration of spatial antibunching [10].

Parametric interaction in a nonlinear crystal has been theoretically shown to be a very efficient source of multimode nonclassical states of light. Many theoretical studies [11,12] have shown in particular that OPAs generate multimode squeezed states. OPOs have also been shown to be a source of multimode squeezed states provided that they use optical cavities with degenerate transverse modes: in particular, detailed theoretical investigations have been performed on subthreshold OPOs in planar [13,14], or quasiplanar cavities [15,16].

From an experimental point of view, such cavities, which are close to instability, are quite difficult to handle and have very high oscillation thresholds. Confocal cavities are much easier to operate, and still exhibit interesting nonclassical transverse effects, such as multimode squeezing in the degenerate case below threshold [17]. The multimode transverse operation of confocal OPOs above threshold has been theoretically investigated at the classical level [18], and experimentally put in evidence in Ref. [20], where it has been shown that the field emitted by a confocal OPO above threshold can be described as a superposition of a great number of TEM_{pq} modes. The quantum description of this regime is unfortunately a difficult task, as the device switches from an uncoupled regime of the different transverse modes to a strongly coupled regime when passing from the subthreshold emission to the regime of intense output.

This paper is devoted to the study of the spatial distribution of quantum fluctuations of such a device, and shows that it generates multimode nonclassical states of light. In Sec. II, we give the precise definition of multimode quantum states of light. We present in Sec. III a criterion unambiguously characterizing such states in our experimental configuration, namely, the measurement of the spatial distribution of the intensity correlations between the signal and idler beams.

*On leave from the Instituto de Fisica, Universidade de São Paulo, P.O. Box 66318 CEP, São Paulo, Brazil.
†Also at the pôle Matériaux et Phénomènes Quantiques, FR CNRS 2437, Université Paris 7, Denis Diderot.

Section IV presents the experimental setup and the procedure for measuring these correlations. Finally, Sec. V presents the experimental results proving that the signal and idler beams emitted by the confocal OPO are multimode and spatially quantum correlated.

II. INTRINSIC CHARACTERIZATION OF MULTIMODE AND SINGLE-MODE BEAMS

A. Definition of single-mode and multimode beams

In the studies on optical patterns, a beam is said to be multimode (in the TEM_{pq} basis), when the far-field patterns appear to be different from the near-field patterns. Actually, this feature is a proof that the beam consists of a superposition of several TEM_{pq} modes. The electric-field positive frequency envelope of such a light beam, $E^{(+)}(\vec{r},z)$, expanded in the basis of TEM_{pq} modes $u_{p,q}(\vec{r},z)$, writes

$$E^{(+)}(\vec{r},z)=\sum_{p,q}\alpha_{p,q}u_{p,q}(\vec{r},z), \tag{1}$$

with more than one $\alpha_{p,q}$ coefficient different from zero. Nevertheless, if the $\alpha_{p,q}$ coefficients are fixed (i.e., if we deal with a *coherent superposition of modes* and not a statistical one), one can always define a new mode $v_0(\vec{r},z)$:

$$v_0(\vec{r},z)=\frac{E^{(+)}(\vec{r},z)}{\int|E^{(+)}(\vec{r},z)|^2d^2r} \tag{2}$$

and construct a new orthonormal basis of modes $\{v_i(\vec{r},z)\}$ in which v_0 is the first element. In this new basis, the field which appeared multimode in the Gauss-Laguerre basis, is proportional to v_0 and is then single mode. This simple reasoning at the classical level seems to show that the single-mode or multimode character of a beam having a well defined and fixed amplitude distribution depends on the choice of the basis, and is not an intrinsic property. A TEM_{00} laser beam is single mode in the Laguerre-Gauss basis, and multimode in the basis of transverse plane waves. We will show here that this statement is no longer true when one describes the beam at the quantum level.

We will now define a single-mode quantum state of light in the following way: $|\Psi\rangle$ is a single-mode quantum state of light if there exists a basis of modes $\{v_i(\vec{r},z)\}$ in which it can be written as

$$|\Psi\rangle=|\Psi_0\rangle\otimes|0\rangle\otimes|0\rangle\otimes\cdots, \tag{3}$$

where the first transverse mode v_0, whatever its shape, is a nonvacuum state $|\Psi_0\rangle$, and all the other modes are in the vacuum state. We will call *intrinsic multimode states* all states defined by a ket $|\Psi\rangle$, which cannot be written as Eq. (3) in any basis. We will give in the following section a characterization of such single-mode or multimode states, which is independent of the basis used to describe it.

This striking difference between the classical and quantum description of a multimode state comes from the fact that a quantum state gives information on the mean electric field, but also on the statistical distribution of quantum fluctuations: a single-mode beam is characterized by a well defined transverse variation that carries all its transverse information. Consequently, in such a state the transverse distribution of quantum fluctuations can be deduced from the transverse variation of the mode itself. In contrast, in intrinsic multimode states, the spatial distribution of fluctuations and correlations cannot be deduced from the structure of the mean field.

Let us finally mention that this problem is modified if one considers *stochastic fields*, i.e., having classical fluctuations. In this case also, the comparison between the spatial (or temporal) distribution of the mean field and of the classical fluctuations is still an intrinsic tool to determine whether the field can be considered as single mode or multimode [9]. We will not consider further this problem here.

B. Characterization of a single-mode quantum state

Let us consider a single-mode state of light $|\Psi\rangle$, written in the adapted basis $\{v_i\}$ as Eq. (3), and let us call $\hat{a}_i$ the annihilation operator of photons in the mode v_i. Let us now introduce any other mode basis of the transverse plane $\{w_j\}$, and the corresponding annihilation operators $\hat{b}_j$. There is a unitary transformation relating the two basis, and correspondingly the two sets of annihilation operators:

$$\hat{b}_i=\sum_j U_{ij}\hat{a}_j. \tag{4}$$

From Eqs. (3) and (4), one deduces that:

$$\hat{b}_i|\Psi\rangle=U_{i0}\hat{a}_0|\Psi_0\rangle. \tag{5}$$

We thus obtain a specific property of a single-mode quantum state: the action on it of all the annihilation operators of any given basis of transverse modes gives vectors which are all proportional. One can show that this feature is a necessary and sufficient condition to be a single-mode state [21]. In contrast, for an intrinsic multimode state, there exists at least one basis of modes in which this property is not true. The condition for single-mode states being very restrictive, the set of single-mode states is a very small subset of the general Hilbert space. The complement of this subspace, namely, the set of intrinsic multimode states, is therefore much larger.

This characterization of single-mode and multimode states appears to be quite mathematical, and seems difficult to implement experimentally. We give in the following a more convenient property of single-mode states, which is not a necessary and sufficient condition, but which can be submitted to an experimental check with our setup.

III. CHARACTERIZATION OF SINGLE-MODE AND MULTIMODE TWIN BEAMS

A. Partial measurement of intensity fluctuations on a single-mode beam

Let us consider an intensity, or photon number, measurement using a detector of variable transverse area S_A. We

have shown in Ref. [6] that if the light is in a single-mode state, the variance of the photon number fluctuations measured with this partial detector is given by

$$\Delta N_A^2 = \langle N_A \rangle + \frac{\langle N_A \rangle^2}{\langle N_{tot} \rangle^2} (\Delta N_{tot}^2 - \langle N_{tot} \rangle), \tag{6}$$

where $\langle N_A \rangle$ is the mean number of photons detected on the area S_A, $\langle N_{tot} \rangle$ is the mean number of photons detected on the whole transverse plane, and ΔN_{tot} is the corresponding variance. One sees that the intensity noise normalized to shot noise, $\Delta N_A^2 / \langle N_A \rangle$, varies linearly with the quantity $T = \langle N_A \rangle / \langle N_{tot} \rangle$. This formula can be understood by considering that in a single-mode state the photons are randomly distributed in the transverse plane, so that a partial detection performed on an area smaller than the tranverse section of the beam will introduce sorting noise in the detection of the photon number, exactly like when one introduces a linear loss of value T in front of the detector. This intuitive picture is no longer true for multimode beams.

B. Partial measurement of intensity correlations on single-mode twin beams

In a nondegenerate OPO, the emitted signal and idler fields present strong intensity correlations at the quantum level (''twin beams''). In particular, the variance of the difference $N_{dif,tot} = N_{1,tot} - N_{2,tot}$ between the signal (labeled 1) and idler (labeled 2) intensities detected over the whole transverse plane is smaller than $\langle N_{1,tot} \rangle + \langle N_{2,tot} \rangle$, which is the shot noise for the sum of the signal and idler beams. When the beams produced by the OPO are both single-mode, one can easily show from Ref. [6] that the following formula, similar to Eq. (6), holds in case of a partial photodetection of signal and idler beams by two detectors having the same areas and positions S_A in the two beams:

$$\Delta N_{dif,A}^2 = (\langle N_{1,A} \rangle + \langle N_{2,A} \rangle) + \frac{(\langle N_{1,A} \rangle + \langle N_{2,A} \rangle)^2}{(\langle N_{1,tot} \rangle + \langle N_{2,tot} \rangle)^2} \times [\Delta N_{dif,tot}^2 - (\langle N_{1,tot} \rangle + \langle N_{2,tot} \rangle)]. \tag{7}$$

Similarly to the interpretation of formula (6), this formula can be understood by considering that in single-mode twin beams there is no spatial correlation between the twin photons inside the signal and idler beams, the photons being randomly distributed inside the two beams. If, instead of small detectors, we use detectors with a broad enough area to detect the whole beams, but preceded by a diaphragm, or iris, of variable transmission T, expression (7) shows that in single-mode twin beams the relative noise on the intensity difference, $n_A = \Delta N_{dif,A}^2 / \langle N_{1,A} \rangle + \langle N_{2,A} \rangle$, is a linear function of the transmitted mean intensity. In contrast, a nonlinear variation of this quantity will be a signature for intrinsic multimode twin beams, for which the twin photons are not randomly distributed inside the two beams.

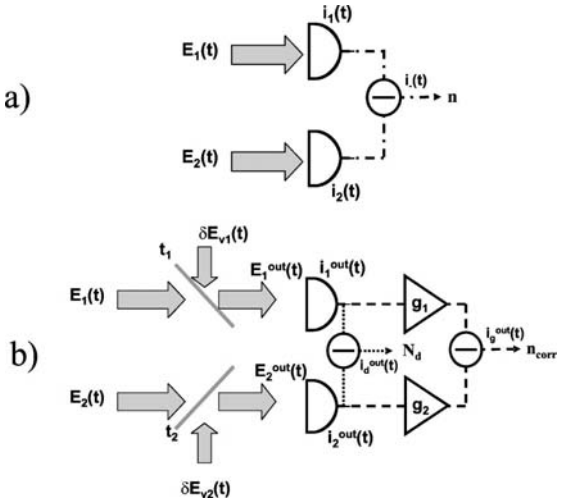

FIG. 1. Measurement of twin beams correlation in the imbalanced case. (a) i_d^{out} : direct difference measurement. (b) i_g^{out} : difference measurement after gain corrections.

C. Partial measurement of intensity correlations on single-mode twin beams undergoing different losses

We have assumed so far that the detected mean intensities of the output beams are always equal, even in partial photodetection. In real experiments, this is not exactly the case, and imbalances of several percents are commonly measured, especially in confocal OPOs, where the patterns observed in the signal and idler beams are different. The imbalance will affect the intensity fluctuations of the two beams in a different way. The imbalance of the whole beams is due to the fact that the signal and idler beams, produced in exact equal amounts in the nonlinear crystal, experience different losses in their propagation. Furthermore, in the case of a partial photodetection, one must also take into account that the signal and idler beams may have different shapes. It is important to precise the way to define the ''twin character'' of such imbalanced beams in a partial measurement. We will first introduce the normalized intensity difference noise n when the whole beams are measured [Fig. 1(a)]. We will then consider a partial measurement [Fig. 1(b)] and define the direct normalized intensity difference noise n_d, with no corrections, as it can be directly calculated from the measurement. We will finally define the corrected normalized intensity difference noise n_{corr}, an attempt to recover the value of n from n_d assuming that the beams are single mode.

Assuming that the mean signal and idler fields are real, and as the fluctuations in the cw regime are very small in comparison to the mean field [19], we can write the field intensity operator as

$$\delta \hat{i}_m = 2 E_m \delta \hat{E}_m, \quad m \in \{1,2\}, \tag{8}$$

where $\delta \hat{E}_m$ is the quadrature fluctuation operator in the amplitude direction. We now introduce the normalized quantity

n, which is the variance of the intensity difference fluctuations normalized to the total shot noise, and can be written as

$$n=\frac{\langle(\delta\hat{i}_1-\delta\hat{i}_2)^2\rangle}{4(i_1+i_2)\Delta^2E_v}, \tag{9}$$

where Δ^2E_v is the noise variance of the vacuum field. $n>1$ for beams with classical correlations (obtained, for example, by using beam splitters) and $n<1$ for quantum correlated beams (twin beams). Let us now assume that the two beams are subject to losses before being incident on the photodetectors [Fig. 1(b)]. We call E_m^{out} the fields which are incident on the photodetectors and i_m^{out} their intensities, and n_d the normalized variance of their intensity difference:

$$n_d=\frac{\Delta^2i_d^{out}}{4(i_1^{out}+i_2^{out})\Delta^2E_v}=\frac{\langle(\delta\hat{i}_1^{out}-\delta\hat{i}_2^{out})^2\rangle}{4(i_1^{out}+i_2^{out})\Delta^2E_v}. \tag{10}$$

In the transverse single-mode case, losses of any origin and partial photodetection have the same effect on the fluctuations mechanism, identical to the effect of a beam splitter of transmission t_m ($m=1,2$) (with $t_m^2=i_m^{out}/i_m$). The field intensity $\hat{i}_m^{out}$ measured by the photodetectors presents fluctuations $\delta\hat{i}_m^{out}(t)$ that can be expressed in the linearization approximation as

$$\delta\hat{i}_m^{out}(t)=2t_n^2E_m\delta\hat{E}_m+2t_m\sqrt{(1-t_m^2)}E_m\delta\hat{E}_{vm}, \quad m\in\{1,2\}. \tag{11}$$

Knowing the effective loss coefficient t_m, it is possible to adjust the gain g_m on the acquisition channels at the value $1/t_m^2$, as shown in Fig. 1, so that the mean values of the corrected intensities $g_m\langle\hat{i}_m^{out}\rangle$ are equal to their value without losses $\langle\hat{i}_m\rangle$. If one assumes that the two beams are single transverse modes, it is possible to recover the original normalized intensity difference noise n of Eq. (9) by subtracting the effect of the vacuum fluctuations $\delta\hat{E}_{vm}$. Writing $\Delta^2i_g^{out}$ the fluctuations of the difference between the two acquisition channels,

$$\Delta^2i_g^{out}=\langle(g_1\delta\hat{i}_1^{out}-g_2\delta\hat{i}_2^{out})^2\rangle, \tag{12}$$

one easily shows that the quantity

$$n_{corr}=\frac{\Delta^2i_g^{out}}{4(g_1i_1^{out}+g_2i_2^{out})\Delta^2E_v}+1-\frac{g_1^2i_1^{out}+g_2^2i_2^{out}}{g_1i_1^{out}+g_2i_2^{out}} \tag{13}$$

is equal to n in the single-transverse-mode case. The last two terms of Eq. (13) correspond to the corrections arising from vacuum fluctuations introduced by the losses or the partial detection.

D. Multimode twin beams

Since for single-mode signal and idler beams $n_{corr}=n$, a constant value n_{corr} with the transmittance t_m for a partial measurement (or a linear variation of n_d) is a good indication (but not a proof) of the single-mode character of the signal and idler mode beams. In contrast, a nonconstant value of n_{corr}, or a nonlinear variation of n_d, with respect to the losses is an unambiguous signature of the multimode character of the two beams generated by the OPO. Furthermore, if these quantities are smaller than 1, we can conclude that we are in presence of multimode nonclassical beams. Strictly speaking, as the vacuum correction in n_{corr} has been derived assuming single-mode beams, n_{corr} do not anymore correspond exactly to a noise correlation in the case of multimode beams. Moreover, for a partial measurement, the mean intensity of both beams may be different, and neither n_d nor n_{corr} are perfectly suited for the exact characterization of quantum intensity correlation. For these reasons, in the case of a *partial* measurement of a *multimode* beam, more sophisticated criteria should be investigated, which will be developed in a forthcoming publication.

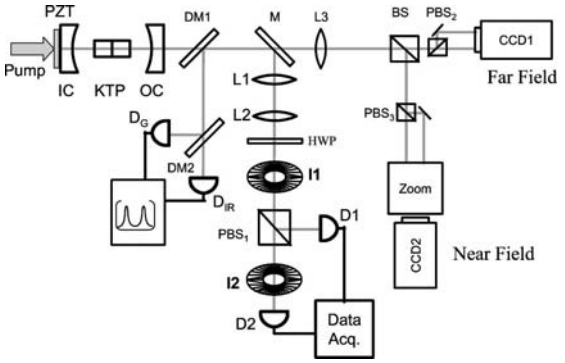

FIG. 2. Experimental setup. PZT, piezoelectric transducer; IC, input coupler; OC, output coupler; DM, dichroï mirror; *M*, mirror; *L*, lens; BS, beam splitter; PBS, polarizing beam splitter; HWP, half-wave plate; *I*, iris; *D*, detector; D_G, detector for green light; D_{IR}, detector for IR light.

IV. EXPERIMENTAL SETUP

For OPOs operating in cavities with degenerate transverse modes, the formation of complex spatial structures has been theoretically [22,23] and experimentally [20,24] studied. Furthermore, quantum multimode operation of the OPO has been already theoretically predicted [14]. But, up to now, to our knowledge, there has been no experimental demonstration that the emission of an OPO is intrinsically multimode. The experiment presented here investigates the spatial distribution of the intensity correlation between the signal and idler beams emitted by a confocal OPO above threshold in order to identify their single-mode or multimode character. The setup, shown in Fig. 2, can be divided into two parts: the triply resonant OPO and the acquisition system of the intensity fluctuations of the beams.

A. The triply resonant OPO

In order to match the desired requirements of power and stability of the experiment, an effective setup was made for

the generation of the pump beam for the OPO. We used an ultrastable single-mode Nd:YAG (yttrium aluminum garnet) laser with 350 mW of output power to lock a flash-lamp-pumped Nd:YAG laser operating in a ring cavity. This configuration [20,24] gives a stable single-mode beam with an output power of 3.5 W at 1064 nm. This beam is injected in a semimonolithic frequency doubler, using a $MgO:LiNbO_3$ crystal and a concave mirror. The output of the second harmonic generator reproduces the frequency stability of the injected Nd:YAG laser and gives a total output power of 1.3 W at 532 nm. The pump is then injected inside the OPO with a waist equal to twice the TEM_{00} waist of the OPO cavity mode like in Ref. [20].

The nonlinear crystal used inside the OPO is a walk-off compensated KTP (potassium titanyl phosphate) cut for type-II phase matching. It is made by two 5-mm-long crystals that are optically contacted, with their orientations compensating the walk-off effect. The triply resonant OPO uses two plane-concave mirrors, whose curvature is $R=100$ mm. The input coupler has a transmittance of 10% for the pump (532 nm) and high reflectance for the Nd:YAG wavelength (1064 nm). The output coupler has a high reflectance at 532 nm and 1% transmittance at 1064 nm. Measured finesse value of the cavity with the crystal is 40 at 532 nm and 300 at 1064 nm and temperature is controlled such that signal (o-polarization) and idler (e-polarization) emitted by the OPO are close to frequency degeneracy. The cavity length can be tuned over a few free spectral ranges with a piezoelectric ceramic (piezoelectric transducer, PZT) attached to the input coupler. A coarse control of the length of the OPO is performed by means of translation stages fixed on both cavity mirrors. A fraction of the infrared output of the Nd:YAG laser can also be injected into the cavity for alignment purposes and to check the transverse-mode separation. The OPO works close to the confocal configuration. In order to define the region of confocality, it is useful to remember that the distance L between two spherical mirrors for a confocal cavity depends not only on the ray of the concave surface but also on the refractive index of the medium inside the cavity. Therefore, considering the diffraction effects inside a crystal of length ℓ and refractive index n in a cavity made by two spherical mirrors of ray R, the distance L between the mirrors for the confocality will be [25]

$$L_{conf}=R+\ell(1-1/n). \tag{14}$$

Since the refractive index for pump, signal, and idler are different (respectively, 1.7881, 1.8296, and 1.7467 [26]), the length of the cavity L_{conf} for which the exact confocality is obtained, is different for each of the three modes (104.41, 104.28, and 104.53 mm). Transverse degeneracy is achieved when different transverse modes are resonant for the same cavity length. Due to the width of the resonance peaks, transverse degeneracy can be obtained even if the cavity is not exactly confocal. The range of confocality can be defined as the region of the cavity length where the fundamental and the first transverse even mode separation is smaller than the cavity bandwidth, and, following Ref. [27], can be expressed as

$$|L-L_{conf}|<\frac{\pi R}{2F}, \tag{15}$$

where F is the finesse of the cavity. In our case, the range of confocality for signal, idler (and pump) is larger than the difference between the confocal lengths for the signal, idler, and pump modes. Transverse degeneracy, essential for multimode emission, is then achievable at the same time for the three modes. Taking the average of the confocal length for signal and idler, we will consider the confocal length as $L_{conf}=104.41$ mm, and express the cavity length in terms of $\Delta L=L-L_{conf}$.

Although the threshold for oscillation is quite low and around 30 mW, significant thermal effects take place inside the cavity even close to threshold, because of the nonnegligible absorption of the green light (3% at 532 nm) and of infrared light (0,45% at 1064 nm): thermal lensing changes the total Gouy phase shift added to the wave in a round trip [27] and even a subconfocal cavity can become transverse degenerate if the pump power injected into it is sufficiently high. Therefore the confocality [20] is obtained for cavity lengths that are shorter than the confocal length L_{conf}, defined above for a "cold" OPO with no thermal effects.

B. Detection and acquisition

The details of the setup used for studying the transverse distribution of noise in twin beams' cavity can be seen in Fig. 2. Near the output coupler, a dichroic mirror (DM1) is used to eliminate the residual green light transmitted through the OPO cavity. A small fraction (2%) of the infrared light that is reflected by this mirror and transmitted by a second dichroic mirror DM2 is monitored by an $In_xGa_{1-x}As$ infrared photodetector D_{IR}. It is used to stabilize the OPO cavity by a servoloop made by a high-voltage amplifier connected to the PZT, controlling the output power of the IR beam and stabilizing it during a time ranging from seconds to minutes of continuous operation. The green light reflected by DM1 and DM2 is detected by a visible photodetector D_G.

After the DM1 at the OPO output, a flipping mirror (M) allows either the imaging of signal and idler far and near fields on a screen, or the recording of their intensities by two $In_xGa_{1-x}As$ infrared four-quadrant photodetectors $D1$ and $D2$ (ETX505Q from Epitaxx). In this experiment, only one quadrant of each photodetector is used. Their quantum efficiencies are very close (less than 1% difference) and equal to $90\%\pm5\%$. In both configurations, polarizing beam splitters (PBS) separate the signal and idler beams. Depending on the orientation of the half-wave plate placed before PBS1, signal and idler can be sent either to $D1$ or $D2$. During the measurement process, two irises of variable diameter are used to select in the far field a circular region of the output beam. Iris $I1$ is used to select a narrow circular region on both signal and idler, while iris $I2$ acts only on a single beam, either signal or idler. The lenses $L1$ and $L2$ are adjusted for each experiment in order to project the far field of the beam into the iris plane. The transmitted intensities are recorded and their fluctuations are monitored by an effective data acquisi-

tion system that is described below.

The data acquisition system used for the noise measurement differs from the usual method of direct measurement and subtraction of noise fluctuations (e.g., Ref. [28]). The high-frequency part of the photocurrent of each photodetector is amplified by a transimpedance amplifier and a broadband 36-dB amplifier. This signal is then mixed in an electronic demodulator at a frequency f_0 equal to 3.5 MHz, which lies inside the cavity bandwidth for the infrared modes and above the excess noise frequencies of the output beams. The output of the mixer has an active low-pass filter, working at 100 kHz. This signal is registered by a fast analog-to-digital acquisition card for measuring the noise correlation of the photocurrents. We used two acquisition cards (PCI6110E from National Instruments) with four simultaneous measurement channels each and 12 bits for signal conversion. The signal is measured with a repetition rate of 200 kHz and registered in the computer. Remaining channels of the data acquisition system are used for the measurement of the average value of the photocurrent of each detector, as well as the photocurrents of detectors D_G and D_{IR}. From the stored information of the average value and noise fluctuations of the photocurrent we can calculate the noise correlation of the intensity, and compare it to a previous calibration of the shot noise level made with a single output of the OPO or with the injected IR light from the Nd:YAG laser. This technique allows us to acquire in a very short time interval both the temporal fluctuations of a given Fourier component of the photocurrents and of their mean values, and then to postprocess the stored data. We can thus determine the different normalized quantities that we have defined earlier in that paper.

C. Experimental procedure

When the OPO oscillation is stabilized for a given cavity length, we perform two kinds of experiments. In the first experiment, we record the simultaneous noise distribution of the signal and idler beams by using the iris $I1$. We continuously close the iris $I1$ in 2 s, while acquiring a long series of values of δi_s, δi_i, i_s, i_i, i_{IR}, and i_G (six series of 400 000 simultaneous values). We analyze the data by groups of 10 000 values, calculating for each group the average photocurrent value $\langle i_m \rangle$ $(m=1,2)$ and the normalized variances n_{corr} and n_d. The corresponding vacuum fluctuation $\Delta^2 E_v$ was previously calibrated, and the electronic noise level is subtracted in the calculation of the variances. The transmittance of the iris for each series of 10 000 points is defined as $T=r/r_{open}$, where r is the ratio $r=\langle i_s+i_i \rangle / \langle i_{IR} \rangle$, and r_{open} corresponds to the initial value of r when the diaphragm is open. The normalized intensity difference noise variances n_{corr} and n_d are then plotted as a function of the transmission of the iris. For $T=1$, $n=n_d=n_{corr}$. When the variation of n_d (n_{corr}) is not linear (flat), one can conclude that the beams are multimode. The quantum correlation between them can be inferred from the intensity difference noise variances obtained for $T=1$. The second kind of experiments consists in setting iris I_2 on either the signal or the idler beam path and taking the unaffected beam as a reference. The procedure is identical to the previous one, except that r, for the iris on the signal beam, is defined as $r=\langle i_s \rangle / \langle i_{IR} \rangle$. Closing the iris I_2 attenuates only one of the beams, and produces a strong imbalance between the photocurrents of the two photodetectors, with a ratio (i_s/i_i) well out of the range 90% to 110%, which was typical in the previous conditions. With such a large imbalance, the value of n_d deduced from the experiment does not give any quantitative information on the quantum correlations between the two beams. On the other hand, the calculation of the corrected value of the normalized noise n_{corr} allows one to recover the information on the quantum correlation only in the case where the two beams are single-mode. Therefore, in this second kind of experiments, we only calculate n_{corr} as a function of the transmittance T.

V. SPATIAL DISTRIBUTION OF THE INTENSITY CORRELATION

A. Experiments with the iris on both signal and idler beams

As described in the preceding section, only iris I_1 is present. We have realized in this configuration two series of measurements: in the first one, the OPO oscillation is stabilized for a cavity length outside the confocality range, ensuring a TEM_{00} output mode for signal and idler beams [20,24]; in the second one, the cavity length is set to a shorter value, inside the confocality range, where complicated patterns can be observed in the signal and idler beams. While closing continuously the iris I_1, we record the transmitted intensity of the signal and idler modes and the normalized intensity noise difference variance n_d. The different normalized variances are then plotted as a function of the transmittance T. In the Fig. (3), the straight line represents the value of n_d that could be calculated with a single-mode beam having the same intensity correlation as the whole beam. One observes that outside the confocality range, where the signal and idler fields are close to TEM_{00}, the calculated straight line fits well the experimental points. Moreover, for an open diaphragm, the normalized intensity difference noise variance is equal to 0.8, demonstrating significant quantum intensity correlations between signal and idler.

In the confocality range, where the signal and idler fields have more complicated, and different, transverse variations, one observes that the variation of n_d is no longer linear with the transmittance, demonstrating that the emission of the OPO is multimode. Moreover, when the iris is open in that confocal configuration, the noise correlation is still below shot noise and close to the value obtained for the single-mode emission: the quantum intensity correlations for the whole beams are preserved even for multimode beams. The increase of noise when the iris is closed shows that the intensity correlation is stronger in the outer parts of the beams than in the center. Unfortunately, with such an experiment it is difficult to describe more precisely the transverse distribution of correlations between the signal and idler beams.

B. Experiments with the iris either on signal or idler beam

1. Single-mode beams

For a length of cavity $L=L_{conf}+5{,}6$ mm, where the OPO is assumed to be far from transverse degeneracy, we com-

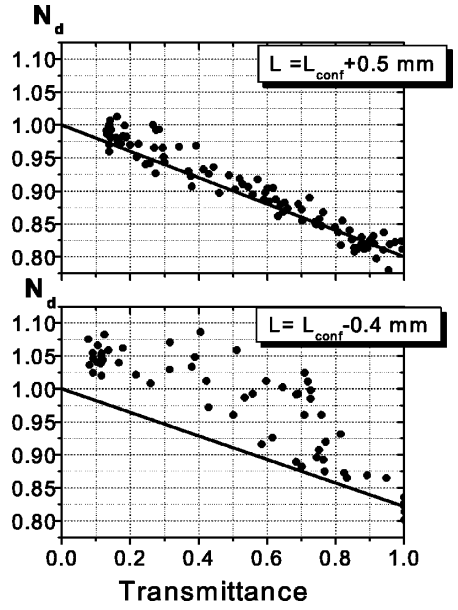

FIG. 3. Spatial distribution of the normalized intensity difference noise n_d as a function of the transmittance T with iris I_1 on signal and idler beams. Points: values of n_d for a cavity length equal to $L_{conf}=L+0{,}5$ mm (beyond the confocality range) and $L_{conf}=L-0{,}4$ mm (inside the confocality range). Straight line: Values of n_d that would be obtained with a single-mode beam having the same squeezing when the iris is fully open.

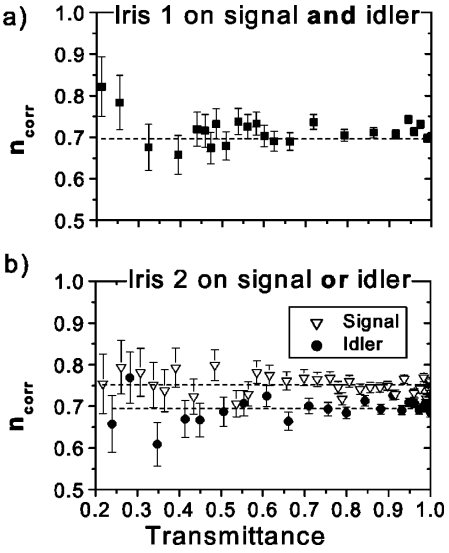

FIG. 4. Experimental values of n_{corr} for quasi-TEM_{00} signal and idler beams. (a) Iris on both beams, (b) Iris on a single beam. Idler (●) and signal (▽). Dashed lines: average corrected noise.

pared the results of the two kinds of experiments for the values of n_{corr} as a function of the transmittance. The results are plotted in Fig. 4. For all those experiments, as the beam intensity on the photodetector is reduced, the fluctuations of the photocurrent approache the electronic level. The dispersion in the calculated data increases when we close the iris. Typically, the variance of the intensity noise reached the dark noise level for an incident power of 0.2 mW, obtained with a typical iris transmittance of 10%.

One observes that all the experimental points are aligned on a horizontal straight line, with a mean value around 70%, which shows that the signal and idler beams are single-mode, quantum-correlated beams. The difference in the obtained level of noise in Fig. 4(b) (69% and 75%) is certainly due to the fact that both experiments are performed at different moments, and therefore on possibly different longitudinal modes. The values of n_{corr} remain stable during a single series of measurements when we close the iris.

2. Beams emitted by an OPO close to confocality

The length for the cavity is chosen to be very close to the exact confocal length L_{conf}. In this configuration, complex structures appear in far and near fields of the signal and idler beams [20]. We performed the same experiments and analysis as in the preceding section, adding the image of the near field and the far field of the beam obtained with the charge-coupled device cameras. Figures 5(a), 5(b), and 5(c) display, respectively, the results obtained for $L-L_{conf}=0.38$, -0.37, and -0.62 mm. In the configuration of Fig. 5(a), one observes a Gaussian-like transverse distribution of the idler beam and a clearly non-Gaussian distribution of the signal beam. When the iris I_2 is placed on the idler beam, n_{corr} does not deviate in a clear way from a flat line, except for lower values of the iris transmittance. In this situation, the dispersion in the results increases, following the attenuation of the idler field intensity. When we set the iris on the signal path, the corrected noise deviates slightly from a constant value for values of the transmittance close to 50%. The same behavior can be observed when we perform the experiment with iris 1 on both signal and idler.

In the configuration of Fig. 5(b), more complex structures appear: a ring pattern can be seen in the outer part of the idler far-field image. In the near field, complex structures appear for both signal and idler beams. In this situation, when iris I_1 is put on both beams, the corrected correlation noise n_{corr} goes up to the shot noise level and stabilizes around this value. It is interesting to observe that the level of squeezing obtained is reduced, and the normalized noise for open iris starts at 85%. When the iris I_2 is put on the signal path and closed, n_{corr} remains constant: from these observations, one can infer that the photons in the signal beams that are correlated to the idler photons are uniformly distributed inside the signal beam. On the contrary, when the diaphragm I_2 is set on the idler beam, the plot of n_{corr} deviates from a flat line. In that case, the results are very close to those obtained when the iris I_1 is set on both signal and idler, showing that most of the correlated photons in the idler are concentrated in the external part of the beam. The central part of the idler is constituted essentially of noncorrelated photons.

In the configuration of Fig. 5(c), both signal and idler beams present a faint external ring out of the central maxi-

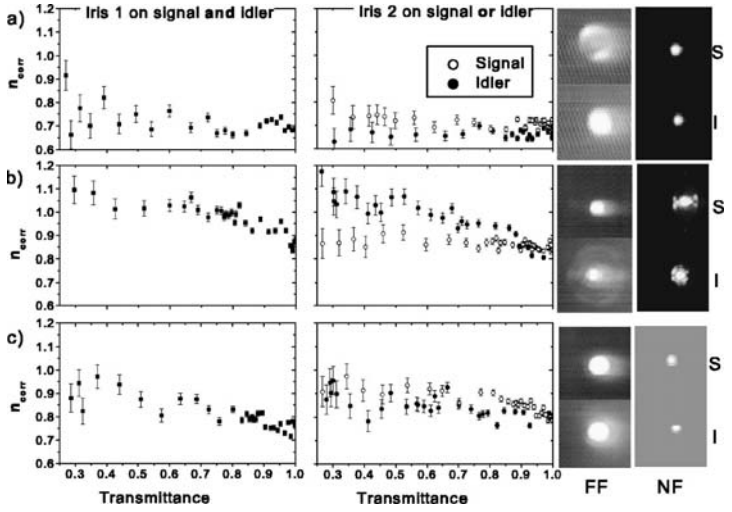

FIG. 5. Experimental values of n_{corr} for signal and idler beams displaying complex transverse distributions. The distance from confocality (ΔL) is equal, respectively, to (a) 0.38, (b) -0.37, and (c) -0.62 mm. Left, iris on both beams: (■). Center, iris on a single beam. Idler (●) and signal (○). Right: Far-field (FF) and near-field (NF) images of signal and idler beams.

mum. In that case, the evolution of the noise when closing iris 1 or closing iris 2 for signal or idler is very close. Both signal and idler corrected noises n_{corr} are reduced when one closes iris $I2$, showing that unlike the centers of signal and idler beams, their outer parts are quantum correlated. We see that these experiments give interesting indications on the details of transverse distribution of the correlations inside the beams. Unfortunately, the great quantity of modes oscillating simultaneously in a confocal cavity, which makes a theoretical approach of the system very difficult, and the lack of long term stability of the setup, which induces a large dispersion on the experimental results, prevent us from a more quantitative comparison between theory and experiments, which has been tackled in the case of the multimode VCSEL, for example [9].

VI. CONCLUSION

The results presented in this paper show that the intensity correlations in a confocal OPO are at the same time below the standard quantum limit and not uniformly distributed inside the beams, which is a clear evidence that the quantum state generated by such an OPO is a multimode nonclassical state of light. This experiment showed also that even in the multimode case, the intensity fluctuations of the signal and idler beams remain quantum correlated. It would be very interesting to find a theoretical explanation, even qualitative, to the fact that, in our experimental configuration, the central part of the beams seems to be less quantum correlated than the outer parts. We plan to extend this study in the case of an OPO working in a lower degeneracy cavity, where only some few modes are allowed to oscillate simultaneously. The small number of oscillating modes can lead to a detailed theoretical description of the system. Another interesting regime is the operation below threshold, where the comparison with theory is somehow simpler, but which requires a spatially resolved homodyne detection. For a more general point, this demonstration of an intrinsic multimode emission of signal and idler beams in the quantum regime of the above threshold OPO, opens interesting prospects for the study and use of transverse quantum effects in bright beams.

ACKNOWLEDGMENTS

Laboratoire Kastler-Brossel, of the Ecole Normale Supérieure and the Université Pierre et Marie Curie, is associated with the Centre National de la Recherche Scientifique. This work was supported by the European Commission in the framework of QUANTIM Project No. IST-2000-26019. M.M. wishes to thank Coordenação de Aperfeiçoamento de Pessoal de Nível Superior (CAPES-BR) and Fundação de Amparo à Pesquisa do Estado de São Paulo (FAPESP-BR) for funding.

[1] L.A. Wu, H.J. Kimble, J.L. Hall, and H. Wu, Phys. Rev. Lett. **57**, 2520 (1986).
[2] J. Mertz, T. Debuisschert, A. Heidmann, C. Fabre, and E. Giacobino, Opt. Lett. **16**, 1234 (1991).
[3] K. Schneider, R. Bruckmeier, H. Hansen, S. Schiller, and J. Mlynek, Opt. Lett. **21**, 1396 (1996).
[4] K. Kasai, Gao Jiangrui, and C. Fabre, Europhys. Lett. **40**, 25 (1997).
[5] M.I. Kolobov and C. Fabre, Phys. Rev. Lett. **85**, 3789 (2000).
[6] C. Fabre, J.B. Fouet, and A. Maître, Opt. Lett. **25**, 76 (2000).
[7] N. Treps, U. Andersen, B. Buchler, P.K. Lam, A. Maître, H.-A. Bachor, and C. Fabre, Phys. Rev. Lett. **88**, 203601 (2002).

[8] M.D. Levenson, W.H. Richardson, and S.H. Perlmutter, Opt. Lett. **14**, 779 (1989).
[9] J.-P. Hermier, A. Bramati, A.Z. Khoury, E. Giacobino, J.-Ph. Poizat, T.J. Chang, and Ph. Grangier, J. Opt. Soc. Am. B **16**, 2140 (1999); A. Bramati, J.-P. Hermier, A.Z. Khoury, E. Giacobino, P. Schnitzer, R. Michalzik, K.J. Ebeling, J.-Ph. Poizat, and Ph. Grangier, Opt. Lett. **24**, 893 (1999); C.L. Garrido Alzar, S.M. de Paula, M. Martinelli, R.J. Horowicz, A.Z. Khoury, and G.A. Barbosa, J. Opt. Soc. Am. B **18**, 1189 (2001).
[10] W.A.T. Nogueira, S.P. Walborn, S. Pádua, and C.H. Monken, Phys. Rev. Lett. **86**, 4009 (2001).
[11] M.I. Kolobov and I.V. Sokolov, Zh. Eksp. Teor. Fiz. **96**, 1945 (1989) [Sov. Phys. JETP **69**, 1097 (1989)].
[12] M.I. Kolobov, Rev. Mod. Phys. **71**, 1539 (1999).
[13] A. Gatti and L.A. Lugiato, Phys. Rev. A **52**, 1675 (1995).
[14] L.A. Lugiato and A. Gatti, Phys. Rev. Lett. **70**, 3868 (1993).
[15] L.A. Lugiato and I. Marzoli, Phys. Rev. A **52**, 4886 (1995).
[16] M. Marte, H. Ritsch, K.I. Petsas, A. Gatti, L.A. Lugiato, C. Fabre, and D. Leduc, Opt. Express **3**, 71 (1998).
[17] L.A. Lugiato and Ph. Grangier, J. Opt. Soc. Am. B **14**, 225 (1997).
[18] C. Schwob, P.F. Cohadon, C. Fabre, M.A.M. Marte, H. Ritsch, A. Gatti, and L. Lugiato, Appl. Phys. B: Lasers Opt. **66**, 685 (1998).
[19] C. Fabre, in *Quantum Fluctuations*, 1995 Les Houches Lectures, edited by S. Reynaud, E. Giacobino, and J. Zinn-Justin (Elsevier Science, Amsterdam, 1997) p. 181.
[20] M. Vaupel, A. Maître, and C. Fabre, Phys. Rev. Lett. **83**, 5278 (1999).
[21] N. Treps, Doctoral thesis, Université Paris VI (unpublished).
[22] G. Izús, M. Santagiustina, M. San Miguel, and P. Colet, J. Opt. Soc. Am. B **16**, 1592 (1999); M. Santagiustina, P. Colet, M. San Miguel, and D. Walgraef, Opt. Lett. **23**, 1167 (1998).
[23] A. Gatti, L.A. Lugiato, G.-L. Oppo, R. Martin, P. di Trapani, and A. Berzanskis, Opt. Express **1**, 21 (1997).
[24] S. Ducci, N. Treps, A. Maître, and C. Fabre, Phys. Rev. A **64**, 023803 (2001).
[25] H. Kogelnik and T. Li, Appl. Opt. **5**, 1550 (1966).
[26] Technical data from the manufacturer Cristal Laser.
[27] Antony E. Siegman, *Lasers* (University Science Books, Mill Valley, 1986).
[28] A. Heidmann, R.J. Horowicz, S. Reynaud, E. Giacobino, C. Fabre, and G. Camy, Phys. Rev. Lett. **59**, 2555 (1987).

PHYSICAL REVIEW A **72**, 013806 (2005)

Multimode squeezing properties of a confocal optical parametric oscillator: Beyond the thin-crystal approximation

L. Lopez, S. Gigan, N. Treps, A. Maître, and C. Fabre
Laboratoire Kastler Brossel, Université Pierre et Marie Curie, Campus Jussieu, Case 74, 75252 Paris cedex 05, France

A. Gatti
INFM, Dipartimento di Scienze Fisiche e Matematiche, Universitá dell'Insubria, Via valleggio 11, 22100 Como, Italy
(Received 4 March 2005; published 8 July 2005)

Up to now, transverse quantum effects (usually labeled as "quantum imaging" effects) which are generated by nonlinear devices inserted in resonant optical cavities have been calculated using the "thin-crystal approximation," i.e., taking into account the effect of diffraction only inside the empty part of the cavity, and neglecting its effect in the nonlinear propagation inside the nonlinear crystal. We introduce in the present paper a theoretical method which is not restricted by this approximation. It allows us in particular to treat configurations closer to the actual experimental ones, where the crystal length is comparable to the Rayleigh length of the cavity mode. We use this method in the case of the confocal optical parametric oscillator, where the thin-crystal approximation predicts perfect squeezing on any area of the transverse plane, whatever its size and shape. We find that there exists in this case a "coherence length" which gives the minimum size of a detector on which perfect squeezing can be observed, and which gives therefore a limit to the improvement of optical resolution that can be obtained using such devices.

DOI: 10.1103/PhysRevA.72.013806 PACS number(s): 42.50.Dv, 42.65.Yj, 42.60.Da

I. INTRODUCTION

Nonlinear optical elements inserted in optical cavities have been known for a long time to produce a great variety of interesting physical effects, taking advantage of the field enhancement effect and of the feedback provided by a resonant cavity [1,2]. In particular, a great deal of attention has been devoted to cavity-assisted nonlinear transverse effects, such as pattern formation [4] and spatial soliton generation [5]. More recently the quantum aspects of these phenomena have begun to be studied, mainly at the theoretical level, under the general name of "quantum imaging," especially in planar or confocal cavities.

Almost all the investigations relative to intracavity nonlinear effects, both at the classical and quantum level, have been performed within the *mean-field approximation*, in which one considers that the different interacting fields undergo only weak changes through their propagation inside the cavity, in terms of their longitudinal and transverse parameters. This almost universal approach simplifies a great deal the theoretical investigations, and numerical simulations are generally needed if one wants to go beyond this approximation [9]. It implies in particular that diffraction is assumed to be negligible inside the nonlinear medium, which limits the applicability of the method to nonlinear media whose length l_c is much smaller than the Rayleigh length z_R of the cavity modes z_c (so-called "thin" medium). This is a configuration that experimentalists do not like much: they prefer to operate in the case $l_c \simeq z_c$ which yields a much more efficient nonlinear interaction for a given pump power [10]. If one wants to predict results of experiments in realistic situations, one therefore needs to extend the theory beyond the usual thin nonlinear medium approximation, and take into account diffraction effects occurring together with the nonlinear interaction inside the medium.

The effects of simultaneous diffraction and nonlinear propagation have already been taken into account in the case of free propagation, i.e., without optical cavity around the nonlinear crystal, and they have been found to have a direct influence on the shape of the propagating beam [3]. These effects have also been studied in detail at the quantum level in the parametric amplifier case [8], and recently for the soliton case [11]. In contrast, they do not play a significant role when the nonlinear medium is inserted in an optical cavity with nondegenerate transverse modes, which imposes the shape of the mode. But they are of paramount importance in the case of cavities having degenerate transverse modes, such as a plane or confocal cavity, which do not impose the transverse structure of the interacting fields, and which are used to generate multimode quantum effects.

Within the thin-crystal approximation, i.e., taking into account diffraction effects only outside the crystal, striking quantum properties have been predicted to occur in a degenerate optical parametric oscillator (OPO) below threshold using a confocal cavity [12,13]: this device generates quadrature squeezed light which is multimode in the transverse domain. It was shown in the case of a plane pump that the level of squeezing measured at the output of such an OPO neither depends on the spatial profile of the local oscillator used to probe it, nor on the size of the detection region. This implies that a significant quantum noise reduction, in principle tending to perfection when one approaches the oscillation threshold from below, can be observed in arbitrarily small portions of the down-converted beam. Therefore in this model there is no limitation in the transverse size of the domains in which the quantum noise is reduced when the OPO works in the exact confocal configuration. Such a multimode squeezed light appears thereby as a very promising tool to increase the resolution in optical images beyond the wavelength limit.

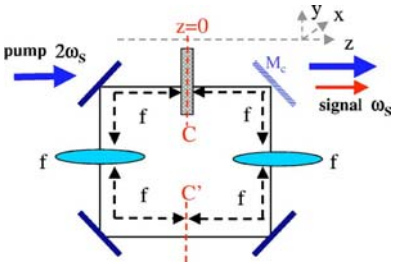

FIG. 1. Confocal ring cavity. The mirrors transmit the pump wave and reflect the signal wave, with the exception of mirror M_c that partially transmits the signal.

It is therefore very important to make a more realistic theoretical model of this system, which is no longer limited by the thin-crystal approximation, to see whether the predicted local squeezing is still present in actual experimental realizations in which the crystal length is of the order of the Rayleigh range of the resonator. This is the purpose of the present paper, in which we will show that the presence of a long crystal inside the resonator imposes a lower limit to the size of the regions in which squeezing can be measured ("coherence area"), which is proportional to $w_c^2 l_c / z_R$, where w_c is the cavity beam waist, l_c is the crystal length, and z_R the Rayleigh range of the resonator.

The following section (Sec. II) is devoted to the general description of the model that is used to treat the effect of diffraction inside the crystal, using the assumption that the single pass nonlinear interaction is weak in the crystal. We then describe in Sec. III the method that is used to determine the squeezing spectra measured in well-defined homodyne detection schemes. We give in Sec. IV and V the results for such quantities respectively in the near field and in the far field, and conclude in Sec. VI.

II. MODEL

A. Assumptions of the model

Let us consider a confocal cavity, that for simplicity we take as a ring cavity of the kind shown schematically in Fig. 1 ([14,15]). It is formed by four plane mirrors and two lenses having a focal length equal to one-quarter of the total cavity length, and symmetrically placed along the cavity, so that the focal points coincide at two positions C and C'. It contains a type-I parametric medium of length l_c, centered on the point C (see figure). It is pumped by a field A_p of frequency $2\omega_s$ having a Gaussian shape and focused in the plane containing the point C. In such a plane the variation of the mean envelope with the transverse coordinate $\mathbf{x}$ is given by

$$A_p(\mathbf{x}) = A_p \exp\left(-\frac{|\mathbf{x}|^2}{w_p^2}\right). \tag{1}$$

We assume that the mirrors are totally transparent for the pump wave, and perfectly reflecting for the field at frequency ω_s, except for the coupling mirror M_c, which has a small transmission t at this frequency. The system was described in Ref. [13] under the thin parametric medium approximation. We will follow here the same approach, generalized to the case of a thick parametric medium of length l_c. The intracavity signal field at frequency ω_s is described by a field envelope operator $\hat{B}(\mathbf{x},z)$, where z is the longitudinal coordinate along the cavity ($z=0$ corresponding to plane C), obeying the standard equal time commutation relation at a given transverse plane at position z:

$$[\hat{B}(\mathbf{x},z,t),\hat{B}^\dagger(\mathbf{x}',z,t)] = \delta(\mathbf{x}-\mathbf{x}'). \tag{2}$$

As we are only interested in the regime below threshold and without pump depletion, the pump field fluctuations do not play any role.

In a confocal resonator the cavity resonances correspond to complete sets of Gauss-Laguerre modes with a given parity for transverse coordinate inversion; we assume that a set of cavity *even* modes is tuned to resonance with the signal field, and that the odd modes are far off resonance. It is then useful to introduce the even part of the field operator:

$$\hat{B}_+(\mathbf{x},z,t) = \frac{1}{2}[\hat{B}(\mathbf{x},z,t) + \hat{B}(-\mathbf{x},z,t)], \tag{3}$$

which obeys a modified commutation relation:

$$[\hat{B}_+(\mathbf{x},z,t),\hat{B}_+^\dagger(\mathbf{x}',z,t)] = \frac{1}{2}[\delta(\mathbf{x}-\mathbf{x}') + \delta(\mathbf{x}+\mathbf{x}')] \tag{4}$$

and can be written as an expansion over the even Gauss-Laguerre modes:

$$\hat{B}_+(\mathbf{x},z,t) = \sum_{p,\text{leven}} f_{p,l}(\mathbf{x},z)\hat{a}_{p,l}(z,t), \tag{5}$$

where $\hat{a}_{p,l}(z,t)$ is the annihilation operator of a photon in mode (p,l) at the cavity position z and at time t.

The interaction Hamiltonian of the system in the interaction picture is given by

$$H_{\text{int}} = \frac{i\hbar g}{2l_c}\int_{-l_c/2}^{l_c/2} dz' \int\int d^2x' \{A_P(\mathbf{x}',z')[\hat{B}_+^\dagger(\mathbf{x}',z',t)]^2 - \text{H.c.}\}, \tag{6}$$

where g is the coupling constant proportional to the second order nonlinear susceptibility $\chi^{(2)}$. This equation generalizes the thin medium parametric Hamiltonian of Ref. [16].

B. Evolution equation in the image plane (near field)

In previous approaches [12,13], the crystal was assumed to be thin, so that one could neglect the longitudinal dependence of A_P and $\hat{B}_+$ along the crystal length in the Hamiltonian (6). This cannot be done in a thick crystal. We will, nevertheless, make a simplifying assumption which turns out to be very realistic in the cw regime, with pump powers below 1 W. We assume that the nonlinear interaction is very weak, so that it does not affect much the field amplitudes in a single pass through the crystal. We will therefore remove the z dependence of the operators $\hat{a}_{p,l}$ in Eqs. (5) and (6), assuming $\hat{a}_{p,l}(z,t)=\hat{a}_{p,l}(z=0,t)=\hat{a}_{p,l}(t)$, where $z=0$ is the

crystal and cavity center C. The longitudinal variation of the signal operator $\hat{B}$ is then only due to diffraction and is described by the well-known z dependence of the modal functions $f_{p,l}(\mathbf{x},z)$. This assumption leads to a rather simple expression of the commutator for the $\hat{B}_+$ field at different positions inside the crystal:

$$[\hat{B}_+(\mathbf{x},z,t),\hat{B}_+^\dagger(\mathbf{x}',z',t')] = G_+^*(z-z';\mathbf{x},\mathbf{x}'). \quad (7)$$

Here $G_+(z;\mathbf{x},\mathbf{x}')$ is the symmetrized part of the Fresnel propagator $G(z;\mathbf{x},\mathbf{x}')$, describing the field linear propagation inside the crystal:

$$G_+(z;\mathbf{x},\mathbf{x}') = \frac{1}{2}[G(z;\mathbf{x},\mathbf{x}') + G(z;\mathbf{x},-\mathbf{x}')] \quad (8)$$

with

$$G(z;\mathbf{x},\mathbf{x}') = \frac{ik_s}{2\pi z} e^{ik_s(|\mathbf{x}-\mathbf{x}'-\boldsymbol{\rho}_s z|^2)/2z}, \quad (9)$$

where $k_s = n_s\omega_s/c$ is the field wave number, with n_s being the index of refraction at frequency ω_s, and we have introduced a walk-off term, present only if the signal wave is an extraordinary one, described by the two-dimensional walk-off angle $\boldsymbol{\rho}_s$.

It is now possible to derive the time evolution of the field operator $\hat{B}(\mathbf{x},z,t)$ due to the parametric interaction. We will, for example, calculate it at the midpoint plane $z=0$ of the crystal:

$$\left.\frac{\partial \hat{B}_+}{\partial t}(\mathbf{x},0,t)\right|_{\text{int}} = g\int\int d^2x'' K_{\text{int}}(\mathbf{x},\mathbf{x}'')\hat{B}_+^\dagger(\mathbf{x}'',0,t) \quad (10)$$

with the integral kernel K_{int} given by

$$K_{\text{int}}(\mathbf{x},\mathbf{x}'') = \frac{1}{l_c}\int_{-l_c/2}^{l_c/2} dz' \times \int\int d^2x' A_P(\mathbf{x}',z') G_+^*(z';\mathbf{x}',\mathbf{x}) G_+^*(z';\mathbf{x}',\mathbf{x}''). \quad (11)$$

In the limit of a thin crystal considered in Refs. [12,13], Eq. (11) is replaced by the simpler expression

$$\left.\frac{\partial \hat{B}_+}{\partial t}(\mathbf{x},0,t)\right|_{\text{int}} = gA_P(\mathbf{x})\hat{B}_+^\dagger(\mathbf{x},0,t). \quad (12)$$

In the thin-crystal case [Eq. (12)], the parametric interaction is local, i.e., the operators at different positions of the transverse plane are not coupled to each other, whereas in the thick-crystal case [Eq. (11)], the parametric interaction mixes the operators at different points of the transverse plane, over areas of finite extension. Note, however, that operators corresponding to different z values are not coupled to each other, because of our assumption of weak parametric interaction. This situation is very close to the one considered in Refs. [6–8] for parametric down-conversion and amplification in a single-pass crystal, where finite transverse coherence areas for the spatial quantum effects arise because of the finite spatial emission bandwidth of the crystal. In a similar way, in our case the spatial extension of the kernel K_{int} will turn out to give the minimum size in which spatial correlation or local squeezing can be observed in such a system. The analogy will become more evident in the next section, where we will explicitly solve the propagation equation of the Fourier spatial modes along the crystal.

In order to get the complete evolution equation for the signal beam, one must add the free Hamiltonian evolution of the intracavity beam and the damping effects. This part of the treatment is standard [17], and is identical to the case of a thin crystal inserted in a confocal cavity [13]. The final evolution equation reads

$$\frac{\partial \hat{B}_+}{\partial t}(\mathbf{x},0,t) = -\gamma(1+i\Delta)\hat{B}_+(\mathbf{x},0,t) + g\int\int d^2x'' K_{\text{int}}(\mathbf{x},\mathbf{x}'')\hat{B}_+^\dagger(\mathbf{x}'',0,t) + \sqrt{2\gamma}\hat{B}_{+in}(\mathbf{x},0,t), \quad (13)$$

where γ is the cavity escape rate, Δ the normalized cavity detuning of the even family of modes closest to resonance with the signal field, and $\hat{B}_{\text{in}}$ the input field operator.

In order to evaluate the coupling kernel, let us first take into account the diffraction of the pump field, focused at the center of the crystal, $z=0$. It is described by the Fresnel propagator $G_p(z;\mathbf{x},\mathbf{x}')$, equal to Eq. (9) when one replaces k_s by the pump wave number k_p, and the signal walk-off angle $\boldsymbol{\rho}_s$ with the pump walk-off angle $\boldsymbol{\rho}_p$. One then gets

$$K_{\text{int}}(\mathbf{x},\mathbf{x}'') = \frac{1}{l_c}\int_{-l_c/2}^{l_c/2} dz' \int d^2x' \int d^2y\, A_p(\mathbf{y}) G_p(z',0;\mathbf{x}',\mathbf{y}) \times G_+^*(z',0;\mathbf{x}',\mathbf{x}) G_+^*(z',0;\mathbf{x}',\mathbf{x}''). \quad (14)$$

Assuming for simplicity exact collinear phase matching $k_p = 2k_s$, and neglecting the walk-off of the extraordinary wave, four of the five integrations can be exactly performed, and one finally gets

$$K_{\text{int}}(\mathbf{x},\mathbf{x}'') = \frac{1}{2}\left[A_p\left(\frac{\mathbf{x}+\mathbf{x}''}{2}\right)\Delta(\mathbf{x}-\mathbf{x}'') + A_p\left(\frac{\mathbf{x}-\mathbf{x}''}{2}\right)\Delta(\mathbf{x}+\mathbf{x}'')\right] \quad (15)$$

with

$$\Delta(\mathbf{x}\pm\mathbf{x}'') = \frac{ik_s}{4\pi l_c}\int_{-l_c/2}^{l_c/2}\frac{dz'}{z'} e^{(ik_s/4z')|\mathbf{x}\pm\mathbf{x}''|^2}. \quad (16)$$

It can be easily shown that the function $\Delta(\mathbf{x}\pm\mathbf{x}'')$ tends to the usual two-dimensional distribution $\delta(\mathbf{x}\pm\mathbf{x}'')$ when $l_c\to 0$, and that it can be written in terms of the integral sine function $\mathrm{Si}(x)=\int_0^x(\sin u du/u)$ [18],

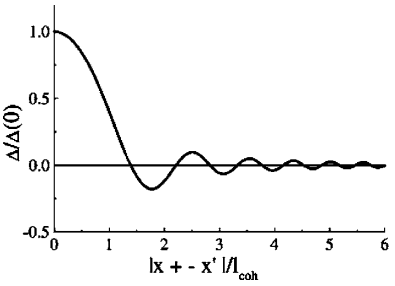

FIG. 2. Evaluation of the coupling kernel. Δ given by Eq. (16) is plotted as a function of $|\mathbf{x}\pm\mathbf{x}''|$ scaled to the coherence length (18). The first zero of Δ is obtained for the value 1.37 of the coordinate.

$$\Delta(\mathbf{x}\pm\mathbf{x}'') = \frac{k_s}{2\pi l_c}\left[\frac{\pi}{2} - \mathrm{Si}\left(\frac{k_s|\mathbf{x}\pm\mathbf{x}''|^2}{2l_c}\right)\right]. \tag{17}$$

This expression shows us that Δ takes negligible values when $|\mathbf{x}\pm\mathbf{x}''| \gg \sqrt{\lambda l_c/\pi n_s}$. Figure 2 plots Δ as a function of the distance $|\mathbf{x}\pm\mathbf{x}''|$ scaled to

$$l_{\mathrm{coh}} = \sqrt{\frac{\lambda l_c}{\pi n_s}} = w_C\sqrt{\frac{l_c}{n_s z_C}}, \tag{18}$$

where w_C and z_C are the cavity waist and Rayleigh range, respectively. This expression shows that when the crystal length is on the order of the Rayleigh range of the resonator, the transverse coherence length is on the order of the cavity waist. Recalling that the pump field has a Gaussian shape of waist w_p, in order to have a multimode operation one must therefore use a defocused pump, with $w_p \gg w_c$, or alternatively use a crystal much shorter than the Rayleigh range of the resonator, which is detrimental for the oscillation threshold of the OPO. The relevant scaling parameter of our problem is therefore

$$b = \frac{w_p^2}{l_{\mathrm{coh}}^2} = 2n_s\frac{z_p}{l_c}, \tag{19}$$

where z_p is the Rayleigh or diffraction length of the pump beam. This parameter sets the number of spatial modes that can be independently excited, and it will turn out to give also the number of modes that can be independently squeezed.

C. Evolution equation in the spatial Fourier domain (far field)

In this section we will investigate the intracavity dynamics of the spatial Fourier amplitude of the signal field, which will offer an alternative formulation of the problem. Fourier modes can be observed in the far-field plane with respect to the crystal center C, which in turn can be detected in the focal plane of a lens placed outside the cavity. Let us introduce the spatial Fourier transform of the signal field envelope operator,

$$\hat{B}_+(\mathbf{q},z,t) = \int\frac{d^2x}{2\pi}\hat{B}_+(\mathbf{x},z,t)e^{-i\mathbf{q}\cdot\mathbf{x}} = \frac{1}{2}[\hat{B}(\mathbf{q},z,t) + \hat{B}(-\mathbf{q},z,t)]. \tag{20}$$

Equation (14) becomes

$$\frac{\partial\hat{B}_+}{\partial t}(\mathbf{q},0,t) = -\gamma(1+i\Delta)\hat{B}_+(\mathbf{q},0,t) + g\int d^2q''\tilde{K}_{\mathrm{int}}(\mathbf{q},\mathbf{q}'')\hat{B}_+^\dagger(\mathbf{q}'',0,t) + \sqrt{2\gamma}\tilde{B}_{+\mathrm{in}}(\mathbf{q},0,t), \tag{21}$$

where the coupling Kernel $\tilde{K}_{\mathrm{int}}(\mathbf{q},\mathbf{q}'')$ is the Fourier transform of the kernel (15) with respect to both arguments. Straightforward calculations show that

$$\tilde{K}_{\mathrm{int}}(\mathbf{q},\mathbf{q}') = \frac{1}{2}\left[\tilde{A}_p(\mathbf{q}+\mathbf{q}')\mathrm{sinc}\left(\frac{l_c}{2k_s}\left|\frac{\mathbf{q}-\mathbf{q}'}{2}\right|^2\right) + \tilde{A}_p(\mathbf{q}-\mathbf{q}')\mathrm{sinc}\left(\frac{l_c}{2k_s}\left|\frac{\mathbf{q}+\mathbf{q}'}{2}\right|^2\right)\right], \tag{22}$$

where $\tilde{A}_p$ is the spatial Fourier transform of the Gaussian pump profile (1), i.e., $\tilde{A}_p(\mathbf{q}) = (w_p^2/2)A_p\exp[-|\mathbf{q}|^2(w_p^2/4)]$. {and where sinc represents the Sinus Cardinal function.}

The result (22) can also be derived by solving the propagation equation of the pump and signal wave inside a $\chi^{(2)}$ crystal directly in the Fourier domain and in the limit of weak parametric gain. We will follow here the same approach as in Refs. [8,19], and write the propagation equation in terms of the spatiotemporal Fourier transform field operators $\hat{A}_j(\mathbf{q},\omega,z)$ of the pump ($j=p$) and signal ($j=s$) waves. Since the cavity linewidth is smaller by several orders of magnitude than the typical frequency bandwidth of the crystal, the cavity filters a very small frequency bandwidth around the carrier frequency ω_s of the signal; moreover, we have assumed that the pump is monochromatic, so that we can safely neglect the frequency argument in the propagation equations, which take the form

$$\frac{\partial\hat{A}_j}{\partial z}(\mathbf{q},z) = ik_{jz}(\mathbf{q})\hat{A}_j(\mathbf{q},z) + \hat{P}_j^{\mathrm{NL}}(\mathbf{q},z), \tag{23}$$

where $\hat{P}_j^{\mathrm{NL}}$ is the nonlinear term, arising from the second-order nonlinear susceptibility of the crystal. $k_{jz}(\mathbf{q}) = \sqrt{k_j^2 - q^2}$ is the projection along the z axis of the wave vector, with $k_j = k_j(\omega_j,\mathbf{q})$ being the wave number, which for extraordinary waves depends also on the propagation direction (identified by $\mathbf{q}$). For the pump wave, we assume an intense coherent beam, that we suppose undepleted by the parametric down-conversion process in a single pass through the crystal, so that

$$\hat{A}_p(\mathbf{q},z) \to \tilde{A}_p(\mathbf{q},z) = e^{ik_{pz}(\mathbf{q})z}A_p(\mathbf{q},0), \tag{24}$$

where we take the crystal center as the reference plane $z=0$. For the signal, the propagation equation is more easily solved by setting $\hat{A}_s(\mathbf{q},z) = \exp[ik_{sz}(\mathbf{q})z]\hat{a}_s(\mathbf{q},z)$. The evolu-

tion along z of the operator $\hat{a}_s$ is only due to the parametric interaction and is governed by the equation (see, e.g., Refs. [8,19] for more details)

$$\frac{\partial \hat{a}_s}{\partial z}(\mathbf{q},z) = \frac{\sigma}{l_c}\int d^2q' A_p(\mathbf{q}+\mathbf{q}',0)\hat{a}_s^\dagger(\mathbf{q}',z)e^{i\delta(\mathbf{q},\mathbf{q}')z}, \tag{25}$$

where σ/l_c is the parametric gain per unit length, and we have introduced the phase mismatch function

$$\delta(\mathbf{q},\mathbf{q}') = k_{pz}(\mathbf{q}+\mathbf{q}') - k_{sz}(\mathbf{q}) - k_{sz}(\mathbf{q}'). \tag{26}$$

Equation (25) has the formal solution

$$\hat{a}_s\left(\mathbf{q},\frac{l_c}{2}\right) = \hat{a}_s\left(\mathbf{q},-\frac{l_c}{2}\right) + \frac{\sigma}{l_c}\int_{-l_c/2}^{l_c/2} dz' \times \int d^2q' A_p(\mathbf{q}+\mathbf{q}',0)\hat{a}_s^\dagger(\mathbf{q}',z')e^{i\delta(\mathbf{q},\mathbf{q}')z'}. \tag{27}$$

Assuming a weak parametric efficiency $\sigma \ll 1$, we can solve this equation iteratively. At first order in σ the solution reads

$$\hat{a}_s\left(\mathbf{q},\frac{l_c}{2}\right) = \hat{a}_s\left(\mathbf{q},-\frac{l_c}{2}\right) + \sigma\int d^2q' K_1(\mathbf{q},\mathbf{q}')\hat{a}_s^\dagger(\mathbf{q}',0), \tag{28}$$

with

$$K_1(\mathbf{q},\mathbf{q}') = \tilde{A}_p(\mathbf{q}+\mathbf{q}',0)\mathrm{sinc}\left(\delta(\mathbf{q},\mathbf{q}')\frac{l_c}{2}\right). \tag{29}$$

We observe that in the paraxial approximation $k_{jz}(\mathbf{q}) \approx k_j - \boldsymbol{\rho}_j\cdot\mathbf{q} - q^2/2k_j$, where ρ_j is the walk-off angle and $k_j = n_j\omega_j/c$. The phase mismatch function is hence given by

$$\delta(\mathbf{q},\mathbf{q}') = k_p - 2k_s + (\boldsymbol{\rho}_s - \boldsymbol{\rho}_p)\cdot(\mathbf{q}+\mathbf{q}') - \frac{|\mathbf{q}+\mathbf{q}'|^2}{2k_p} + \frac{1}{2k_s}(q^2+q'^2). \tag{30}$$

Assuming exact phase matching $k_p = 2k_s$, and neglecting the walk-off term, the argument of the sinc function in Eq. (29) becomes

$$\delta(\mathbf{q},\mathbf{q}')\frac{l_c}{2} = \frac{l_c}{2k_s}\left|\frac{\mathbf{q}-\mathbf{q}'}{2}\right|^2. \tag{31}$$

In this way we start to recover the result of the Hamiltonian formalism used to derive Eqs. (22) and (14), where, however, the effect of walk-off and phase mismatch were neglected for simplicity. Indeed, it is not difficult to show that the variation of the intracavity field operator $\hat{B}_+(\mathbf{q},0,t)$ per cavity round-trip time τ, due to the parametric interaction in a single pass through the crystal, is

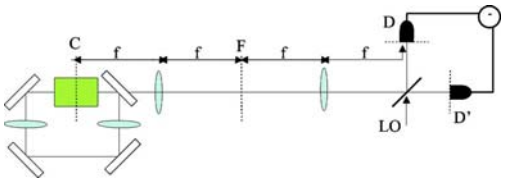

FIG. 3. Balanced homodyne detection scheme in the near field. Two matching lenses of focal f are used to image the cavity center C at the detection planes D and D'.

$$\frac{1}{\tau}\Delta\hat{B}_+(\mathbf{q},0,t)\bigg|_{\mathrm{int}} = \frac{\sigma}{\tau}\int d^2q'\frac{1}{2}[K_1(\mathbf{q},\mathbf{q}') + K_1(\mathbf{q},-\mathbf{q}')]\hat{B}_+^\dagger(\mathbf{q}',0,t). \tag{32}$$

This approach permits us to understand the physical origin of the sinc terms in the coupling kernel of Eq. (22) [which are the Fourier transform of the Δ terms in Eq. (15)], that is, the limited phase-matching bandwidth of the nonlinear crystal. For a crystal of negligible length, phase matching is irrelevant and there is no limitation in the spatial bandwidth of down-converted modes, whereas for a finite crystal the cone of parametric fluorescence has an aperture limited to a bandwidth of transverse wave vectors $\Delta q \approx 1/l_{\mathrm{coh}} \propto 1/\sqrt{\lambda l_c}$. As a consequence of the confocal geometry, the cavity ideally transmits all the Fourier modes, so that the only limitation in spatial bandwidth is that arising from phase matching along the crystal.

We notice that if the pump is defocused enough, the phase-matching limitation results in a limitation of the spot size $\propto 1/l_{\mathrm{coh}}$ in the far field with respect to the cavity center. Inside this spot, modes are coupled because of the finite size of the pump beam [the terms $\propto\tilde{A}_P$ in Eq. (22)], inside a region of size $\propto w_p^{-1}$. The relevant parameter which sets the number of Fourier modes that can be independently excited is again given by $b = w_p^2/l_{\mathrm{coh}}^2$ [see Eq. (19)].

III. HOMODYNE DETECTION AND SQUEEZING SPECTRUM

A. Homodyne detection scheme in the far field and near field

The method used for measuring the noise-spectrum outside the cavity is a balanced homodyne detection scheme [20]. We will use two configurations: the near-field configuration (x-position basis described in Sec. II B) and the far-field configuration (q-vector basis described in Sec. II C). The complete detection scheme in the near-field case is schematically shown in Fig. 3. The two matching lenses of focal length f image the crystal and cavity center plane C onto the detection planes D and D'. The image focal plane F of the first lens coincides with the object focal plane of the second one, and represents the far-field plane with respect to the cavity center C. In planes C, F, D the signal field has its minimum waist, and it has a flat wave front.

The detection scheme in the far field is obtained by using only one lens as depicted in Fig. 4. The focal length f lens is used to image the far-field plane with respect of the cavity center C onto the detection plane D.

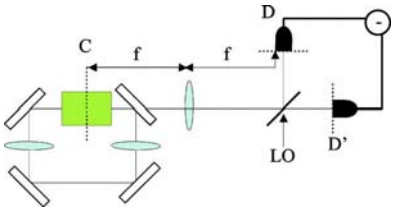

FIG. 4. Balanced homodyne detection scheme in the far field. A matching lens of focal f is used to make the far-field image of the cavity center C at the detection planes D and D'.

The symmetrical beam-splitter BS (reflection and transmission coefficients $r=1/\sqrt{2}$ and $t=1/\sqrt{2}$) mixes the output signal field with an intense stationary and coherent beam $\alpha_L(\mathbf{x},z)$, called local oscillator (LO). Note that for all the fields being evaluated at the beam-splitter location, we will omit the z dependence in the following. The difference photocurrent is a measure of the quadrature operator:

$$E_H(\Omega)=\int_{\text{det}} d\mathbf{x}[B^{\text{out}}(\mathbf{x},\Omega)\alpha_L^*(\mathbf{x})+B^{\text{out}+}(\mathbf{x},-\Omega)\alpha_L(\mathbf{x})], \tag{33}$$

where "det" is the reciprocal image of the photodetection region at the beam-splitter plane, and assumed to be identical for the two photodetectors. We have also assumed here that the quantum efficiency of the photodetector is equal to 1. Here B^{out} is the sum of its odd and even part:

$$B^{\text{out}}(\mathbf{x},\Omega)=B_+^{\text{out}}(\mathbf{x},\Omega)+B_-^{\text{out}}(\mathbf{x},\Omega). \tag{34}$$

The fluctuations $\delta E_H(\Omega)$ of the homodyne field around steady state are characterized by a noise spectrum:

$$V(\Omega)=\int_{-\infty}^{+\infty} d\Omega'\langle \delta E_H(\Omega)\delta E_H(\Omega')\rangle = N+S(\Omega), \tag{35}$$

where E_H is normalized so that N gives the mean photon number measured by the detector,

$$N=\int_{\text{det}} dx|\alpha_L(x)|^2. \tag{36}$$

N represents the shot-noise level, and S is the normally ordered part of the fluctuation spectrum, which accounts for the excess or decrease of noise with respect to the standard quantum level.

B. Input-output relation

The relation linking the outgoing fields $B_\pm^{\text{out}}(\mathbf{x},t)$ with the intracavity and input fields at the cavity input-output port [17] is

$$B_\pm^{\text{out}}(\mathbf{x},t)=\sqrt{2\gamma}B_\pm(\mathbf{x},t)-B_\pm^{\text{in}}(\mathbf{x},t). \tag{37}$$

Equation (13) in the near-field [or Eq. (21) in the far-field case] is easily solved in the frequency domain, by introducing

$$B_\pm^{\text{in/out}}(\mathbf{x},\Omega)=\int \frac{dt}{\sqrt{2\pi}}B_\pm^{\text{in/out}}(\mathbf{x},t)e^{-i\Omega t}.$$

Taking into account the boundary condition (37), we obtain the input-output relation:

$$\begin{aligned}[i\Omega+\gamma(1+i\Delta)][B_+^{\text{out}}(\mathbf{x},\Omega)+B_+^{\text{in}}(\mathbf{x},\Omega)]&\\ =2\gamma B_+^{\text{in}}(\mathbf{x},\Omega)+\frac{\gamma}{i\Omega+\gamma(1-i\Delta)}\int\int d^2\mathbf{x}' K_{\text{int}}(\mathbf{x},\mathbf{x}')&\\ \times\Bigg(2\gamma B_+^{\text{in}+}(\mathbf{x}',-\Omega)+\int\int d^2\mathbf{x}''\gamma K_{\text{int}}^*(\mathbf{x}',\mathbf{x}'')[B_+^{\text{in}}(\mathbf{x}'',\Omega)&\\ +B_+^{\text{out}}(\mathbf{x}'',\Omega)]\Bigg).&\end{aligned} \tag{38}$$

In the case of a thin crystal in the near field [13] or a plane pump in the far field, this relation describes an infinite set of independent optical parametric oscillators. In these cases the squeezing spectrum can be calculated analytically as we will see in the following. But in other cases, this relation links all points in the transverse plane. In order to get the input-output relation, we have to inverse relation (38) by using a numerical method.

C. Numerical method

In order to inverse relation (38) by numerical means, we need to discretize the transverse plane in order to replace integrals by discrete sums. For the sake of simplicity, we will only describe here the solution in the single transverse dimension model: the cavity is assumed to consist of cylindrical mirrors, so that the the transverse fields depend on a single parameter y. In this case the electromagnetic fields are represented by vectors and the interaction terms by matrices. Straightforward calculations show that we can introduce the interaction functions $U(y,y')$ and $V(y,y')$ (calculated at resonance $\Delta=0$ and at zero frequency in near-field or far-field configurations) linking two different points in the transverse plane, so that relation (38) becomes

$$B_+^{\text{out}}(y)=\int_{-\infty}^{\infty} dy' U(y,y')B_+^{\text{in}}(y')+\int_{-\infty}^{\infty} dy' V(y,y')B_+^{in+}(y'). \tag{39}$$

Since we assumed that the odd part of the output field is in the vacuum state, B_-^{out} gives no contribution to the normally ordered part of the spectrum S, which can be calculated by using the input-output relation (21) for the even part of the field, and by using the commutation rules for the even part:

$$[B_\pm^{\text{in/out}}(x,t),B_\pm^{\text{in/out}+}(x',t')]=\frac{1}{2}[\delta(x-x')\pm\delta(x+x')]\delta(t-t'). \tag{40}$$

In the following, we will assume, as in Refs. [13,12], that the local oscillator has a constant phase profile $\varphi_L(\mathbf{x})=\varphi_L$, so that $\alpha_L(x)=|\alpha_L(x)|e^{i\varphi_L}$. We obtain the ordered part of the spectrum, normalized to the shot noise:

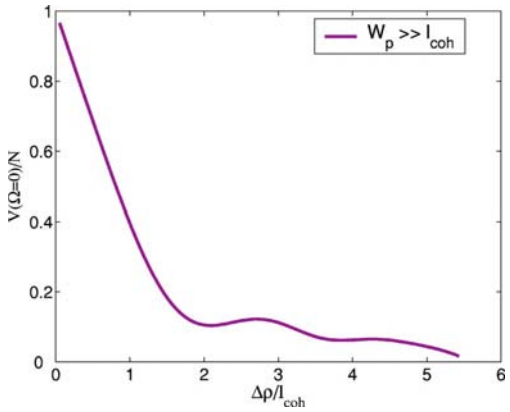

FIG. 5. Squeezing spectrum at zero frequency, normalized to the shot noise, as a function of the detector radius (scaled to l_{coh}).

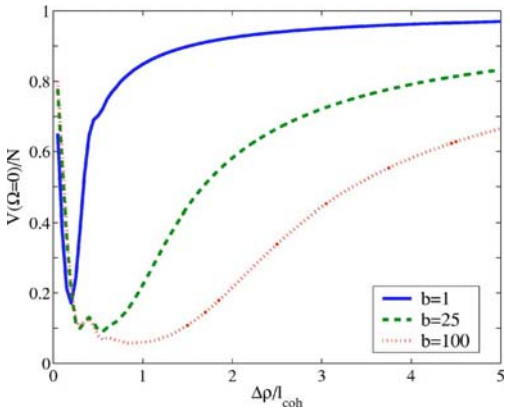

FIG. 6. Squeezing spectrum at zero frequency, normalized to the shot noise, as a function of the radial amplitude of the detector scaled to l_{coh}, plotted for several values of b.

$$\frac{S(0)}{N} = \frac{1}{\int_{\mathrm{det}} dy|\alpha_L|^2} \int\int_{\mathrm{det}^2} dxdx' \int_{-\infty}^{+\infty} dy|\alpha_L(x)||\alpha_L(x')| \times\{[V(x,y)V(x',y) + V(x,y)V(x,-y)] + \cos(2\varphi_L) \times[U(x,y)V(x',y) + U(x,y)V(x',-y)]\}. \quad (41)$$

Now, knowing the $U(y,y')$ and $V(y,y')$ interaction functions, we are able to calculate the squeezing spectrum in both near- and far-field cases.

IV. SQUEEZING SPECTRUM IN THE NEAR FIELD

In this section, we use the near-field homodyne detection (Fig. 3) described in Ref. [13]. As already said in Sec. II, in the near field, the thick crystal couples pixels contained in a region whose size is in the order of l_{coh} (18).

Let us study first the case of a plane-wave pump and a plane-wave local oscillator. As pointed out in Ref. [12], in this case and in the thin-crystal approximation, the level of squeezing does not depend on the width of the detection region. Figure 5 shows results predicted for a measurement performed with a circular detector of radius $\Delta\rho$ centered on the cavity axis (which is a symmetric detection area, as pointed out in Ref. [13]). We represent the squeezing spectrum at zero frequency as a function of the size of the detector, scaled to the coherence length $l_{\mathrm{coh}}=\sqrt{\lambda l_c/\pi n_s}$. We can see that for $\Delta\rho<l_c$, the squeezing tends to zero when $\Delta\rho \rightarrow 0$, as already predicted. For larger values of the detector size, perfect squeezing can be achieved. We can also see that the squeezing evolution is comparable to the Δ function evolution (Fig. 2).

In the more realistic case of finite-size pump, the squeezing level depends on the parameter $b=w_p^2/l_{\mathrm{coh}}^2=2n_s(z_p/l_c)$, as pointed out in Sec. I. Figure 6 represents the squeezing spectrum at zero frequency as a function the detector radius, normalized to l_{coh}, for different b parameters, using a plane local oscillator. As already seen in Fig. 5, for $\Delta\rho\rightarrow 0$, the noise reduction effect tends to zero. But we see now that there is also no squeezing effect for large values of the detector radius, because of the finite size of the pump, as already shown in Ref. [13].

Figure 7 shows theoretical results in the case of a detector consisting of two symmetric pixels (pixel of size equal to the coherence length), for different b values, in function of the distance between the two pixels. For large values of ρ, the noise level goes back to shot noise because of the finite size of the pump, as already depicted in Ref. [13]. But now, for small ρ values, the squeezing does not tend to zero, as in the thin-crystal case.

V. SQUEEZING SPECTRUM IN THE FAR FIELD

In this section, we will consider the spatial squeezing spectrum in the far field (Fig. 4) and in the q-vector basis. As already said in Sec. II C, the coupling between q-vector modes is now due to the finite length of the pump. We will see that a new coherence length $l_{\mathrm{coh}\,f}$ appears in such a case, given by

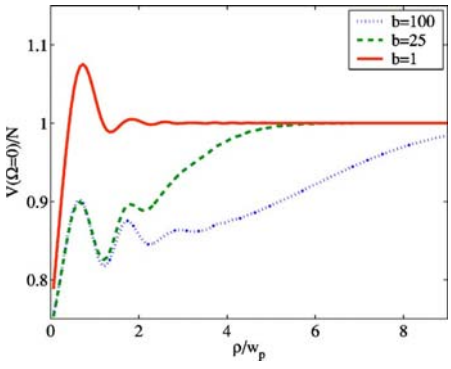

FIG. 7. Squeezing spectrum at zero frequency, normalized to the shot noise, as a function of the pixel distance between the two pixels ρ from the cavity axis (scaled to l_{coh}), plotted for several values of b.

$$l_{\mathrm{coh}\,f} \propto \frac{1}{w_p}.$$

We will successively investigate two configurations: the plane-wave pump regime (where the squeezing spectrum can be calculated analytically), and the case of a finite pump size (where a numerical method is necessary).

A. Plane-wave pump regime in the far field

In order to evaluate the far-field case, we introduce the spatial Fourier transforms of the electromagnetic field temporal frequency components:

$$\tilde{B}_{\pm}^{\mathrm{in/out}}(\mathbf{q},\Omega) = \int\int \frac{d^2x}{2\pi} \hat{B}_{\pm}^{\mathrm{in/out}}(\mathbf{x},\Omega) e^{-i\mathbf{q}\cdot\mathbf{x}}.$$

In the case of a plane-wave pump, $A_p(\mathbf{x},z)=A_p$, so that Eq. (22) becomes

$$\frac{\partial \tilde{B}_+}{\partial t}(\mathbf{q},0,t) = -\gamma\Bigg[(1+i\Delta)\tilde{B}_+(\mathbf{q},0,t) + \sqrt{2\gamma}\tilde{B}_{+\mathrm{in}}(\mathbf{q},0,t) - A_p\,\mathrm{sinc}\left(\frac{l_c\mathbf{q}^2}{2k_s}\right)\tilde{B}_+^{\dagger}(\mathbf{q},0,t)\Bigg]. \tag{42}$$

This equation, which does not mix different $\mathbf{q}$ values, can be solved analytically. It is similar to Eq. (14) in Ref. [13]. Taking into account the boundary condition

$$\tilde{B}_{\pm}^{\mathrm{out}}(\mathbf{q},t) = \sqrt{2\gamma}\tilde{B}_{\pm}(\mathbf{q},t) - \tilde{B}_{\pm}^{\mathrm{in}}(\mathbf{q},t) \tag{43}$$

we obtain

$$\tilde{B}_+^{\mathrm{out}}(\mathbf{q},\Omega) = U(\mathbf{q},\Omega)\tilde{B}_+^{\mathrm{in}}(\mathbf{q},\Omega) + V(\mathbf{q},\Omega)\tilde{B}_+^{\mathrm{in}+}(-\mathbf{q},-\Omega), \tag{44}$$

where

$$U(\mathbf{q},\Omega) = \frac{[1-i(\Delta-\Omega/\gamma)][1-i(\Delta+\Omega/\gamma)] + A_p^2\,\mathrm{sinc}^2\left(\frac{l_c\mathbf{q}^2}{2k_s}\right)}{[1+i(\Delta+\Omega/\gamma)][1-i(\Delta-\Omega/\gamma)] - A_p^2\,\mathrm{sinc}^2\left(\frac{l_c\mathbf{q}^2}{2k_s}\right)} \tag{45}$$

and

$$V(\mathbf{q},\Omega) = \frac{2A_p\,\mathrm{sinc}\left(\frac{l_c\mathbf{q}^2}{2k_s}\right)}{[1+i(\Delta+\Omega/\gamma)][1-i(\Delta-\Omega/\gamma)] - A_p^2\,\mathrm{sinc}^2\left(\frac{l_c\mathbf{q}^2}{2k_s}\right)}. \tag{46}$$

In the case of the plane-wave regime, the input-output relation in the spatial Fourier space describes therefore an infinite set of independent optical parametric oscillators below threshold. This can be simply understood: the q-vector basis is the eigenbasis of the diffraction, so that no coupling between q-vector modes due to the crystal appears.

Let us now consider the homodyne-detection scheme, schematically shown in Fig. 4. The lens provides a spatial Fourier transform of the output field $B_{\mathrm{out}}(x,\Omega)$, so that at the location of plane D the field $B_{\mathrm{out}}^D(x,\Omega)$ is

$$B_{\mathrm{out}}^D(x,\Omega) = \frac{2\pi}{\lambda f}\tilde{B}_{\mathrm{out}}\left(\frac{2\pi}{\lambda f}x,\Omega\right). \tag{47}$$

In this plane, $B_{\mathrm{out}}^D(x,\Omega)$ is mixed with an intense stationary and coherent beam $\alpha_{\mathrm{LO}}^D(x)=(2\pi/\lambda f)\tilde{\alpha}_{\mathrm{LO}}(2\pi x/\lambda f,\Omega)$, where $\alpha_L(x)$ has a Gaussian shape, with a waist w_{LO}. The homodyne field has thus an expression similar to the near-field case, where functions of x are now replaced by their spatial Fourier transforms:

$$E_H(\Omega) = \int_{\mathrm{det}} d\mathbf{q}[\tilde{B}^{\mathrm{out}}(\mathbf{q},\Omega)\tilde{\alpha}_{\mathrm{LO}}^*(\mathbf{q}) + \tilde{B}^{\mathrm{out}+}(\mathbf{q},-\Omega)\tilde{\alpha}_{\mathrm{LO}}(\mathbf{q})]. \tag{48}$$

This analogy shows that, in the case of a local oscillator that has an even parity with respect to coordinate inversion, the squeezing spectrum is given by (like in Ref. [13])

$$V(\Omega) = \int_{\mathrm{det}} d\mathbf{q}\{|\tilde{\alpha}_{\mathrm{LO}}(\mathbf{q})|^2[1-\sigma(\mathbf{q})]\} + \int_{\mathrm{det}} d\mathbf{q}\{|\tilde{\alpha}_{\mathrm{LO}}(\mathbf{q})|^2\sigma(\mathbf{q})R(\mathbf{q},\Omega)\}, \tag{49}$$

where the noise spatial density $R(\mathbf{q},\Omega)$ is given by

$$R(\mathbf{q},\Omega) = |U(\mathbf{q},\Omega) + e^{2i\varphi_{\mathrm{LO}}(\mathbf{q})}V^*(\mathbf{q},-\Omega)|^2 \tag{50}$$

and where

$$\sigma(\mathbf{q}) = \int_{\mathrm{det}} d\mathbf{q}'\,\delta_+(\mathbf{q},\mathbf{q}'). \tag{51}$$

In order to minimize $R(\mathbf{q},\Omega)$, the local oscillator phase should be chosen as $\varphi_{\mathrm{LO}}(\mathbf{q})=\arg[U(\mathbf{q},\Omega)V(\mathbf{q},\Omega)]/2$. In particular, at resonance and at zero frequency $U(\mathbf{q},0)$ and $V(\mathbf{q},0)$ are real and the optimal local oscillator phase would correspond to $\varphi_{\mathrm{LO}}(\mathbf{q})=\pi/2$, when $\mathrm{sinc}(l_c\mathbf{q}^2/2k_s)\geqslant 0$, and $\varphi_{\mathrm{LO}}(\mathbf{q})=0$, when $\mathrm{sinc}(l_c\mathbf{q}^2/2k_s)\leqslant 0$, which is not indeed very practical. However, modes for which $\mathrm{sinc}(l_c\mathbf{q}^2/2k_s)\leqslant 0$ are quite outside the phase matching curve, so that the choice $\varphi_{\mathrm{LO}}(\mathbf{q})=\pi/2$ everywhere should give good results. The squeezing spectrum at resonance and zero frequency, for $\varphi_{\mathrm{LO}}(\mathbf{q})=\pi/2$ can be analytically calculated and as a function of the radius r of a detector centered on the optical axis is given by

$$\frac{V(r,0)}{N} = \frac{1}{\int_0^{r/r_0} u\exp\left(\frac{-w_{\mathrm{LO}}^2k_su^2}{l_c}\right)}\int_0^{r/r_o} u\exp\left(\frac{-w_{\mathrm{LO}}^2k_su^2}{l_c}\right) \times\left(\frac{1+A_p\,\mathrm{sinc}(u^2)}{1-A_p\,\mathrm{sinc}(u^2)}\right)^2, \tag{52}$$

where

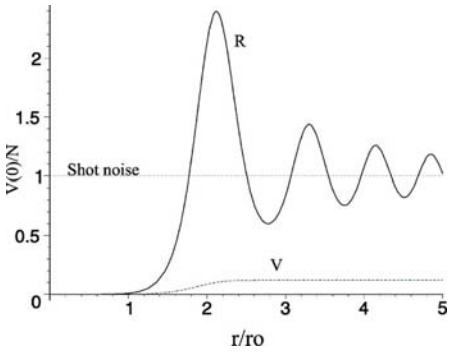

FIG. 8. Squeezing spectrum normalized to the shot noise, at zero frequency, at resonance, in the plane pump regime and far-field case, for two measurement configurations. V is obtained using a circular detector of radial amplitude r (scaled to r_0). R is obtained using a pair of symmetrical pixels in function of the pixel distance from the axis r (scaled to r_0).

$$r_0 = \frac{\lambda f}{2\pi}\sqrt{\frac{2k_s}{l_c}} = \frac{\lambda f}{\pi}\frac{1}{l_{\mathrm{coh}}}. \tag{53}$$

Figure 8 shows the results obtained in the case of two different detection configurations: the V curve shows results in the case of a circular detector of variable radius r (scaled to r_0), using a local oscillator waist $w_{\mathrm{LO}}=r_0$. As already said in Sec. II, the limitation of the squeezing level is due to the nonperfect phase matching along the crystal. For $r>r_0$, the squeezing level decreases. So, in the plane-wave pump regime in the far field, the thickness of the crystal has a role comparable with the finite size of the pump in the near field, as reported in Ref. [13]. The R curve shows results obtained in the case of two small symmetrical pixels and a plane-wave local oscillator as a function of the pixel distance from the cavity axis r, scaled to r_0. We can see that the noise level goes back to the shot-noise level for $r>r_0$, because of the nonperfect phase matching along the crystal.

B. Squeezing spectrum in the far-field case and finite-size pump regime

When one takes into account the finite size of the pump, a coupling between different q vectors appear, and one needs to solve equations numerically, as in the near-field case. A new coherence length $l_{\mathrm{coh}\,f}$ appears in the far field: $l_{\mathrm{coh}\,f}=1/w_P$.

Figure 9 shows the evolution of the squeezing spectrum at zero frequency, and at resonance, for different b parameters, in a function of the detector radius scaled to $l_{\mathrm{coh}\,f}$. We see the same evolution as in the analytical case, except that the noise level tends to shot noise for small values of the detector.

Figure 10 shows the results obtained in the case of two symmetrical pixels (pixel of size equal to the coherence length $l_{\mathrm{coh}\,f}$), for different b values, in a function of the distance between the two pixels ρ. The evolution is similar to the one given by Fig. 6 for large distances, but there is also a decrease of the squeezing effect for small distances.

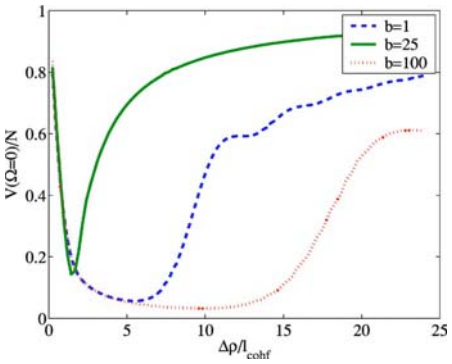

FIG. 9. Squeezing spectrum normalized to the shot noise at zero frequency, and at resonance, as a function of the radial amplitude of the detector $\Delta\rho$ (scaled to the coherence area $l_{\mathrm{coh}\,f}$), in the finite pump regime and far-field approach and for different values of b.

VI. DISCUSSIONS AND CONCLUSIONS

We have seen that when one takes into account the effect of diffraction inside the nonlinear crystal in a confocal OPO, the local squeezing predicted for any shape and size of the detectors in the thin-crystal approximation is now restricted to detection areas lying within a given range, characterized by a coherence length l_{coh}. This prediction introduces serious limitations to the success of an experiment, and must be taken into account when designing the experimental setup. With the purpose of producing a light beam that is squeezed in several elementary portions of its transverse cross section, either a crystal short compared to z_R should be used or, alternatively, a defocused pump, with a waist much larger than the cavity waist. In both cases the efficiency of the nonlinear coupling is reduced. For instance, with a 1-cm-long crystal, l_{coh} is equal to 40 μm, and one must choose a pump waist much larger than this value in order to observe multimode squeezing (the number of modes being roughly equal to the ratio $b=w_p^2/l_{\mathrm{coh}}^2$). This defocused pump will imply a much

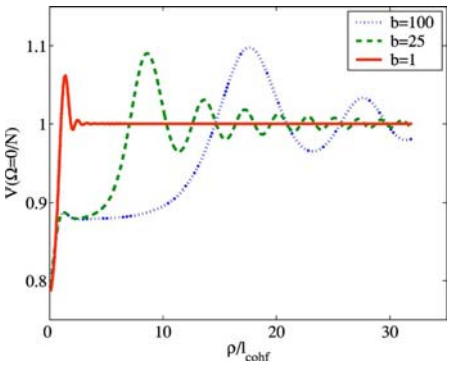

FIG. 10. Squeezing spectrum normalized to the shot noise at zero frequency, and at resonance, as a function of the distance between the two pixels ρ (scaled to the coherence area $l_{\mathrm{coh}\,f}$), in the finite pump regime and far-field approach and for different values of b.

higher threshold for the OPO oscillation, which is multiplied by a factor also close to b. The conclusion of this analysis is that one cannot have multimode squeezing "for free," and that with a given pump power, one will be able to excite a number of modes which is roughly equal to the ration of the injected pump power to the threshold power for single mode operation.

ACKNOWLEDGMENTS

Laboratoire Kastler-Brossel, of the Ecole Normale Supérieure and the Université Pierre et Marie Curie, is associated with the Centre National de la Recherche Scientifique. This work was supported by the European Commission in the frame of QUANTIM Project No. IST-2000-26019.

[1] W. Boyd, *Nonlinear Optics* (Academic Press, New York, 1992).
[2] A. Siegman, *Lasers* (University Science Books, Sausalito, CA, 1986).
[3] Y. R. Shen, *The Principles of Nonlinear Optics* (Wiley, New York, 1984).
[4] L. A Lugiato, M Brambilla, and A Gatti, Adv. At., Mol., Opt. Phys. **40**, 229 (1998).
[5] S. Barland, J. R. Tredicce, M. Brambilla, L. A. Lugiato, S. Balle, M. Giudici, T. Maggipinto, L. Spinelli, G. Tissoni, T. Koedl, M. Miller, and R. Jaeger, Nature (London) **419**, 699 (2002).
[6] M. I. Kolobov and I. V. Sokolov, Sov. Phys. JETP **69**, 1097 (1989).
[7] M. I. Kolobov, Rev. Mod. Phys. **71**, 1539 (1999).
[8] E. Brambilla, A. Gatti, M. Bache, and L. A. Lugiato, Phys. Rev. A **69**, 023802 (2004).
[9] M. LeBerre, D. Leduc, E. Ressayre, and A. Tallet, J. Opt. B: Quantum Semiclassical Opt. **1**, 153 (1999).
[10] G. Boyd and D. Kleinman, J. Appl. Phys. **39**, 3597 (1968).
[11] E. Lantz, T. Sylvestre, H. Maillotte, N. Treps, and C. Fabre, J. Opt. B: Quantum Semiclassical Opt. **6** S295 (2004).
[12] L. A. Lugiato and Ph. Grangier, J. Opt. Soc. Am. B **31**, 3761 (1985).
[13] K. I. Petsas, A. Gatti, L. A. Lugiato, and C. Fabre, Eur. Phys. J. D **22**, 501 (2003).
[14] C. Schwob, P. F. Cohadon, C. Fabre, M. A. Marte, H. Ritsch, A. Gatti, and L. Lugiato, Appl. Phys. B: Lasers Opt. **66**, 685 (1998).
[15] S. Mancini, A. Gatti, and L. Lugiato, Eur. Phys. J. D **12**, 499 (2000).
[16] A. Gatti and L. Lugiato, Phys. Rev. A **52**, 1675 (1995).
[17] C. W. Gardiner and M. J. Collett, Phys. Rev. A **31**, 3761 (1985).
[18] M. Abramowitz and I. A. Stegun, *Handbook of Mathematical Functions* (U.S. Department of Commerce, 1972).
[19] A. Gatti, R. Zambrini, and M. San Miguel, Phys. Rev. A **68**, 053807 (2003).
[20] J. Mod. Opt. **34** (6/7), 1 (1987), special issue on squeezed light.

Noiseless Optical Amplifiaction of Images using transverse degenerate OPOs

L.Lopez, N.Treps, C. Fabre, A. Maître
Laboratoire Kastler Brossel, Université Pierre et Marie Curie, Campus Jussieu, Case 74, 75252 Paris cedex 05, France
(Dated: July 28, 2006)

PACS numbers: 42.50.Dv, 42.65.Yj, 42.60.Da

I. INTRODUCTION

II. THEORIE

Noiseless amplification in a type II parametric crystal has been performed either in a single mode [1] or multimode [2, 3] configuration, and each time the single path system had to be pumped with pulsed lasers. It is well known [1] that the noise figure of such a system depends on the input polarisation : if only the signal mode is injected, the amplification is phase insensitive (PIA) and the noise figure of the system F is given by $F = 2 - 1/G$. If both signal and idler mode are injected (at 45° of the optical axes), we are in a phase sensitive amplification case (PSA) and no noise is added during the process. The signal to noise ratio is preserved: $F = 1$.

With continuous lasers, in order performe the same type of experiments one has to insert the non-linear crystal in an optical cavity in order to create a so called optical parametric oscillator (OPO). However, the presence of the cavity changes the noise figure of the system, that depends on the input and output coupler of the cavity. This problem is usually omitted in the literature dealing with noiseless amplification [4, 5]. In fact, the models consider ring cavities with the input and the output on the same mirror. Intracavity losses are neglected. In this case, the noise figure is equivalent to the simple path case ($F = 2 - 1/G$ in the PIA case and $F = 1$ in the PSA case).

In our experiment, which is a proof of principle of the possibility of noiseless amplification within a parametric oscillator, consists of a linear cavity with different input and output ports. This configuration facilitates the measurement of quantum effects and the experimental proof of the quantum operation of the amplifier, but is far away from this ideal model. To design our system, we introduce a new ring OPO scheme represented in fig.1.

In order to model the linear cavity, the input and output mirrors are separated. The amplitude transmission losses on the input and the output mirrors are called respectively γ_{in} and γ_{out}. An outside coupling (represented by the modes s_i with $i = 1, 2$ corresponding to signal and idler polarisations) appears due to the output mirror. In a same way, intra-cavity losses are represented by a second outside coupling (represented by the modes c_i with $i = 1, 2$ corresponding to signal and idler polarisations) with a mirror of transmission losses γ_c. The presence of

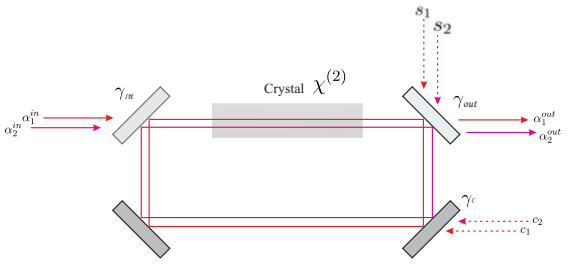

FIG. 1:

the losses will degrade the signal to noise ratio, even when the amplification is phase sensitive. It can be shown that the noise figure F is related to the gain G by the formula:

$$F = 1 + \frac{\gamma_c}{\gamma_{in}} + \frac{\gamma_{out}}{\gamma_{in}} + \frac{1}{G} - 2\sqrt{\frac{\gamma_{out}}{\gamma_{in} G}} \qquad (1)$$

Experimentally, we don't measure directly the noise figure of our system. Like in the experiments [2, 3], all the measurements are done at the output of the system. We compare the signal to noise ratio with amplification and the signal to noise ratio without amplification. Corresponding values of the gain $\tilde{G}$ and of the noise figure $\tilde{F}$ are calculated. We call them the "normalized" parameter of the system as they are equal to one without amplification, which would not be the case if one would compare the input beam to the output beam. In that procedure, we get rid of the transmission of the cavity, which is a problem if one want to apply directly our amplifier to practical configuration but is not in order to evaluate its quantum behavior. We will propose at the end of this article how to adapt the system for applications.

Thanks to our model, we can plot the evolution of the normalised noise factor in function of the normalised gain in the phase sensitive (injection at 45° of the optical axes) or phase insensitive case (see fig.4). In our experiment, the amplification is called noiseless, when for a given value of the normalised gain, the noise factor is lower than the theoretical value of an amplifier equivalent in terms of losses but which works in a phase insensitive configuration.

The previous results have been obtained in the monomode case. Nevertheless it can be shown [6] that, for a perfectly spatially degenerate cavity, these results can be generalised locally provided the detector used has

a size superior to a coherence area, whose caracteristic size is $l_{coh} = \sqrt{\frac{\lambda l_c}{\pi n_s}}$, with l_c length of the crystal, n_s linear indice and λ wavelength of the infra-red beam. In order to amplify many transverses modes a large pump waist w_p has to be used [5, 6]. The relevant parameter of such an experiment is $b = \frac{w_p^2}{l_{coh}^2}$ [6] which corresponds to the number of amplified transverse modes for a cavity of degeneracy 1 [7]. This number has to be divided by the cavity degeneracy if it is different from 1. (C'est VRAI ??).

III. EXPERIMENTAL SCHEME

The experiment scheme is depicted in fig. 2.

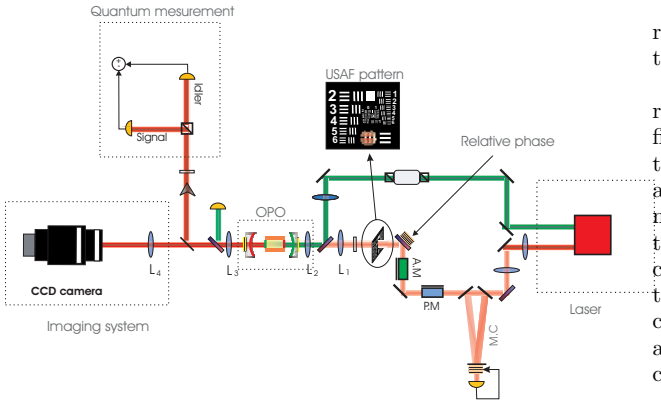

FIG. 2: Noiseless amplification of image in an hemi-confocal cavity: experimental scheme

We use a continuous wave Nd:Yag laser, frequency doubled with two coherent outputs. One at 532 nm to pump the OPO, the second at 1064 nm to generate the image, that will be amplified. In order to eliminate technical noise the infra-red beam is injected into an impedance-matched ring Fabry-Perot cavity of high finesse (mode cleaner).

To get a high stability of the experiment, we use a peculiar system, a dual-cavity configuration already depicted in [8]. In this configuration (depicted in fig. 3) where signal and idler fields are resonant in a cavity which is different from the one of the pump, the three fields are overlapping in the crystal. We use a non critical phase matched, type II, $3 * 3 * 10mm$ KTP crystal ($l_{coh} = 45\mu m$). A very good temperature stabilization ($\sim mK$), obtained thanks to a Peltier unit, is used to reach, by fine tuning, the triple resonance of the cavity.

The pump cavity is bounded by the high reflecting mirrors at 532nm M_1 (90%@532nm, 5%@1064nm) and M_3 (99.3%@532nm, 0.11%@1064nm), the infra-red one by M_2 (5.25%@532nm, 99.96%@1064nm) and M_4 (6.6%@532nm, 98.93%@1064nm). The M_1 and M_4 mirros are mounted on translation stages to reach the exact transverse degeneracy.

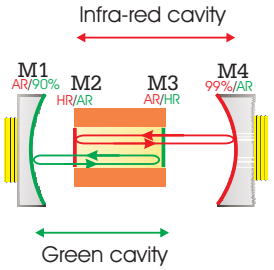

FIG. 3: The dual cavity configuration. The infra-red cavity is a transverse degenerate, hemi-confocal cavity made of a plane mirror and a curve mirror of radius of curvature R, separated by a distance $R/2$

In order to amplify many transverse modes, the infra-red cavity has to be transverse degenerate. In our configuration, the infra-red cavity is a hemi-confocal cavity, that consist of a plane and a curve mirror separated by a distance equal to half the radius of curvature of the mirror. In our experiment, $R = 100mm$ so the length of the infra-red cavity is about $50mm$. The hemi-confocal cavity is a partially transmitting cavity, whose classical transmission properties have been studied in [7]. In this cavity, only half of the even (or odd) modes are resonant at the same time for a given length of the cavity. In this configuration, the OPO threshold is about $30mW$.

The radius of curvature of the M_1 mirror is large: $R = 2000mm$, so that the waist of the green cavity is large in order to amplify many transverse modes. The length of the green cavity is $50mm$ so that $w_{532nm} = 230\mu m$. The number of amplified transverse modes is about $b = \frac{w_p^2}{l_{coh}^2} =$ 25 (DIVISER PAR l'ORDRE DE DEGENERESCENCE ??)

The image, which will be amplified is created thanks to a USAF resolution target, that intercepts the infra-red beam. The target plane is image on the mirror M_2 in a both amplitude and phase preserving near field transformation thanks to a telescopic system (lenses (L_1, L_2)).

At the output of the OPO, the green and infra-red beams are separated thanks to a dichroic mirror. The green beam is sent onto a photodiode to monitor the green cavity and to stabilize it. For the infra-red, the detection system is made of two levels. A flipping mirror enable us to send the signal and idler beams onto an imaging set-up, which consists of a CCD camera that record the transverse distribution of infra-red beam, either in the near or the far field. For a quantum study, signal and idler are separated thanks to a polarizing beam spitter and sent to two InGaAs photodetectors having matched high quantum efficiency around 95%.

The different optical cavities are stabilized using the Pond-Drever-Hall method [11]. For the green, we use

the $12MHz$ phase modulation present at the output of the laser. For the infra-red, a new phase modulation at $8,5Mhz$ is added thanks to an electro-optic modulator (P.M) at the output of the mode cleaner. The relative phase between the pump, signal and idler is controlled by a mirror placed on a piezo-electric transducer which modifies the optical length of the infra-red beam. We work in two different regimes : either the piezo-electric is continuously modulated, so that we can monitor simultaneously amplification and deamplification, either the relative phase is locked. To do so, we use a technique already introduce in [9]: the infra-red beam is demodulated at $12MHz$ at the output of the OPO.

IV. RESULTS

The results shown in this article have been obtained with different images shapes: two vertical slits, two horizontal slits, a large mode (3 times the size of the eigen mode of the hemi-confocal cavity).

Classical properties of the amplification have been studied in [8]. Thanks to the spatial gain repartition, it can be shown that many transverse modes are amplified.

The first studied performed consisted of the proof of the quantum multimode operation of our system. We thus studied the quantum fluctuations of the images at the output of the cavity, either or the amplification or the de-amplification regime, with a digital acquisition system described in [10]. However, in our system the local properties of the output beams are difficult to analyse, as the complex geometry of the semi-confocal cavity mixes them together. Furthermore, due to the walk-off inside the cavity, signal and idler beam are slightly different. We thus choose, instead of this local study, to analyse the quantum fluctuations of the whole output beams, the proof of the multimode operation then made by varying the input image instead of varying the detector geometry, which is mathematically equivalent, as far as we assume a linear response of our system and that it stays stable while we chage the input image, which is the case in our experiment.

The results are the following : whatever the shape of the input image, we see a quantum noise reduction of 30% on the difference between signal and idler (twin beams behavior). These results are in good agrement with theory (45%). In the de-amplification case, we see a reduction of the intensity noise on the sum of signal and idler of 30% (theoretically $< 45\%$). This is, to our knowledge, the first proof of a multimode operation of a continuous wave OPO, appart from the preliminary studied we performed in [10], and shows also that we are able to taylor the quantum fluctuations of whatever beam shape resonnant in the cavity, which is of most use in multipixel image analysis [12].

Having proven the quantum multimode operation of our system, we can investigate its noise figure. An intensity modulation at $5Mhz$ of the infra red beam is realized at the output of the mode cleaner thanks to an amplitude modulator (A.M). This modulation correspond to the "signal" that will be amplified. As already said, we mesure normalised values corresponding to the comparison of the system with and without amplification. In order to investigate the noise of the system, the high frequency channels of the photodiodes signal and idler are summed and sent into a spectrum analyser. We have access to the normalised gain and the normalised noise figure of the amplifier.

The experimental results of normalised noise factor are represented in figure 4.

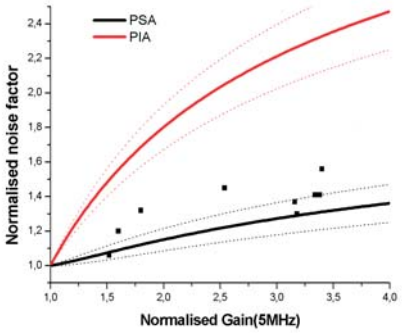

FIG. 4: Experimental values of normalised noise factor using the hemi-confocal OPO. Added to this points, the theoretical values of normalised noise factor in function of the normalised gain for the PIA ans PSA cases. The dotted lines represent the incertitude of this curves

Added to this results, the theoretical values of normalised noise factor in function of the normalised gain for our system in the phase sensitive and phase insensitive cases. Our system add less noise than an equivalent one, whose losses are the same but who works in a phase insensitive configuration: we are in a noiseless regime of amplification.

We extend the study of the normalised noise factor to a confocal OPO, using a non critical phase matched, type I crystal ($MgO : LiNbO_3$), whose temperature of degeneracy is about 120°. In this case, only a defocalised mode was amplified, because the goal of the experiment was to test the response of the normalised noise factor in function of the different losses. In this case, we had $\gamma_{out}/\gamma = 1/3$. The experimental results of normalised noise factor and the theoretical values in the PSA and PIA cases are represented in figure 5. Our system add less noise than an equivalent one, whose losses are the same but who works in a phase insensitive configuration: we are in a noiseless regime of amplification.

Some general comments on these results are necessary. First of all, one can see that the actuals values of the measured signal to noise ratio varry a lot from shot to shot. We should stress that we did not do any post selection of

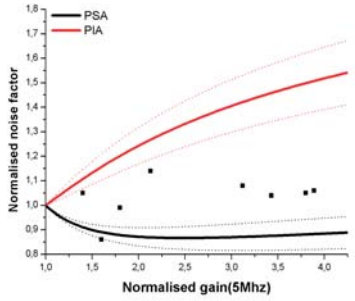

FIG. 5: Experimental values of normalised noise factor using the confocal OPO. Added to this points, the theoretical values of normalised noise factor in function of the normalised gain for the PIA ans PSA cases. The dotted lines represent the incertitude of this curves

our experimental results, and thus the fluctuations come essentially from the quality of the locking, which is critical due to high thermal effects inside the crystal. However, all our experimental data lie within the quantum regime. Secondly, one can argue that this is not trully noiseless amplification due to the normalization procedure. Even is this is true and has to be assess for practical application, as we will propose in the conclusion, we have indedd demonstrated here the quantum behavior of our amplifier, as the signal to noise ratio obtained at the output is in complete agreement with the non-classical properties demonstrated without signal. The quantum correlations are preserved in the presence of signal, and are responsible for the improvement of the noise factor, thus demonstrating the quantum noiseless amplification regime achieved here.

V. CONCLUSION

We have demonstrated in this letter the first experimental evidence of multimode noiseless amplification in the continuous wave regime, along with the quantum multimode behavior of a degenerate OPO. In order to move to practical application, it is however necessary to modify the properties of the cavity to get rid of the normalization procedure and analyse a "true" noise figure. Calculations shows that, in an approach similar to an impedance matched cavity where all the input power is transmitted by the cavity, an OPO with an input coupler of ?? transmission and output coupler of ?? transmission will achieve this goal for gain comprised between 4 and 10 and cavity threashold comparable to our setup. In that configuration, reflected power from the cavity would be neglectible and noiseless amplification is predicted for the input/output noise figure.

Finally, we would like to stress that this experiments also demonstrate the possibility to modify the quantum fluctuation of any transverse mode within the same experimental setup, and thus easily switched from one to another transverse squeezing configuration. This is what is needed for optical read-out bellow the standard quantum limit, is for instance compact disc read out [13].

Acknowledgments

Laboratoire Kastler-Brossel, of the Ecole Normale Supérieure and the Université Pierre et Marie Curie, is associated with the Centre National de la Recherche Scientifique.
This work was supported by the European Commission in the frame of the QUANTIM project (IST-2000-26019).

[1] J. A. Levenson, I. Abram, T.Rivera, P. Fayolle, J. C. Garreau, and P. Grangier, Phys. Rev. Lett. **70**, 267-270 (1993)
[2] S.-K. Choi, M. Vasilyev, and P. Kumar, Phys. Rev. Lett. **83**, 1938-1941 (1999)
[3] A. Mosset, F. Devaux, E. Lantz, Phys. Rev.Lett. **94**, 223603 (2005)
[4] M. Kolobov and L. Lugiato, Phys. Rev. A **52**,4930 (1995)
[5] S.Mancini, A.Gatti, L.A.Lugiato, Eur.Phys.J.D **12**, 499 (2000)
[6] L. Lopez, S. Gigan,N. Treps, A. Matre, C. Fabre, A. Gatti, Phys. Rev. A **67**, 023808 (2005)
[7] S. Gigan, L. Lopez, N. Treps, A. Maitre, C. Fabre, Phys. Rev. A **72**, 023804 (2005)
[8] S. Gigan, L. Lopez, V .Delaubert, N. Treps, C. Fabre, A. Maitre, Journal of Modern Optics, **53**, Nos 5-6, 809-820 (2006)
[9] P. K. Lam, PhD thesis
[10] Martinelli M., Treps N., Ducci S., Gigan S., Matre A., Fabre C., Phys. Rev. A **67**, 023808 (2003)
[11] Drever R. W. P, Hall J.L.,Kowalski F.V., Hough J., Ford G.M., Munley A.J. et Ward H., Applied Physics B **31**, 97-105 (1983)
[12] N. Treps, V. Delaubert, A. Matre, J.M. Courty and C. Fabre, Phys. Rev. A **71**, 013820 (2005)
[13] V. Delaubert, N. Treps, G. Bo, C. Fabre, Phys. Rev. A

Multimode en temps et fréquence : futures directions

Article 20, reproduit en page 178

Squeezing frequency combs

G.J. de Valcarcel, G. Patera, N. Treps and C. Fabre

Soumis à Phys. Rev. A

Abstract : We have developed the full multimode theory of a synchronously pumped type I optical parametric oscillator (SPOPO). We derive expressions for the oscillation threshold and the characteristics of the generated mode-locked signal beam. We calculate the output quantum fluctuations of the device, and find that, in the degenerate case (coincident signal and idler set of frequencies), significant squeezing is obtained when one approaches threshold from below for a set of well defined "super-modes", or frequency combs, consisting of a coherent linear superposition of signal modes of different frequencies which are resonant in the cavity.

Multimode Squeezing of Frequency Combs

G. J. de Valcárcel ([1,2]), G. Patera ([1]), N. Treps([1]), C. Fabre([1])

([1]) *Laboratoire Kastler Brossel, Université Pierre et Marie Curie-Paris6, 4 place Jussieu CC 74, 75252 Paris cedex 05, France and*

([2]) *Departament d'Òptica, Universitat de València, Dr. Moliner 50, 46100 Burjassot, Spain*

(Dated: September 27, 2006)

Abstract

We have developed the full multimode theory of a synchronously pumped type I optical parametric oscillator (SPOPO). We calculate the output quantum fluctuations of the device, and find that, in the degenerate case (coincident signal and idler set of frequencies), significant squeezing is obtained when one approaches threshold from below for a set of well defined "super-modes", or frequency combs, consisting of a coherent linear superposition of signal modes of different frequencies which are resonant in the cavity.

PACS numbers: 42.50.Dv, 42.65.Yj, 42.65.Re

Optical Parametric Oscillators are among the best sources of squeezed [1], correlated [2] and entangled [3] light in the so-called continuous variable regime. They have allowed physicists to successfully implement demonstration experiments for high sensitivity optical measurements and quantum information protocols. In order to maximize the quantum effects, one needs to optimize the parametric down-conversion process. This has been achieved so far by using either intense pump lasers or resonant cavities. Having in mind that the parametric process is an almost instantaneous one, femtosecond mode-locked lasers are the best pump sources in this respect, as they generate very high peak optical powers with high coherence properties. Furthermore, they minimize the thermal effects in the linear crystal which often hamper the normal operation of parametric devices. Mode-locked lasers have been already used extensively to generate non classical light, either to pump a parametric crystal [4, 5] or an optical fiber [6]. However in such single-path configurations, perfect quantum properties are only obtained when the pump power goes to infinity. This is the reason why mode-locking is often associated to Q-switching and pulse amplification [7] in order to reach even higher peak powers, at the expense of a loss in the coherence properties between the successive pump pulses. In contrast, intracavity devices produce perfect quantum properties for a finite power, namely the oscillation threshold of the device. It is therefore tempting to consider devices in which one takes advantage of the beneficial effects of both high peak powers and resonant cavity build-up. Such devices exist: they are the so-called synchronously pumped OPOs or SPOPOs. In a SPOPO, the inter-pulse separation time is equal to the repetition rate of the mode-locked laser, so that the effect of the successive intense pump pulses add coherently, thus reducing considerably its oscillation threshold. Such SPOPOs have already been implemented as efficient sources of tunable ultra-short pulses [8–13] and their temporal properties have been theoretically investigated [14–16]. Let us mention that mode-locked OPOs have also been developed: in such devices, the cavity is resonant only for the signal modes and idler modes, and the pump pulses are not re-circulating. Degenerate mode-locked OPOs have been used to generate pulsed squeezed light in the picosecond regime[5].

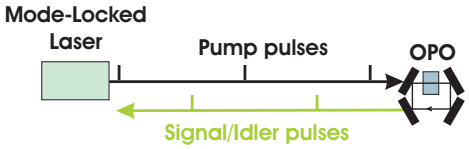

FIG. 1: Synchronously pumped OPO

In this paper, we make a complete multimode quantum analysis of SPOPOs, and show theoretically that these devices are very efficient to produce squeezed states. Squeezing is effective not in a single frequency mode, as usual, but instead in a whole set of "super-modes", which are well defined linear combinations of signal modes of different frequencies. Similar "super-modes" have been independently introduced by Wasilewski *et. al* [17] in the different context of transient degenerate down-conversion in a single-pass, single-pulse configuration. In their case, the "super-modes" are continuous linear superpositions of the annihilation operators in free space, whereas in our case, because of the resonant cavity, they are a discrete combination of modes.

Let us first precise the model that we use (figure 1). We consider a ring cavity of optical length L containing a type I parametric crystal of thickness l. Degenerate phase matching is assumed, meaning that the phase-matching condition is fulfilled for frequencies $2\omega_0$ and ω_0. This amounts to saying that $n(2\omega_0) = n(\omega_0) \equiv n_0$, $n(\omega)$

being the refractive index of the crystal at frequency ω. The mode-locked pump laser, having a repetition rate $\Omega/2\pi = c/L$, is tuned so that the frequency of one of its modes is equal to $2\omega_0$. The electric field generated by the pump mode-locked laser can be expressed as:

$$E_{\text{ext}}(t) = \left(\frac{P}{2\varepsilon_0 c}\right)^{\frac{1}{2}} \sum_m i\alpha_m e^{-i(2\omega_0 + m\Omega)t} + \text{c.c.}, \quad (1)$$

where P is the average laser power per unit area, α_m the normalized ($\sum_m |\alpha_m|^2 = 1$) complex spectral component of longitudinal mode labelled by the integer index m, and $m = 0$ corresponds to the phase-matched mode. For the sake of simplicity in this first approach of the problem, we will take the modal coefficients α_m as real numbers, thus excluding chirped pump pulses. As already mentioned, the SPOPO cavity length is adjusted so that its free spectral range coincides with that of the pumping laser. In the nonlinear crystal, pump photons belonging to all the different longitudinal pump modes are converted into signal and idler photons via the parametric interaction. In addition we will assume here that we are in the ideal case of *doubly resonant degenerate operation*, meaning that among all the OPO cavity resonant frequencies, there are all the pump mode frequencies $\omega_{p,m} = 2\omega_0 + m\Omega$ but also all the frequencies $\omega_{s,q} = \omega_0 + q\Omega$ around the phase-matched subharmonic frequency ω_0. The intracavity electric field generated by the parametric interaction will then be a superposition of fields oscillating at frequencies $\omega_{s,q}$. We will finally call γ_p and γ_s, the cavity damping rates for the pump and signal modes. Note that the free spectral range Ω is assumed to be the same in the pump and in the signal spectral regions. This is necessary for an efficient intracavity parametric down conversion and requires, from the experimental viewpoint, the use of extra dispersive elements inside the cavity that compensate for the dispersion of the crystal. At the quantum level, the signal field, taken at the middle of the crystal, is represented by the quantum operator $\hat{E}_s$ which can be written as:

$$\hat{E}_s(t) = \sum_q i\mathcal{E}_{s,q}\hat{s}_q(t)e^{-i\omega_{s,q}t} + \text{H.c.}, \quad (2)$$

where $\hat{s}_q$ is the annihilation operator for the q^{th} signal mode in the interaction picture. $\mathcal{E}_{s,q}$ is the single photon field amplitude, equal to $\sqrt{\hbar\omega_{s,q}/2\varepsilon_0 n(\omega_{s,q}) AL}$, and A its effective transverse area.

The following Heisenberg equations for the field operators can be derived using the standard methods. The detail of the derivation will be given in a forthcoming publication[18]. Below threshold, and in the linearized regime for the pump fluctuations, they read:

$$\frac{d\hat{s}_m}{dt} = -\gamma_s \hat{s}_m + \gamma_s \sigma \sum_q \mathcal{L}_{m,q}\hat{s}_q^\dagger + \sqrt{2\gamma_s}\hat{s}_{\text{in},m}, \quad (3)$$

where σ is the normalized pump amplitude

$$\sigma = \sqrt{P/P_0} \quad (4)$$

in which P_0 is the single mode c.w. oscillation threshold:

$$P_0 = 2\gamma_s^2\gamma_p n_0^3 c^3 \varepsilon_0 / \left(4\sqrt{2}\chi l\omega_0\right)^2 \quad (5)$$

with χ the crystal nonlinear susceptibility. $\mathcal{L}_{m,q}$ is the product of a phase-mismatch factor by the pump spectral normalized amplitude α_{m+q}:

$$\mathcal{L}_{m,q} = \frac{\sin\phi_{m,q}}{\phi_{m,q}}\alpha_{m+q}, \quad (6)$$

where $\phi_{m,q}$ is the phase mismatch angle:

$$\phi_{m,q} = \frac{l}{2}\left(k_{p,m+q} - k_{s,m} - k_{s,q}\right) \quad (7)$$

which can be computed using a Taylor expansion around $2\omega_0$ for the pump wave vectors $k_{p,m}$ and around ω_0 for the signal wave vectors $k_{s,q}$:

$$\phi_{m,q} \simeq \beta_1(m+q) + \beta_{2p}(m+q)^2 - \beta_{2s}\left(m^2+q^2\right), \quad (8)$$

where $\beta_1 = \frac{1}{2}\Omega\left(k_p' - k_s'\right)l$, $\beta_{2p} = \frac{1}{4}\Omega^2 k_p'' l$, $\beta_{2s} = \frac{1}{4}\Omega^2 k_s'' l$. k' and k'' are the first and second derivative of the wave vector with respect to frequency. Finally $\hat{s}_{\text{in},m}$ are the input signal field operators at frequency $\omega_{s,m}$ transmitted through the coupling mirror. When the input is the vacuum state, which we consider here, their only non-null correlations are:

$$\left\langle \hat{s}_{\text{in},m_1}(t_1)\,\hat{s}_{\text{in},m_2}^\dagger(t_2)\right\rangle = \delta_{m_1,m_2}\delta(t_1 - t_2). \quad (9)$$

In order to get Eqs. (3), we assumed, as usual, that $\mathcal{E}_{s,m} \simeq \mathcal{E}_{s,0}$ for all m and we neglected the dispersion of the nonlinear susceptibility. Therefore the present approach is not valid for ultra-short pulses, the spectrum of which extends over the whole visible region.

Let us first determine the average values of the generated fields. They are determined by the "classical" counterpart of Eq. (3), removing the input noise terms, and replacing the operators by complex numbers. The solution of these equations is of the form $s_m(t) = S_{k,m}e^{\lambda_k t}$, where k is an index labelling the different solutions. The parameters $S_{k,m}$ and λ_k obey the following eigenvalue equation:

$$\lambda_k S_{k,m} = -\gamma_s S_{k,m} + \gamma_s\sigma\sum_q \mathcal{L}_{m,q}S_{k,q}^*. \quad (10)$$

As matrix $\mathcal{L}$ is both self-adjoint and real ($\mathcal{L}_{m,q} = \mathcal{L}_{q,m}$ real, see Eqs. (6)–(8)), its eigenvalues Λ_k and eigenvectors $\vec{L}_k$, of components $L_{k,m}$, are all real. As γ_s and σ are also real, there exist two sets of solutions of Eqs. (10), that we will call $S_{k,m}^{(+)}$ and $S_{k,m}^{(-)}$. The first set is given by $S_{k,m}^{(+)} = L_{k,m}$ and the second one is $S_{k,m}^{(-)} = iL_{k,m}$, with corresponding eigenvalues:

$$\lambda_k^{(\pm)} = \gamma_s\left(-1 \pm \sigma\Lambda_k\right), \quad (11)$$

Let us now label by index $k = 0$ the solution of maximum value of $|\Lambda_k|$: $|\Lambda_0| = \max\{|\Lambda_k|\}$. When $\sigma|\Lambda_0|$ is smaller than 1, all the rates $\lambda_k^{\pm}$ are negative, which implies that the null solution for the steady state signal field is stable. For the simplicity of notations, we will take Λ_0 positive in the following [19]. The SPOPO reaches its oscillation threshold when σ takes the value $1/\Lambda_0$, i.e. for a pump power $P = P_{\rm thr}$ equal to:

$$P_{\rm thr} = P_0/\Lambda_0^2, \tag{12}$$

The exact value of Λ_0, and therefore of the SPOPO threshold, depends on the exact shape of the phase matching curve and on the exact spectrum of the pump laser[18]. In the most favorable situation, the theoretical SPOPO threshold can be extremely low, of the order of the single mode threshold divided by the number of pump modes.

Let us now define the normalized amplitude pumping rate r by $r = \sqrt{P/P_{th}} = \sigma\Lambda_0$. We will call eigen-spectrum the set of $S_{k,m}$ values for a given k, which corresponds physically to the different spectral components of the signal field, and critical eigen-spectrum $S_{0,m}^{(+)}$, the one associated with $\lambda_0^{(+)}$, which changes sign at threshold. Above threshold, this critical mode will be the "lasing" one, i.e. the one having a non-zero mean amplitude when $r > 1$. Let us note that the eigen-spectrum in quadrature with respect to the critical one, $S_0^{(-)} = iS_0^{(+)}$, has an associated eigenvalue $\lambda_0^{(-)} = -2\gamma_s$ at threshold. Furthermore, equation (11) implies that all the damping rates $\lambda_k^{(\pm)}$ are comprised below threshold between $-2\gamma_s$ and 0, and that, whatever the pump intensity, all the eigenvalues $\lambda_k^{(\pm)}(r)$ lie between $\lambda_0^{(+)}(r)$ and $\lambda_0^{(-)}(r)$. These properties will be useful for the study of squeezing.

We can now determine the squeezing properties of the signal field in a SPOPO below threshold. This is done by using the SPOPO linearized quantum equations. Let us introduce the operator $\hat{S}_{in,k}(t)$ by:

$$\hat{S}_{in,k}(t) = \sum\nolimits_m L_{k,m}\hat{s}_{in,m}(t) \tag{13}$$

As $\sum_m |L_{k,m}|^2 = 1$, one has $\left[S_{in,k}(t), S_{in,k'}^{\dagger}(t')\right] = \delta(t-t')\delta_{k,k'}$: $\hat{S}_{in,k}$ is the annihilation operator of a combination of modes of different frequencies, which are the eigen-modes of the linearized evolution equation (3). The corresponding creation operator applied to vacuum state creates a photon in a single mode, which can be labelled as "super-mode", which globally describes a frequency comb. Defining in an analogous way as in (13) the intracavity operator $\hat{S}_k(t)$, one can then write:

$$\frac{d}{dt}\hat{S}_k = -\gamma_s\hat{S}_k + \gamma_s\sigma\Lambda_k\hat{S}_k^{\dagger} + \sqrt{2\gamma_s}\hat{S}_{\rm in,k}, \tag{14}$$

Let us now define quadrature hermitian operators $\hat{S}_k^{(\pm)}$ by:

$$\hat{S}_k^{(+)} = \hat{S}_k + \hat{S}_k^{\dagger} \tag{15}$$

$$\hat{S}_k^{(-)} = -i\left(\hat{S}_k - \hat{S}_k^{\dagger}\right) \tag{16}$$

which obey the following equations:

$$\frac{d}{dt}\hat{S}_k^{(\pm)} = \lambda_k^{(\pm)}\hat{S}_k^{(\pm)} + \sqrt{2\gamma_s}\hat{S}_{\rm in,k}^{(\pm)}, \tag{17}$$

with $\lambda_k^{(\pm)}$ given by Eq. (11). These relations enable us to determine the intracavity quadrature operators in the Fourier domain $\tilde{S}_k^{(\pm)}(\omega)$

$$i\omega\tilde{S}_k^{(\pm)}(\omega) = \lambda_k^{(\pm)}\tilde{S}^{\pm}(\omega) + \sqrt{2\gamma_s}\tilde{S}_{\rm in,k}^{(\pm)}(\omega). \tag{18}$$

Finally, the usual input-output relation on the coupling mirror:

$$\tilde{s}_{{\rm out},m}(\omega) = -\tilde{s}_{{\rm in},m}(\omega) + \sqrt{2\gamma_s}\tilde{s}_m(\omega), \tag{19}$$

extends by linearity to any super-mode operator as the mirror is assumed to have a transmission independent of the mode frequency. One then obtains the following expression for the quadrature component in Fourier space of any signal super-mode:

$$\tilde{S}_{{\rm out},k}^{(\pm)}(\omega) = \frac{\gamma_s\left(1 \pm r\Lambda_k/\Lambda_0\right) - i\omega}{\gamma_s\left(-1 \pm r\Lambda_k/\Lambda_0\right) + i\omega}\tilde{S}_{{\rm in},k}^{(\pm)}(\omega), \tag{20}$$

These expressions are particularly simple for the critical mode quadrature components ($k = 0$):

$$\tilde{S}_{{\rm out},0}^{(\pm)}(\omega) = \frac{\gamma_s\left(1 \pm r\right) - i\omega}{-\gamma_s\left(1 \mp r\right) + i\omega}\tilde{S}_{{\rm in},0}^{(\pm)}(\omega), \tag{21}$$

The variance of these operators can be measured using the usual balanced homodyne detection scheme: the local oscillator is in the present case a coherent mode-locked multimode field $E_{\rm L}(t)$ having the same repetition rate as the pump laser:

$$E_{\rm L}(t) = i\epsilon_L\sum_m e_m e^{-i\omega_{s,m}t} + {\rm c.c.}, \tag{22}$$

where $\sum_m |e_m|^2 = 1$, and ϵ_L is the local oscillator field total amplitude factor. Assuming that the photodetectors measure the intensity of the Fourier components of the photocurrent averaged over many successive pulses, the balanced homodyne detection scheme measures the variance of the fluctuations of the projection of the output field on the local oscillator mode when the mean field generated by the OPO is zero, which is the case below threshold. As a result, when the coefficients e_m of the local oscillator field spectral decomposition are equal to the coefficients $L_{k,m}$ of the k-th super-mode, one measures the two following variances, depending on the local

oscillator phase:

$$V_k^- (\omega) = \frac{\gamma_s^2 \left(1 - r\Lambda_k/\Lambda_0\right)^2 + \omega^2}{\gamma_s^2 \left(1 + r\Lambda_k/\Lambda_0\right)^2 + \omega^2} \quad (23)$$

$$V_k^+ (\omega) = V_k^- (\omega)^{-1} \quad (24)$$

Eqs. (23,24) show that the device produces, as expected, a minimum uncertainty state and that quantum noise reduction below the standard quantum limit (equal here to 1) is achieved for any super-mode characterized by a non-zero Λ_k value and that the smallest fluctuations are obtained close to threshold and at zero Fourier frequency:

$$(V_k)_{\min} = \left(\frac{\Lambda_0 - |\Lambda_k|}{\Lambda_0 + |\Lambda_k|}\right)^2 \quad (25)$$

In particular, if one uses as the local oscillator the critical mode $k = 0$, identical to the one oscillating just above the threshold $r = 1$, one then gets perfect squeezing just below threshold and at zero noise frequency, just like in the c.w. single mode case. But modes of $k \neq 0$ may be also significantly squeezed, provided that $|\Lambda_k/\Lambda_0|$ is not much different from 1. This occurs in particular when the pump spectrum width is much smaller than the phase-matching bandwidth[18]. Our multi-mode approach of the problem has therefore allowed us to extract from all the possible linear combinations of signal modes the ones in which the quantum properties are concentrated [20].

In conclusion, we have studied the quantum behaviour of a degenerate synchronously-pumped OPO, which seems at first sight a highly multi-mode system, since it involves roughly 10^5 different usual single frequency modes for a $100fs$ pulse. We have shown that its properties are more easily understood if one considers the "super-modes", linear combinations of all these modes that are eigen-modes of the SPOPO set of evolution equations and describe in a global way the frequency comb -or, equivalently, the train of pulses- generated by the SPOPO. The super-mode of minimum threshold plays a particular role, as it is the one which turns out to be perfectly squeezed at threshold and will oscillate above threshold, but all the super-modes have non-classical character and can be significantly squeezed. The present paper gives a first example of the high interest of studying frequency combs at the quantum level, as they merge the advantages of two already well-known non-classical states of light: the c.w. light beams, with their high degree of coherence and reproducibility and the single pulses of light, with their high peak power enhancing the non-linear effects necessary to produce pure quantum effects.

Laboratoire Kastler Brossel, of the Ecole Normale Supérieure and the Université Pierre et Marie Curie-Paris6, is UMR8552 of the Centre National de la Recherche Scientifique. G.J. de V. has been financially supported by grant PR2005-0246 of the Secretaría de Estado de Universidades e Investigación del Ministerio de Educación y Ciencia (Spain).

[1] L.A. Wu, H.J. Kimble, J. Hall, H. Wu, Phys. Rev. Lett. **57**, 2520 (1986).
[2] A. Heidmann, R. Horowicz, S. Reynaud, E. Giacobino, C. Fabre, G. Camy, Phys. Rev. Lett. **59**, 2555 (1987).
[3] Z. Y. Ou, S. F. Pereira, H. J. Kimble, K. C. Peng, Phys. Rev. Lett. **68**, 3663 (1992).
[4] R. E. Slusher, P. Grangier, A. LaPorta, B. Yurke, M. J. Potasek, Phys. Rev. Lett. **59**, 2566 (1987).
[5] R. M. Shelby and M. Rosenbluh, Appl. Phys. B **55**, 226 (1992).
[6] M. Rosenbluh, R. Shelby, Phys. Rev. Lett. **66**, 153 (1991).
[7] J. A. Levenson, I. Abram, T. Rivera, P. Fayolle, J. C. Garreau, P. Grangier, Phys. Rev. Lett. **70**, 267 (1993).
[8] A. Piskarskas, V. J. Smil'gyavichyus and A. Umbrasas, Sov. Quantum Electron. **18**, 155 (1988).
[9] D. C. Edelstein, E. S. Wachman, C. L. Tang, Appl. Phys. Lett. **54**, 1728 (1989).
[10] G. Mak, Q. Fu, H. M. van Driel, Appl. Phys. Lett. **60**, 542 (1992).
[11] G. T. Maker and A. I. Ferguson, Appl. Phys. Lett **56**, 1614 (1990).
[12] M. Ebrahimzadeh, G. J. Hall and A. I. Ferguson, Opt. Lett. **16**, 1744 (1991).
[13] M. J. McCarty and D. C. Hanna, Opt. Lett. **17**, 402 (1992).
[14] E. C. Cheung and J. M. Liu, J. Opt. Soc. Am. B **7**, 1385 (1990) and **8**, 1491 (1991).
[15] M. J. McCarthy and D. C. Hanna, J. Opt. Soc. Am. B **10**, 2180 (1993).
[16] M. F. Becker, D. J. Kuizenga, D. W. Phillion, A. E. Siegman, J. Appl. Phys. **45**, 3996 (1974).
[17] W. Wasilewski, A.I. Lvovsky, K. Banaszek and C. Radzewicz, PRA **73**, 063819 (2006).
[18] G. Patera, G. De Valcarcel, N. Treps, C. Fabre, to be published
[19] Should $\Lambda_0 < 0$ then the null eigenvalue at threshold would be $\lambda_0^{(-)}$ instead of $\lambda_0^{(+)}$ and the following analysis should be accordingly modified.
[20] Our result is different from the "frequency comb of squeezing" reported in A. E. Dunlop *et al.* Phys. Rev. A **73**, 013817 (2006), which deals with single-mode cw OPOs and shows that squeezing is effective in a comb of noise frequencies.

Résumé

Nous considérons la description quantique de la lumière dans le régime des variables continues, où les photons ne sont pas distinguables individuellement. Dans la limite des petites fluctuations quantiques, nous cherchons à augmenter la richesse, et les possibles applications, des états quantiques produits en multipliant le nombre de "modes" -ou degrés de libertés- mis en jeu par le processus de détection. C'est ce que nous appelons l'optique quantique multimode. Dans ce cadre, nous voyons comment, en pratique, compter le nombre de modes pertinents au sein d'un faisceau lumineux. Puis nous reprenons la théorie de la mesure optique pour associer le caractère multimode de la lumière à la recherche d'information dans un faisceau. Par cette approche, nous redéfinissons les limites ultimes de la mesure et nous considérons l'intrication quantique à partir de n'importe quelle grandeur mesurable. Nous illustrons cette théorie par des expériences mettant en jeu de plus en plus de modes : mesures de photons jumeaux, intrication et téléportation quantique, mesure et réduction du bruit de polarisation, nano-positionnement d'un faisceau au delà de la limite quantique standard, intrication spatiale, amplification sans bruit d'images et optique quantique multimode avec des peignes de fréquence. Nous évoquons également les possibles applications à l'accroissement des capacités de stockage et de transfert d'information, au traitement en parallèle de l'information quantique et à l'amélioration les techniques d'imagerie et de métrologie.

We consider the quantum description of light in the continuous wave regime, where photons are not distinguishable individually. In the small quantum fluctuations limit, we intend to increase both the richness and possible applications of non-classical light by the increase of the number of modes -or degree of freedom- involved in the detection process. This is what is called multimode quantum optics. Within this frame, we describe a practical way to extract the number of relevant modes in a beam of light. Then, measurement theory is reconsidered to link the multimode character of light to information processing with a beam of light. Limits to optical measurement are thus redefined, and quantum entanglement for any measurable observable described. Experiments involving more and more optical modes are demonstrated to illustrate that theory : twin beams, entanglement and quantum teleportation measurement, polarization squeezed and entangled state generation, nano-positioning of a beam of light beyond the standard quantum limit, spatial entanglement, noiseless amplification of images and multimode quantum optics with frequency combs. On the way, we evoke the possible applications to the increase of optical read-out capacity and information transfer, to parallel processing of quantum information and to quantum imaging and metrology.